Universidad de Valladolid

Escuela de Doctorado Universidad de Valladolid

PROGRAMA DE DOCTORADO EN QUÍMICA: QUÍMICA DE SÍNTESIS, CATÁLISIS Y MATERIALES AVANZADOS

TESIS DOCTORAL:

Study of relevant steps in bimetallic Cu-catalysed cross-coupling reactions

Presentada por Guillermo Marcos Ayuso para optar al grado de
Doctor/a por la Universidad de Valladolid

Dirigida por:
Juan A. Casares González

La Tesis Doctoral titulada "*Study of relevant steps in bimetallic Cu-catalysed cross-coupling reactions*" ha sido realizada gracias al apoyo económico de la Junta de Castilla y León (VA224P20) y de la Dirección General de Investigación Científica y Técnica del MICINN o del MINECO (PID2019-111406GB-I00).

.

Publicaciones

Parte de los resultados presentados en esta memoria de Tesis Doctoral fueron publicados en los siguientes artículos científicos:

1. “Copper(I) activation of C–X bonds: bimolecular vs. unimolecular reaction mechanism”.

Marcos-Ayuso, G.;Lledós A.; Casares, J. A. ***Chem. Commun.***, 2022, **58**, 2718–2721. doi: 10.1039/D1CC07027D

2. “Pd/Cu bimetallic catalysis to access highly fluorinated biaryls from aryl halides and fluorinated arenes”.

Ponce-de-León, J.; Marcos-Ayuso, G.; Casares, J. A.; Espinet, P. ***Chem. Commun***., 2022, **58**, 3146–3149. doi: 10.1039/D2CC00141A

RESUMEN GENERAL DE LA TESIS DOCTORAL

En esta memoria se presentan los resultados de la investigación realizada en el Instituto Universitario CINQUIMA de la Universidad de Valladolid, en el departamento de Química Inorgánica y Química Física, durante el transcurso de la presente tesis doctoral. Algunos de los resultados aquí expuestos ya están publicados en revistas científicas por lo que sus contenidos pueden coincidir parcialmente o en su totalidad.

En el capítulo I se presenta un sistema bimetálico Pd/Cu para la síntesis de biarilos fluorados. En este capítulo, se detalla la contribución de cada uno de los catalizadores al ciclo catalítico, así como la optimización de condiciones de dicho sistema. Se muestran numerosos compuestos sintetizados utilizando esta metodología, asi como su purificación y exhaustiva caracterización. Finalmente, se contribuye al entendimiento de las diferentes etapas mediante estudios mecanísticos.

En el capítulo II se realiza el estudio de la etapa de adición oxidante de haluros de arilo fluorados a complejos de Cu^{I} del tipo [Cu(Ar^{F})(NHC)] (Ar^{F} = arilo fluorado, NHC = carbeno N-heterocíclico). Este trabajo muestra de forma sistemática el estudio mecanístico de dicha etapa elemental, empleando diferentes técnicas espectroscópicas, especialmente RMN de ^{19}F y experimentos de difusión en disolución. Para confirmar el mecanismo propuesto se emplean cálculos computacionales, que se llevaron a cabo en colaboración con el Prof. Agustí Lledós de la Universidad Autónoma de Barcelona.

En el capítulo III se lleva cabo la puesta a punto de un sistema fotocatalítico de cobre para la síntesis de biarilos fluorados a partir de carboxilatos de arilo y haluros de arilo. Este sistema muestra por primera vez la fotodescarboxilación de acidos carboxílicos fluorados con complejos de cobre en estado de oxidación +1 para dar acoplamientos C–C, no descritos hasta la fecha empleando esta metodología.

El capítulo IV detalla la etapa de transmetalación entre complejos de Cu(I) del tipo [Cu(Ar^F)(bipy)] a complejos de Fe(II) del tipo [Fe(Cp)I($CO)_2$]. En este estudio, se demuestra la gran sinergia que existe entre estos dos metales, pese a ser ambos de la primera serie de transición. El mecanismo explica la necesidad de la formación de una especie activa en la etapa de transmetalación, así como diferentes propuestas para facilitar dicha disociación. Finalmente, se comentan aspectos electrónicos y orbitales, cuya investigación se continúa en la actualidad a nivel computacional, en colaboración con el Prof. Agustí Lledós de la Universidad Autónoma de Barcelona.

El capítulo V detalla las diferencias, tanto termodinámicas como cinéticas, de la etapa de transmetalación entre el complejo *trans*-[PdCl($C_6F_3Cl_2$)($AsPh_3)_2$] y los complejos del tipo [M(C_6F_5)(NHC)] (M = Cu, Ag, Au). Este estudio se lleva a cabo de forma casi exclusiva empleando técnicas de resonancia magnética nuclear, así como determinación estructural mediante difracción de rayos x. El mecanismo se está desarrollando en profundidad a nivel computacional por la Profesora Rosana Álvarez, de la Universidad de Vigo.

INTRODUCCIÓN GENERAL

Esta memoria está organizada en cinco capítulos escritos en su totalidad en inglés, y por motivos de forma, se han incluido una introducción general, donde se expone de forma breve el hilo conductor de esta tesis doctoral y las conclusiones en castellano. Todos los capitulos cuentan con una introducción donde se enmarca el estudio llevado a cabo, así como las necesidades dentro de sus campos. Seguidamente, una sección donde se exponen detalladamente los resultados obtenidos y su discusión, la cual da paso a la exposición de las conclusiones. Por último, se detallan los procedimientos experimentales. La bibliografía correspondiente se recoge en el pie de página en cada capítulo.

La catálisis homogénea que emplea metales de transición es una de las herramientas más poderosas a la hora de romper o generar nuevos enlaces químicos.[1] Su uso se extiende por la mayoría de las vertientes de la química sintética, desde la química médica y farmacéutica, que permite diseñar y sintetizar moléculas pequeñas de alto valor añadido, a la síntesis de polímeros y nuevos materiales. Tradicionalmente, estas transformaciones se han llevado a cabo mediante catalizadores monometálicos de transición, empleando metales como por ejemplo el rodio, el paladio o el oro. Sin embargo, este tipo de catalizadores pueden experimentar ciertas limitaciones dentro de los ciclos catalíticos, bien por no poder realizar ciertas transformaciones, o bien por ser energéticamente muy costosas. Una solución para estos problemas es el empleo de nuevas estrategias, como la catálisis multimetálica.[2] En un sistema multimetálico, cada catalizador desempeña un papel independiente en la activación o funcionalización de los reactivos, y se conectan en una de las etapas de reacción, normalmente la etapa de transmetalación, como se observa en la Figura 1. Esta nueva metodología tiene grandes ventajas sobre la catálisis monometálica tradicional, como la aparición de nuevas reactividades,

[1] Behr A., Neubert P. John Wiley & Sons. Applied Homogeneous Catalysis. Wiley-VCH, **2012.** ISBN: 978-3-527-32641-9.
[2] Shibasaki, Masakatsu.; Yamamoto, Y.; John Wiley & Sons. Multimetallic Catalysts in Organic Synthesis; Wiley-VCH, **2004**. ISBN:9783527308286.

mejoras en la regio- y estereoselectividad, el empleo de condiciones de reacción más suaves o una mayor tolerancia de grupos funcionales.[3]

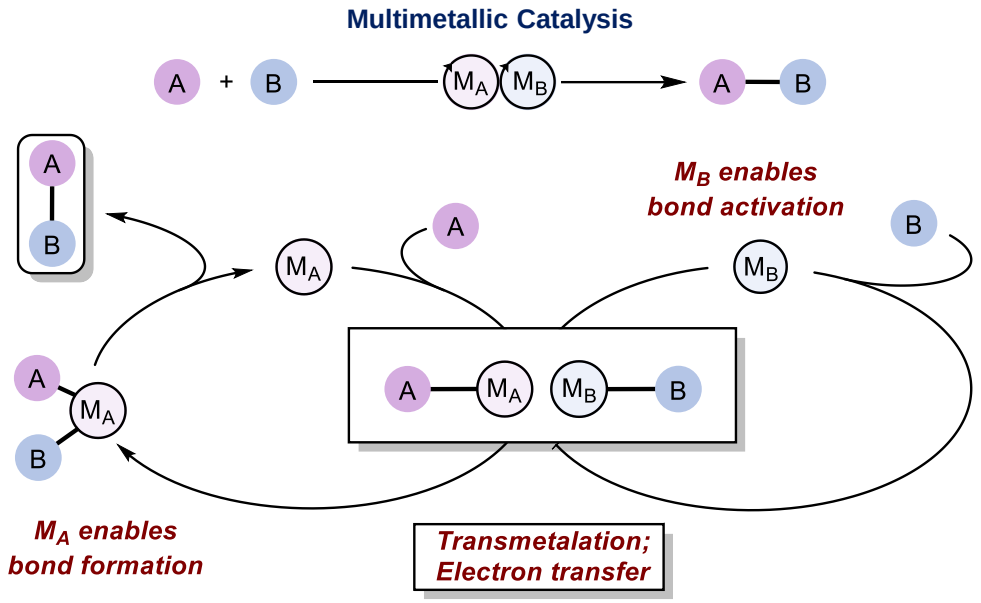

Figura 1. Esquema general de los ciclos catalíticos multimetálicos.

En las últimas décadas, muchos de los esfuerzos desempeñados en investigación están relacionados con el perfeccionamiento y el descubrimiento de nuevos sistemas multimetálicos.[4] Dentro del gran número de estudios, un importante porcentaje pertenece a la formación de enlaces C–C, uno de los más importantes debido a la gran cantidad de transformaciones que permite llevar a cabo.[5] Una de las reacciones más importantes dentro de este campo, es la reacción de Sonogashira.[6] En ella, dos metales de transición, el cobre y el paladio, cooperan para dar la formación de un enlace $C(sp^2)–C(sp^3)$. En este proceso, podemos encontrar

[3] A) Pérez-Temprano, M. H.; Casares, J. A.; Espinet, P. Bimetallic Catalysis Using Transition and Group 11 Metals: An Emerging Tool for C–C Coupling and Other Reactions. *Chem. Eur. J.* **2012**, *18*, 1864–1884. B) In Science of Synthesis: Dual Catalysis in Organic Synthesis 1 and 2; Molander, G. A., Ed.; Georg Thieme Verlag: Stuttgart, Germany, **2020**.

[4] A) Lee, J. M.; Na, Y.; Han, H.; Chang, S. Cooperative Multi-Catalyst Systems for One-Pot Organic Transformations. *Chem. Soc. Rev*. **2004**, *33*, 302–312. B) Allen, A. E.; MacMillan, D. W. C. Synergistic Catalysis: A Powerful Synthetic Strategy for New Reaction Development. *Chem. Sci.* **2012**, *3*, 633–658.

[5] Pye, D. R.; Mankad, N. P. Bimetallic Catalysis for C–C and C– X Coupling Reactions. *Chem. Sci*. **2017**, 8, 1705–1718.

[6] Chinchilla, R.; Najera, C. The Sonogashira Reaction: A Booming Methodology in Synthetic Organic Chemistry. *Chem. Rev*. **2007**, *107*, 874–922.

diferentes etapas químicas fundamentales dentro de cada uno de los ciclos catalíticos, como se observa en la Figura 2.

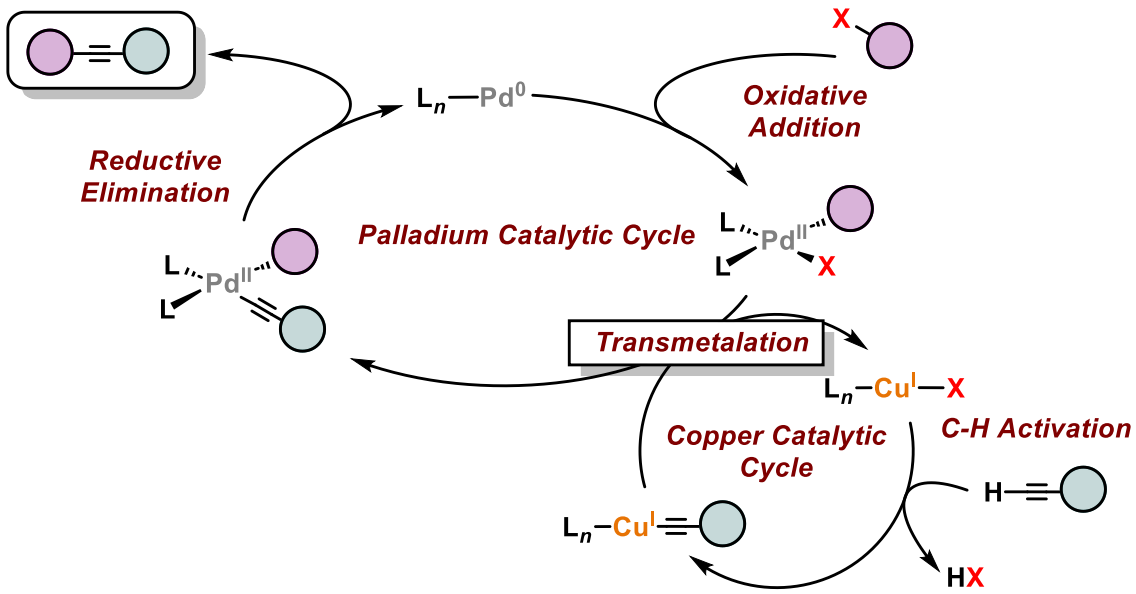

Figura 2. Esquema general de la reacción de Sonogashira.

En el ciclo catalítico del paladio, encontramos las etapas elementales conocidas como adición oxidante, donde un haluro de arilo experimenta la ruptura del enlace X–C, que resulta en la oxidación de dos electrones del centro metálico, pasando de Pd(0) a Pd(II). Por otro lado, el complejo organometálico de Cu(I) es capaz de reaccionar con un alquino terminar en presencia de base, para formal el acetiluro de cobre correspondiente, mediante un proceso de activación C–H. Ambos ciclos están conectados por la etapa de transmetalación, donde el acetiluro y el halógeno se intercambian formando la especie inicial de Cu(I) y el complejo de Pd(II) con los dos restos orgánicos. Por último, en la etapa de eliminación reductora se forma un nuevo enlace C–C, y el centro metálico sufre una reducción, pasando de Pd(II) a Pd(0), regenerando el catalizador.

La sinergia que existe entre ambos metales en la reacción de Sonogashira, se puede desarrollar en diferentes sistemas catalíticos, empleando parejas de metales muy distintas, como por ejemplo, sistemas catalíticos entre el Pd y metales del grupo 11 (Cu, Ag y Au), metales de una misma serie de transición, como el Cu y el Fe o Cu y Ni, o metales de una mismo grupo, como la catálisis entre Ni y Pd.[7] Todos estos

[7] Kim, U. B.; Jung, D. J.; Jeon, H. J.; Rathwell, K.; Lee, S. Synergistic Dual Transition Metal Catalysis. *Chem. Rev.* **2020**, *120*, 13382–13433.

sistemas catalíticos se han descubierto en parte, gracias al estudio mecanístico de sus reacciones elementales. El análisis en profundidad y de forma exhaustiva de las componentes físico-químicas que gobiernan estos procesos, como son la termodinámica y la cinética, ha permitido un mayor entendimiento del desarrollo de estos procesos. Este conocimiento se traduce en mejoras a diferentes niveles, especialmente a nivel medioambiental, reduciendo la cantidad de energía necesaria para llevar a cabo determinadas transformaciones, y a nivel económico, permitiendo emplear metales mucho más abundantes. Es por ello, que dichos estudios mecanísticos han aumentado su número exponencialmente en los últimos años en la literatura científica.

Por otro lado, de forma paralela al descubrimiento de nuevos sistemas multimetálicos, se han desarrollado otras metodologías capaces de cooperar con un metal de transición en la funcionalización de uno o varios reactivos. Este es el caso de los procesos fotoquímicos, que se pueden llevar a cabo empleando diferentes estrategias.[8] Entre las más utilizadas encontramos, el uso de fotocatalizadores, bien orgánicos u organometálicos, capaces de funcionalizar uno de los reactivos mediante un proceso redox. Otra variante es el empleo de la fotoquímica para generar estados excitados, capaces de dar reactividades imposibles en los estados fundamentales. Las principales ventajas conceptuales que ofrece esta tecnología son la posibilidad de generar especies radicalarias altamente reactivas en condiciones suaves simplemente irradiando las reacciones químicas, y el acceso a distintos modos de reactividad inalcanzables en el estado fundamental. Es importante destacar que el desarrollo técnico de fuentes de luz sintonizables, seguras y ampliamente disponibles ha contribuido a impulsar la rápida adopción de la fotoquímica en las metodologías sintéticas.

Los metales de la primera serie de transición son generalmente baratos y abundantes, por lo que la catálisis con ellos activada por luz visible es muy atractiva para el objetivo de desarrollar métodos sintéticos sostenibles. Sin embargo, la sustitución del iridio o el rutenio como fotocatalizadores va más allá de un simple propósito económico o de sostenibilidad, y abre nuevas oportunidades ofrecidas por

[8] Melchiorre, P. Introduction: Photochemical Catalytic Processes. *Chem. Rev.* **2022**,*122*,1483–1484.

los complejos metálicos de la primera serie de transición. Así, la exploración de complejos de Ni, Cu o Fe como fotocatalizadores ofrece una gran oportunidad con aplicaciones en reacciones de acoplamiento cruzado y en la generación de especies de capa abierta con una reactividad no explorada hasta el momento. Estos aspectos han impulsado recientemente a los químicos a centrar su atención en la fotoexcitación directa de complejos metálicos con fines sintéticos, explotando reactividades más allá de los procesos bien establecidos de transferencia de electrones (*Single Electron Transfer*) que conforman la base de la catálisis fotorredox. De hecho, muchas etapas elementales de la química organometálica, como la adición oxidante, la eliminación reductora, la β-eliminación de hidrógeno o la homólisis de enlaces, pueden habilitarse o acelerarse bajo irradiación lumínica, explotando la distintiva reactividad de complejos metálicos en los estados excitados.[9] Entre ellos, una de las estrategias más generalizadas es la transferencia de carga ligando-metal (*Ligand to Metal Charge Transfer*) de complejos metálicos que generan especies de capa abierta que pueden utilizarse en reacciones radicalarias, como se observa en la Figura 3.

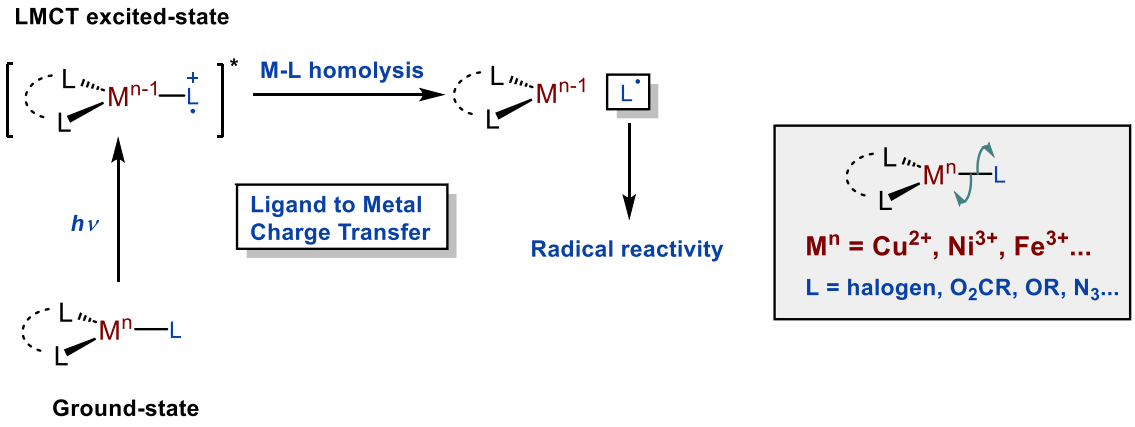

Figura 3. Esquema general de la fotoquímica de los procesos de transferencia de carga ligando-metal.

Para diseñar y entender sistemas fotoactivos con reactividad LMCT es necesario comprender las propiedades fotofísicas y fotoquímicas de este tipo de estados excitados. Los estados LMCT son el resultado de una transición electrónica de un orbital lleno que se localiza en gran medida en un ligando a un orbital vacío del

[9] Juliá, F. Ligand-to-Metal Charge Transfer (LMCT) Photochemistry at 3d-Metal Complexes: An Emerging Tool for Sustainable Organic Synthesis. *Chem. Cat. Chem*. **2022,** *14*.

centro metálico (Figura 3). Dado que el orbital del metal vacío (d*) debe ser relativamente bajo en energía para ser accesible, este tipo de estados excitados son característicos de complejos que soportan centros metálicos electrófilos y de alto estado de oxidación. Algunos ejemplos dentro del bloque 3d son el Ti(IV), Fe(III)o Cu(II), entre otros. Por otra parte, dado que el ligando actúa como fuente interna de electrones en esta transición electrónica, la presencia de ligandos donantes ricos en electrones, como los halogenuros, los carboxilatos o las azidas también favorecen la aparición de transiciones π-LMCT.

A lo largo de esta tesis doctoral, se abordarán las diferentes metodologías resumidas en esta introducción general, que buscan poder mejorar problemas existentes en la formación de enlaces C–C utilizando la catálisis multimetálica y los procesos fotocatalizados. Por otro lado, se van a desarrollar diferentes estudios mecanísticos, buscando arrojar luz sobre etapas elementales (adición oxidante y transmetalación) en sistemas potencialmente empleables en reacciones catalíticas de acoplamiento.

Table of contents

CHAPTER I: Pd/Cu bimetallic catalysis to access highly fluorinated biaryls from aryl halides and fluorinated arenes.

1.1 Introduction

Bimetallic catalysis is defined as a homogeneous process in which two transition metals (TM) or a transition metal and another chemical element, cooperate in a catalytic process. Nowadays, this type of reaction is widely used in synthetic chemistry, as it represents a very useful alternative where traditional homogeneous catalysis cannot operate. That is why it is one of the main topics within the research.[10,11,12] Over the last decades, the reactions catalysed by Cu/Pd organometallic complexes have attracted the interest of numerous research groups and have become one of the most studied topics in organic and organometallic chemistry.[13,14,15,16] In addition, numerous catalytic systems have been discovered and in many cases, their mechanisms have been studied in detail.[17,18]

So far, the most frequent synthetic protocol in bimetallic catalysis, although not the only one, is C–C bond formation. One of the most important reactions is the Sonogashira process.[19] This type of bimetallic catalysis uses a Pd/Cu system.[20] As we can see in Scheme 1, the role of copper is to react with the alkyne in the presence

---

[10] Kim, U.; Jung, D. J.; Jeon, H. J.; Rathwell, K.; Lee, S. G. Synergistic Dual Transition Metal Catalysis. *Chem. Rev.* **2020**, *120*, 13382–13433. DOI: 10.1021/acs.chemrev.0c00245.

[11] Pye, D. R.; Mankad, N. P. Bimetallic Catalysis for C–C and C–X Coupling Reactions. *Chem. Sci.* **2017**, *8*, 1671–2466. DOI: 10.1039/c6sc05556g.

[12] Pérez-Temprano, M. H.; Casares, J. A.; Espinet, P. Bimetallic Catalysis Using Transition and Group 11 Metals: An Emerging Tool for C–C Coupling and Other Reactions. *Chem. – Eur. J.* **2012**, *18*, 1864–1884. DOI: 10.1002/CHEM.201102888.

[13] Chen, Q.; Fu, L.; Nishihara, Y. Palladium/Copper-Cocatalyzed Decarbonylative Alkynylation of Acyl Fluorides with Alkynylsilanes: Synthesis of Unsymmetrical Diarylethynes. *Chem. Commun.* **2020**, *56*, 7977–7980. DOI: 10.1039/D0CC03309J.

[14] Shibasaki, Masakatsu.; Yamamoto, Y.; John Wiley & Sons. *Multimetallic Catalysts in Organic Synthesis*; Wiley-VCH, **2004**.

[15] Rivada-Wheelaghan, O.; Comas-Vives, A.; Fayzullin, R. R.; Lledós, A.; Khusnutdinova, J. R. Dynamic Pd^{II}/Cu^{I} Multimetallic Assemblies as Molecular Models to Study Metal–Metal Cooperation in Sonogashira Coupling. *Chem. – Eur. J.* **2020**, *26*, 12168–12179. DOI: 10.1002/CHEM.202002013.

[16] Hackenberger, D.; Song, B.; Grünberg, M. F.; Farsadpour, S.; Menges, F.; Kelm, H.; Groß, C.; Wolff, T.; Niedner-Schatteburg, G.; Thiel, W. R.; Gooßen, L. J. Bimetallic Cu/Pd Catalysts with Bridging Aminopyrimidinyl Phosphines for Decarboxylative Cross-Coupling Reactions at Moderate Temperature. *Chem. Cat. Chem.* **2015**, *7*, 3579–3588. DOI: 10.1002/CCTC.201500769.

[17] Ponce-De-León, J.; Espinet, P. Selective Synthesis of Fluorinated Biaryls by [MCl_2(PhPEWO-F)] (M = Ni, Pd) Catalysed Negishi Cross-Coupling. *Chem. Commun.* **2021**, *57*, 10875-10879. DOI: 10.1039/d1cc04915a.

[18] Fromm, A.; van Wüllen, C.; Hackenberger, D.; Gooßen, L. J. Mechanism of Cu/Pd-Catalyzed Decarboxylative Cross-Couplings: A DFT Investigation. *J. Am. Chem. Soc.* **2014**, *136*, 10007–10023. DOI: 10.1021/JA503295X.

[19] Chinchilla, R.; Nájera, C. The Sonogashira Reaction: A Booming Methodology in Synthetic Organic Chemistry. *Chem. Rev.* **2007**, *107*, 874–922. DOI: 10.1021/cr050992x.

[20] Wu, Y.; Huo, X.; Zhang, W. Synergistic Pd/Cu Catalysis in Organic Synthesis. *Chem. – Eur. J.* **2020**, *26*, 4895–4916. DOI: 10.1002/chem.201904495.

of a base to give a copper acetylide in a C–H activation process. Then, acetylide undergoes transmetalation from copper to palladium to give the key palladium(II) acetylide, which experiments reductive elimination to generate the desired cross-coupling product.[21]

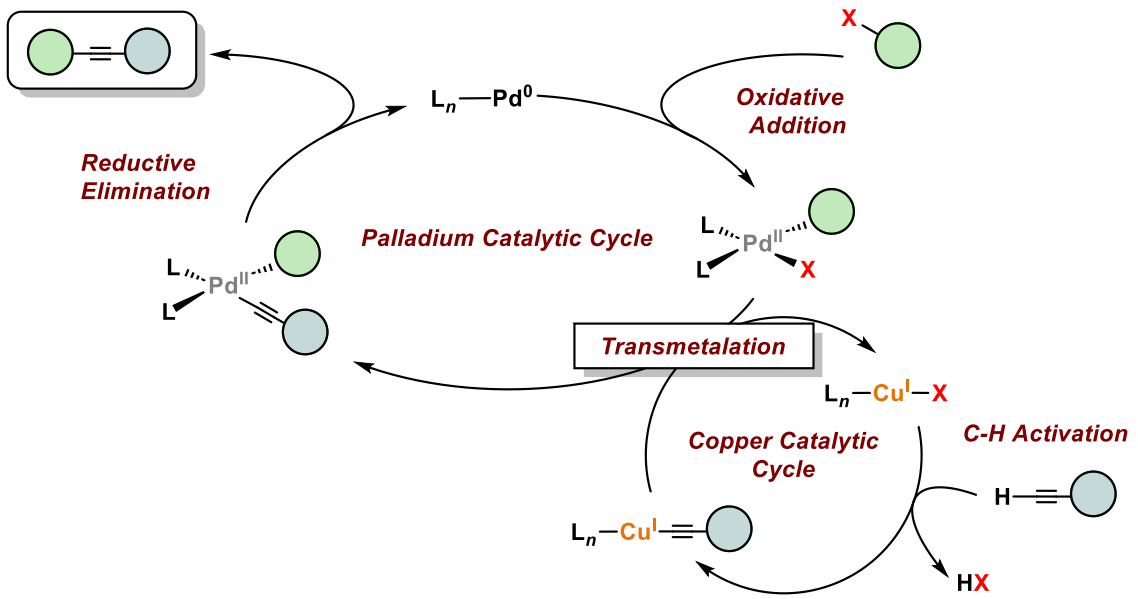

Scheme 1. Two cycles connected by transmetalation in the Sonogashira reaction. Green and blue circles represent organic moieties.

If we pay attention to this type of bimetallic catalysis, we can observe several interesting features. The palladium catalytic cycle is composed by some elementary steps, oxidative addition, reductive elimination, transmetalation and, sometimes, isomerization processes. The copper catalytic cycle is formed by the C–H activation of an acetylene in the presence of a base. Finally, both cycles are linked in the transmetalation step, where the organic moiety is transferred from one metal to the other. This synergy has a beneficial effect on the overall yield, since the transmetalation step is the slow step of this reaction. Proof of this is that when the coupling of alkynyls with organic halides is carried out using only a Pd catalyst (Heck/Cassar reaction), the catalyst loadings, reaction times and temperatures are usually higher.[22]

[21] Chinchilla, R.; Nájera, C. N. Recent Advances in Sonogashira Reactions. *Chem. Soc. Rev.* **2011**, *12*, 5084–5121. DOI: 10.1039/c1cs15071e.

[22] Gazvoda, M.; Virant, M.; Pinter, B.; Košmrlj, J. Mechanism of Copper-Free Sonogashira Reaction Operates through Palladium-Palladium Transmetallation. *Nat. Commun.* **2018**, *9*, 1–9. DOI: 10.1038/s41467-018-07081-5.

Although the transmetalation step in palladium-copper systems is known to work, it is worth commenting on the thermodynamics of this process. In a simplistic manner, Cu–C and Pd–X bonds are broken and Pd–C and Cu–X bonds are formed. Concerning the copper species, experimental data of various Cu–X bond dissociation energies (BDE) are available.[23] Considering X–Cu dissociation energies series, the Cu–C bond dissociation energy is 53 kcal·mol^{-1}, whereas the Cu–I BDE is 72 kcal·mol^{-1}.[24] The affinity of halogens for copper centers are indeed well known, and it acts as the thermodynamic driving force of the transmetalation, as we can see in Equation 1. In the case of Pd–halogen bonds of actual complexes, calculated and experimental energies are available. The energy balance between the Pd–X and the Pd–C bonds is endergonic, (from about 14 kcal·mol^{-1} for Pd–I, up to 30 kcal·mol^{-1} if a Pd–Cl bond is broken).[25] Nevertheless, much smaller differences are handled if compared with the copper ones, which would have a greater contribution to the overall ΔG (the energy balance between the Cu–X and the Cu–C bonds is 19 kcal·mol^{-1} for X=I, and 41 kcal·mol^{-1} for X=Cl).

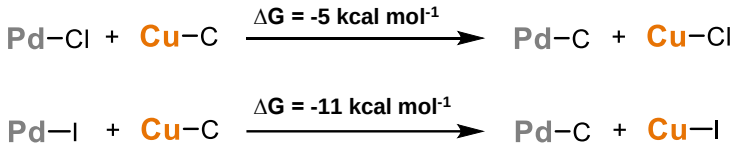

Equation 1. Thermodynamic values of the general transmetalation reaction between Pd–X and Cu–C.

However, in a multistep reaction the whole balance of ΔG does not depend only on the transmetalation step, but also on the other steps. A cross-coupling reaction involves the formation of a C–C bond, which is enough driving force for the overall balance in most cases. As a matter of fact, usually the transmetalation is

[23] Luo, Y. R. Comprehensive Handbook of Chemical Bond Energies. *Comprehensive Handbook of Chemical Bond Energies* **2007**, 1–1656. DOI: 10.1201/9781420007282.

[24] Casares, J. A.; Coco, S.; Espinet, P.; Lin, Y. S. Observation of a Slow Dissociative Process in Palladium(II) Complexes. *Organometallics* **1995**, *14*, 3058–3067. DOI: 10.1021/om00006a055.

[25] Golubeva, E. N.; Zubanova, E. M.; Zhidomirov, G. M. The Nature of Cu–C Bond and Copper Oxidation State in Chloroorganocuprates $[CuClCH_3]_2$. *J. Phys. Org. Chem.* **2013**, *26*, 724–729. DOI: 10.1002/poc.3093.

reversible,[26,27,28] but the coupling proceeds as the irreversible reductive elimination pulls forward the catalytic cycle. Consequently, kinetic factors are usually more relevant than thermodynamic ones, if the transmetalation itself is not too much disfavoured.[29]

Inspired by this type of reaction, taking advantage of the good synergy between these two metals, and with favourable thermodynamics for the formation of C–C cross-coupling, new bimetallic models have been discovered over the years. Optimizing the reaction conditions, it has been possible to activate less acidic C–H bonds than those described by the Sonogashira reaction. An example published by Huang and co-workers in 2010, *''A Highly Efficient Palladium/Copper Cocatalytic System for Direct Arylation of Heteroarenes*'' where the C–H activation of different heteroarenes is described using a copper organometallic complex, to couple it with different aryls.[30] As we can see in Scheme 2, the complex [CuI(XantPhos)] is capable to activate different heteroarenes in the presence of Cs_2CO_3 at 100 °C in toluene. The organic moiety goes to the Pd complex through the transmetalation step. The Pd^{II} complex now formed gives a reductive elimination process, generating the cross-coupling product and regenerating the initial Pd catalyst.

[26] Gallego, A. M.; Peñas-Defrutos, M. N.; Marcos-Ayuso, G.; Martin-Alvarez, J. M.; Martínez-Ilarduya, J. M.; Espinet, P. Experimental Study of Speciation and Mechanistic Implications When Using Chelating Ligands in Aryl-Alkynyl Stille Coupling. *Dalton Trans.* **2020**, *49*, 11336–11345. DOI: 10.1039/d0dt02335c.

[27] García-Melchor, M.; Fuentes, B.; Lledós, A.; Casares, J. A.; Ujaque, G.; Espinet, P. Cationic Intermediates in the Pd-Catalyzed Negishi Coupling. Kinetic and Density Functional Theory Study of Alternative Transmetalation Pathways in the Me-Me Coupling of $ZnMe_2$ and Trans -[$PdMeCl(PMePh_2)_2$]. *J. Am. Chem. Soc.* **2011**, *133*, 13519–13526. DOI: 10.1021/ja204256x.

[28] Pérez-Temprano, M. H.; Nova, A.; Casares, J. A.; Espinet, P. Observation of a Hidden Intermediate in the Stille Reaction. Study of the Reversal of the Transmetalation Step. *J. Am. Chem. Soc.* **2008**, *130*, 10518–10520. DOI: 10.1021/ja802994v.

[29] Amatore, C.; Jutand, A.; Le Duc, G. Kinetic Data for the Transmetalation/Reductive Elimination in Palladium-Catalyzed Suzuki-Miyaura Reactions: Unexpected Triple Role of Hydroxide Ions Used as Base. *Chem. – Eur. J.* **2011**, *17*, 2492–2503. DOI: 10.1002/chem.201001911.

[30] Huang, J.; Chan, J.; Chen, Y.; Borths, C. J.; Baucom, K. D.; Larsen, R. D.; Faul, M. M. A Highly Efficient Palladium/Copper Cocatalytic System for Direct Arylation of Heteroarenes: An Unexpected Effect of Cu(Xantphos)I. *J. Am. Chem. Soc*. **2010**, *132*, 3674–3675. DOI: 10.1021/ja100354j.

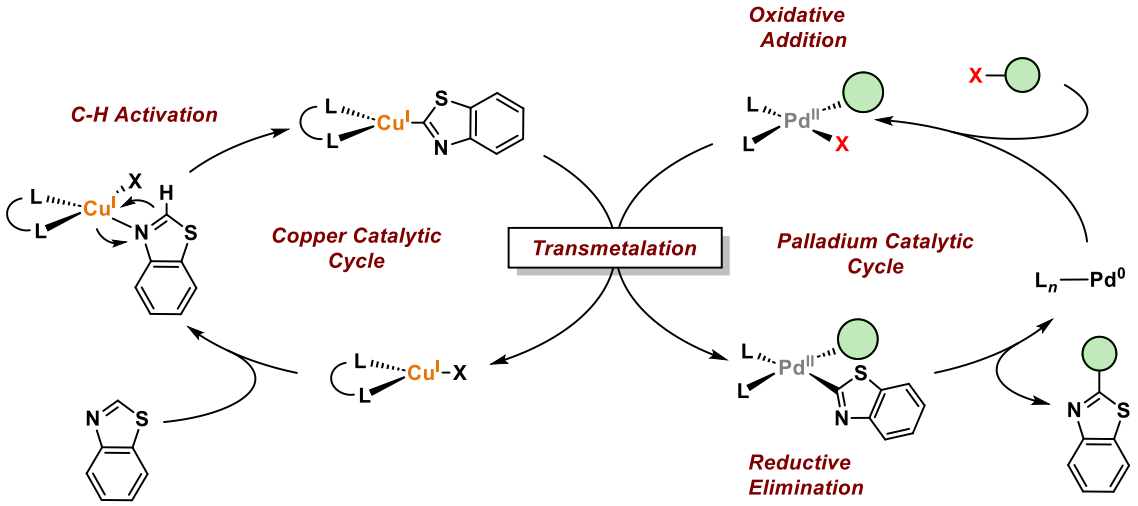

Scheme 2. Proposed Mechanism for the Direct C–H Arylation. Green circle represents generic aryls.

Nowadays, the synthesis of polyfluorinated asymmetric biaryls is one of the synthetic challenges to be solved. Many transition metals complexes can generate C–C couplings from conventional aryls, or even when one of the aryls is a fluorinated aryl, but it is much less easy when it comes to two fluorinated aryls (Ar^F). Fluorinated biaryls have interest in different areas, such as materials science,[31,32] and pharmaceuticals building blocks.[33] The synthesis of high fluorinated biaryls is well known to be challenging. Traditionally, these couplings have been achieved using transition metals such as palladium or nickel. The challenge in the synthesis of fluorinated biaryls is that the reductive elimination from the Pd complex of two highly fluorinated residues, involved the use of high temperatures, special ligands and additives.[34] In addition, the use of these high temperatures leads to the appearance of some by-products (homocoupling and hydrolysis) due to undesired side reactions, such as transmetalation between two palladium complexes,[35] or the

[31] Maiti, B.; Wang, K.; Bhandari, S.; Bunge, S. D.; Twieg, R. J.; Dunietz, B. D. Enhancing Charge Mobilities in Selectively Fluorinated Oligophenyl Organic Semiconductors: A Design Approach Based on Experimental and Computational Perspectives. *J. Mater. Chem. C.* **2019**, *7*, 3881-3889. DOI: 10.1039/c8tc06517a.

[32] Sakamoto, Y.; Suzuki, T.; Miura, A.; Fujikawa, H.; Tokito, S.; Taga, Y. Organofluorine Chemistry: Principle and Commercial Applications. *Top. Curr. Chem.* **1996**, *273*, 1832–1833. DOI: 10.1021/ja994083z.

[33] Inoue, M.; Sumii, Y.; Shibata, N. Contribution of Organofluorine Compounds to Pharmaceuticals. *ACS Omega.* **2020**, *5*, 10633–10640. DOI: 10.1021/ACSOMEGA.0C00830.

[34] Gioria, E.; del Pozo, J.; Martínez-Ilarduya, J. M.; Espinet, P. Promoting Difficult Carbon–Carbon Couplings: Which Ligand Does Best? *Angew. Chem. Int. Ed.*- **2016**, *55*, 13276–13280. DOI: 10.1002/ANIE.201607089.

[35] Marcos-Ayuso, G.; Lledós, A.; Casares, J. A. Copper(I) Activation of C–X Bonds: Bimolecular vs. Unimolecular Reaction Mechanism. *Chem. Commun.* **2022**, *58*, 2718–2721. DOI: 10.1039/d1cc07027d.

reaction with the solvent residual water.[36] For this reason, there are not many examples involving two polyfluoroaryls.

One of the first examples of cross-coupling involving at least one fluorinated aryl was published by Cazin and co-workers in 2014, represented in Scheme 3. They reported a dual system involving [Cu(Cl)(SIPr)] and [Pd(Cl)(cinnamyl)(I^{t}Bu)] that has been employed to very effective perform the direct arylation of C–H bonds using CsOH as base.[37] The mechanistic studies indicate that the CuOH species performs an activation involving acid–base reactions, which then transmetalates to Pd to undergo an aryl or heteroaryl fragment. This methodology is efficient for a broad range of aryl, benzyl and alkenyl bromides and chlorides reacting with high fluorinated aromatic and heteroaromatic substrates. The drawback of this reaction is the absence of cross-coupling products when both reactants are high fluorinated moieties, that leaves out of scope a wide variety of interesting products.

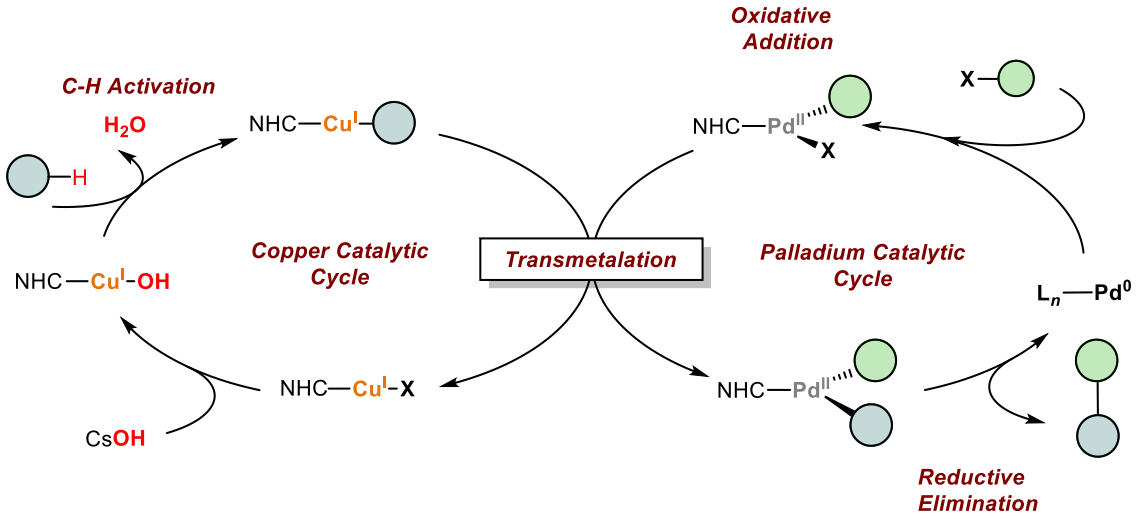

Scheme 3. Proposed mechanism for the direct diarylation using a Pd/Cu system (reference 37).

The challenge of the cross-coupling of high fluorinated aryls was approached by Huber et al., in 2017.[38] In this work, polyfluorinated biphenyls are synthesized by the Suzuki-Miyaura reaction, using high fluorinated boronic acids and high

[36] Del Pozo, J.; Salas, G.; Álvarez, R.; Casares, J. A.; Espinet, P. The Negishi Catalysis: Full Study of the Complications in the Transmetalation Step and Consequences for the Coupling Products. *Organometallics* **2016**, *35*, 3604–3611. DOI: 10.1021/acs.organomet.6b00660.

[37] Lesieur, M.; Lazreg, F.; Cazin, C. S. J. A Cooperative Pd-Cu System for Direct C–H Bond Arylation. *Chem. Commun.* **2014**, *50*, 8927-8929. DOI: 10.1039/c4cc03201b.

[38] Bulfield, D.; Huber, S. M. Synthesis of Polyflourinated Biphenyls; Pushing the Boundaries of Suzuki-Miyaura Cross Coupling with Electron-Poor Substrates. *J. Org. Chem.* **2017**, *82*, 13188–13203. DOI: 10.1021/ACS.JOC.7B02267.

fluorinated aryl halides. To carry out the reaction, high temperatures (95 °C) and long reaction times (60 h) are necessary. In addition, when both aryls are very fluorinated, especially in ortho positions, the yields decrease dramatically. This is because the reductive elimination step of the complex $[Pd(Ar^F)(Ar^{F'})(PPh_3)_2]$ has a high energetic barrier, which blocks the reaction. The triphenylphosphine ligand is not able to give enough electron density to the metal center to give efficient the reductive elimination step when the two aryls are highly fluorinated.[34]

In contrast with that, Marder et al. published in 2020, the homocoupling of high fluorinated aryls using an oxidative coupling.[39] In this case, the transformation takes place under milder conditions (75 °C, 5h) and they obtain high fluorinated biaryls in good yields but stoichiometric amounts of Ag_2O are needed.

More recently, our research group reported the cross-couplings of polifluoroaryls using the Negishi cross-coupling reaction.[17] The synthesis of biaryls, including highly fluorinated species, is made easily accessible to Ni- or Pd-catalysed Negishi cross-coupling using the chelating ligand PhPEWO-F, as we can see in Equation 2. This ligand facilitates fast and selective coupling even for highly fluorinated aryls.[34]

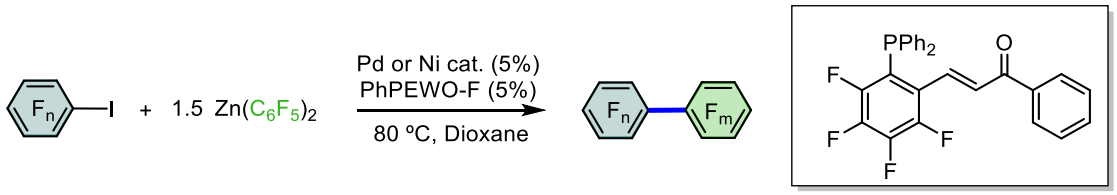

Equation 2. Synthesis of biaryls by Ni or Pd catalysed Negishi cross-coupling using PEWO-F ligand.

The drawbacks of this work are found in the formation of different by-products, very common in the Negishi reaction due to de retro-transmetalation step or decomposition of the substrates, such as homocoupling and hydrolysis of the aromatic rings.[36] In addition, an over-stoichiometric amount of $Zn(C_6F_5)_2$ is necessary for the reaction to have a high conversion due to the low nucleophilicity of this reagent. This type of zinc compounds are extremely expensive, and only C_6F_5 moiety was employed.

[39] Budiman, Y. P.; Jayaraman, A.; Friedrich, A.; Kerner, F.; Radius, U.; Marder, T. B. Palladium-Catalyzed Homocoupling of Highly Fluorinated Arylboronates: Studies of the Influence of Strongly vs Weakly Coordinating Solvents on the Reductive Elimination Process. *J. Am. Chem. Soc.* **2020**, *142*, 6036–6050. DOI: 10.1021/JACS.9B11871.

Due to all these disadvantages, we decided to face the challenge of synthesizing highly fluorinated biaryls using a bimetallic system. As we have already mentioned, the synergy that exists between Pd and Cu is extraordinary. If we review the strengths of each catalyst, we consider using a copper catalyst, whose function was to give C–H activation of fluorinated arenes. While the Pd, would be responsible for carrying out the oxidative addition and reductive elimination steps, represented in Scheme 4.

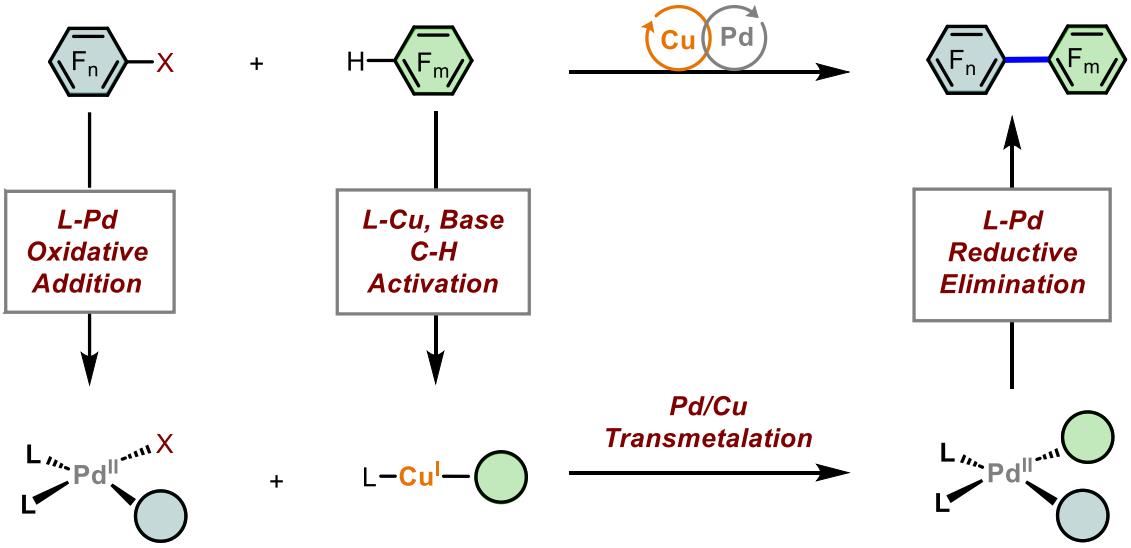

Scheme 4. Mechanistic proposal for the formation of high fluorinated aryls using Pd/Cu bimetallic system.

1.2 Results and discussion

Optimization Conditions

In order to meet the challenge of designing an effective bimetallic catalysis for the formation of fluorinated biaryls, we started our study by looking at the extent to which Cu complexes can play a role in the C–H activation of acidic protons in this type of system.[40,41,42,43,44] As mentioned in the introduction, [CuX(NHC)] complexes are widely used in catalytic reactions as generators of Cu–C or Cu–N bonds by C–H activation.[45,46,47,48] For this reason, we use the complex [Cu(O^{t}Bu)(IMes)] (IMes = 1,3-Bis(2,4,6-trimethylphenyl)-1,3-dihydro-2H-imidazol-2-ylidene) as organometallic complex, which we will react with different fluorinated arenes, observing the differences between the reaction rates. For this examination we choose different arenes, with different electronic properties and number of fluorine atoms.

Our first approximation was that the complex [Cu(O^{t}Bu)(IMes)] cannot activate arenes with 2 or 3 fluorine atoms.[39,40] This behavior can be explained by the proton acidity of the arene. Protons with a pK_a higher than 29 (calculated in DMSO),[49,50]

---

[40] Fortman, G. C.; Slawin, A. M. Z.; Nolan, S. P. A Versatile Cuprous Synthon: [Cu(IPr)(OH)] (IPr = 1,3 Bis(Diisopropylphenyl)Imidazol-2-Ylidene). *Organometallics* **2010**, *29*, 3966–3972. DOI: 10.1021/om100733n.

[41] Aneeja, T.; Neetha, M.; Afsina, C. M. A.; Anilkumar, G. Progress and Prospects in Copper-Catalyzed C–H Functionalization. *RSC Adv.* **2020**, *10*, 34429-34458. DOI: 10.1039/d0ra06518h.

[42] Eisenstein, O.; Milani, J.; Perutz, R. N. Selectivity of C–H Activation and Competition between C–H and C–F Bond Activation at Fluorocarbons. *Chem. Rev.* **2017**, *117*, 8710–8753. DOI: 10.1021/acs.chemrev.7b00163.

[43] Do, H.-Q.; Khan, R. M. K.; Daugulis, O. A General Method for Copper-Catalyzed Arylation of Arene C–H Bonds. *J. Am. Chem. Soc*. **2008**, *130*, 15185–15192 DOI: 10.1021/ja805688p.

[44] Molteni, R.; Edkins, K.; Haehnel, M.; Steffen, A. C-H Activation of Fluoroarenes: Synthesis, Structure, and Luminescence Properties of Copper(I) and Gold(I) Complexes Bearing 2-Phenylpyridine Ligands. *Organometallics* **2016**, *35*, 629–640. DOI: 10.1021/acs.organomet.5b00904.

[45] Gaillard, S.; Cazin, C. S. J.; Nolan, S. P. N-Heterocyclic Carbene Gold(I) and Copper(I) Complexes in C–H Bond Activation. *Acc. Chem. Res*. **2012**, *45*, 778–787. DOI: 10.1021/ar200188f.

[46] Xie, W.; Yoon, J. H.; Chang, S. (NHC)Cu-Catalyzed Mild C–H Amidation of (Hetero)Arenes with Deprotectable Carbamates: Scope and Mechanistic Studies. *J. Am. Chem. Soc.* **2016**, *138*, 12605–12614. DOI: 10.1021/jacs.6b07486.

[47] Xie, W.; Chang, S. [Cu(NHC)]-Catalyzed C–H Allylation and Alkenylation of Both Electron-Deficient and Electron-Rich (Hetero)Arenes with Allyl Halides. *Angew. Chem. Int. Ed.* **2016**, *128*, 1908–1912. DOI: 10.1002/ange.201510180.

[48] Wendlandt, A. E.; Suess, A. M.; Stahl, S. S. Copper-Catalyzed Aerobic Oxidative C-H Functionalizations: Trends and Mechanistic Insights. *Angew. Chem. Int. Ed* **2011**, *50*, 11062–11087. DOI: 10.1002/anie.201103945.

[49] Shen, K.; Fu, Y.; Li, J. N.; Liu, L.; Guo, Q. X. What Are the PKa Values of C-H Bonds in Aromatic Heterocyclic Compounds in DMSO? *Tetrahedron.* **2007**, *63*, 1568–1576. DOI: 10.1016/j.tet.2006.12.032.

[50] Salamanca, V.; Albéniz, A. C. Deuterium Exchange between Arenes and Deuterated Solvents in the Absence of a Transition Metal: Synthesis of D-Labeled Fluoroarenes. *Eur. J. Org. Chem.* **2020**, *22*, 3206–3212. DOI: 10.1002/EJOC.202000284.

cannot be activated by this type of complexes, as we can see in Figure 1. Therefore, only tetrafluorobenzenes and pentafluoroarenes can be used. [51]

As we observed in Figure 1, the reaction can be monitored by ^{19}F NMR. The experimental results confirm the expected trend of acidity, but there are no significate-differences in the rate constants in each of the reactions.

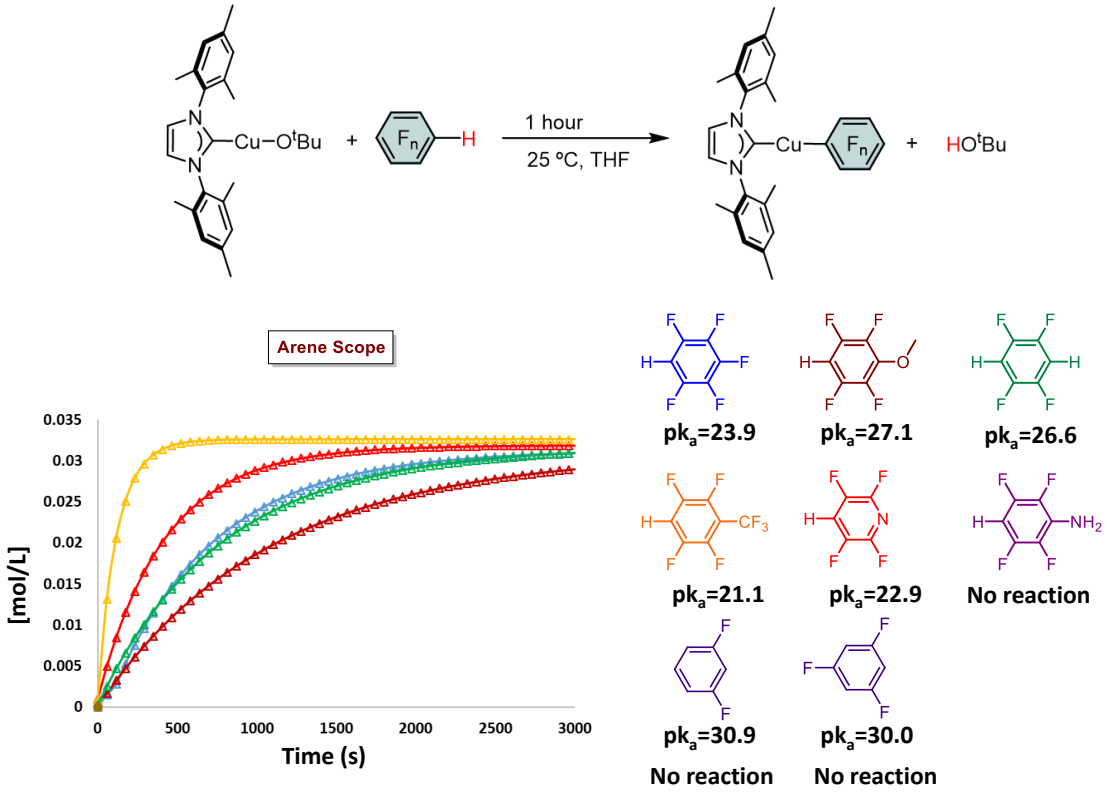

Figure 1. Reaction between [Cu(O^{t}Bu)(IMes)] and high fluorinated arenes. Concentration/time plots (dots) and best least-squares fitting (continuous lines) for the C–H activation (0.5 mL DMF) from [Cu(OtBu)(IMes)] = 0.035 mol L^{-1} + [Arene^F] = 0.35 mol L^{-1} (1:10) at 298 K, monitored by ^{19}F NMR.

The kinetic analysis using copasi software estimates an energy barrier between $\Delta G^{\ddagger} \approx$ 22-20 kcal mol^{-1}, which leads us to believe that this step will be carried out efficiently within the Pd/Cu catalytic cycle but does not allow for a wide variety of substrates. Moreover, tetrafluoroaniline also does not give C–H activation, probably due to the coordination of the nitrogen atom to the metal center.

This correlation is in agreement with the hypothesis that the rate of C–H activation of arenes depends on the acidity of the proton to be activated, and the

[51] Wang, M.; Fan, T.; Lin, Z. DFT Studies on Copper-Catalyzed Arylation of Aromatic C–H Bonds. *Organometallics.* **2012**, *31*, 560–569. DOI: 10.1021/om2007612.

relative dissociation energies of the C–Cu and C–H bonds.[52] This behavior will be commented in Chapter IV.

We embarked on our studies by examining a model reaction of 1-Br-2,6-$C_6H_3F_2$ (**1a**) as fluorinated aryl and C_6F_5H (**2n**) as precursor of Cu–C_6F_5. First of all, we essayed a system similar to the one used by Lesieur et al. formed by [Pd(allyl)Cl(IPr)] and [CuCl(IPr)] as catalyst due to the good results that they observed.[37] However, no cross-coupling of biaryl product was formed and only C_6F_5–allyl and undetermined Pd–C_6F_5 species was detected. This result was consistent with the previous observations about the reductive elimination of high fluorinated aryls. The Pd^{II} complexes of the type [Pd(Ar^F)($Ar^{F'}$)(NHC)] cannot undergo reductive elimination with carbene ligand.[34] This result suggests that the C–H activation of C_6F_5H and the Cu-to-Pd transmetalation steps are working but the ligand on Pd probably is not efficient enough to undergo reductive elimination of Ar^F–$Ar^{F'}$ and regenerate the palladium cycle.

With this first result, we focus on a systematic work testing different ligands in the Pd center. These ligands must be able to promote difficult reductive elimination processes.[34] Therefore, we began by testing Buchwald Phosphine Ligands, and alkyl phosphines that can undergo an efficient reductive elimination of high fluorinated aryls.[34] As shown in Figure 2, the coupling results are quite different. The ligands with the best results turned out to be Buchwald-type phosphines, as we can see for (2-Dicyclohexylphosphino-2′,4′,6′-triisopropyl-1,1′-biphenyl)[2-(2′-amino-1,1′-biphenyl)] palladium(II) methanesulfonate (XPhos-Pd-G3). However, ligands such as P^{t}Bu$_3$, did not prove to be very effective in generating the cross-coupling product.

[52] Lu, Q.; Yuz, H.; Fu, Y. Linear Correlation between the C–H Activation Barrier and the C–Cu/C–H Bond Dissociation Energy Gap in Cu-Promoted C–H Activation of Heteroarenes. *Chem. Commun.* **2013**, *49*, 10847–10852. DOI: 10.1039/c3cc46069j.

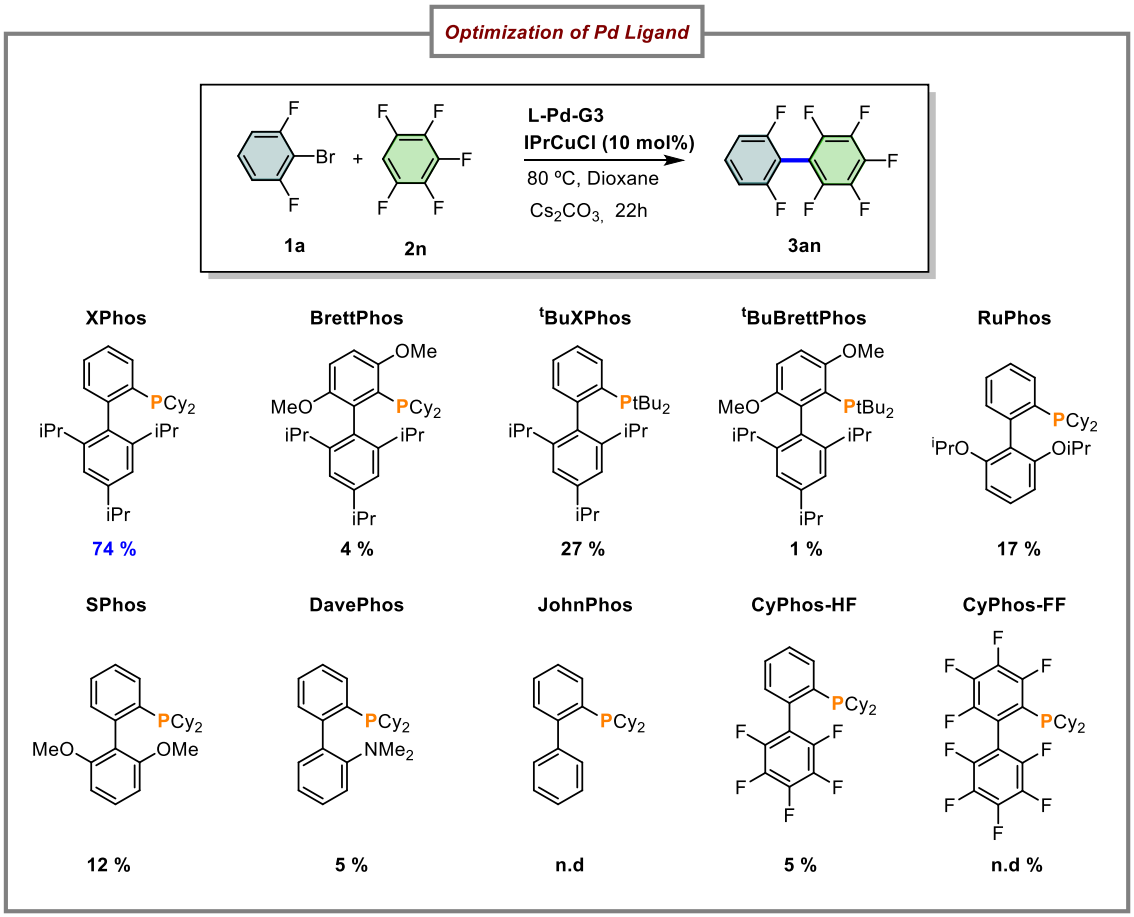

Figure 2. Different L-Pd-G3 complexes as well as [Pd(allyl)Cl(IPr)] were tested as precatalyst. Standard conditions: **1a** (0.16 mmol), **2n** (0.16 mmol), L-Pd-G3 (5 %), [CuCl(IPr)] (10 %), Cs_2CO_3 (0.16 mmol), dioxane (2 mL), 80 °C, 22 h. a Yield determined by ^{19}F NMR.

The use of the bulkier, electron-rich ^{t}BuXPhos and P^{t}Bu$_3$, which are excellent promoters of C_6F_5–C_6F_5 coupling,[26] afforded the product in 27 and 10 % yield respectively, probably because the transmetalation step becomes more difficult as both the ligand in Pd and in Cu are very bulky. In contrast with these frustrating results, the precatalysts XPhos-Pd-G3 (5%) and [CuCl(IPr)] (10%) combined with Cs_2CO_3 as base, at 80 °C, gave the best yield (74%).

Along with the desired cross-coupling product **3an**, very small amounts of the hydrolysis product 1,3-difluorobenzene (**4a**, 4%) and the homocoupling biaryls of both aryls (**3aa**, 4% and **3nn**, 3%) were identified by ^{19}F NMR or GS/Ms spectrometry.

Once we had a reaction that generated a good performance in the C–C cross coupling, we focused on trying to optimize the conditions to improve this reaction.

To do this, we continued with the optimization of the ligand for the other catalyst. It is well known that copper organometallic complexes with carbene ligands are good promoters of C–H activations of acidic protons in the presence of base.[53] For that, we decided to explore the field of copper carbenes (Figure 3). Surprisingly, the less bulky ligands turned out to be the worst for this type of reaction, possibly because they had some difficulty in giving the C–H activation reaction. The results of testing several carbene ligands for the copper catalyst in no case exceeded 10% of coupling, except in the case of the IPr (1,3-Bis-(2,6-diisopropylphenyl)-imidazolinium) ligand.

One of the advantages of this system is that no ligand exchange is observed between the Pd and Cu complexes, although it is a relatively common reaction.[54] This behavior is quite common, especially when [Cu(NHC)] complexes are used. This ligand exchange reaction usually occurs when one of the two complexes has labile ligands ($AsPh_3$,THF, tht…) and the carbene ligand is small,[55] and this generates an equilibrium between the two species, giving rise to ligand-exchanged intermediates. In our case, as there is a very bulky and relatively donor complex such as a Buchwald-type phosphine in the Pd complex, and rather bulky NHC-type ligands in the Cu complex, no ligand exchange is observed at any time.

[53] Lazreg, F.; Nahra, F.; Cazin, C. S. J. Copper-NHC Complexes in Catalysis. *Coord. Chem. Rev*. **2015**, 48–79. DOI: 10.1016/j.ccr.2014.12.019.

[54] Toledo, A.; Salamanca, V.; Pérez-Moro, T.; Albéniz, A. C. Transmetalation of Acyclic Tungsten Carbenes to Coinage Metals: Distinct Behavior of Silver toward Carbene Transfer and Hydrolysis. *Organometallics* **2021**, *40*, 38–47. DOI: 10.1021/acs.organomet.0c00675.

[55] del Pozo, J.; Casares, J. A.; Espinet, P. The Decisive Role of Ligand Metathesis in Au/Pd Bimetallic Catalysis. *Chem. Commun.* **2013**, *49*, 7246–7248. DOI: 10.1039/c3cc43133a.

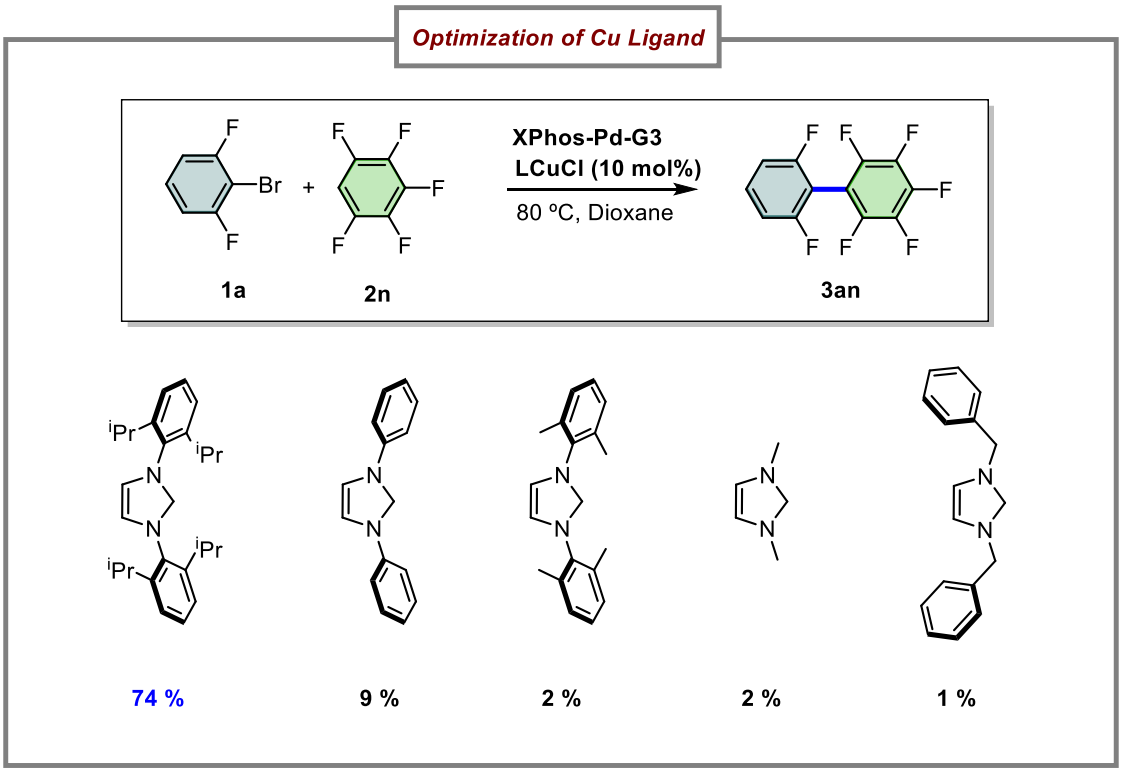

Figure 3. Standard conditions: **1a** (0.16 mmol), **2n** (0.16 mmol), XPhos-Pd-G3 (5 %), [CuCl(L)] (10 %), Cs_2CO_3 (0.16 mmol), dioxane (2 mL), 80 °C, 22 h. Yield determined by ^{19}F NMR.

Aiming to improve the catalytic results, different solvents were tested. The use of toluene diminished the reaction yield, while employing a coordinating solvent such as acetonitrile did not afford the coupling product. The explanation is the low solubility of the base in these solvents. For instance, THF and 1,4-Dioxane were the best options for this reaction, as we can see in Table 1.

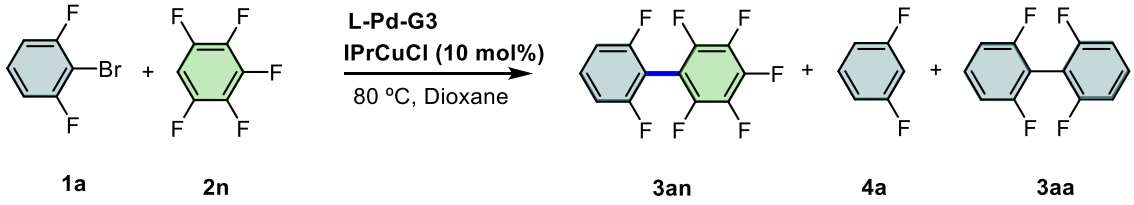

Entry	Conditions	3an (%)	4a/3aa (%)
1	1,4-dioxane	74	4/4
2	THF	64	8/-
3	Toluene	18	3/2
4	Acetonitrile	<1	6/-

Table 1. Standard conditions: **1a** (0.16 mmol), **2n** (0.16 mmol), XPhos-Pd-G3 (5%), [CuCl(IPr)] (10%), Cs_2CO_3 (0.16 mmol) solvent (2 mL), 80 °C, 22h.

Different mechanisms are well known for C–H activation with copper complexes.[51,56] When coordinating bases are used, concerted transition state for the deprotonation–metalation are obtained in DFT calculations.[57] Furthermore, in the case of non-coordinating bases (these differences are commented in Chapter IV), the base assist the deprotonation transition state with no interactions with the metal center.[56] Coordinating bases are efficient in this catalytic step, generating a reactive specie (Cu–OR) that react with the C–H bond in a non-redox process. For that reason, we tested different bases, as summarized in Table 2.

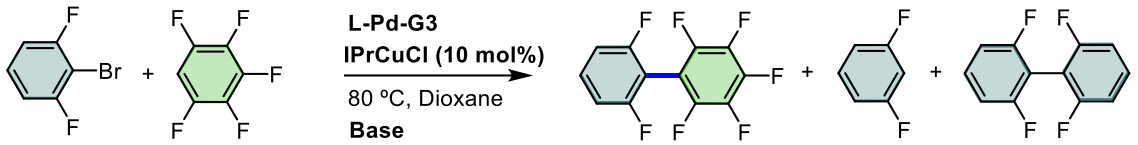

1a **2n** **3an** **4a** **3aa**

Entry	**Conditions**	**3an** (%)[a]	**4a/3aa** (%)[a]
1	Cs_2CO_3	74	4/4
2	CsOH	55	4/5
3	K_2CO_3	3	4/2
4	Na_2CO_3	<1	-/-
5	NaO^{t}Bu	17	4/2
6	K_3PO_4	3	3/2

Table 2. Standard conditions: **1a** (0.16 mmol), **2n** (0.16 mmol), XPhos-Pd-G3 (5 %), [CuCl(IPr)] (10 %), *base* (0.16 mmol), dioxane (2 mL), 80 °C, 22 h. [a] Yield determined by ^{19}F NMR.

CsOH gave the product in a moderate yield (entry 2), while the use of other carbonate salts did not afford the product, probably due to their lower solubility (entries 3,4). Employing NaO^{t}Bu yielded 17% of the product, moreover, activation of the para-C–F bond of the C_6F_5 moiety was observed (entry 5). These results are in agreement with the solubility of the base. Bases like Na_2CO_3 are not soluble in the reaction media, stopping the reaction.

[56] Yuan, R.; Lin, Z. Mechanism for the Carboxylative Coupling Reaction of a Terminal Alkyne, CO_2, and an Allylic Chloride Catalyzed by the Cu(I) Complex: A DFT Study. *ACS Catal.* **2014**, *4*, 4466–4473. DOI: 10.1021/cs5011184.
[57] Xie, W.; Heo, J.; Kim, D.; Chang, S. Copper-Catalyzed Direct C–H Alkylation of Polyfluoroarenes by Using Hydrocarbons as an Alkylating Source. *J. Am. Chem. Soc.* **2020**, *142*, 7487–7496. DOI: 10.1021/jacs.0c00169.

Another interesting point was the evaluation of the temperature. For this type of reaction, to increase the temperature can improve the result of the catalysis. In contrast with this hypothesis, we observe that 80 °C was the optimal temperature, and that to increase it in 10 or 20 degrees give lowers yields and more by-products.

Finally, we tested the influence of the concentration of the reagents and the catalysts. As we can see in Table 3, the optimal concentration was 0.32 M in aryl bromide, generating the cross-coupling product (**3an**) in high yield, and also minimizing the generation of the hydrolysis product $C_6F_2H_4$ (**4a**) and the homocoupling product (**3aa**). This agrees with the importance of the solubility of the catalysts and the base.

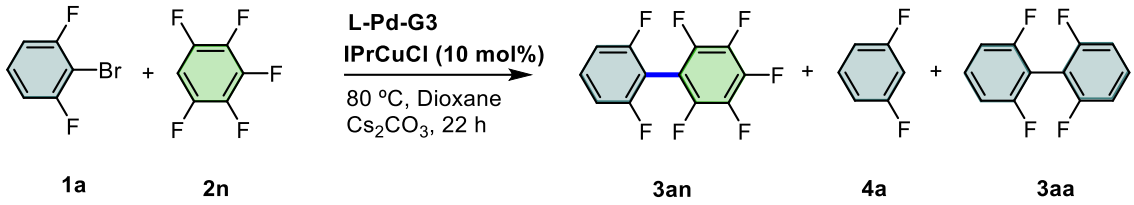

Entry	**[Ar-Br]** (mol L^{-1})	**3an** (%)[a]	**4a/3aa** (%)[a]
1	0.04	46	16/-
2	0.04[b]	6	1/2
3	0.08	74	4/4
4	**0.32**	**80**	**2/3**
5	0.32[c]	20	1/2

Table 3. Standard conditions: **1a** (0.16 mmol), **2n** (0.16 mmol), XPhos-Pd-G3 (5 %), [CuCl(IPr)] (10 %), Cs_2CO_3 (0.16 mmol), dioxane (*V*), 80 °C, 22 h. [a] Yield determined by ^{19}F NMR. [b] [CuCl(IPr)] (5 %). [c] XPhos-Pd-G3 (2.5 %), [CuCl(IPr)] (5 %).

Reducing the amount of copper precatalyst reduced the product yield at the same time (entry 2). Increasing the concentration of the aryl bromide in the system slightly increased the yield, obtaining the product in 80 % yield (Table 3, entry 4). At this concentration, reducing the amount of catalysts to a half led to a much lower yield (Table 3, entry 5) due to it is a bimolecular reaction. Finally, when the reaction was carried out in the absence of one or both precatalyst, only the hydrolysis

product of the aryl bromide (**4a,** $C_6F_2H_4$) or homocoupling product of the arene (**3aa,** C_6F_5–C_6F_5) was detected, as we can see in Table 4.

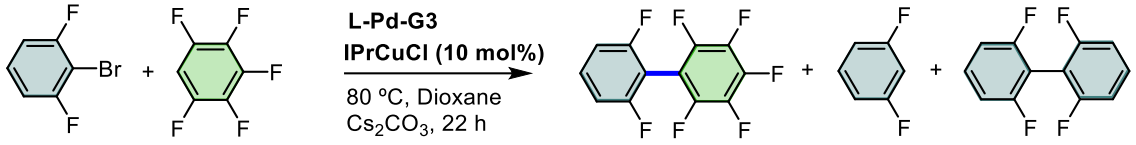

1a **2n** **3an** **4a** **3aa**

Entry	**Conditions**	**3an** (%)[a]	**4a/3aa** (%)[a]
1	Standard	74	4/4
2	No Cu	2	3/3
3	No Pd	<1	-/-
4	No Cu, no Pd	<1	-/-

Table 4. Standard conditions: **1a** (0.16 mmol), **2n** (0.16 mmol), XPhos-Pd-G3 (5 %), [CuCl(IPr)] (10 %), Cs_2CO_3 (0.16 mmol), dioxane (2 mL), 80 °C, 22 h. [a] Yield determined by ^{19}F NMR. [b] [CuCl(IPr)] (5 %). [c] XPhos-Pd-G3 (2.5 %), [CuCl(IPr)] (5 %).

With the optimized conditions in hand, the scope of fluorinated aryls was next explored in a reaction with C_6F_5–H (**2n**) as a representative arene, as we can see in Figure 4.

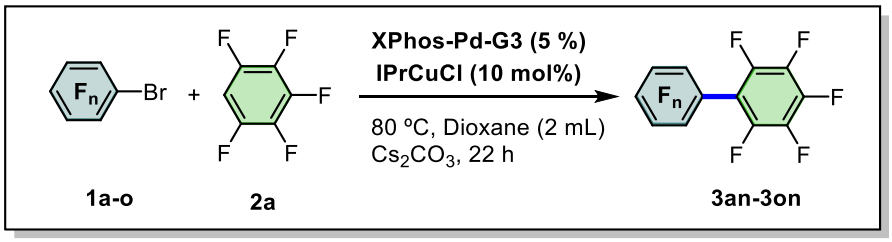

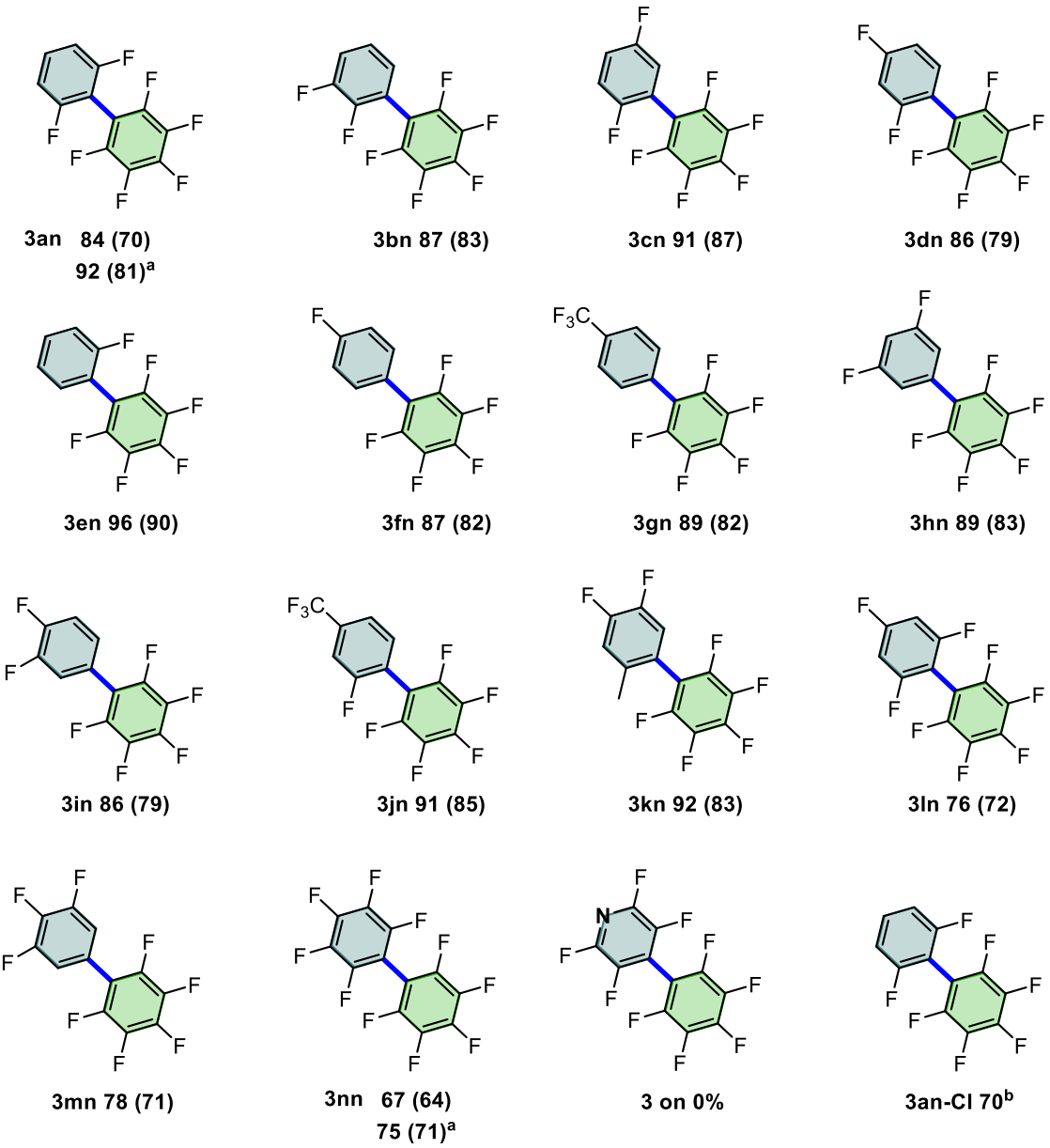

Figure 4. Standard conditions: **1** (0.16 mmol), **2n** (0.16 mmol), XPhos-Pd-G3 (5 %), [CuCl(IPr)] (10 %), Cs_2CO_3 (0.16 mmol), dioxane (2 mL), 80 °C, 22 h. Fluoroaryl bromide scope. Yield determined by ^{19}F NMR (Isolated yield in parenthesis). [a] 1.5 equiv. of C_6F_5H (**2n**). [b] The reaction was carried out with the aryl chloride. The X-ray structures of **3bn**, **3fn** and **3gn** are given in the experimental section.

Firstly, a wide variety of fluorinated aryl bromides, with different substitution patterns, were tested (Figure 4). The coupling products were obtained in high yields

(up to 90 %), with the higher yields for the less fluorinated aryl bromides. The fluoridation degree of the aromatic ring, especially in ortho positions, influences drastically within the Pd catalytic cycle. This is probably because if the number of fluorine atoms is higher, the oxidative addition step is easier, and in contrast, the reductive elimination is slower, so this must be a kinetic effect and reflect build-up of negative charge on the substrate during the transition state.[34] For this reason, couplings involving moieties where the aryl bromide has more fluoride atoms, especially in ortho positions, always have a lower yield if the reductive eliminations energetic barrier is higher than the oxidative addition one. Interestingly, homocoupling (Ar–Ar) and hydrolysis products (Ar–H and Ar'–H) were detected in all cases in very low yield (<4%). These results demonstrate that the retro-transmetalation process is not very effective in this Pd/Cu catalytic cycle, improving the previous results obtained with the Negishi coupling. [17]

Alkyl or fluoroalkyl substituents at the bromo aryl ring, such as Me (**3kn**) and CF_3 (**3gn** and **3jn**), are compatible with this synthetic protocol. In contrast, the presence of tetrafluoro-pyridine blocks the reaction, and no cross-coupling product is observed (**3on**). This quenching is probably due to coordination of the nitrogen to some intermediate. Furthermore, when 1-X-2,6-$C_6F_2H_3$ (X = Cl, Br, I) was used as a reactant with the optimised conditions, 70% of cross-coupling product was obtained in the case of the aryl chloride, showed in Table 5. This opens the door to use aryl chlorides for this synthetic protocols.

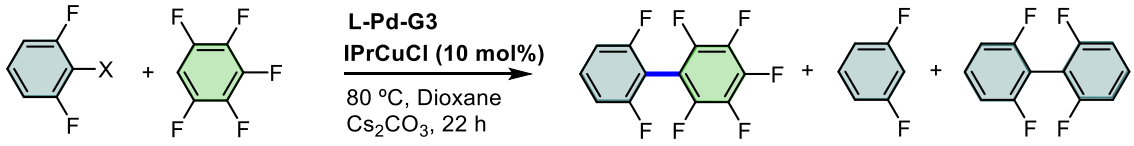

1a **2n** **3an** **4a** **3aa**

Entry	Aryl halide	**3an** (%)[a]	**4a/3aa** (%)[a]
1	Aryl bromide	74	4/4
2	Aryl chloride	70	5/1
3	Aryl iodide	38	4/2

Table 5. Standard conditions: **1a** (0.16 mmol), **2n-X** (0.16 mmol), XPhos-Pd-G3 (5 %), [CuCl(IPr)] (10 %), Cs_2CO_3 (0.16 mmol), dioxane (2 mL), 80 °C, 22 h. [a] Yield determined by ^{19}F NMR.

Surprisingly, when aryl iodide is used, the yield decreases drastically. The explanation for this behavior is that aryl iodides can give easier oxidative addition than bromides or chlorides, due to the varying strength of the C–X bond. This implies that the aryl iodide can give the oxidative addition step to the copper complex as well and blocking part of the reaction.[35]

After surveying the scope of aryl bromides, the availability of fluoroarene substrates was further investigated in reactions with 2,6-$C_6F_2H_3$-Br (**1a**) and 3,4,5-$C_6F_3H_2$-Br (**1m**) as a representative coupling partner, represented in Figure 5. As previously reported, the formation of [Cu(Ar^F)(IPr)] precursors in the presence of base is efficient for the tetrafluorinated reagents.

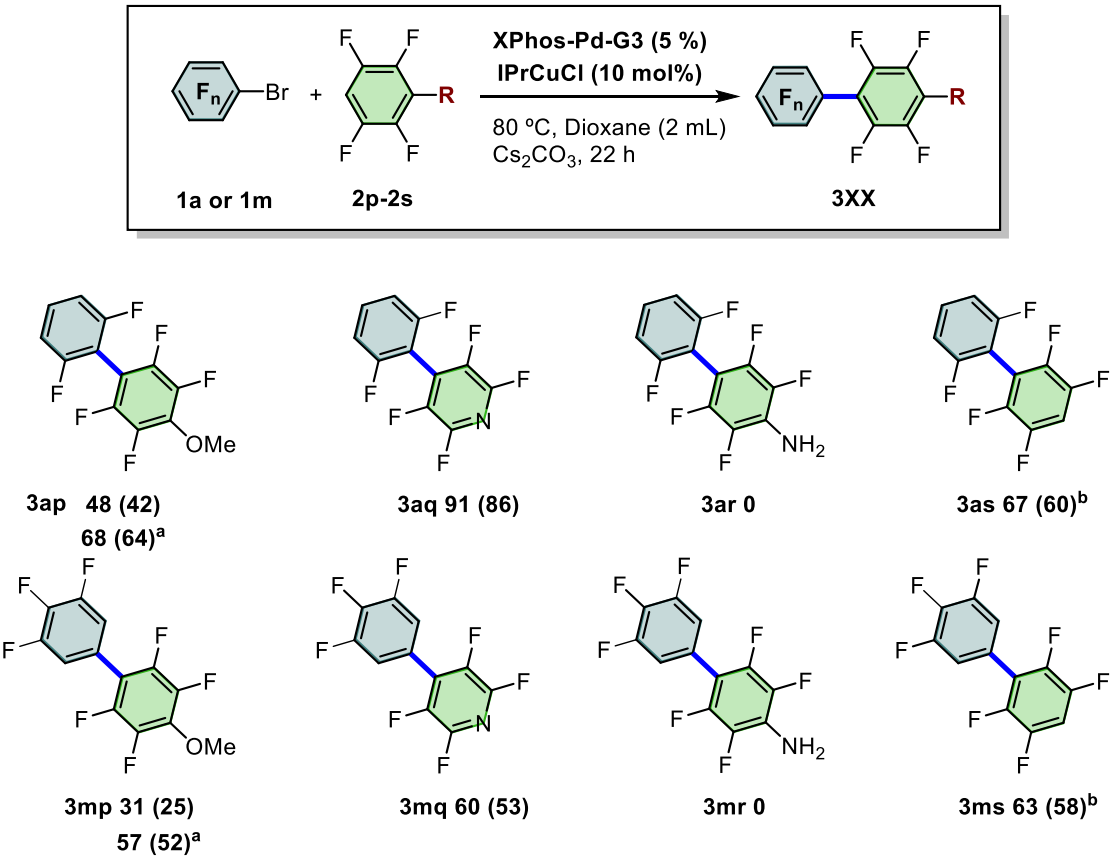

Figure 5. Standard conditions: **1** (0.16 mmol), **2** (0.16 mmol), XPhos-Pd-G3 (5 %), [CuCl(IPr)] (10 %), Cs_2CO_3 (0.16 mmol), dioxane (2 mL), 80 °C, 22 h. Fluoroarenes scope. Yield determined by ^{19}F NMR (Isolated yield in parenthesis). [a] 1.5 equiv. of **2p** were used instead of 1 equiv. [b] 3.0 equiv. of **2s** were used instead of 1 equiv.

As we can observe in Figure 5, good yields were obtained for all the subtracted instead of the aniline. This result shows that the biphenyl yield is very sensitive to

the coordinative capability of the substituents, supporting the idea of the coordination of the reactant quenches the reaction. In contrast, 2,3,5,6-tetrafluoropyridine gives high yields of **3aq** or **3mq** because of the well-known that the donor ability of the N electron pair of this tetrafluoropiridine is practically zero; in the middle, OMe leads to lower yields due to a weaker OMe coordination ability compared to NH_2.

As expected, the reaction with 1,2,4,5-tetrafluorobenzene, with two C–H bonds, gave the competition of the mono and diarylated products. Using an excess of the arene **2s** (3 equivalents) we can diminish the diarylated product, obtained a 67% of yield in the monoarylated product. Besides, full conversion of the aryl bromide was observed.

Mechanistic Studies.

To obtain mechanistic insight into the present cross-coupling reactions, a number of experimental studies were carried out. First of all, the C–H activation of C_6F_5–H by the complex [CuCl(IPr)] with Cs_2CO_3 was tested, as we can see in Equation 3. The obtained result is the complex [Cu(C_6F_5)(IPr)] (**5**) in high yield (>99%).

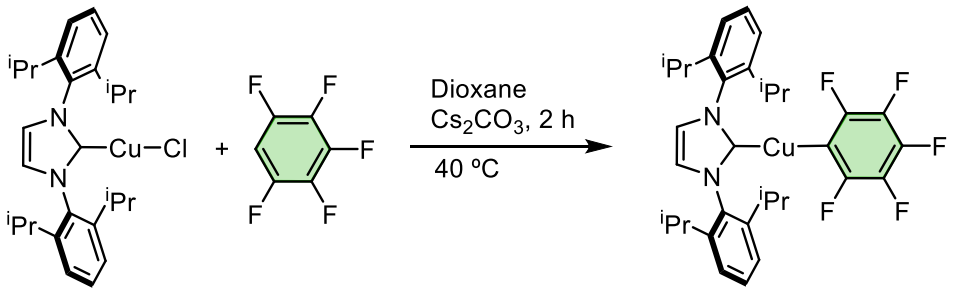

Equation 3. Stoichiometry reaction for the C–H activation of fluoroarenes.

The reductive eliminaton reaction of the complex [Pd(C_6F_5)$_2$(XPhos)] was also tested. To do this, the complex was synthesized using the *cis*-[Pd(C_6F_5)$_2$(THF)$_2$] precursor with Xphos phosphine (1 equivalent). This reaction afforded the complex [Pd(C_6F_5)$_2$(XPhos)] (**7**) in good yield, and allows us to obtained a X-ray diffraction, as shown in Figure 6.

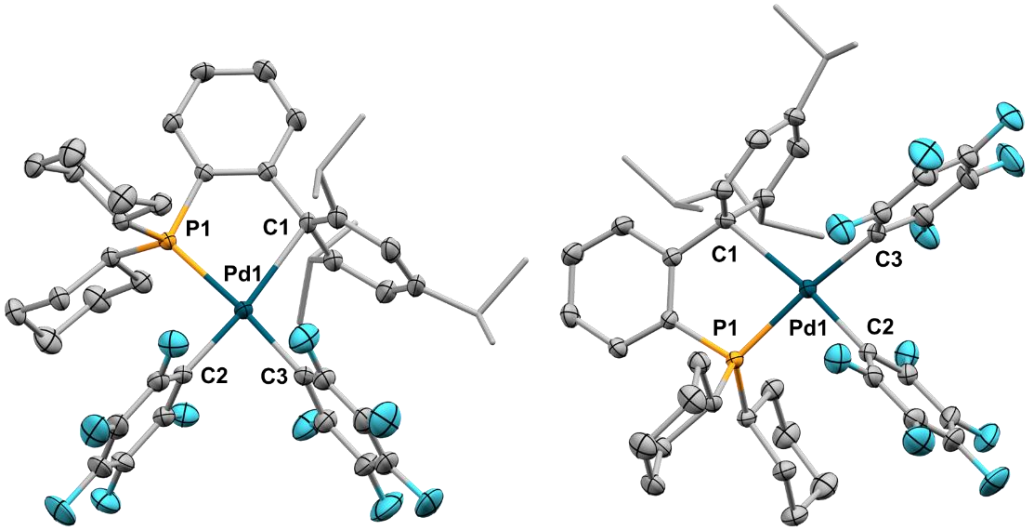

Figure 6. X-ray structure of *cis*-[Pd(C_6F_5)$_2$(XPhos)] (**7**). H atoms omitted for clarity. Selected bond distances (Å) and angles (°): Pd1–P1 = 2.328, Pd1–C1 = 2.478, Pd1–C2 = 2.013, Pd1–C3 = 2.080. P1–Pd1–C1 = 81.58, P1–Pd1–C2 = 91.72, C2–Pd1–C3 = 82.32, C1– Pd1–C3 = 104.32. Pd1–C distances to the two distal ring atoms ortho to C1 = 2.784, 3.002.

When a solution of *cis*-[Pd(C_6F_5)$_2$(XPhos)] (**7**) in dioxane was heated at 80 ˚C in the presence of C_6F_5–Br, reductive elimination of C_6F_5–C_6F_5 followed by instantaneous oxidative addition to the in situ generated [Pd^0(XPhos)] complex was complete in 180 min, generating [PdBr(C_6F_5)(XPhos)] (**8**). At room temperature, **8** shows an equilibrium in solution between monomers and halogen bridged dimers [Pd(μ-Br)(C_6F_5)(XPhos)]$_2$, giving rise to broadening of its ^{19}F and ^{31}P NMR signals, represented in Equation 4. This kind of ligand fluxionality in halogen-bridged Pd dimers with Buchwald-type phosphine ligands has been previously reported.[58] Moreover, aryl exchange between the Pd species does not take place as no signals of *cis*-[Pd(C_6F_5)$_2$(XPhos)] (**7**) are observed in the spectra.

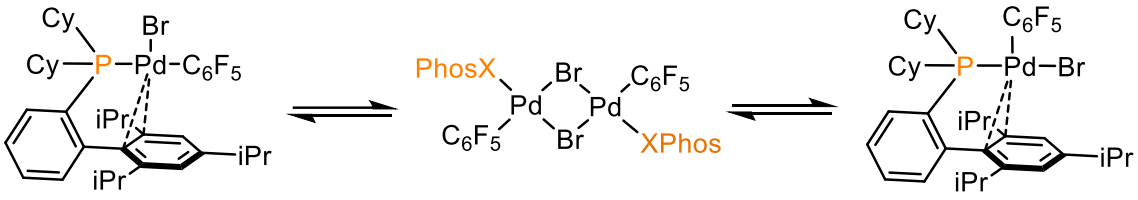

Equation 4. Dynamic equilibria of **8** in solution. For clarity, only one dimeric species is shown and iPr substituents have been omitted on it.

[58] Melvin, P. R.; Nova, A.; Balcells, D.; Hazari, N.; Tilset, M. DFT Investigation of Suzuki-Miyaura Reactions with Aryl Sulfamates Using a Dialkylbiarylphosphine-Ligated Palladium Catalyst. *Organometallics* **2017**, *36*, 3664–3675. DOI: 10.1021/ACS.ORGANOMET.7B00642.

Based on the analysis of the NMR spectra, an equilibrium between different species is proposed (Figure 7).

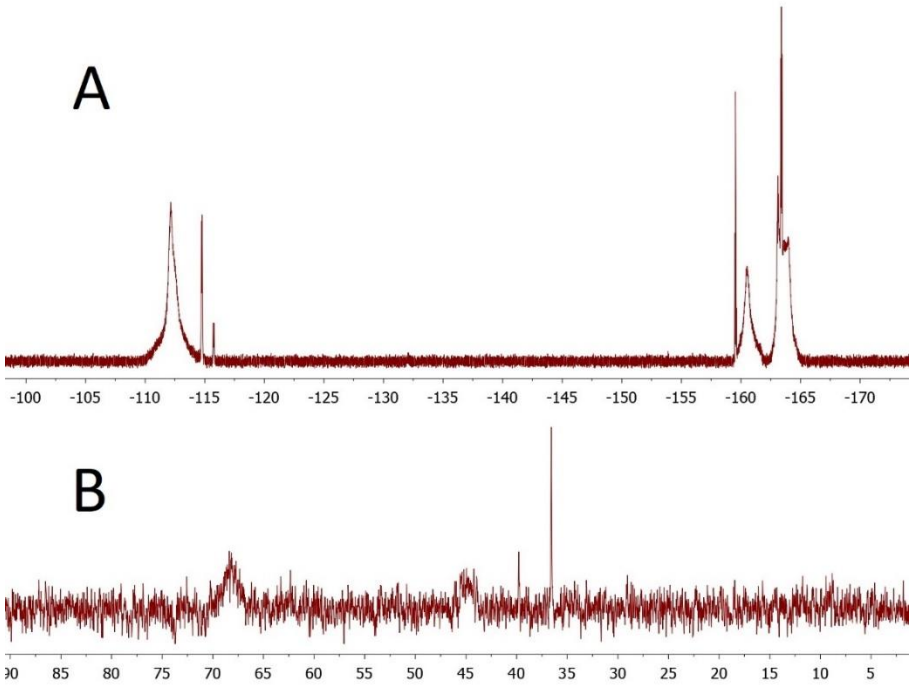

Figure 7. ^{19}F (top, A) and ^{31}P (bottom, B) NMR spectra of **8** at 298 K in $CDCl_3$.

The sharp doublets can be assigned to the *cis* and *trans* monomers of [PdBr(C_6F_5)(XPhos)] (**8**). The broad signal observed at room temperature in both spectra is due to signal coalescence of species in equilibrium, which can be proposed as *μ-Br* Pd dimers. These dimeric species have two intrinsic isomers, *syn* and *anti*, along with conformational isomers due to the unrestricted rotation of the biaryl moiety of the ligand in solution. This kind of ligand fluxionality in halogen-bridged Pd dimers with Buchwald-type phosphine ligands has been previously studied and reported.[59] Moreover, aryl exchange between the Pd species does not take place as no signals of *cis*-[Pd(C_6F_5)$_2$(XPhos)] (**7**) are observed in the spectra.

Besides, an inspection of the ^{19}F NMR of the catalytic reactions using C_6F_5Br (**1n**) and C_6F_5H (**2n**) as reagents, led us to identify the [Cu(C_6F_5)(IPr)] (**5**) and [Pd(C_6F_5)$_2$(XPhos)] (**7**) in the reaction mixture. This suggests that, for **1n** and **2n** as

[59] Pérez-Iglesias, M.; Infante, R.; Casares, J. A.; Espinet, P. Intriguing Behavior of an Apparently Simple Coupling Promoter Ligand, PPh_2(p-C_6H_4-C_6F_5), in Their Pd Complexes. *Organometallics* **2019**, *38*, 3688–3695. DOI: 10.1021/acs.organomet.9b00460.

reagents, the reductive elimination of [Pd(C_6F_5)$_2$(XPhos)] (**7**) is the slowest step in the catalytic cycle.

The transmetalation and reductive elimination sequence was evaluated for different aryl halides. In both cases the transmetalation step between [Cu(C_6F_5)(IPr)] (**5**) and [Pd(Ar^F)(Br)(XPhos)] (Ar^F=C_6F_5 (**8**); *p*-C_6H_4F (**9**)) was fast at room temperature. This fast transmetalation probably occurred due to the facility of XPhos ligand to generate an unoccupied position.[51] The reaction of **8** with **5** at room temperature did not produce the biaryl product (**3nn**), but full conversion to Pd biaryl complex **7** in 4 hours. Obviously, the reductive elimination is much slower than the transmetalation for these highly fluorinated reagents. That indicated the reductive eliminations is the rds (rate determining state). In contrast, when [Cu(C_6F_5)(IPr)] (**5**) and [Pd(C_6H_4F)Br(XPhos)] (**9**) were mixed at room temperature the reaction took place in two hours, and only the cross-coupling product (**3fn**) was detected along the reaction, showing that in this case, with only 2 fluorine atoms in the aromatic ring, the reductive elimination is faster than the transmetalation.[26]

For Cu, the [Cu(C_6F_5)(IPr)] (**5**) concentration depends on a deprotonation equilibrium of aryl–H, which is influencing the Cu availability at the transmetalation and, consequently, the rate of this step. Information about the influence of the arene deprotonation step in the transmetalation/reductive elimination process could be obtained from KIE (kinetic isotopic effect) experiments with C_6F_5–H/D.[60] One of the most powerful and common techniques for studying reaction mechanisms is the measurement of KIEs. When conducted in a good way, these experiments can provide important information about which bonds are broken or formed at different stages of a reaction, and in some cases, about the properties of the transition state or intermediates. Simons and Hartwig have discussed the different KIE experiments that can be used to get experimental information about C–H activation processes.[60] A short summary of what these experiments consist of:

[60] Simmons, E. M.; Hartwig, J. F. On the Interpretation of Deuterium Kinetic Isotope Effects in C–H Bond Functionalizations by Transition-Metal Complexes. *Angew. Chem. Int. Ed.* **2012**, *51*, 3066–3072. DOI: 10.1002/ANIE.201107334.

a) The experiments are carried out in different vessels with C–D and C–H substrates. This experiment gives valuable information on whether the cleavage of the C–H bond is really the limiting step of the reaction. It should be noted that the main drawback of this experiment is that in catalytic systems, the result can be influenced by different factors, such as catalyst decomposition or induction periods.

b) The experiments are carried out in the same vessel with C–D and C–H substrates. This type of experiment has the advantage that since both reagents are in the same vessel, the k_H and k_D measurements are more precise, and the reaction is always carried out under the same conditions, with no possibility of variation. The disadvantage with respect to the previous experiment is that it does not provide the same information, since it does not establish that the activation of the C–H bond is the limiting step of the reaction.

c) The third type of experiment is conceptually similar to the second one but involves an intramolecular competition between functionalization of a C–H bond and a C–D bond in a single substrate.

For these experiments, we used the highest fluorinated system and 1-Br-4-C_6FH_4 aryl bromide in two different vessels as we can see in Equation 5.

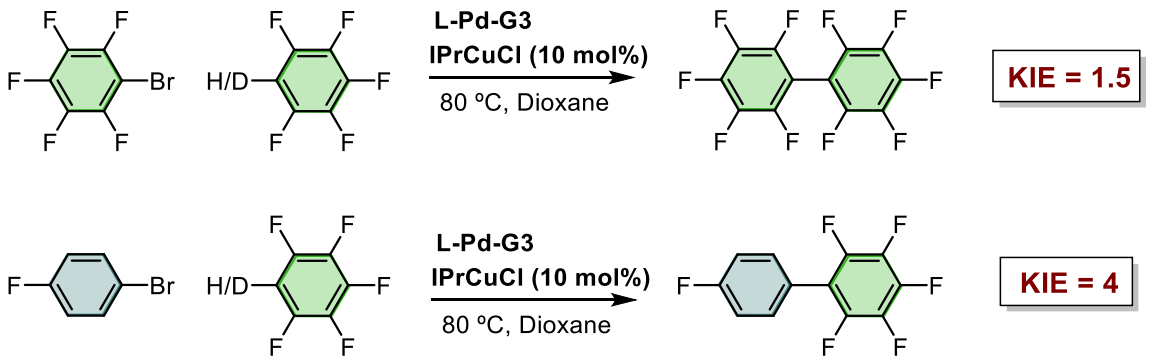

Equation 5. KIE experiments.

Two Schlenk flasks equipped with a screw cap and a teflon stirring bar were charged in a nitrogen atmosphere with [Pd-G3-XPhos] and [CuCl(IPr)] in dry dioxane. Aryl halide (1-Br-4-C_6FH_4 or C_6F_5–Br) was added to each flask. Then, C_6F_5–H was added to one flask and C_6F_5–D to the other. Then, the schlenk flasks were placed in a pre-heated oil bath at 80 °C with constant stirring. After 30 minutes, an

aliquot was taken and analysed by ^{19}F NMR. The concentration of the product was determined by integration of the distinct signals of reagent and products. The ratio of product concentrations in these independently experiments determine the ratio of reaction rate constants (k_H/k_D) giving the reported KIE value.

If we analysed these results, for the first case the KIE is ≈ 1.5, and we can conclude that the C–H activation is not de rds. On the other hand, when 1-Br-4-C_6FH_4 was used, the result is absolutely different. We obtained a KIE ≈ 4.0, indicating that the C–H activation is largely determinant on the overall reaction rate. In both cases, the C–H activation is the same, but the oxidative addition and the reductive elimination are different. In the first case, the reductive elimination will be the most difficult step in this reaction, due to the difficult of generate C_6F_5–C_6F_5 when 1-Br-4-C_6FH_4 was used the reductive elimination will be easier than the C_6F_5 one, because the carbon bonded to the Pd is less activated, because the ring contains few fluorine atoms. This makes the reductive elimination much faster, thus leaving the activation of the C–H bond above in energy, becoming the limiting step of the reaction.

This is an extreme case of difficult cross-coupling but, in less clear cases with fast oxidative addition, the KIE experiments can determine which step, reductive elimination or C–H activation, is more rate determining. Considering that the reductive elimination of two fluorinated aryls is one of the limiting steps of the reaction, it is presumable to think that in Pd/Cu systems improving the C–H activation will make an incredible difference in the reaction rate of the whole process. All of this information allows us to conclude the following mechanistic proposal, represented in Scheme 5.

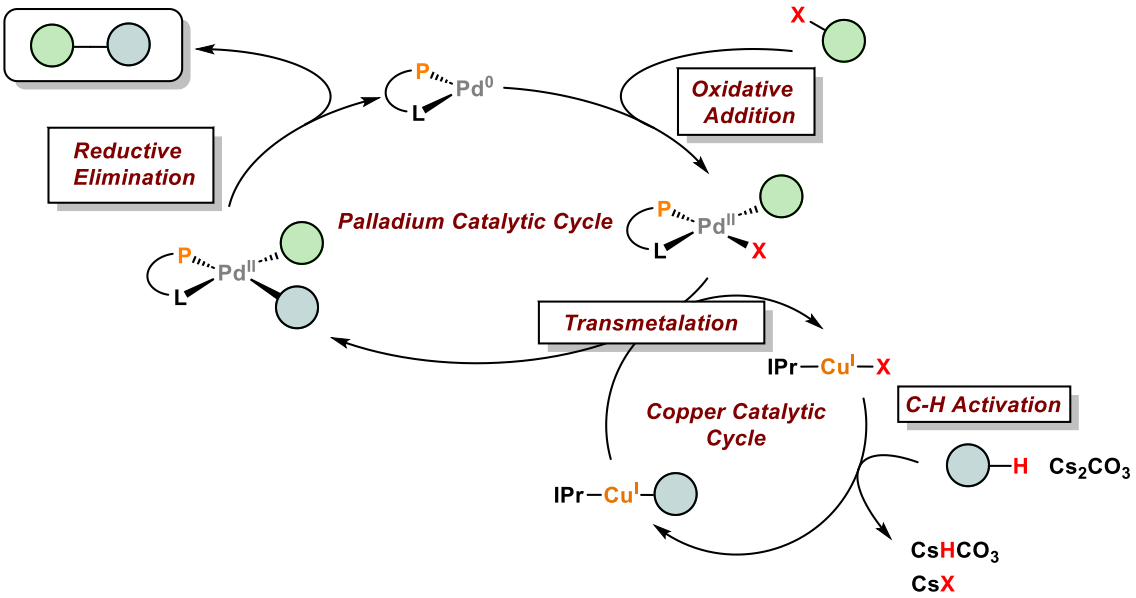

Scheme 5. Bimetallic mechanism proposal for cross coupling between arenes containing an acidic proton and aryl halides.

1.3 Summary and conclusions

In summary, we have developed a new efficient system to prepare highly fluorinated biaryls in good to excellent yields, using a Pd/Cu bimetallic catalytic system, employing commercially available Ar^F–H active reagents and not needing previous nucleophile preparation for the copper catalytic cycle, and high fluorinated aryl bromides or chlorides for the palladium catalytic cycle.

The choice of ligands for Pd and Cu is crucial for the good outcome of the reaction, since all the steps in the mechanism can be limiting for the overall reaction rate. The choice of the carbene ligand IPr for the organometallic copper complex and the Buchwald-type phosphine XPhos for the palladium has proved to be perfectly synergistic in this catalytic system. This ligand facilitates fast and selective coupling even for highly fluorinated aryls, reducing the undesired hydrolysis and homocoupling products, produced by outside catalytic cycles and allows for general application and mild conditions. Furthermore, the election of the ligands also allows the selective steps in the different catalytic cycles and avoiding ligand exchange.
The mechanistic investigation shows a key cooperative behaviour between both metals, demonstrating that the *rds.* depends on the nature of the reactants. That makes the process feasible and generates interesting synergy between metals, that can allow to improve new Pd/Cu bimetallic catalysis.

1.4 Experimental section

All the manipulations were performed in a dry glovebox or by means of standard Schlenk techniques under N_2 or Ar atmosphere. Solvents were dried using a solvent purification system SPS PS-MD-5 or distilled from appropriate drying agents and were sparged with nitrogen gas. Solvents for experiments in an inert atmosphere were stored into flame-dried Schlenk flasks over freshly activated 3 or 4 Å molecular sieves. Commercially available chemicals were purchased from Sigma Aldrich, Alfa Aesar, Fluorochem and Acros Organics and were used without further purification.

CyPhos-HF and CyPhos-FF, [CuCl(NHC)] complexes, [29] [$Cu(C_6F_5)$(IPr)], [29] and C_6F_5–D, were prepared by reported methods. Flash chromatography was carried out using silica gel (230-240 mesh). Chemical yields refer to pure isolated substances. NMR spectra were recorded with Bruker Avance 400 Ultrashield and Varian 500/54 Premium Shielded instruments. Chemical shifts are reported in ppm referenced to tetramethylsilane (^{1}H), CCl_3F (^{19}F), and 85% H_3PO_4 (^{31}P), with positive shifts downfield, at 298 K unless otherwise stated. In the ^{19}F and ^{31}P NMR spectra registered in non-deuterated solvents, a coaxial tube containing acetone-d_6 was used to maintain the ^{2}H lock signal. HRMS (EI) were performed with a MALDI Bruker Autoflex at the LTI facilities of Valladolid University.

Optimization of catalytic conditions

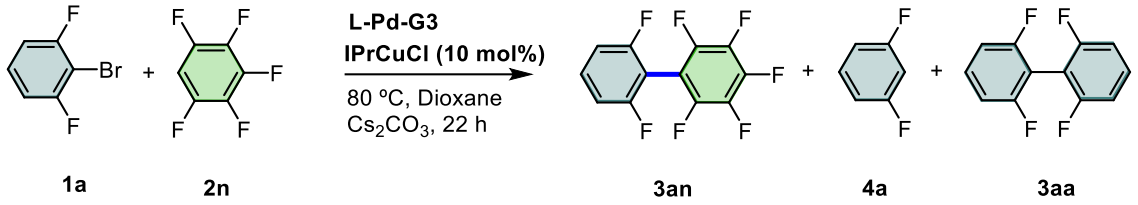

Equation 6. Products obtained in the catalytic reaction.

Screening reactions were conducted on a 0.160 mmol scale of aryl halide, in 2.0 mL of solvent (0.08 M). [Pd] precatalyst (0.016 mmol), [Cu] precatalyst (0.032 mmol) and base (0.160 mmol) were added to a flame-dried screwed-capped Schlenk flask with a magnetic stirrer. Then, the corresponding aryl halide (**1a**, 0.160 mmol), arene (**2n**, 0.160 mmol) and solvent (2 mL) were added to the flask. α,α,α-trifluorotoluene was added as internal standard (12.5 µL, 0.100 mmol). The Schlenk was placed in an oil bath at 80 °C and stirred for 22 hours. Then, it was taken out of the bath, cooled to room temperature, and an aliquot was checked by ^{19}F NMR. **3an** was obtained in 74 % yield employing the standard conditions stated in the image.

General procedure for catalysis

To a flame-dried screwed-capped Schlenk flask with a magnetic stirrer, XPhos-Pd-G3 precatalyst (27.1 mg, 0.032 mmol), [CuCl(IPr)] (31.2 mg, 0.064 mmol) and Cs_2CO_3 (209.0 mg, 0.640 mmol) were added. Then, the corresponding aryl bromide (**1**, 0.640 mmol), fluorinated arene (**2**, 0.640 mmol) and dioxane (2 mL) were added to the flask. The Schlenk was placed in an oil bath at 80 °C and stirred for 22 hours. Then, the flask was taken out of the bath and 5 mL of aqueous saturated NH_4Cl solution were added. The aqueous layer was extracted with Et_2O (3 x 5 mL). The organic fraction was dried over $MgSO_4$ and filtered through a short path of silica gel. The coloured solution was concentrated, and the residue was purified by flash column chromatography.

Catalysis products characterization

2,2',3,4,5,6,6'-heptafluoro-1,1'-biphenyl (3an)

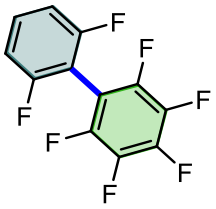

Following general procedure with 2-bromo-1,3-difluorobenzene (**1a**) and pentafluorobenzene (**2n**). The product was obtained as a colourless volatile liquid after column chromatography employing *n*-pentane as eluent (125.5 mg, 70 % yield).

HRMS (EI) Calculated for $C_{12}H_3F_7$ $[M]^+$: 280.0123. Experimental $[M]^+$: 280.0116.

^{1}H NMR (499.72 MHz, Chloroform-*d*) δ 7.48 (tt, *J* = 8, 6 Hz, 1H), 7.09 – 7.04 (m, 1H).

^{13}C{^{1}H} NMR (125.67 MHz, Chloroform-*d*) δ 160.3 (dd, *J* = 252, 5 Hz), 144.5 (d, *J* = 254 Hz), 141.6 (d, *J* = 242 Hz), 137.7 (d, *J* = 255 Hz), 132.1(t, *J* = 10 Hz), 111.6 (d, *J* = 25 Hz). C_{ipso} not observed.

^{19}F NMR (470.17 MHz, Chloroform-*d*) δ -110.17 – -110.31 (m), -137.91 – -138.05 (m), -152.60 (tt, *J* = 21, 2 Hz), -161.74 – -161.90 (m).

2,2',3,3',4,5,6-heptafluoro-1,1'-biphenyl (3bn)

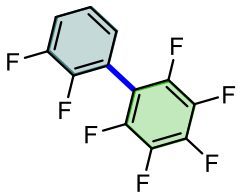

Following general procedure with 1-bromo-2,3-difluorobenzene (**1b**) and pentafluorobenzene (**2n**). The product was obtained as a colourless volatile liquid after column chromatography employing *n*-pentane as eluent (148.8 mg, 83 % yield).

HRMS (EI) Calculated for $C_{12}H_3F_7$ $[M]^+$: 280.0123. Experimental $[M]^+$: 280.0127.

^{1}H NMR (499.72 MHz, Chloroform-*d*) δ 7.36 – 7.28 (m, 1H), 7.25 – 7.18 (m, 1H), 7.16 – 7.08 (m, 1H).

^{13}C{^{1}H} NMR (125.67 MHz, Chloroform-*d*) δ 151.0 (dd, *J* = 249, 12 Hz), 148.50 (dd, *J* = 252, 13 Hz), 144.4 (dddt, *J* = 250, 11, 7, 4 Hz), 141.6 (dddd, *J* = 255, 13, 8, 5-Hz), 139.6 – 136.1 (dm, *J* = 253 Hz), 126.85 (d, *J* = 3 Hz), 124.5 (dd, *J* = 7, 5 Hz), 118.9 (d, *J* = 17 Hz), 116.5 (d, *J* = 12 Hz), 109.1 (tt, *J* = 18, 3 Hz).

^{19}F NMR (470.17 MHz, Chloroform-*d*) δ -136.21 – -136.53 (m, 1F), -136.85 – -137.16 (m, 1F), -139.98 – -140.15 (m, 2F), -153.10 (tt, J = 21, 2 Hz, 1F), -161.52 – -161.73 (m, 2F).

2,2',3,4,5,5',6-heptafluoro-1,1'-biphenyl (3cn)

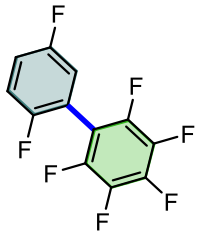

Following general procedure with 2-bromo-1,4-difluorobenzene (**1c**) and pentafluorobenzene (**2n**). The product was obtained as a colourless volatile liquid after column chromatography employing *n*-pentane as eluent (156.0 mg, 87 % yield).

HRMS (EI) Calculated for $C_{12}H_3F_7$ $[M]^+$: 280.0123. Experimental $[M]^+$: 280.0129.

^{1}H NMR (499.72 MHz, Chloroform-*d*) δ 7.22 – 7.14 (m, 2H), 7.11 – 7.03 (m, 1H).

^{13}C{^{1}H} NMR (125.67 MHz, Chloroform-*d*) δ 158.4 (d, *J* = 244 Hz), 156.1-(d, *J* = 247 Hz), 144.4 (d, *J* = 254 Hz), 141.6 (d, *J* = 255 Hz), 137.9-(d, *J* = 252 Hz), 118.5 (d, *J* = 25 Hz), 118.4 (dd, *J* = 23, 9 Hz, 117.4 (dd, *J* = 24, 9 Hz), 115.4 (dd, *J* = 18, 10 Hz), 109.2 (s).

^{19}F NMR (470.17 MHz, Chloroform-*d*) δ -117.98 – -118.17 (m, 1F), -118.55 – -118.72 (m, 1F), -140.06 (dddd, *J* = 23, 11, 7, 3 Hz, 2F), -152.98 (t, *J* = 21 Hz, 1F), -161.44 – -161.62 (m, 2F).

2,2',3,4,4',5,6-heptafluoro-1,1'-biphenyl (3dn)

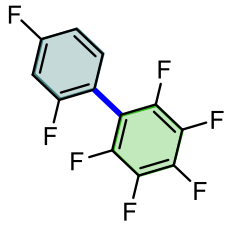

Following general procedure with 1-bromo-2,4-difluorobenzene (**1d**) and pentafluorobenzene (**2n**). The product was obtained as a colourless solid after column chromatography employing *n*-pentane as eluent (141.6 mg, 79 % yield).

HRMS (EI) Calculated for $C_{12}H_3F_7$ $[M]^+$: 280.0123. Experimental $[M]^+$: 280.0119.

^{1}H NMR (499.72 MHz, Chloroform-*d*) δ 7.38 – 7.30 (m, 1H), 7.06 – 6.96 (m, 2H).

^{13}C{^{1}H} NMR (125.67 MHz, Chloroform-*d*) δ 164.1 (dd, *J* = 252, 12 Hz), 160.4 (dd, *J* = 253, 12 Hz), 146.0– 143.3 (m, *J* = 243 Hz), 142.9 – 140.0 (m, *J* = 253 Hz), 139.3 – 135.8 (m, *J* = 248 Hz), 133.0 (dd, *J* = 10, 4 Hz), 112.1 (dd, *J* = 21, 4 Hz), 110.4 (d, *J* = 16 Hz,), 109.4 (td, *J* = 18, 4 Hz), 104.9 (t, *J* = 25 Hz).

^{19}F NMR (470.17 MHz, Chloroform-*d*) δ -106.69 – -106.80 (m, 1F), -108.13 (h, *J* = 10 Hz, 1F), -140.28 – -140.42 (m, 2F), -153.63 (t, *J* = 21 Hz, 1F), -161.74 – -161.94 (m, 2F).

2,2',3,4,5,6-hexafluoro-1,1'-biphenyl (3en)

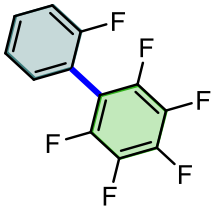

Following general procedure with 1-bromo-2-fluorobenzene (**1n**) and pentafluorobenzene (**2n**). The product was obtained as a colourless liquid after column chromatography employing *n*-pentane as eluent (151.0 mg, 90 % yield).

HRMS (EI) Calculated for $C_{12}H_4F_6$ $[M]^+$: 262.0217. Experimental $[M]^+$: 262.0221.

^{1}H NMR (499.72 MHz, Chloroform-*d*) δ 7.52 – 7.47 (m, 1H), 7.39 – 7.34 (m, 1H), 7.28 (td, *J* = 7.5, 1.1 Hz, 1H), 7.26 – 7.20 (m, 1H).

^{13}C{^{1}H} NMR (125.67 MHz, Chloroform-*d*) δ 160.0 (d, *J* = 250 Hz), 144.5 (dddt, *J* = 249, 11, 7, 4 Hz), 141.2 (dtt, *J* = 254, 13, 5 Hz), 139.1 – 136.4 (dm, *J* = 251 Hz), 132.1 (t, *J* = 2 Hz), 131.8 (d, *J* = 8 Hz), 124.4 (d, *J* = 4 Hz), 116.2 (s), 114.3 (dq, *J* = 16, 2 Hz), 110.3 (td, *J* = 18, 4 Hz).

^{19}F NMR (470.17 MHz, Chloroform-*d*) δ -112.73 – -113.12 (m, 1F), -140.29 – -140.52 (m, 2F), -154.29 (t, *J* = 2 Hz, 1F), -162.18 – -162.34 (m, 2F).

2,3,4,4',5,6-hexafluoro-1,1'-biphenyl (3fn)

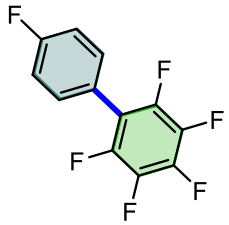

Following general procedure with 1-bromo-4-fluorobenzene (**1f**) and pentafluorobenzene (**2n**). The product was obtained as a colourless solid after column chromatography employing *n*-pentane as eluent (137.6 mg, 82 % yield).

HRMS (EI) Calculated for $C_{12}H_4F_6$ $[M]^+$: 262.0217. Experimental $[M]^+$: 262.0215.

^{1}H NMR (499.72 MHz, Chloroform-*d*) δ 7.45 – 7.37 (m, 2H), 7.24 – 7.15 (m, 2H).

^{13}C{^{1}H} NMR (125.67 MHz, Chloroform-*d*) δ 163.3 (d, *J* = 250 Hz), 144.2-(dddt, *J* = 247, 11, 7, 4 Hz), 141.9 – 139.3 (m, *J* = 252 Hz), 139.3 – 136.4 (m, *J* = 248 Hz), 132.2 (dd, *J* = 8, 2 Hz), 122.4 (s), 116.1 (d, *J* = 22 Hz), 115.1 (td, *J* = 17, 4 Hz).

^{19}F NMR (470.17 MHz, Chloroform-*d*) δ -111.33 (tt, *J* = 8, 5 Hz, 1F), -143.36 (m, 2F), -155.25 (t, *J* = 21 Hz, 1F), -161.21 – -163.05 (m, 2F).

2,3,4,5,6-pentafluoro-4'-(trifluoromethyl)-1,1'-biphenyl (3gn)

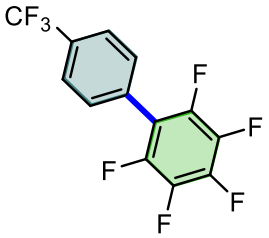

Following general procedure with 4-bromobenzotrifluoride (**1g**) and pentafluorobenzene (**2n**). The product was obtained as a colourless solid after column chromatography employing *n*-pentane as eluent (163.8 mg, 82 % yield).

HRMS (EI) Calculated for $C_{13}H_4F_8$ $[M]^+$: 312.0185. Experimental $[M]^+$: 312.0190.

^{1}H NMR (499.72 MHz, Chloroform-*d*) δ 7.77 (d, *J* = 8.1 Hz, 2H), 7.57 (d, *J* = 8.1 Hz, 2H).

^{13}C{^{1}H} NMR (125.67 MHz, Chloroform-*d*) δ 144.3 (d, *J* = 248 Hz), 141.1 (d, *J* = 255 Hz), 138.1 (d, *J* = 253 Hz), 131.6 (q, *J* = 32 Hz), 130.8 (s), 130.2 (s), 126.0 – 125.6 (m), 123.9 (q, *J* = 272 Hz), 114.7 (td, *J* = 17, 4 Hz).

^{19}F NMR (470.17 MHz, Chloroform-*d*) δ -62.99 (s, 3F), -142.90 – -143.02 (m, 2F), -153.78 (t, *J* = 21 Hz, 1F), -161.32 – -161.50 (m, 2F).

2,3,3',4,5,5',6-heptafluoro-1,1'-biphenyl (3hn)

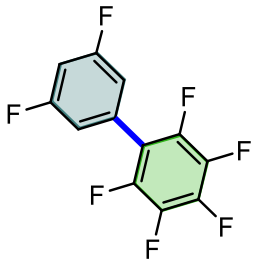

Following general procedure with 1-bromo-3,5-difluorobenzene (**1h**) and pentafluorobenzene (**2n**). The product was obtained as a colourless solid after column chromatography employing *n*-pentane as eluent (148.8 mg, 83 % yield).

HRMS (EI) Calculated for $C_{12}H_3F_7$ $[M]^+$: 280.0123. Experimental $[M]^+$: 280.0126.

^{1}H NMR (499.72 MHz, Chloroform-*d*) δ 7.00 – 6.96 (m, 2H), 6.93 (tt, *J* = 8.8, 2.3 Hz, 1H).

^{13}C{^{1}H} NMR (125.67 MHz, Chloroform-*d*) δ 163.0 (dd, *J* = 250, 13 Hz), 144.22 (d, *J* = 250 Hz), 141.2-(d, *J* = 256 Hz), 138.0 (d, *J* = 258 Hz), 129.2 (d, *J* = 11 Hz), 113.9 (t, *J* = 15 Hz), 113.8 – 112.3 (m), 105.1-(t, *J* = 25 Hz).

^{19}F NMR (470.17 MHz, Chloroform-*d*) δ -101.14 – -112.97 (m, 2F), -138.39 – -145.19 (m, 2F), -153.35 (t, *J* = 21 Hz, 1F), -156.20 – -164.29 (m, 2F).

2,3,3',4,4',5,6-heptafluoro-1,1'-biphenyl (3in)

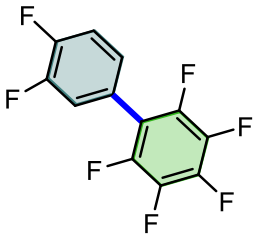

Following general procedure with 4-bromo-1,2-difluorobenzene (**1i**) and pentafluorobenzene (**2n**). The product was obtained as a colourless solid after column chromatography employing *n*-pentane as eluent (141.6 mg, 79 % yield).

HRMS (EI) Calculated for $C_{12}H_3F_7$ $[M]^+$: 280.0123. Experimental $[M]^+$: 280.0128.

^{1}H NMR (499.72 MHz, Chloroform-*d*) δ 7.33 – 7.27 (m, 2H), 7.21 – 7.14 (m, 1H).

^{13}C{^{1}H} NMR (125.67 MHz, Chloroform-*d*) δ 151.0 (dd, *J* = 252, 12 Hz), 150.5-(dd, *J* = 250, 12 Hz), 145.5 – 142.7 (m, *J* =248 Hz), 142.3 – 139.6 (m, *J* =254 Hz), 139.3 – 136.4 (m, *J* = 253 Hz), 126.9 (dq, *J* = 6, 3 Hz), 123.1 (s), 119.6-(d, *J* = 19.0 Hz), 118.0 (d, *J* = 18 Hz), 114.0 (td, *J* = 17, 17, 4 Hz).

^{19}F NMR (470.17 MHz, Chloroform-*d*) δ -135.55 – -135.69 (m, 1F), -136.26 – -136.40 (m, 1F), -143.00 – -143.11 (m, 2F), -154.10 (t, *J* = 21 Hz, 1F), -161.35 – -161.60 (m, 2F).

2,2',3,4,5,6-hexafluoro-5'-(trifluoromethyl)-1,1'-biphenyl (3jn)

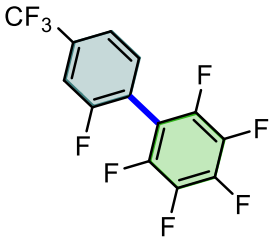

Following general procedure with 1-bromo-3-fluoro-5-(trifluoromethyl)benzene (**1j**) and pentafluorobenzene (**2n**). The product was obtained as a colourless volatile liquid after column chromatography employing *n*-pentane as eluent (179.6 mg, 85 % yield).

HRMS (EI) Calculated for $C_{13}H_3F_9$ $[M]^+$: 330.0091. Experimental $[M]^+$: 330.0083.

^{1}H NMR (499.72 MHz, Chloroform-*d*) δ 7.83 – 7.76 (m, 1H), 7.71 – 7.65 (m, 1H), 7.37 (t, *J* = 8.8 Hz, 1H).

^{13}C{^{1}H} NMR (125.67 MHz, Chloroform-*d*) δ 161.9 (d, *J* = 257 Hz), 144.5 (dddt, *J* = 250, 11, 7, 4 Hz), 141.9 (dtt, *J* = 256, 13, 5 Hz), 139.6 – 136.3 (dm, *J* = 252 Hz), 130.1 – 129.6 (m), 129.3 (dq, *J* = 9, 3 Hz), 127.5 (qd, *J* = 33, 3 Hz), 123.5 (q, *J* = 272 Hz), 117.1 (d, *J* = 23 Hz), 115.4 (dq, *J* = 17, 2 Hz), 108.9 (td, *J* = 18, 4 Hz).

^{19}F NMR (470.17 MHz, Chloroform-*d*) δ -62.48 (s, 3F), -104.00 – -109.23 (m, 1F), -138.19 – -141.72 (m, 2F), -152.79 (t, *J* = 20 Hz, 1F), -158.37 – -165.37 (m, 2F).

2,3,4,4',5,5',6-heptafluoro-2'-methyl-1,1'-biphenyl (3kn)

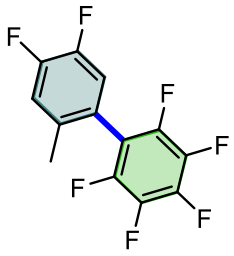

Following general procedure with 1-bromo-4,5-difluoro-2-methylbenzene (**1k**) and pentafluorobenzene (**2n**). The product was obtained as a colourless volatile liquid after column chromatography employing *n*-pentane as eluent (156.3 mg, 83 % yield).

HRMS (EI) Calculated for $C_{13}H_5F_7$ $[M]^+$: 294.0279. Experimental $[M]^+$: 294.0285.

^{1}H NMR (499.72 MHz, Chloroform-*d*) δ 7.16 (dd, *J* = 11.1, 7.9 Hz, 1H), 7.04 (dd, *J* = 10.4, 7.9 Hz, 1H), 2.15 (s, 3H).

^{13}C{^{1}H} NMR (125.67 MHz, Chloroform-*d*) δ 150.9 (dd, *J* = 251, 12 Hz, 1C), 148.5 (dd, *J* = 247, 13 Hz, 1C), 144.26 (dddt, *J* = 247, 11, 7, 4 Hz, 2C), 141.2 (dtt, *J* = 255, 13, 5 Hz, 1C), 139.3 – 136.2 (dm, *J* = 251 Hz, 2C), 134.9 (dd, *J* = 6, 4 Hz, 1C), 122.0 (dp, *J* = 6, 2 Hz, 1C), 119.6 (d, *J* = 18 Hz, 1C), 119.3 (d, *J* = 17 Hz, 1C), 113.7 (td, *J* = 19, 4 Hz, 1C), 19.1 (s, 1C).

^{19}F NMR (470.17 MHz, Chloroform-*d*) δ -136.59 (ddd, *J* = 21, 11, 8 Hz, 1F), -140.39 – -140.76 (m, 2F), -141.37 (dt, *J* = 21, 9 Hz, 1F), -154.29 (t, *J* = 20 Hz, 1F), -161.80 – -161.96 (m, 2F).

2,2',3,4,4',5,6,6'-octafluoro-1,1'-biphenyl (3ln)

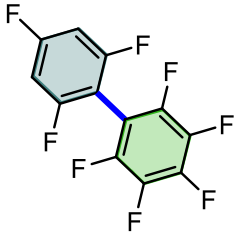

Following general procedure with 2-bromo-1,3,5-trifluorobenzene (**1l**) and pentafluorobenzene (**2n**). The product was obtained as a colourless volatile liquid after column chromatography employing *n*-pentane as eluent (137.4 mg, 72 % yield).

HRMS (EI) Calculated for $C_{12}H_2F_8$ $[M]^+$: 298.0029. Experimental $[M]^+$: 298.0036.

^{1}H NMR (499.72 MHz, Chloroform-*d*) δ 6.88 – 6.81 (m, 2H).

^{13}C{^{1}H} NMR (125.67 MHz, Chloroform-*d*) δ 164.3 (dt, *J* = 253, 15 Hz), 160.8 (ddd, *J* = 253 15, 9 Hz), 144.8 (dddt, *J* = 250, 11, 7, 4 Hz), 142.1 (dtt, *J* = 256, 13, 5 Hz), 139.5 – 136.2 (dm, *J* = 251 Hz), 103.6 (td, *J* = 18, 4.0 Hz), 101.5 – 100.7 (m), 100.6 (d, *J* = 3 Hz).

^{19}F NMR (470.17 MHz, Chloroform-*d*) δ -104.0 (p, *J* = 8.2 Hz, 1F), -107.12 (p, *J* = 8 Hz, 2F), -138.09 – -138.29 (m, 2F), -152.31 (tt, *J* = 21, 2 Hz, 1F), -161.68 – -161.8 (m, 2F).

2,3,3',4,4',5,5',6-octafluoro-1,1'-biphenyl (3mn)

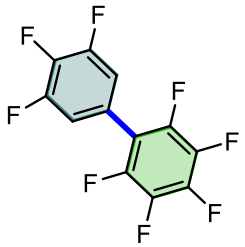

Following general procedure with 5-bromo-1,2,3-trifluorobenzene (**1m**) and pentafluorobenzene (**2n**). The product was obtained as a colourless volatile liquid after column chromatography employing *n*-pentane as eluent (135.5 mg, 71 % yield).

HRMS (EI) Calculated for $C_{12}H_2F_8$ $[M]^+$: 298.0029. Experimental $[M]^+$: 298.0025.

^{1}H NMR (499.72 MHz, Chloroform-*d*) δ 7.09 (t, *J* = 6.9 Hz, 1H).

^{13}C{^{1}H} NMR (125.67 MHz, Chloroform-*d*) δ 151.5 (ddd, *J* = 251, 10, 4 Hz), 144.2 (dddt, *J* = 249, 11, 7, 4 Hz), 142.6 – 139.9 (dm, *J* = 256 Hz), 140.60 (dt, *J* = 255, 15 Hz), 139.3 – 136.3 (dm, *J* = 252 Hz), 122.3 – 121.9 (m), 115.0 (ddt, *J* = 17, 4, 2 Hz), 113.2 (t, *J* = 16 Hz).

^{19}F NMR (470.17 MHz, Chloroform-*d*) δ -132.88 – -133.04 (m, 2F), -142.68 – -142.81 (m, 2F), -152.93 (t, *J* = 21 Hz, 1F), -157.91 (tt, *J* = 21, 6 Hz, 1F), -160.80 – -161.00 (m, 2F).

Perfluoro-1,1'-biphenyl (3nn)

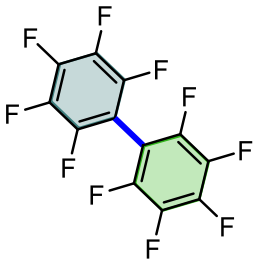

Following general procedure with bromopentafluorobenzene (**1n**) and pentafluorobenzene (**2n**). The product was obtained as a colourless solid after column chromatography employing *n*-pentane as eluent (136.9 mg, 64 % yield).

HRMS (EI) Calculated for $C_{12}F_{10}$ $[M]^+$: 333.9840. Experimental $[M]^+$: 333.9837.

$^{13}C\{^1H\}$ NMR (125.67 MHz, Chloroform-*d*) δ 144.8 (ddt, *J* = 253, 11, 3 Hz), 144.4 – 141.0 (m, *J* = 258 Hz), 139.8 – 136.4 (m, *J* = 252 Hz), 102.1 – 101.1 (m).

^{19}F NMR (376.21 MHz, Chloroform-*d*) δ -135.34 – -139.60 (m), -149.81 (t, *J* = 21 Hz), -160.23 – -160.45 (m).

2,2',3,5,6,6'-hexafluoro-4-methoxy-1,1'-biphenyl (3ap)

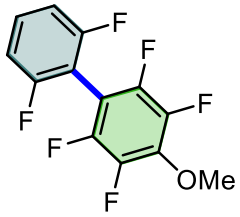

Following general procedure with 2-bromo-1,3-difluorobenzene (**1a**) and 1,2,4,5-tetrafluoroanisole (**2p**). The product was obtained as a colourless liquid after column chromatography employing *n*-pentane as eluent (78.5 mg, 42 % yield).

HRMS (EI) Calculated for $C_{13}H_6F_6O$ $[M]^+$: 292.0323. Experimental $[M]^+$: 292.0319.

^{1}H NMR (499.72 MHz, Chloroform-*d*) δ 7.44 (tt, *J* = 8, 6 Hz, 1H), 7.04 (dd, *J* = 8, 7 Hz, 2H), 4.15 (t, *J* = 1 Hz, 3H).

^{13}C{^{1}H} NMR (125.67 MHz, Chloroform-*d*) δ 160.4 (dd, *J* = 251, 6 Hz), 144.7 (dddd, *J* = 248, 12, 7, 3 Hz), 142.3 – 139.6 (d of m, *J* = 247.0 Hz), 139.0 (tt, *J* = 11, 3 Hz), 131.5 (t, *J* = 10 Hz), 112.1 – 110.9 (m), 104.6 (tt, *J* = 20, 2 Hz), 102.1 (t, *J* = 19 Hz), 62.0 (td, *J* = 4, 2 Hz).

^{19}F NMR (470.17 MHz, Chloroform-*d*) δ -110.39 (p, *J* = 7 Hz, 2F), -140.01 – -140.26 (m, 2F), -158.06 – -158.27 (m, 2F).

4-(2,6-difluorophenyl)-2,3,5,6-tetrafluoropyridine (3aq)

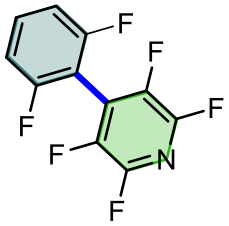

Following general procedure with 2-bromo-1,3-difluorobenzene (**1a**) and 2,3,5,6-tetrafluoropyridine (**2q**). The product was obtained as a colourless solid after column chromatography employing *n*-pentane as eluent (144.8 mg, 86 % yield).

HRMS (EI) Calculated for $C_{11}H_3F_6N$ $[M]^+$: 263.0170. Experimental $[M]^+$: 263.0173.

^{1}H NMR (499.72 MHz, Chloroform-*d*) δ 7.56 (tt, *J* = 8, 6 Hz, 1H), 7.11 (t, *J* = 8 Hz, 2H).

^{13}C{^{1}H} NMR (125.67 MHz, Chloroform-*d*) δ 159.7 (dd, *J* = 254, 6 Hz), 143.4 (dddd, *J* = 246, 16, 13, 3 Hz), 141.4 – 137.3 (d of m, *J* = 262 Hz), 133.2 (t, *J* = 10 Hz), 122.5 (tt, *J* = 17, 3 Hz), 111.9 (dd, *J* = 20, 4 Hz), 103.5 (t, *J* = 20 Hz).

^{19}F NMR (470.17 MHz, Chloroform-*d*) δ -90.18 (tt, *J* = 26, 13 Hz, 2F), -109.52 (dh, *J* = 17, 9, 9 Hz, 2F), -139.35 (dpd, *J* = 23, 14, 7 Hz, 2F).

2,2',3,5,6,6'-hexafluoro-1,1'-biphenyl (3as)

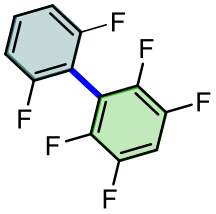

Following general procedure with 2-bromo-1,3-difluorobenzene (**1a**) and 1,2,4,5-tetrafluorobenzene (**2s**). The product was obtained as a colourless solid after column chromatography employing *n*-pentane as eluent (100.7 mg, 60 % yield).

HRMS (EI) Calculated for $C_{12}H_4F_6$ $[M]^+$: 262.0217. Experimental $[M]^+$: 262.0213.

^{1}H NMR (499.72 MHz, Chloroform-*d*) δ 7.47 (tt, *J* = 8, 6 Hz, 1H), 7.18 (tt, *J* = 9, 7 Hz, 1H), 7.10 – 7.01 (m, 2H).

^{13}C{^{1}H} NMR (125.67 MHz, Chloroform-*d*) δ 160.4 (dd, *J* = 252, 6 Hz), 147.3 – 144.7 (dm, *J* = 252 Hz), 144.3 (ddt, *J* = 252, 16, 4 Hz), 132.0 (t, *J* = 10 Hz), 111.8 (dd, *J* = 20, 4 Hz), 110.0 (tdd, *J* = 18, 3, 1 Hz), 107.5 – 106.1 (m), 105.0 (tt, *J* = 20, 2 Hz).

^{19}F NMR (470.17 MHz, Chloroform-*d*) δ -110.31 (p, *J* = 7 Hz, 2F), -138.72 – -139.12 (m, 4F).

2,3,3',4',5,5',6-heptafluoro-4-methoxy-1,1'-biphenyl (3mp)

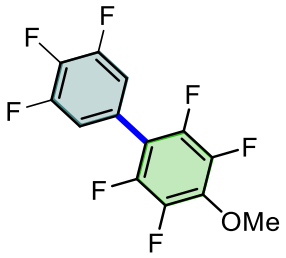

Following general procedure with 5-bromo-1,2,3-trifluorobenzene (**1m**) and 1,2,4,5-tetrafluoroanisole (**2p**). The product was obtained as a colourless solid after column chromatography employing *n*-pentane as eluent (49.6 mg, 25 % yield).

HRMS (EI) Calculated for $C_{13}H_5F_7O$ $[M]^+$: 310.0229. Experimental $[M]^+$: 310.0234.

^{1}H NMR (499.72 MHz, Chloroform-*d*) δ 7.22 – 6.89 (m, 2H), 4.14 (t, *J* = 1 Hz, 3H).

^{13}C{^{1}H} NMR (125.67 MHz, Chloroform-*d*) δ 151.3 (ddd, *J* = 250, 10, 4 Hz), 145.5 – 143.1 (dm, *J* = 247 Hz), 141.2 (ddt, *J* = 248, 15, 4 Hz), 140.2 (dt, *J* = 255, 14 Hz), 138.8 – 137.0 (m), 123.1 (tdd, *J* = 8, 5, 2 Hz), 114.9 (ddt, *J* = 17, 5, 2 Hz), 111.5 – 110.4 (m), 62.3 (t, *J* = 4 Hz).

^{19}F NMR (470.17 MHz, Chloroform-*d*) δ -133.71 (dd, *J* = 20, 8 Hz, 2F), -144.93 – -145.03 (m, 2F), -157.36 – -157.50 (m, 2F), -159.05 (tt, *J* = 20, 6 Hz, 1F).

2,3,5,6-tetrafluoro-4-(3,4,5-trifluorophenyl)pyridine (3mq)

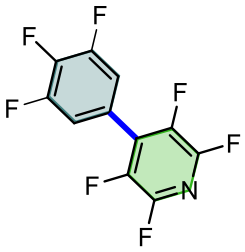

Following general procedure with 5-bromo-1,2,3-trifluorobenzene (**1m**) and 1,2,4,5-tetrafluoropyridine (**2q**). The product was obtained as a colourless liquid after column chromatography employing *n*-pentane as eluent (95.4 mg, 53 % yield).

HRMS (EI) Calculated for $C_{11}H_2F_7N$ $[M]^+$: 281.0075. Experimental $[M]^+$: 281.0078.

^{1}H NMR (499.72 MHz, Chloroform-*d*) δ 7.26 – 7.21 (m, 2H).

^{13}C{^{1}H} NMR (125.67 MHz, Chloroform-*d*) δ 151.4 (ddd, *J* = 252, 10, 4 Hz), 145.5 – 142.7 (m), 141.1 (dt, *J* = 258, 15 Hz), 140.3 – 137.6 (m), 130.6 – 129.6 (m), 121.7 – 121.0 (m), 114.9 – 114.4 (m).

^{19}F NMR (470.17 MHz, Chloroform-*d*) δ -89.19 – -89.46 (m, 2F), -132.08 (dd, *J* = 20, 7 Hz, 2F), -144.54 – -144.72 (m, 2F), -155.61 (tt, *J* = 20, 6 Hz, 1F).

2,3,3',4',5,5',6-heptafluoro-1,1'-biphenyl (3ms)

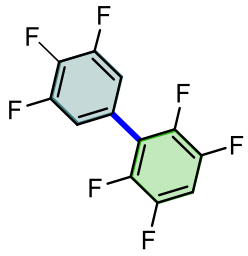

Following general procedure with 5-bromo-1,2,3-trifluorobenzene (**1m**) and 1,2,4,5-tetrafluorobenzene (**2s**). The product was obtained as a colourless solid after column chromatography employing *n*-pentane as eluent (104.0 mg, 58 % yield).

HRMS (EI) Calculated for $C_{12}H_3F_7$ $[M]^+$: 280.0123. Experimental $[M]^+$: 280.0117.

^{1}H NMR (499.72 MHz, Chloroform-*d*) δ 7.19 – 7.07 (m, 3H).

^{13}C{^{1}H} NMR (125.67 MHz, Chloroform-*d*) δ 151.4 (ddd, *J* = 250, 10, 4 Hz), 146.4 (dddd, *J* = 249, 14, 10, 4 Hz), 143.7 (ddt, *J* = 248, 14, 4 Hz), 140.50 (dt, *J* = 255, 15 Hz), 123.2 (tdt, *J* = 8, 5, 2 Hz), 118.6 (t, *J* = 16 Hz), 115.5 – 114.0 (m), 106.2 (t, *J* = 22 Hz).

^{19}F NMR (470.17 MHz, Chloroform-*d*) δ -133.49 (dd, *J* = 20.4, 7.9 Hz, 2F), -137.99 – -138.17 (m, 2F), -143.59 (ddd, *J* = 21, 12, 7 Hz, 2F), -158.43 (td, *J* = 14, 7 Hz, 1F).

X-ray structure of 3bn, 3fn and 3gn

X-ray quality crystals of compounds **3bn**, **3fn** and **3gn** were obtained by slow evaporation of an *n*-pentane solution of the corresponding biaryls. Their X-ray structures are shown in Figure 8, Figure 9 and Figure 10, respectively.

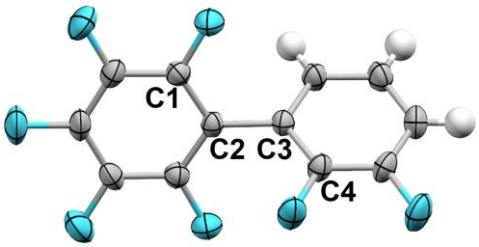

Figure 8. *X-ray structure of 3bn. Selected bond distances (Å) and angles (°): C2-C3 = 1.484, C1-C2-C3-C4 = 120.70.*

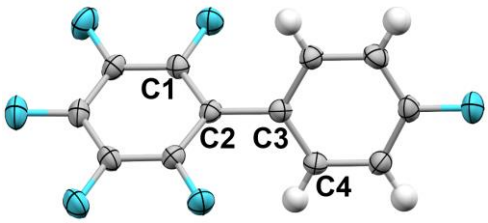

Figure 9*. X-ray structure of 3fn. Selected bond distances (Å) and angles (°): C2-C3 = 1.487, C1-C2-C3-C4 = 123.02.*

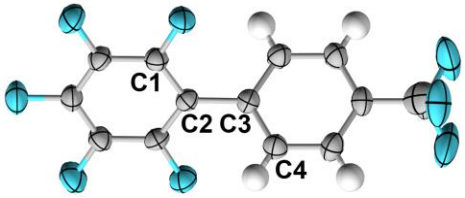

Figure 10*. X-ray structure of 3gn. Selected bond distances (Å) and angles (°): C2-C3 = 1.489, C1-C2-C3-C4 = 122.70.*

Synthesis of palladium intermediates

cis-[Pd(C$_6$F$_5$)$_2$(XPhos)] (7) and its X-ray structure

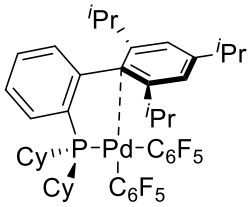

In a flame-dried Schlenk, *cis*-[Pd(C$_6$F$_5$)$_2$(THF)$_2$] (97.5 mg, 0.167 mmol) and XPhos (86.2, 0.177 mmol) were dissolved in 3 mL of CH_2Cl_2 at room temperature. The solution was stirred for 1 hour, *n*-hexane (3 mL) was added to induce precipitation of the product and the solvent was removed under vacuum. The colourless solid obtained was sonicated with *n*-pentane, filtered under air and washed with *n*-pentane (2 x 5 mL). It was dried under vacuum affording the title compound as a colourless solid (130.7 mg, 86 % yield).

X-ray-quality crystals were grown by slow diffusion of a CH_2Cl_2/*n*-hexane mixture at –20 °C.

The X-ray structure of **7** (Figure 11) shows a P,C-chelating coordination of XPhos involving predominantly C1 of the distal ring (the Kochi hapticity of this interaction is h = 1.37). The most remarkable structural aspect of **7** is the small C2-Pd-C3 angle (82.3°) forced by the crowding with the biaryl phosphine. This forced angle shortens the distance between C2 and C3 to 2.69 Å, reducing the activation energy for aryl-aryl reductive elimination.

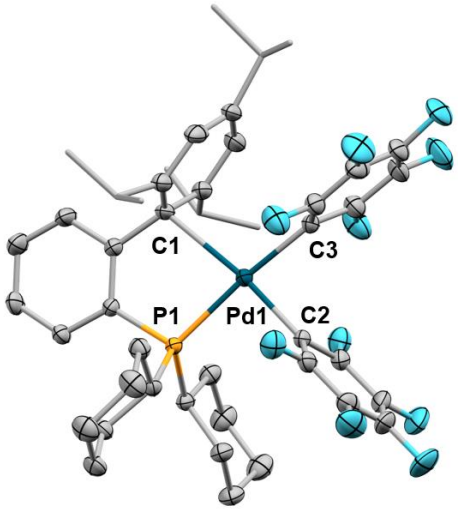

Figure 11. X-ray structure of cis-[Pd(C$_6$F$_5$)$_2$(XPhos)] (7). H atoms omitted for clarity. Selected bond distances (Å) and angles (°): Pd1–P1 = 2.328, Pd1–C1 = 2.478, Pd1–C2 = 2.013, Pd1–C3 = 2.080. P1–Pd1–C1 = 81.58, P1–Pd1–C2 = 91.72, C2–Pd1–C3 = 82.32, C1–Pd1–C3 = 104.32. Pd1–C distances to the two distal ring atoms ortho to C1 = 2.784, 3.002.

HRMS (EI) Calculated for $C_{45}H_{49}F_{10}NaPPd$ $[M+Na]^+$: 939.2356. Experimental $[M+Na]^+$: 939.2381.

^{1}H NMR (499.72 MHz, Chloroform-*d*) δ 7.68 – 7.62 (m, 1H), 7.50 – 7.41 (m, 2H), 7.06 (s, 2H), 6.89 – 6.85 (m, 1H), 2.47 (hept, J = 6 Hz, 2H), 2.15 – 2.00 (m, 5H), 1.86 – 1.78 (m, 2H), 1.77 – 1.64 (m, 14H), 1.31 – 1.17 (m, 6H), 0.99 (d, J = 7 Hz, 6H), 0.87 (d, J = 7 Hz, 6H), 0.80 – 0.68 (m, 2H).

^{19}F NMR (470.17 MHz, Chloroform-*d*) δ -111.10 – -111.46 (m, 2F), -112.88 (t, J = 27 Hz, 2F), -160.41 (t, J = 20 Hz, 1F), -162.44 (t, J = 20 Hz, 1F), -163.07 – -163.31 (m, 2F), -163.61 – -163.82 (m, 2F).

^{13}P{^{1}H} NMR (202.30 MHz, Chloroform-*d*) δ 27.8 (s).

[PdBr(C$_6$F$_5$)(XPhos)] (8)

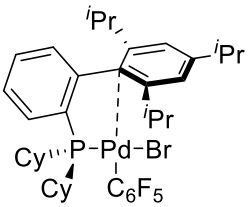

In a flame-dried Schlenk, *cis*-[Pd(CH$_2$TMS)$_2$(COD)] (97.5 mg, 0.167 mmol), XPhos (86.2 mg, 0.177 mmol) and C$_6$F$_5$Br (**1n**, 42 µL, 0.33 mmol) were dissolved in 3 mL of THF. The solution was stirred for 3 hours at room temperature, *n*-hexane (3 mL) was added, and the mixture was removed under vacuum. The yellowish residue obtained was sonicated with *n*-hexane (*it may be fully redissolved*) and a precipitate appears upon stirring (*overnight stirring is recommended*). It was filtered under air and washed with *n*-pentane (3 x 5 mL). The solid obtained was dried under vacuum affording the title compound as a yellowish solid (80.7 mg, 57 % yield).

In solution this solid shows an equilibria between several species, as observed by low temperature NMR (*vide infra, fluxionality of [PdBr(C$_6$F$_5$)(XPhos)]*) which precluded a detailed characterization.

HRMS (EI) Calculated for C$_{39}$H$_{49}$F$_5$PPd [M-Br]$^+$: 749.2536. Experimental [M-Br]$^+$: 749.2556.

[PdBr(p-C$_6$H$_4$F)(XPhos)] (9)

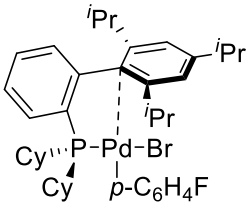

This complex was prepared following the procedure described to obtain **8** employing 1-bromo-4-fluorobencene (**1f**, 30 µL, 0.27 mmol), The title compound was obtained as a colourless solid (69.2 mg, 67 % yield). The complex is observed as a *cis*/*trans* isomer mixture in solution. (*Major isomer* 88%, *minor isomer* 12%, based on ^{19}F and ^{31}P NMR)

HRMS (EI) Calculated for C$_{39}$H$_{53}$FPPd [M-Br]$^+$: 677.2913. Experimental [M-Br]$^+$: 677.2935.

^{1}H NMR (499.72 MHz, Chloroform-*d, only for major isomer*) δ 7.66 (td, J = 6, 3 Hz, 1H), 7.45 – 7.39 (m, 2H), 7.13 (s, 2H), 6.99 – 6.93 (m, 2H), 6.87 (dt, J = 6, 3 Hz, 1H), 6.77 – 6.68 (m, 2H), 3.12 (hept, J = 7 Hz, 1H), 2.44 (hept, J = 7 Hz, 2H), 2.20 (dtd, J = 12, 10, 3 Hz, 2H), 1.96 (bs, 2H), 1.80 (d, J = 12 Hz, 2H), 1.75 – 1.65 (m, 6H), 1.59 (d, J = 7 Hz, 8H), 1.39 (d, J = 7 Hz, 6H), 1.24 – 1.08 (m, 6H), 0.89 (d, J = 7 Hz, 6H), 0.74 – 0.56 (m, 2H).

^{19}F NMR (470.17 MHz, Chloroform-*d*) δ -122.64 – -122.75 (m, *minor isomer*), -122.78 – -122.90 (m, *major isomer*).

^{13}P{^{1}H} NMR (202.30 MHz, Chloroform-*d*) δ 28.5 (d, J = 3 Hz, *minor isomer*), 26.5 (d, J = 3 Hz, *major isomer*).

Fluxionality of [PdBr(C_6F_5)(XPhos)] (8)

A solution of **8** in $CDCl_3$ was analysed by ^{19}F and ^{31}P NMR at room temperature. When a closer look to the ortho fluorine region of the C_6F_5 moiety is taken in the ^{19}F spectra, it is possible to distinguish a broad signal (-112.1 ppm) and two doublets (-114.8 and -115.8 ppm) in an integer ratio of 45:4:1 (Figure 12, top). This behaviour is also observed for the para and meta fluorine atoms of the C_6F_5 moiety, although signal overlapping precludes a clean analysis of this region of the spectra. To obtain more information, ^{19}F and ^{31}P NMR spectra acquisition was performed at 233 K (Figure 13). At this temperature, the broad signal observed in the ortho region of the ^{19}F NMR at room temperature is resolved in at least 5 sharp signals (mainly doublets and triplets), along with the doublets previously observed at room temperature (Figure 12, bottom).

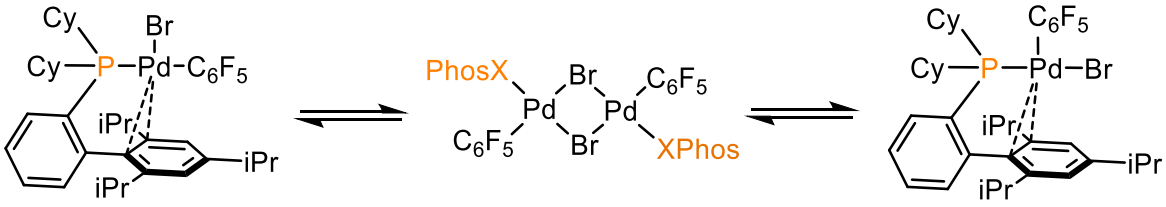

Scheme 6. Dynamic equilibria of **8** in solution. For clarity, only one dimeric species is shown and ^{i}Pr substituents have been omitted in it.

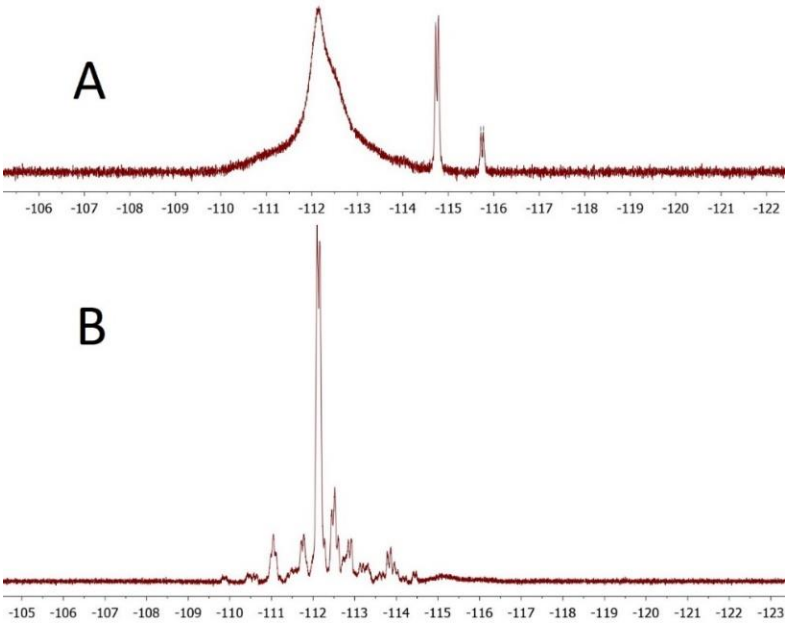

Figure 12. Ortho fluorine spectra region of **8** at 298 K (top, A) and 233 K (bottom, B).

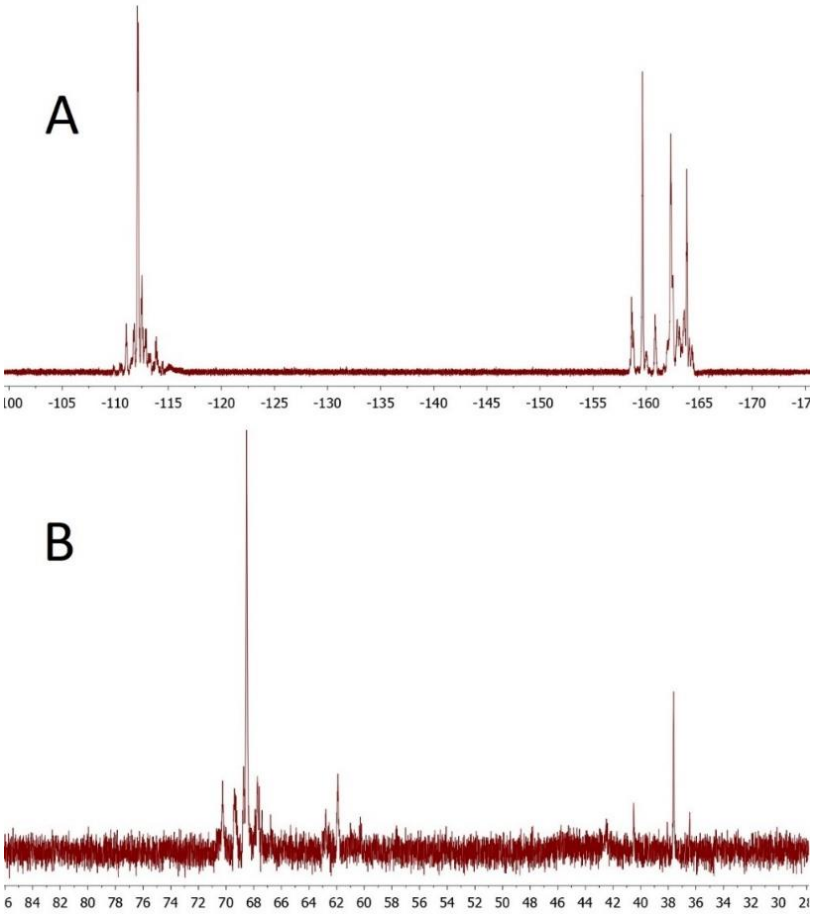

Figure 13. ^{19}F (top, A) and ^{31}P (bottom, B) NMR spectra of **8** at 233 K in $CDCl_3$.

Stoichiometric studies

C–H activation

In a flame-dried Schlenk under N_2 atmosphere, [CuCl(IPr)] (15.8 mg, 32.4 µmol), Cs_2CO_3 (10.6 mg, 32.4 µmol) and C_6F_5H (5.0 µL, 45.0 µmol) were dissolved in 1 mL of dioxane. The solution was stirred at 40 °C. After 2 hours, an aliquot of the mixture was analysed by ^{19}F NMR, showing full conversion to the C–H activation product, [Cu(C_6F_5)(IPr)] (**5**) (Figure 14).

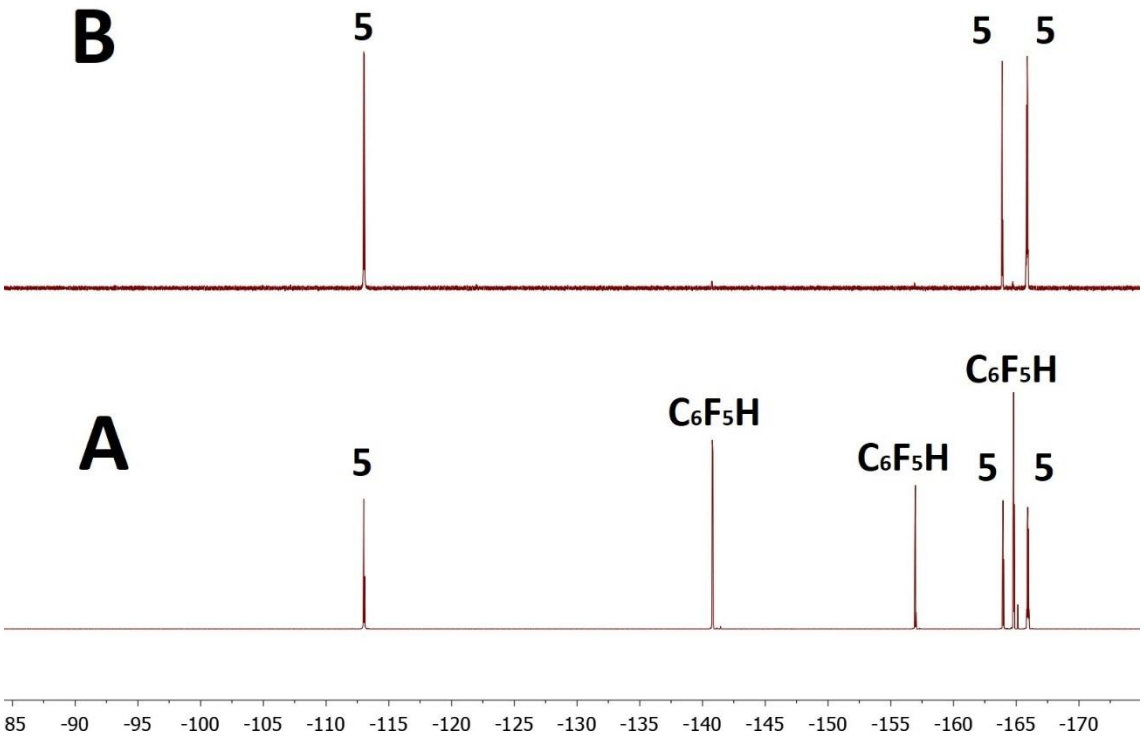

Figure 14. ^{19}F NMR spectra after 1 hour (A, bottom) and 2 hours (B, top) of the C–H activation experiment.

Reductive elimination from *cis*-[Pd(C_6F_5)$_2$(XPhos)] (7) and oxidative addition to [PdBr(C_6F_5)(XPhos)] (8)

In a flame-dried Schlenk under N_2 atmosphere, **7** (7.10 mg, 7.75 µmol) and C_6BrF_5 (**1n**, 3.0 µL, 23.2 µmol, 3 eq) were dissolved in 500 µL of dioxane. The mixture was stirred in an oil bath at 80 °C. The reaction was followed by ^{19}F and ^{31}P NMR. After 180 min, signals of **7** had fully disappeared and only signals of **8** were observed in the ^{19}F NMR spectra (Figure 15).

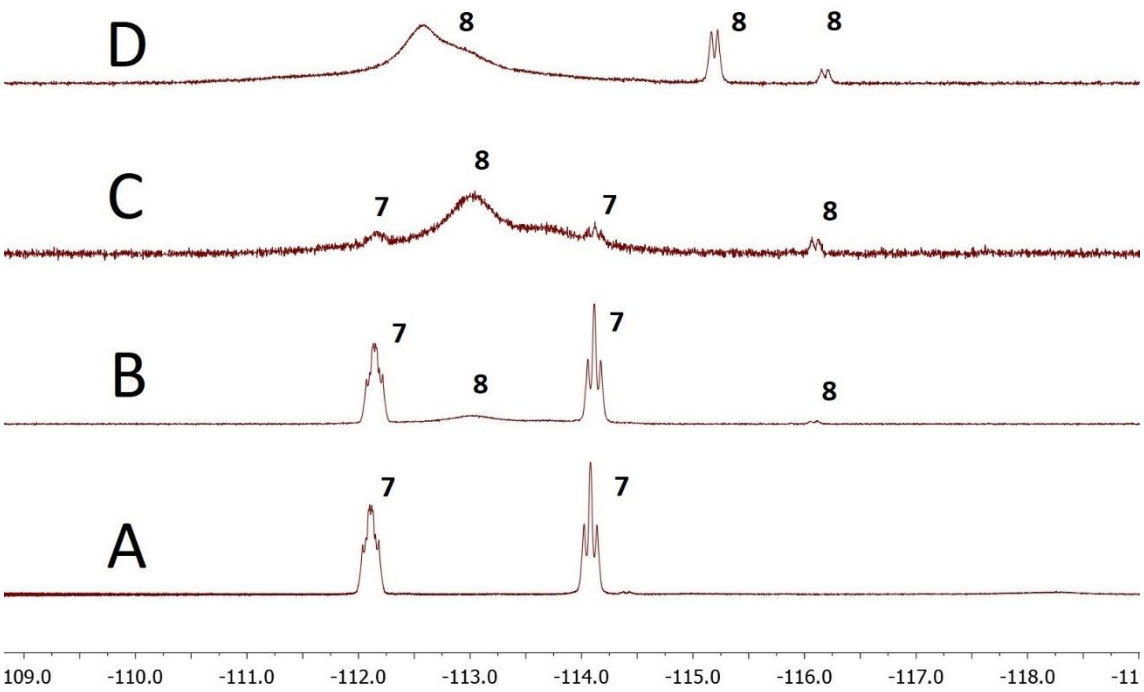

Figure 15. Ortho fluorine region of the ^{19}F NMR spectra at 298 K. A (bottom): mixture of cis-[Pd(C_6F_5)$_2$(XPhos)] (**7**) and C_6F_5Br (**1n**) at room temperature; B (middle) mixture after 60 min at 80 °C; C (middle) mixture after 120 min at 80 °C; D (top) mixture after 180 min at 80 °C.

Cu to Pd aryl transmetalation

In a flame-dried NMR tube under N_2 atmosphere, [Cu(C_6F_5)(IPr)] (**5**) (5.00 mg, 8.1 µmol) and the corresponding oxidative addition Pd complex, **8** or **9** (1 eq, 8.1 µmol), were dissolved in 500 µL of dioxane at room temperature. The tube was vigorously shaken and ^{19}F and ^{31}P NMR spectra were acquired.

When complex **8** was employed, disappearance of its broad signals and formation of the signals corresponding to *cis*-[Pd(C_6F_5)$_2$(XPhos)] (**7**) was observed (Figure 16). In contrast, for **9** not only transmetalation but also reductive elimination took place. Hence, formation of the coupling product *p*-C_6H_4F–C_6F_5 (**3fn**) was observed. This transformation finished in less than 2 hours at room temperature, when no remaining **5** was observed (Figure 17, top).

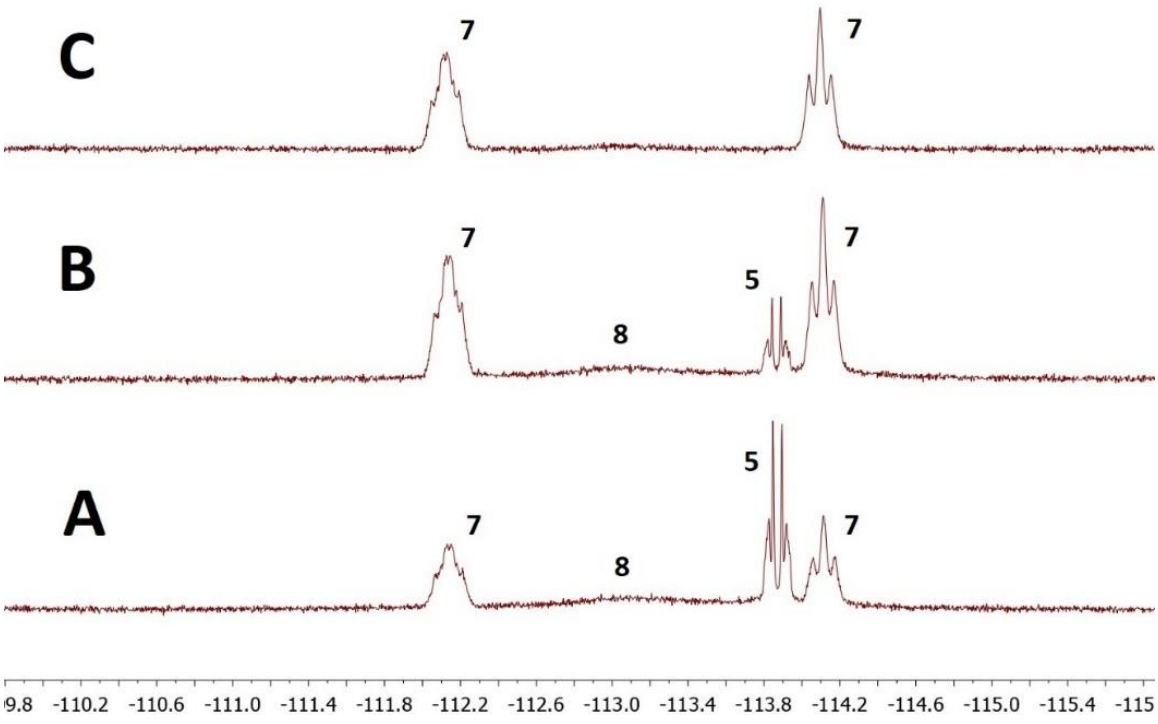

Figure 16. ^{19}F NMR spectra of the reaction between **8** and **5** in dioxane at 298 K. A (bottom): acquisition after tube preparation. B (middle): acquisition after 2 hours at 298 K. C (top) acquisition after 4 hours at 298 K.

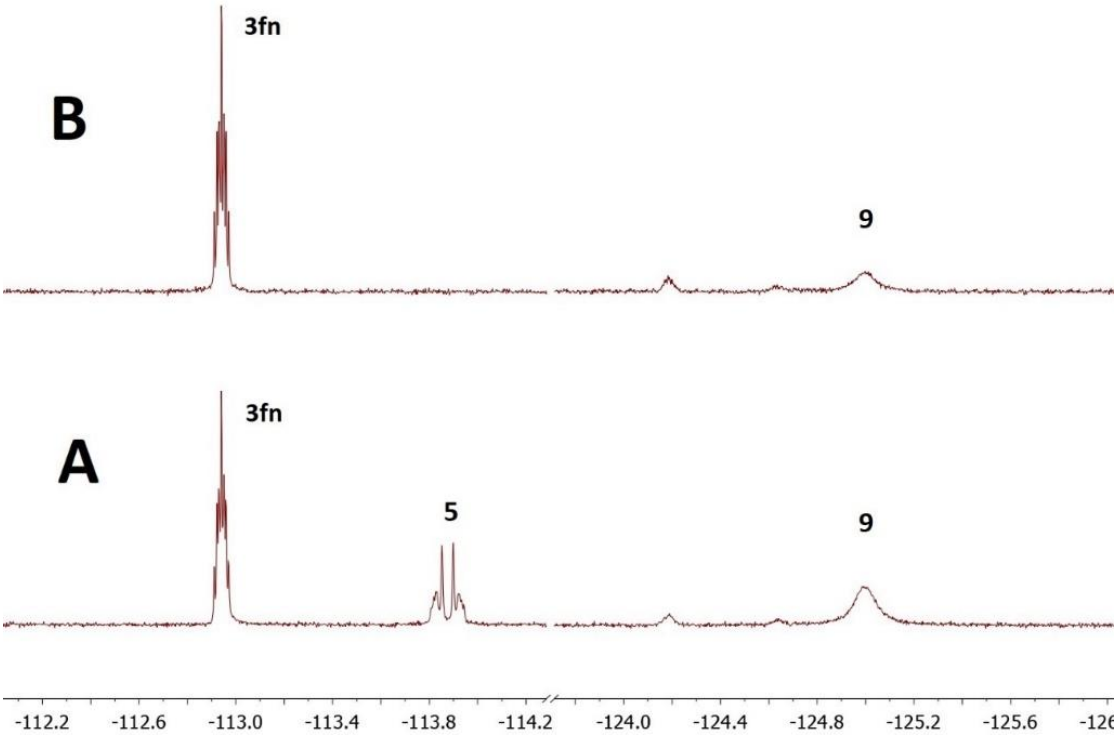

Figure 17. ^{19}F NMR spectra of the reaction between **9** and **5** in dioxane at room temperature. A (bottom): acquisition after tube preparation. B (top): acquisition after 2 hours at 298 K.

Detection of reaction intermediates

Following the general procedure for catalysis, when an aliquot of the reaction employing C_6BrF_5 (**1n**) and C_6F_5H (**2n**) was analysed by NMR before hydrolysis, signals of complexes **5** and **7** were detected in the ^{19}F NMR spectra (Figure 18). This observation suggests that reductive elimination is the rate determining step in this reaction.

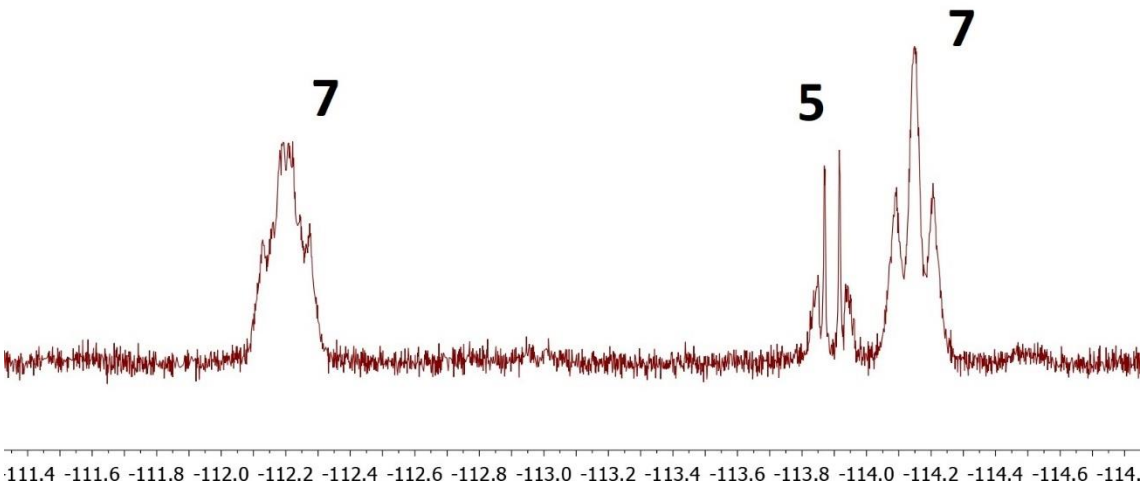

Figure 18. Ortho region of the ^{19}F NMR spectra of an aliquot of the catalysis employing 1n and 2n as substrates before hydrolysis.

KIE experiments

KIE experiments were performed by measuring the ratio of product formation between the activation of deuterated and protic reagents in experiments carried out in separated vessels (Figure 19, Table 6). KIE experiments were conducted following the general procedure for catalysis. α,α,α-trifluorotoluene was added as internal standard. C_6F_5–D was employed instead of C_6F_5–H in the deuterium labelled experiments.

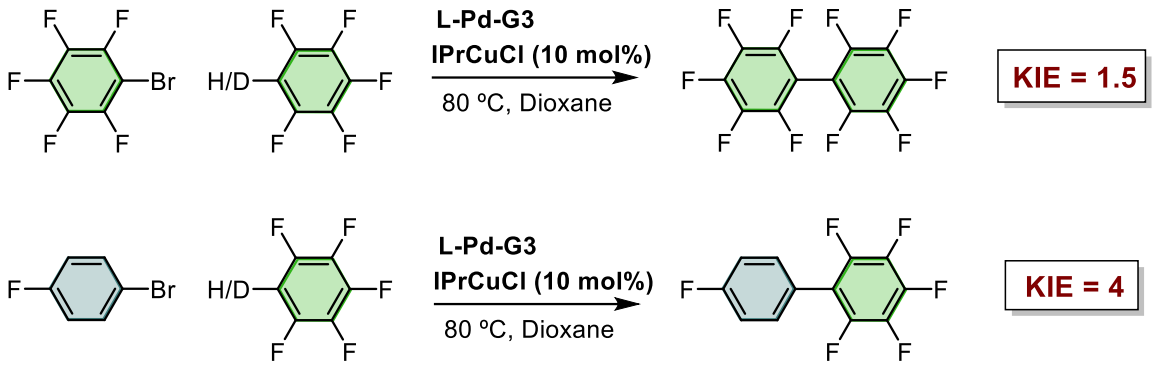

Figure 19. KIE experiments employing two different aryl bromides (**1f**, **1n**).

Table 6. Product formation in the KIE experiments.

Aryl Bromide	Arene	Time (h)	[Product] (mol L^{-1})	Product Yield (%)	$KIE_{H/D}$
1f	**2n**	1	0.032	10.1	4.0
1f	**2n-*D***	1	0.008	2.5	
1f	**2n**	3	0.168	52.4	4.0
1f	**2n-*D***	3	0.042	13.2	
1n	**2n**	3	0.036	11.2	1.5
1n	**2n-*D***	3	0.023	7.4	

X-ray crystallographic data

A crystal was attached to a glass fiber and transferred either to an Agilent Supernova diffractometer with an Atlas CCD area detector (Valladolid University facilities). The crystal was kept at constant temperature during data collection. Data collection was performed with Mo-Kα radiation (0.71073 Å). Data integration, scaling and empirical absorption correction were carried out using the CrysAlisPro program package. Using Olex2, the structure was solved with the olex2.solve structure solution program and refined with ShelX program. The non-hydrogen atoms were refined anisotropically and hydrogen atoms were placed at idealized positions and refined using the riding model. Refinement proceeded smoothly to give the residuals shown in CCDC contains the supporting crystallographic data for this paper. These data can be obtained free of charge at www.ccdc.cam.ac.uk/conts/retrieving.html [or from the Cambridge Crystallographic Data Centre, 12, Union Road, Cambridge CB2 1EZ, UK; fax: (internat.) +44-1223/336-033;

Identification code	**3bn**	**3fn**	**3gn**
CCDC deposition N°	2131398	2131399	2131400
Empirical formula	$C_{12}H_3F_7$	$C_{12}H_4F_6$	$C_{13}H_4F_8$
Formula weight	280.14	262.15	312.16
Temperature/K	294	294	294
Crystal system	triclinic	monoclinic	monoclinic
Space group	P-1	$P2_1/c$	$P2_1/c$
a/Å	7.3590(9)	13.3244(14)	14.5626(17)
b/Å	7.5748(9)	5.9453(5)	5.8525(7)
c/Å	9.8836(10)	13.0908(15)	14.0383(11)
α/°	75.019(9)	90	90
β/°	79.707(9)	108.653(13)	93.599(10)
γ/°	78.279(10)	90	90
Volume/Å^3	516.46(11)	982.55(19)	1194.1(2)
Z	2	4	4
ρ_{calc}g/cm^3	1.801	1.772	1.736
μ/mm^{-1}	0.194	0.183	0.189
F(000)	276	520	616
Crystal size/mm^3	0.539 × 0.491 × 0.082	0.744 × 0.479 × 0.189	0.423 × 0.329 × 0.102
Radiation	MoKα (λ = 0.71073)	MoKα (λ = 0.71073)	Mo Kα (λ = 0.71073)
2Θ range for data collection/°	6.674 to 58.896	7.576 to 58.966	6.614 to 59.4
Index ranges	-9 ≤ h ≤ 9, -7 ≤ k ≤ 9, -12 ≤ l ≤ 13	-18 ≤ h ≤ 14, -7 ≤ k ≤ 5, -12 ≤ l ≤ 17	-19 ≤ h ≤ 16, -8 ≤ k ≤ 4, -14 ≤ l ≤ 19
Reflections collected	4325	4255	5001
Independent reflections	2392 [R_{int} = 0.0258, R_{sigma} = 0.0517]	2292 [R_{int} = 0.0346, R_{sigma} = 0.0526]	2778 [R_{int} = 0.0289, R_{sigma} = 0.0508]
Data/restraints/parameters	2392/0/172	2292/0/163	2778/0/227
Goodness-of-fit on F^2	1.066	0.963	1.03
Final R indexes [I>=2σ (I)]	R_1 = 0.0504, wR_2 = 0.1023	R_1 = 0.0581, wR_2 = 0.1328	R_1 = 0.0532, wR_2 = 0.1182
Final R indexes [all data]	R_1 = 0.1160, wR_2 = 0.1472	R_1 = 0.1060, wR_2 = 0.1862	R_1 = 0.1408, wR_2 = 0.1764
Largest diff. peak/hole / e Å^{-3}	0.16/-0.23	0.35/-0.37	0.16/-0.21

Identification code	$[Pd(C_6F_5)_2(XPhos)]$ (**7**)
CCDC deposition N°	2131401
Empirical formula	$C_{45}H_{49}F_{10}PPd$
Formula weight	917.16
Temperature/K	294
Crystal system	monoclinic
Space group	$P2_1/c$
a/Å	20.2800(5)
b/Å	11.8689(3)
c/Å	17.7116(4)
α/°	90
β/°	104.392(2)
γ/°	90
Volume/Å^3	4129.42(18)
Z	4
ρ_{calc}g/cm^3	1.475
μ/mm^{-1}	0.565
F(000)	1880
Crystal size/mm^3	0.286 × 0.177 × 0.145
Radiation	Mo Kα (λ = 0.71073)
2Θ range for data collection/°	6.826 to 59.26
Index ranges	-25 ≤ h ≤ 27, -16 ≤ k ≤ 15, -15 ≤ l ≤ 23
Reflections collected	17887
Independent reflections	9636 [R_{int} = 0.0289, R_{sigma} = 0.0553]
Data/restraints/parameters	9636/1/542
Goodness-of-fit on F^2	1.045
Final R indexes [I>=2σ (I)]	R_1 = 0.0441, wR_2 = 0.0775
Final R indexes [all data]	R_1 = 0.0837, wR_2 = 0.0987
Largest diff. peak/hole / e Å^{-3}	0.44/-0.48

CHAPTER II: Cu^{I} activation of C–X bonds: bimolecular vs. unimolecular reaction mechanism

2.1 Introduction

Copper catalysed cross-coupling reactions to form C–C or C–E (heteroatom) bonds is nowadays one of the most powerful tools in synthetic chemistry.[61,62,63,64,65] The Ullman C–C and C–N cross-coupling reactions (Figure 20) were discovered over a century ago and their development has really operated over the past twenty-five years. These types of couplings have opened up a large number of possibilities within organic chemistry because they are capable of generating bonds that are difficult to build by other ways.[66]

Traditionally, two steps are commonly present in copper catalysed cross-coupling catalytic cycles, the oxidative addition and the reductive elimination, although other processes such as ligand substitution or transmetalations may occur. (Figure 20).

---

[61][61] Guo, X.-X.; Gu, D.-W.; Wu, Z.; Zhang, W. Copper-Catalyzed C−H Functionalization Reactions: Efficient Synthesis of Heterocycles. *Chem. Rev*. **2015**, *115*, 1622–1651. DOI: 10.1021/cr500410y.

[62] Evano, G.; Blanchard, N.; Toumi, M. Copper-Mediated Coupling Reactions and Their Applications in Natural Products and Designed Biomolecules Synthesis. *Chem. Rev*. **2008**, *108*, 3054–3131. DOI: 10.1021/cr8002505

[63] Trammell, R.; Rajabimoghadam, K.; Garcia-Bosch, I. Copper-Promoted Functionalization of Organic Molecules: From Biologically Relevant Cu/O Model Systems to Organometallic Transformations. *Chem. Rev*. **2019**, *119*, 2954–3031. DOI: 10.1021/acs.chemrev.8b00368.

[64] Allen, S. E.; Walvoord, R. R.; Padilla-Salinas, R.; Kozlowski, M. C. Aerobic Copper-Catalyzed Organic Reactions. *Chem. Rev*. **2013**, *113*, 6234–6458. DOI: 10.1021/cr300527g.

[65] Reymond, S.; Cossy, J. Copper-Catalyzed Diels-Alder Reactions. *Chem. Rev*. **2008**, *108,* 5359–5406 DOI: 10.1021/cr078346g.

[66] Cheng, L.-J.; Mankad, N. P. C–C and C–X Coupling Reactions of Unactivated Alkyl Electrophiles Using Copper Catalysis. *Chem. Soc. Rev.* **2020**, *49*, 8036–8064. DOI: 10.1039/d0cs00316f

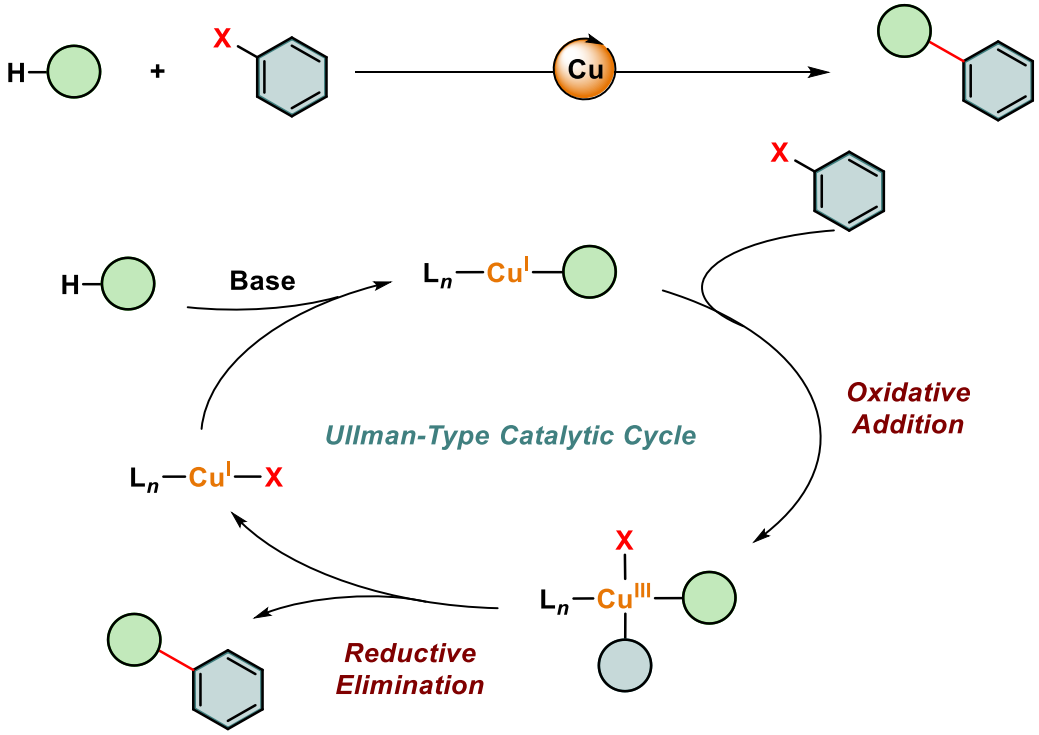

Figure 20. Mechanism of Ullman-Type catalytic cycle.

Exhaustive studies of the mechanism of Cu^I-based cross-coupling reactions have provided strong evidence that oxidative addition to a Cu^I complex to form a formally Cu^{III} intermediate is the rate limiting step (*rds*) and is followed by facile reductive elimination to furnish the coupled product and recovering the catalyst.[67,68,69,70,71,72] On this way, Lan *et al*. investigated whether the Cu^{III} intermediate is really necessary in the catalytic cycle after an oxidative addition process.[73] Different reaction paths were planted in cross-coupling reactions catalysed by different copper complexes.

---

[67] Yu, H.-Z.; Jiang, Y.-Y.; Fu, Y.; Liu, L. Alternative Mechanistic Explanation for Ligand-Dependent Selectivities in Copper-Catalyzed N-and O-Arylation Reactions. *J. Am. Chem. Soc.* **2010**, *132*, 18078–18091 DOI: 10.1021/ja104264v

[68] Lefè, G.; Grégory, G.; Tlili, A.; Adamo, C.; Taillefer, M.; Ciofini, I.; Jutand, A. Contribution to the Mechanism of Copper-Catalyzed C–N and C–O Bond Formation. *Organometallics* **2012**, *31*, 7694–7707. DOI: 10.1021/om300636f.

[69] Tye, J. W.; Weng, Z.; Giri, R.; Hartwig, J. F. Copper(I) Phenoxide Complexes in the Etherification of Aryl Halides. *Angew. Chem. - Int. Ed.* **2010**, *49*, 2185–2189. DOI: 10.1002/ANIE.200902245

[70] Zhang, S.-L.; Liu, L.; Fu, Y.; Guo, Q.-X. Theoretical Study on Copper(I)-Catalyzed Cross-Coupling between Aryl Halides and Amides. *Organometallics* **2007**, *26*, 4546–4554. DOI: 10.1021/om700573h.

[71] Cristau, H. J.; Cellier, P. P.; Spindler, J. F.; Taillefer, M. Highly Efficient and Mild Copper-Catalyzed N- and C-Arylations with Aryl Bromides and Iodides. *Chem. - Eur. J.* **2004**, *10*, 5607–5622. DOI: 10.1002/CHEM.200400582.

[72] Tye, J. W.; Weng, Z.; Johns, A. M.; Incarvito, C. D.; Hartwig, J. F. Copper Complexes of Anionic Nitrogen Ligands in the Amidation and Imidation of Aryl Halides. *J. Am. Chem. Soc.* **2008**, *130*, 9971–9983. DOI: 10.1021/ja076668w.

[73] Li, S.-J.; Lan, Y. Is Cu(III) a Necessary Intermediate in Cu-Mediated Coupling Reactions? A Mechanistic Point of View. *Chem. Commun.* **2020**, *56*, 6609–6619. DOI: 10.1039/d0cc01946a.

It is discovered that in many cases, generating a Cu^{III} intermediate is usually thermodynamically unfavorable, preventing the classical oxidative addition. That is why reaction pathways such as coproportion between Cu^{I} and Cu^{III}, or radical species can be possible.

The oxidative addition step is usually thought of as a concerted double-electron oxidative addition process but can be organized into different types, following by the cross-coupling process, as we can see in Figure 21:

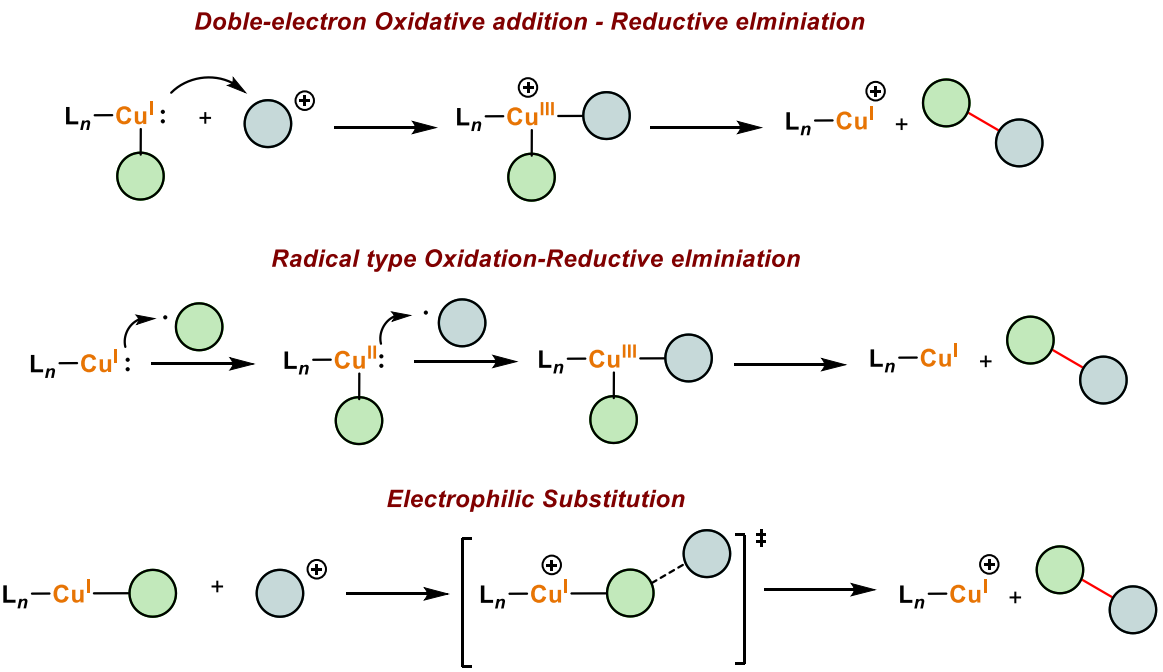

Figure 21. Possible modes for copper-mediated coupling reactions proposed by Lan and co-workers.

a) Copper-mediated coupling reaction by double-electron oxidative addition–reductive elimination

The typical catalytic cycle by double-electron oxidative addition–reductive elimination is often used to understand the mechanism of copper catalysed Ullmann-type couplings. A clear example of this type of reaction is C–S cross-coupling of thioacetate with aryl halides.[74] The oxidative addition–reductive elimination mechanism via an unstable Cu^{III} intermediate is energetically more

[74] Soria-Castro, S. M.; Andrada, D. M.; Caminos, D. A.; Argüello, J. E.; Robert, M.; Peñéñory, A. B. Mechanistic Insight into the Cu-Catalyzed C–S Cross-Coupling of Thioacetate with Aryl Halides: A Joint Experimental-Computational Study. *J. Org. Chem.* **2017**, *82*, 11464–11473. DOI: 10.1021/acs.joc.7b01991

feasible than other possible mechanisms such as single electron transfer, halogen atom transfer, and σ-bond metathesis, that were also tested. The rapid reductive elimination process from this proposed Cu^{III} intermediates generates the desired products. This mechanism is favoured by reagents that can oxidize the metal center with a relatively simple cleavage of the bond involved, as is the case with aryl iodides.

The oxidative addition step is highly dependent on the geometry of the Cu^{I} complex (lineal, trigonal or tetrahedral) and the electron density of the metal center. Usually, electrondonating ligands, which increase the electron density at the metal center, facilitate this type of double-electron oxidative addition. In contrast with this hypothesis, Hartwig's group reported that reactions of aryl halides with Cu^{I} perfluoroalkyl complex with substituted bipyridine ligands, are faster for complexes with less electron-donating ligands than for those of more electron-donating ligands (Scheme 7).[75]

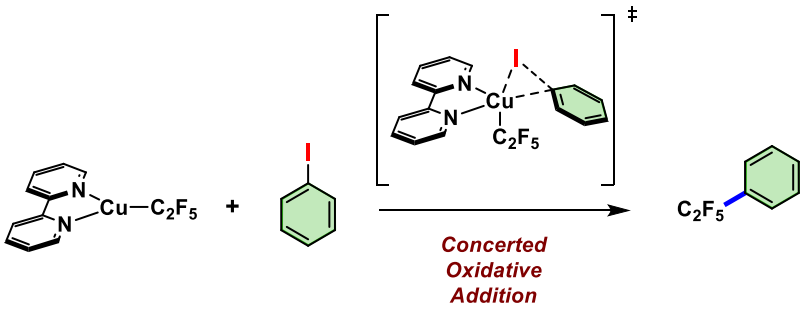

Scheme 7. Reaction between [Cu(bipy)(C_2F_5)] and Ar–I.

This effect contrasts with the trend of the electronic effects of ligands on the rate of oxidative addition of aryl halides previously reported,[12] and highlights the unusual behaviour of Cu^{I} complexes in this step. However, clear trend was observed between the computed free energies of activation and the experimental results. The computed free energy barriers of concerted oxidative addition of unsubstituted iodobenzene to [Cu(C_2F_5)(L)] (L= substituted bipyridines) ($\Delta G_{calc}^{\ddagger}$= 25 kcal/mol) were similar in magnitude to those determined experimentally from k_{obs} ($\Delta G_{expt}^{\ddagger}$=24 kcal/mol). On the other hand, no clear trend was observed between the computed free energies of activation and the σ_p values of the substituents on the bipy ligand.

[75] Kalkman, E. D.; Mormino, M. G.; Hartwig, J. F. Unusual Electronic Effects of Ancillary Ligands on the Perfluoroalkylation of Aryl Iodides and Bromides Mediated by Copper(I) Pentafluoroethyl Complexes of Substituted Bipyridines. *J. Am. Chem. Soc*. **2019**, *141*, 19458–19465. DOI: 10.1021/jacs.9b10540.

More recently, our group investigated the oxidative addition between perfluoroaryl Cu^{I} complexes with bipyridine ligand [Cu(Pf)(bipy)] and perfluoroaryl halide $C_6F_3Cl_2I$ (Rf–I),[76] represented in Scheme 8. This study presents a case in which the abundant Cu^{I} reagents reacts with Cu^{III} intermediates in an electron-transfer coproportionation reaction, followed by a fast transmetalation, and generates all possible products (two homocouplings (C_6F_5–C_6F_5; $C_6F_3Cl_2$–$C_6F_3Cl_2$) and the heterocoupling ($C_6F_3Cl_2$–C_6F_5)).

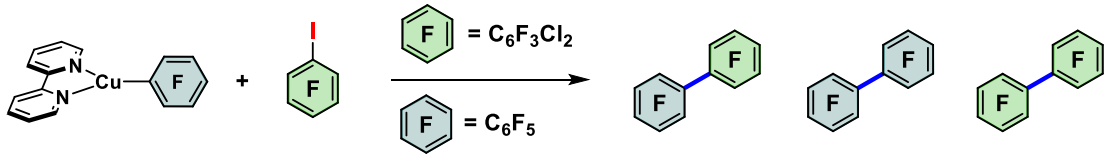

Scheme 8. Reaction between [Cu(bipy)(Pf)] and Rf–I. Pf=C_6F_5, Rf=$C_6F_3Cl_2$.

The oxidative addition process was calculated using DFT methos, and the Cu^{III} intermediate was generated by a concerted transition step, represented in Figure 22.

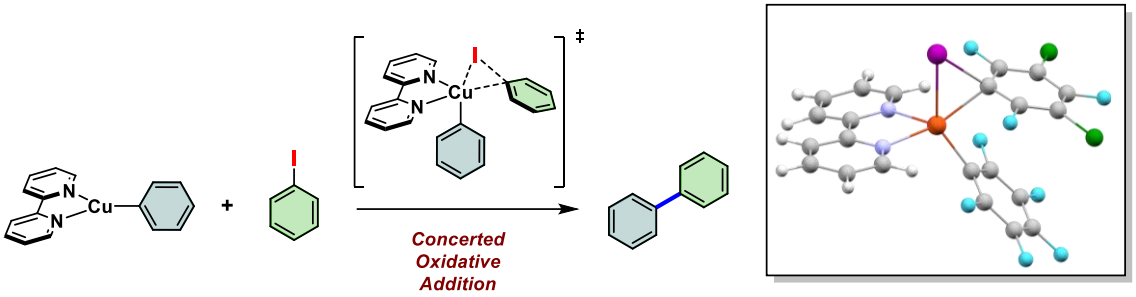

Figure 22. Representation of the concerted transition step for the oxidative addition of aryl iodide to [Cu(C_6F_5)(bipy)].

DFT calculations and kinetic experiments clearly show the easiness of the electron transfer and the transmetalation between different copper complexes. Heterocoupling product (Rf–Pf) follows the expected oxidative addition (O.A.)/reductive elimination (R.E.) pathway. Homocoupling products requires the presence of another copper complex to facilitates the aryl exchange. This interaction

[76] Lozano-Lavilla, O.; Gómez-Orellana, P.; Lledós, A.; Casares, J. A. Transmetalation Reactions Triggered by Electron Transfer between Organocopper Complexes. *Inorg. Chem.* **2022**, *18*, 11633–11639. DOI: 10.1021/acs.inorgchem.1c01595

generates a minimum-energy crossing point (MECP). DFT calculations show that the interaction between these Cu^{III} species and the starting Cu^{I} complex involves a Cu^{I}–Cu^{III} electron transfer (calculated by MECP) with the formation of an iodine bridge between the metals and a fast transmetalation takes place in a dimer in a triplet state between two Cu^{II} units, as we can see in Figure 23.

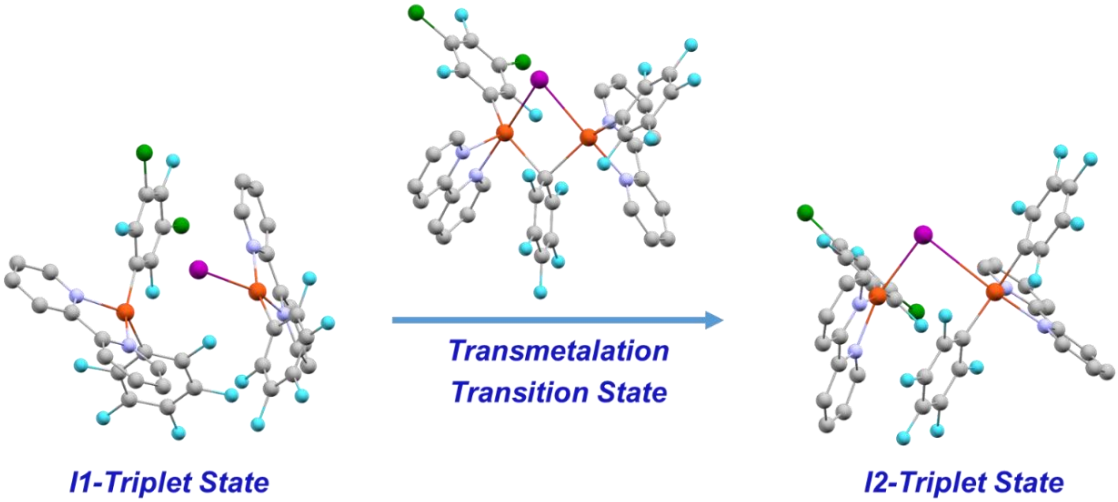

Figure 23. DFT calculations of the transmetalation step between 2 Cu^{II} in the triplet state.

More interestingly, when the oxidative addition was calculated for non-fluorinated aryls, the Cu^{III} intermediate was not found by DFT calculations. The oxidative addition/reductive elimination process occurs in the same step, and only the cross-coupling product was obtained. These results suggest that the reaction behaves as a nucleophilic attack of the copper complex to the C_{ipso} of the aryl iodide, in agreement with previous studies in other Cu^{I} systems.[76]

As we can observed in the examples commented previously, in the copper-mediated coupling reaction by two-electron oxidative addition/reductive elimination the oxidative addition step is always the *rds*. In general, it can be concluded that in this type of reaction, the highest energetic step is the oxidative addition, to form an unstable Cu^{III} intermediate, which undergoes a fast reductive elimination process, to generate the Cu^{I} complex.

Although mechanistically much remains to be explored in the field of oxidative additions pathways to organometallic Cu^{I} complexes, concerted oxidative addition

has been the most studied, especially in DFT calculations.[77,78,79,80,81,82,83] Within the large amount of bibliographic data that we can find, it is important to note that in most of the reactions, the limiting step is always the oxidative addition step, many times above the C–H activation or transmetalation reactions. It is therefore necessary to pay attention to the step that in most cases determines the total energy of the process.

b) Copper-mediated coupling reaction by radical-type oxidation.

Sometimes copper is mechanistically unpredictable because it can easily access to Cu^0, Cu^I, Cu^{II}, and Cu^{III} oxidation states allowing it to act through one or two-electron processes.[84] As a result, radical pathways can occur. Due to this, the existence of other pathways to give the oxidative addition process cannot be discarded.[85] The accepted mechanism of the copper mediated coupling reaction by radical-type oxidation is based on the formation of a Cu^{II} species from a Cu^I by oxidation with a R· radical. In this Cu^{II} intermediate, copper and the coordinated substituent show radical character. Therefore, another incoming radical R'· can react with copper to afford a Cu^{III} intermediate through a second radical oxidation. After rapid reductive elimination, the cross-coupling product is obtained with

---

[77] Tye, J. W.; Weng, Z.; Johns, A. M.; Incarvito, C. D.; Hartwig, J. F. Copper Complexes of Anionic Nitrogen Ligands in the Amidation and Imidation of Aryl Halides. *J. Am. Chem. Soc.* **2008**, *130*, 9971–9983. DOI: 10.1021/ja076668w

[78] Konovalov, A. I.; Lishchynskyi, A.; Grushin, V. V. Mechanism of Trifluoromethylation of Aryl Halides with $CuCF_3$and the Ortho Effect. *J. Am. Chem. Soc.* **2014**, *136*, 13410–13425. DOI: 10.1021/ja507564p.

[79] Deshmukh, K. M.; Madyal, R. S.; Qureshi, Z. S.; Gaikar, V. G.; Bhanage, B. M. Experimental and Theoretical Investigations of Consequence of Ionic Liquid Anion on Copper(I) Catalyzed Reaction of Aryl Iodide and Thiols. *Ind. Eng. Chem. Res.* **2013**, *52*, 4747–4757. DOI: 10.1021/ie3035338.

[80] Lefèvre, G.; Franc, G.; Adamo, C.; Jutand, A.; Ciofini, I. Influence of the Formation of the Halogen Bond ArX-N on the Mechanism of Diketonate Ligated Copper-Catalyzed Amination of Aromatic Halides. *Organometallics* **2012**, *31*, 914–920. DOI: 10.1021/om200952v.

[81] Zhang, S.; Ding, Y. Theoretical Study on Mechanism of Copper(I)-Catalyzed Cross-Coupling between Aryl Halides and Alkylamines. *Organometallics* **2011**, *30*, 633–641. DOI: 10.1021/om100996e

[82] Jones, G. O.; Liu, P.; Houk, K. N.; Buchwald, S. L. Computational Explorations of Mechanisms and Ligand-Directed Selectivities of Copper-Catalyzed Ullmann-Type Reactions. *J. Am. Chem. Soc.* **2010**, *132*, 6205–6213. DOI: 10.1021/ja100739h.

[83] Tye, J. W.; Weng, Z.; Johns, A. M.; Incarvito, C. D.; Hartwig, J. F. Copper Complexes of Anionic Nitrogen Ligands in the Amidation and Imidation of Aryl Halides. *J. Am. Chem. Soc.* **2008**, *130*, 9971–9983. DOI: 10.1021/ja076668w.

[84] Dong, X.-Y.; Li, Z.-L.; Gu, Q.-S.; Liu, X.-Y. Ligand Development for Copper Catalyzed Enantioconvergent Radical Cross-Coupling of Racemic Alkyl Halides. *J. Am. Chem. Soc*. **2022**, *144*, 17319–17329. https://doi.org/10.1021/jacs.2c06718

[85] Clark, A. J. Copper Catalyzed Atom Transfer Radical Cyclization Reactions. *Eur. J. Org. Chem.* **2016**, *13*, 2231–2243. DOI: 10.1002/ejoc.201501571

regeneration of the Cu^{I} species. For this type of reactions, the Xiao's work represents the first asymmetric propargylic radical cyanation through a dual photoredox and copper catalysis.[86] An organic photocatalyst serves to generate propargyl radicals and oxidise Cu^{I} species to Cu^{II}. Moreover, mechanistic investigations including experimental support and density functional theory calculations were performed to illustrate the reaction pathway and stereochemical results. This type of reactions are favoured by the use of reagents with great facility to form radicals, and ligands in the Cu complex capable of stabilizing them.

Furthermore, Chang and co-workers presented in 2020 the coupling of fluorinated aryls with alkenes through the good synergy of copper with C–H activation reactions and radical oxidation (Figure 24).[87] This is another awesome example of this kind of one electron oxidative addition and two electron reductive elimination. The study demonstrates for the first time that copper-catalysed selective alkylation of polyfluoroarenes is enabled by using hydrocarbons as radical precursor.

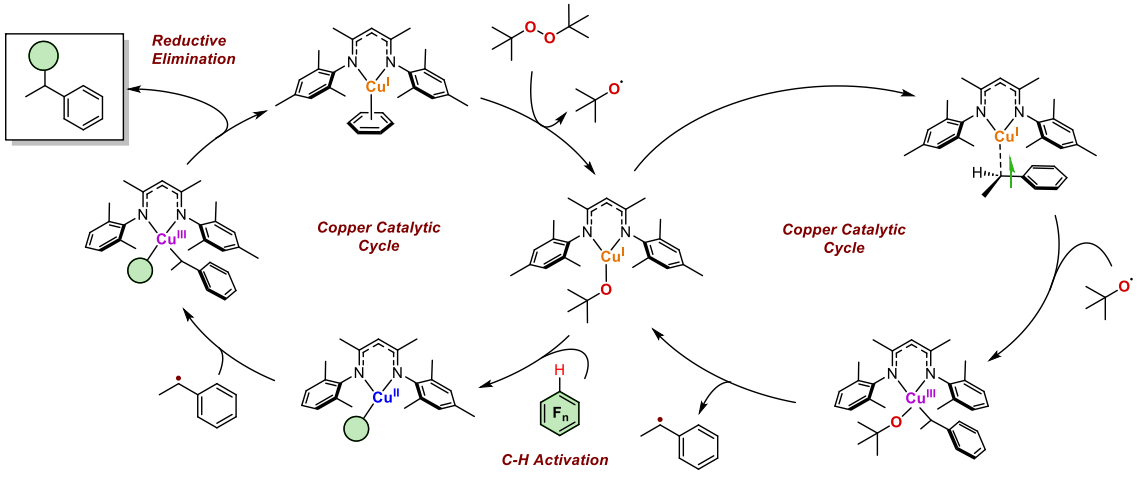

Figure 24. Mechanistic proposed pathway of the alkane–fluoroarene coupling reaction.

As we can see in Figure 24, two different catalytic cycles operate in this cross-coupling reaction. One of them is responsible for the C–H activation step by means of a Cu^{II}–O^{t}Bu complex. To obtain this complex, the use of an anionic diamine ligand

[86] Floriani, C.; Fiaschi, P.; Chiesi-Villa, A.; Guastini, C.; Zanazzi, P. F. A Reactive and Versatile Fourteen-Electron Copper(I) Fragment for Binding Carbon Monoxide, Isocyanides, and Phosphines: Synthesis, Crystal Structure, and Reactivity of (2-Methylquinolin-8-Olato) Copper(1) Derivatives. *J. Chem. Soc. Dalton Trans.* **1988**, *40*, 1607-1615. DOI: 10.1039/DT9880001607.

[87] Xie, W.; Heo, J.; Kim, D.; Chang, S. Copper-Catalyzed Direct C–H Alkylation of Polyfluoroarenes by Using Hydrocarbons as an Alkylating Source. *J. Am. Chem. Soc.* **2020**, *142*, 7487–7496. DOI: 10.1021/jacs.0c00169.

is essential. On the other hand, ditertbutyl peroxide is able to generate an R· radical of the hydrocarbon used, in presence of the copper catalyst. This radical recombines with the Cu^{II}–Ar^F complex to form a Cu^{III} complex, which undergoes a fast reductive elimination step, generating the Cu^I complex and the desired product. Besides, the radical oxidation is lower in energy than the double-electron oxidative addition. This kind of oxidation is also beneficial when anionic ligands are used, due to the facile oxidation to Cu^{III}, the only oxidation state that can undergo reductive elimination in copper chemistry.

If we pay attention to the results obtained by computational calculations, we observe that the reaction can be separated into two steps:

1) The first one would be the C–H activation part of the Csp^2–H and Csp^3–H bonds for the formation of the [$Cu(Ar^F)(L)$] complex and the benzyl radical, as we shown in Figure 24. Within the Csp^3–H activation different activation methods are studied. Direct hydrogen atom abstraction by a free *tert*-BuO· radical could be conceived, but copper-mediated activation was also considered. The observation of the primary kinetic isotope effects (KIE) of ethylbenzene implies that the irreversible cleavage of Csp^3 C–H bonds would be relevant to be rate-limiting, which was consistent with the computational investigations ($\Delta G^{\ddagger}$ = 26.0 kcal/mol) and the experimental results. In the other way, the Csp^2–H activation of fluoroarenes was previously reported for the same group for Cu-alkoxide,[88] and in this case provides the Cu^{II}–Ar^F intermediate with the same energetic barrier ($\Delta G^{\ddagger}$ = 25.9 kcal/mol).
2) The radical oxidation step to form the [$Cu^{III}(Alk)(Ar^F)(L)$] complex, unlike in the case of concerted double-electron oxidative additions, is not the limiting step, and occurs at low energy. Cu^{II}–Ar^F intermediate interacts with an alkyl radical to generate the proposed intermediate. Product will be released upon the reductive elimination of this Cu^{III} species along with the regeneration of active copper complex.

c) Copper-mediated coupling reaction by electrophilic substitution

[88] Xie, W.; Chang, S. [Cu(NHC)]-Catalyzed C–H Allylation and Alkenylation of Both Electron-Deficient and Electron-Rich (Hetero)Arenes with Allyl Halides. *Angew. Chem. Int. Ed.* **2016**, *55*, 1876–1880. DOI: 10.1002/anie.201510180

Traditionally, in the cross-coupling reactions catalysed by transition metals, the electrophile E^+ can be an oxidant that reacts with the transition metal to afford a high valent metal for further reductive elimination or another reductive process. However, in some cases, the electrophile E^+ can directly react with the metal-activated nucleophile by electrophilic substitution. This kind of reactions can also be considered when special reactants are used. This is the case of the Togni's reagent that can be an electrophile, which can react with either the copper species to achieve oxidation or bond with the nucleophile by electrophilic substitution.[89] The electron deficiency of the trifluoromethyl group (CF_3) results in the generation of an unstable high valent Cu^{III} intermediate. In contrast, the electrophilic substitution would be favourable.

Currently, another type of complexes widely used in copper chemistry for their great versatility are copper carbenes.[90] Copper(I) complexes with NHC ligands also activate efficiently C–X (X = halogen or pseudo-halogen) bonds in several catalytic processes, such as the C–H activation of several substrates, cross-coupling of aryl and allyl halides, or the carbonylative coupling of alkyl halides.[88,91,92] In addition, copper-NHC complexes are extremely efficient in bimetallic catalysis, for example, in Pd/Cu systems (demonstrated in Chapter I).[93,94,95,96] Although they are widely

[89] Ye, J. H.; Zhu, L.; Yan, S. S.; Miao, M.; Zhang, X. C.; Zhou, W. J.; Li, J.; Lan, Y.; Yu, D. G. Radical Trifluoromethylative Dearomatization of Indoles and Furans with CO_2. *ACS Catal.* **2017**, *7*, 8324–8330. DOI: 10.1021/acscatal.7b02533

[90] Lazreg, F.; Nahra, F.; Cazin, C. S. J. Copper-NHC Complexes in Catalysis. *Coor. Chem. Rev.* **2015**, *25*, 48–79. DOI: 10.1016/j.ccr.2014.12.019.

[91] Yu, D. H.; Shao, J. N.; He, R. X.; Li, M. Mechanism of Trifluoromethylation Reactions with Well-Defined NHC Copper Trifluoromethyl Complexes and Iodobenzene: A Computational Exploration. *Chin. Chem. Lett.* **2015**, *26*, 564–566. DOI: 10.1016/J.CCLET.2014.12.017

[92] Danopoulos, A. A.; Simler, T.; Braunstein, P. N-Heterocyclic Carbene Complexes of Copper, Nickel, and Cobalt. *Chem. Rev*. **2019**, *119*, 3730–3961. DOI: 10.1021/acs.chemrev.8b00505

[93] Rodionov, V. O.; Fokin, V. V.; Finn, M. G. Mechanism of the Ligand-Free CuI-Catalyzed Azide-Alkyne Cycloaddition Reaction. *Angew. Chem. Int. Ed.* **2005**, *44*, 2210–2215. DOI: 10.1002/anie.200461496

[94] Ponce-de-León, J.; Marcos-Ayuso, G.; Casares, J. A.; Espinet, P. Pd/Cu Bimetallic Catalysis to Access Highly Fluorinated Biaryls from Aryl Halides and Fluorinated Arenes. *Chem. Commun.* **2022**, *58*, 3146–3149. DOI: 10.1039/d2cc00141a

[95] Gooßen, L. J.; Deng, G.; Levy, L. M. Synthesis of Biaryls via Catalytic Decarboxylative Coupling. *Science* **2006**, *313*, 662–664. DOI: 10.1126/science.1128684

[96] Gooßen, L. J.; Rodríguez, N.; Linder, C.; Lange, P. P.; Fromm, A. Comparative Study of Copper- and Silver-Catalyzed Protodecarboxylations of Carboxylic Acids. *Chem. Cat. Chem.* **2010**, *2*, 430–442. DOI: 10.1002/cctc.200900277.

used, there are few mechanistic studies involving linear Cu^{I} complexes with carbene-type ligands.

As we have said before, the geometry and electronic density of the metal center is fundamental to understand how are the processes in which it participates. Consequently, we have started the study of linear copper complexes in copper mediated C–X activation reactions. We have tested the cross-coupling reactions of [Cu(NHC)R] (R = Pf = C_6F_5, or R = Rf = 3,5-$C_6F_3Cl_2$, NHC = DPI = 1,3-Diphenylimidazolium) with allyl, benzyl and aryl halides.

2.2 Results and discussion

Our investigations began with the synthesis of a series of pentafluorophenyl-copper(I) complexes ligated by NHC ligand (DPI = 1,3-Diphenylimidazolium), represented in Scheme 9.

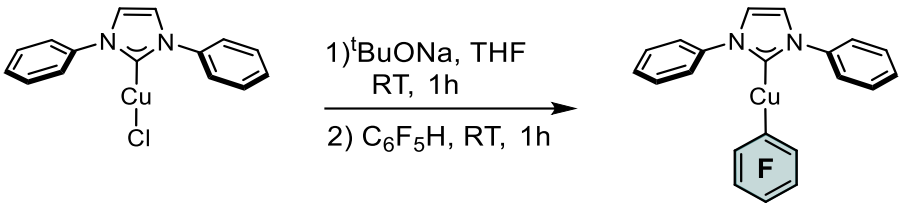

Scheme 9. General procedure for the synthesis of [Cu(Pf)(DPI)] **(1-Pf)**

These organometallic Cu^{I} complexes have been well known for many years and have been used for different types of reactions.[90] These complexes are sensitive to oxygen and water, and as most of the Cu^{I} complexes are in equilibrium with cationic and anionic species. Once we had synthesized the compounds, our research began with the study of the oxidative addition of different allyl halides. This reaction was studied by Chang and co-workers, and allows us to obtain initial data on the reactivity of these compounds.[88] We rapidly saw that the reaction rate between [Cu(Pf)(DPI)] and allyl bromide is extremely fast (5 minutes at 273 K). This reaction can be easily monitored by ^{19}F NMR and obtain kinetic constants. The same results are obtained when the chloro-derivative is used as reagent, as we can see in Figure 25. In the case of using the tosyl group (TsO) or benzyl bromide we also obtained the cross-coupling product. However, when allyl iodides were used as substrates, a mixture of cross-coupling and metathesis products have been observed in a 10-90 ratio.

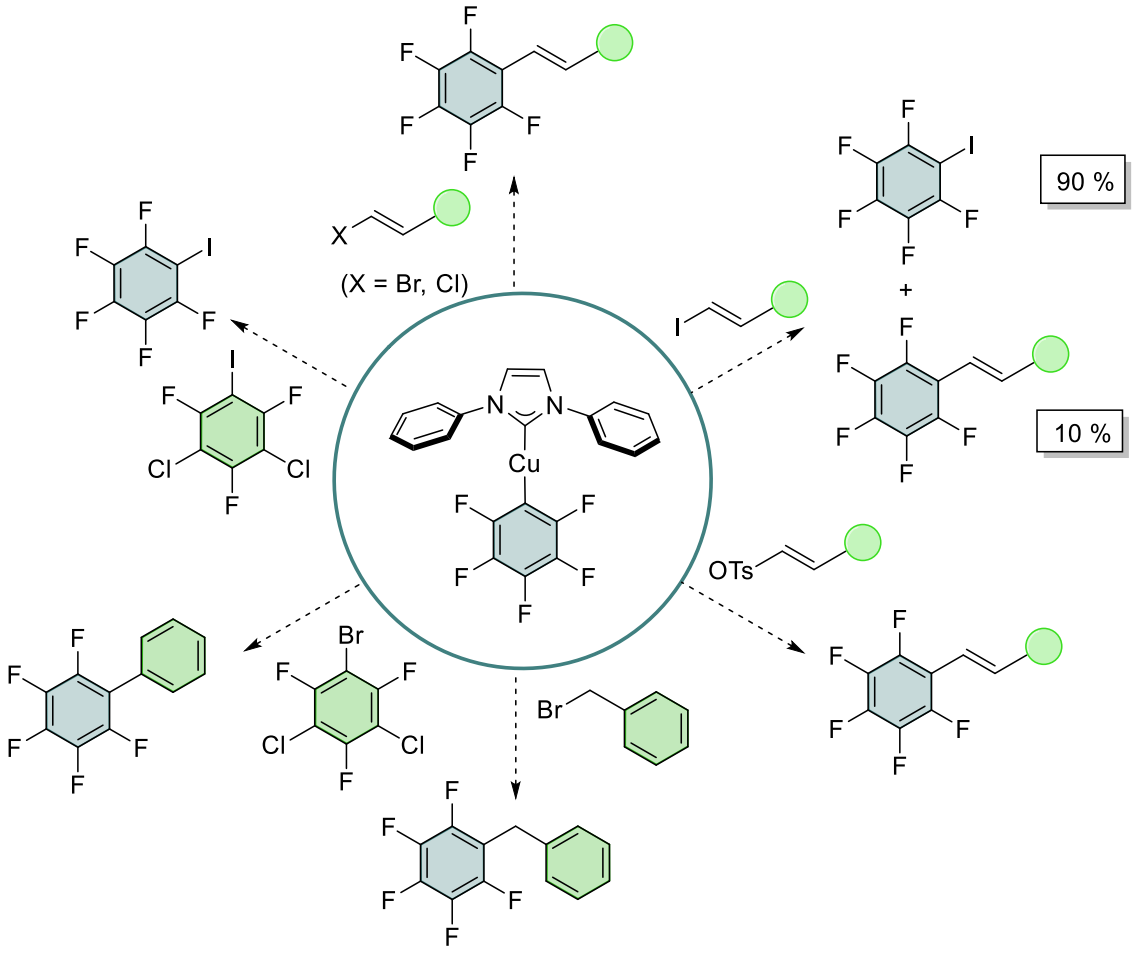

Figure 25. Qualitative results of cross-coupling reactions with different organic halides with the [Cu(Pf)(DPI)] (**1-Pf**) complex.

The reaction with allyl iodide is too fast to allow its study by NMR, but fortunately similar reactivity and selectivity, although with slower kinetics, was observed for fluorinated aryls: when Rf–I (Rf = $C_6F_3Cl_2$-3,5) is used the reaction yields Pf–I and [Cu(Rf)(NHC)] as only products. In contrast with the reaction with allyl iodide, no traces of cross-coupling product (Rf–Pf) was detected by Gs-Ms or NMR spectroscopy.

The metathesis reaction between the complexes [Cu(Pf)(DPI)] and Rf–I can be monitored by ^{19}F NMR (Figure 26). These two fluoroaryl rings (Pf and Rf) are practically identical in terms of their reactivity, thus the reaction can be considered a quasi-self-exchange system, simplifying the kinetic treatment of data. The kinetic study lead to a value of $\Delta G^{\ddagger}_{298} = 21$ kcal mol^{-1} for the reaction using COPASI software. For this kinetic simulation, the metathesis reaction and the hydrolysis of both Cu^{I} complexes were used as kinetic model.

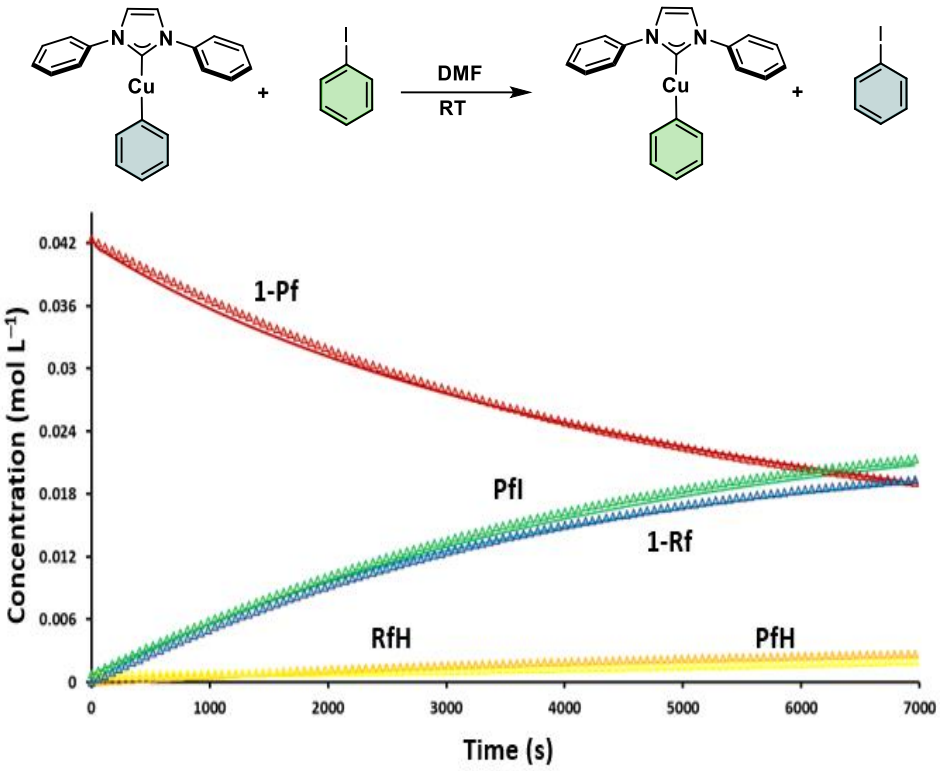

Figure 26. Experimental (Triangles) and best least square fitted (continuous line) concentration vs time plot of the formed species in the reaction of **1–Pf** ($4.2 \cdot 10^{-2}$ mol L^{-1}) with **Rf–I** ($4.2 \cdot 10^{-1}$ mol L^{-1}) in DMF at 298K. Blue aryl represents C_6F_5 and green aryl represents $C_6F_3Cl_2$-3,5.

To complete the investigation, we decided to do more kinetic studies and computational calculations to try to understand this unusual reaction pathway. To incorporate the computational calculations, an analysis of the possible reactions that can be studied was made. If we look at the stereochemistry, in order to give the metathesis product (Rf–I), it is essential that these groups are in *cis* arrangement in the assumed Cu^{III} intermediate that would be formed after the oxidative addition step. In contrast, the oxidative addition step which generate the two aryls in *cis* arrangement, will undergo the reductive elimination of the C–C bond formation. The possible reaction paths were examined using DFT calculations (details in Experimental Section), as we can observe in Figure 27.

The first one (***Cis* Pathway**) represents the classic double-electron oxidative addition and reductive elimination mechanism. This oxidative addition would leave the two aryls in *cis* arrangement in the Cu^{III} intermediate with a square plane geometry. This geometry is the most common in this type of reaction, which allows to continue with a facile reductive elimination step. This *cis* pathway was discarded

for several reasons. The first, and most important, is that no cross-coupling product is observed under the reaction conditions. Second, although the oxidative addition is the *rds.* as is common in this type of reaction, the total energy barrier is 23.9 kcal mol^{-1}, about 3 kcal mol^{-1} above the experimental value.

At this point, the second pathway of the reaction, ***trans* pathway**, is proposed. In this energy profile, we observe that the desired product would be formed, since the oxidative addition step would generate a Cu^{III} intermediate with the two aryls in *trans* arrangement. This would prevent the reductive elimination to give the cross coupling, generating the metathesis product. Besides, the Cu^{III} intermediate is hihgher in energy than in the case of *cis* pathway due to de *trans influence* of the fluorinated aryls. The high energy barrier of this energy profile made us to discard it as a possible explanation for the unusual behavior of this reaction.

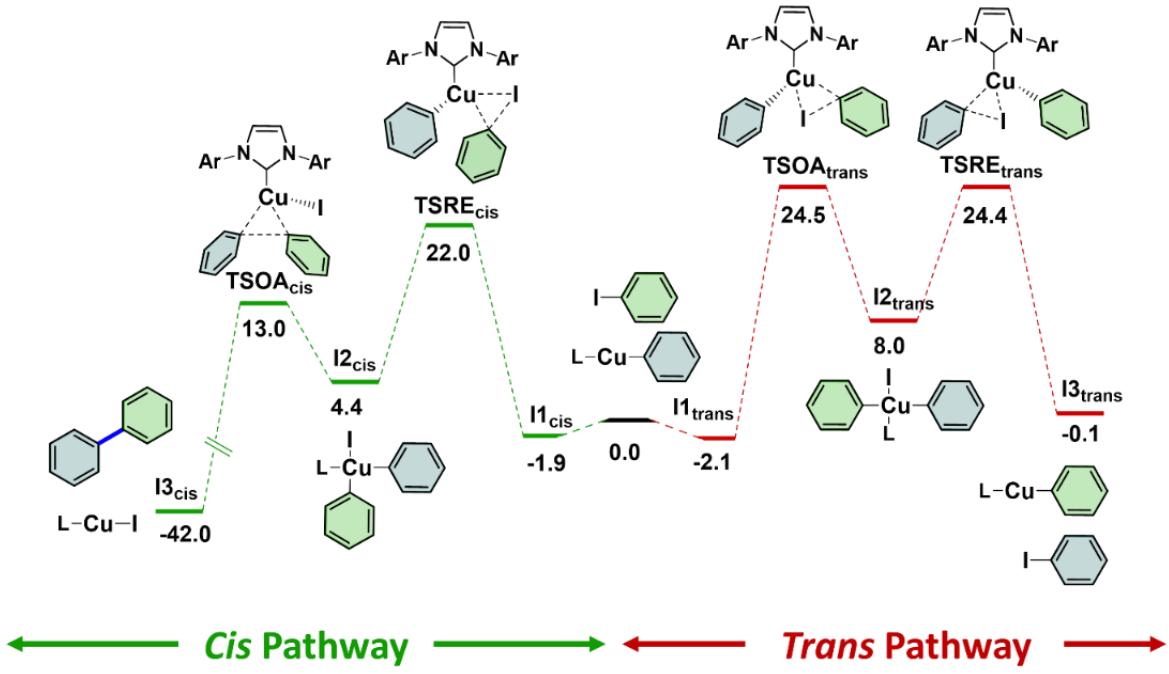

Figure 27. Calculated Gibbs energy profiles (kcal mol^{-1}) for the reaction between (**1–Pf**) and Rf–I. Color code: blue aryl = Pf; green aryl = Rf. (DFT at B3LYP-D3/BS2 level, SMD solvent model (DMF), 298 K).

Apart from these reaction pathways, transmetalation reactions were also calculated between several Cu^{II} or Cu^{I}/Cu^{III} complexes, due to the results obtained

in similar systems.[97] Different isomerization processes of the **I2$_{trans}$** complex were also tested to generate **I2$_{cis}$**. None of the hypotheses gave a satisfactory result.

Since the computational calculations failed to explain the behaviour of this reaction, more kinetic experiments were made. This kinetic study of the system showed that the reaction rate is first order on Rf–I and second order on [Cu(Pf)(DPI)] (**1-Pf**), and lead to a value of $\Delta G^{\ddagger}_{298}$ = 19.9 kcal mol^{-1} for the reaction. This result is of great importance, because there are not many examples of second order reactions in copper.[98,99,100] We explored the bimolecular pathways, which means association of two of the three reagents before the rate determining step (*rds*). Copper(I) organometallics complexes have the ability to produce dimers or oligomers in solution,[101,102] besides it could be also possible the coordination of Rf–I to the 14e$^-$ (**1-Pf**). These equilibria may be reached very fast in solution precluding the individual observation of ''[Cu(DPI)(Pf)]$_n$'' or {[Cu(DPI)(Pf)],I–Rf} species. In addition, a change in the chemical shift of the F$_{ortho}$ of Rf–I about 0.2 ppm is observed in ^{19}F NMR, which indicates a possible interaction in solution between the reactants.

To determine the nature of the involved species, diffusion-in-solution experiments (DOSY) were conducted.[103,104] These experiments may shed some light on a possible association between reactants ({[Cu(DPI)(Pf)],I–Rf}) or interactions between different copper complexes (''[Cu(DPI)(Pf)]$_n$''). First of all, a calibration line

---

[97] Lozano-Lavilla, O.; Gómez-Orellana, P.; Lledós, A.; Casares, J. A. Transmetalation Reactions Triggered by Electron Transfer between Organocopper Complexes. *Inorg. Chem.* **2022**, *18*, 11633–11639. DOI: 10.1021/ACS.INORGCHEM.1C01595

[98] Jin, L.; Tolentino, D. R.; Melaimi, M.; Bertrand, G. Isolation of Bis(Copper) Key Intermediates in Cu-Catalyzed Azide-Alkyne "Click Reaction." *Sci. Adv.* **2015**, *1*, e1500304. DOI: 10.1126/sciadv.1500304

[99] Presolski, S. I.; Hong, V.; Cho, S.-H.; Finn, M. G. Tailored Ligand Acceleration of the Cu-Catalyzed Azide–Alkyne Cycloaddition Reaction: Practical and Mechanistic Implications. *J. Am. Chem. Soc.* **2010**, *132*, 14570–14576. DOI: 10.1021/ja105743g.

[100] Haines, B. E.; Kawakami, T.; Kuwata, K.; Murakami, K.; Itami, K.; Musaev, D. G. Cu-Catalyzed Aromatic C-H Imidation with N-Fluorobenzenesulfonimide: Mechanistic Details and Predictive Models. *Chem. Sci.* **2017**, *8*, 988–1001. DOI: 10.1039/c6sc04145k.

[101] Pérez-Iglesias, M.; Lozano-Lavilla, O.; Casares, J. A. [Cu($C_6Cl_2F_3$)(tht)]$_4$: An Extremely Efficient Catalyst for the Aryl Scrambling between Palladium Complexes. *Organometallics* **2019**, *38*, 739–742. DOI: 10.1021/acs.organomet.8b00885.

[102] Yoshikai, N.; Nakamura, E. Mechanisms of Nucleophilic Organocopper(I) Reactions. *Chem. Rev*. **2012**, *112*, 2339–2372. DOI: 10.1021/cr200241f.

[103] Johnson Jr., C. S. Diffusion Ordered Nuclear Magnetic Resonance Spectroscopy: Principles and Applications. *Prog. Nucl. Magn. Reson. Spectrosc.* **1999**, *34*, 203–256. DOI: 10.1016/S0079-6565(99)00003-5.

[104] Dal Poggetto, G.; Antunes, V. U.; Nilsson, M.; Morris, G. A.; Tormena, C. F. ^{19}F NMR Matrix-Assisted DOSY: A Versatile Tool for Differentiating Fluorinated Species in Mixtures. *Magn. Reson. Chem.* **2017**, *55*, 323–328. DOI: 10.1002/mrc.4534

is prepared. To do this, the diffusion coefficient of substances whose speciation in solution is known was measured, using substances with different molecular weights and hydrodynamic radii, in order to obtain a calibration line as long and linear as possible, as shown in Table 7. Once the calibration line has been determined, the problem substances are chosen, in this case, the complexes **1-Pf**, Rf–I, Rf–Br and **1-Pf** + Rf–I.

For calibration line, different tubes were charged with similar quantities of the standard substances (0.0199 mmol) in dry DMF (0.5 mL). When the substance got dissolved, the sample was placed into the NMR probe thermostated at 273.15 K. An empirical relation between diffusion coefficient and molecular weight was established and its expressed as: $D = K \cdot M_W^{\alpha}$ where K is a molecule-dependent constant and α is a parameter that depends highly on the particle shape.[105,106,107,108] This equation was transformed into a linear equation in order to obtain the α parameter, as we can see in Figure 28, and the data is collected in Table 7.

$$\mathbf{\ln D = \ln K + \alpha \cdot \ln M_W}$$

[105] Neufeld, R.; Stalke, D. Accurate Molecular Weight Determination of Small Molecules via DOSY-NMR by Using External Calibration Curves with Normalized Diffusion Coefficients. *Chem. Sci.* **2015**, *6*, 3354–3364. DOI: 10.1039/c5sc00670h.

[106] Johnson Jr., C. S. Diffusion Ordered Nuclear Magnetic Resonance Spectroscopy: Principles and Applications. *Prog. Nucl. Magn. Reson. Spectrosc.* **1999**, *34*, 203–256. DOI: 10.1016/S0079-6565(99)00003-5.

[107] Gounarides, J. S.; Chen, A.; Shapiro, M. J. Nuclear Magnetic Resonance Chromatography: Applications of Pulse Field Gradient Diffusion NMR to Mixture Analysis and Ligand-Receptor Interactions. *J. Chromatogr. B. Biomed. Sci. App.* **1999**, *725*, 79–90. DOI: 10.1016/S0378-4347(98)00512-X.

[108] Valencia, D. P.; González, F. J. Understanding the Linear Correlation between Diffusion Coefficient and Molecular Weight. A Model to Estimate Diffusion Coefficients in Acetonitrile Solutions. *Electrochem. Commun.* **2011**, *13*, 129–132. DOI: 10.1016/j.elecom.2010.11.032

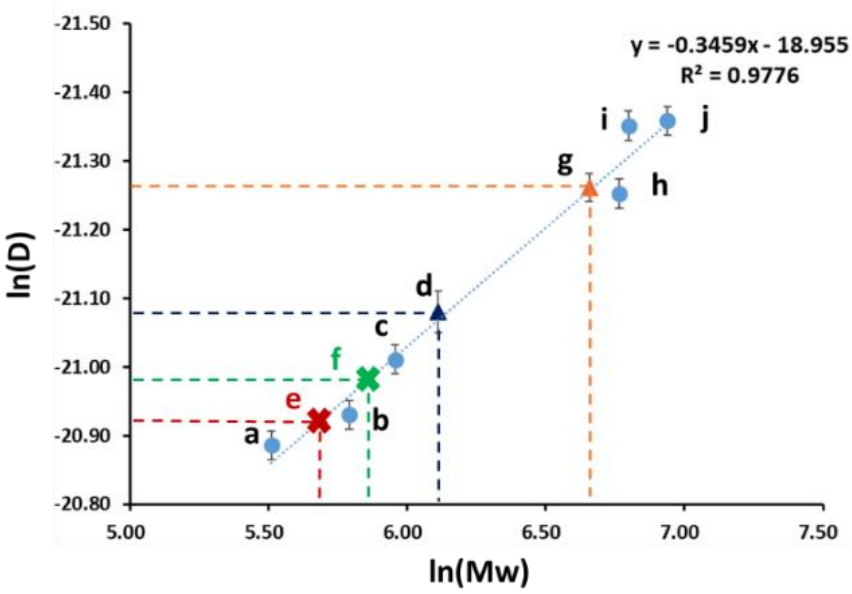

Figure 28. Plot of lnD versus lnMw. Blue dots represent experimental values obtained for known complexes for the calibration line. Other than blue dots correspond to the problem compounds or mixtures.

Name	Compound	Signal	Mw (calc) / g mol^{-1}	ln Mw	lnD
a	**PfBr**	F_{ortho}	246.93	5.51	20.89
b	**RfI**	F_{ortho}	326.87	5.79	20.93
c	**[Cu(Pf)(bipy)]**	F_{ortho}	385.99	5.96	21.01
d	**[Cu(Pf)(DPI)]**	F_{ortho}	450.88	6.11	21.08
e	**[Cu(Pf)(DPI)] + PfBr**	F_{ortho} of PfBr	**284.62**	**5.65**	20.91
f	**[Cu(Pf)(bipy)] + RfI**	F_{ortho} of RfI	**337.71**	**5.82**	20.97
g	**[Cu(Pf)(DPI)] + RfI**	F_{ortho} of RfI	**777.75**	**6.66**	21.26
h	**[PdCl(Rf)(PPh$_3$)$_2$]**	F_{ortho}	866.41	6.76	21.25
i	**[PdCl(Rf)(dppf)]**	F_{ortho}	896.22	6.80	21.35
j	**[Pd(Rf)$_2$(PPh$_3$)$_2$]**	F_{ortho}	1030.93	6.94	21.36

Table 7. Results of diffusion experiments of different compounds in DMF for the calibration line.

Compound	D (m^2s^{-1})	1/D^3
[PdRfCl(PPh_3)$_2$]	5.9 ± 0.12E-10	4.9E+27
RfI	8.3 ± 0.19E-10	1.7E+27
[Cu(Pf)(DPI)]	7.0 ± 0.10E-10	2.9E+27
[Cu(Pf)(Bipy)]	7.5 ± 0.16E-10	2.3E+27
[Pd(Rf)$_2$(PPh_3)$_2$]	5.3 ± 0.09E-10	6.7E+27
Pf-Br	8.5 ± 0.17E-10	1.6E+27
[PdCl(Rf)(dppf)]	5.3 ± 0.21E-10	6.5E+27
[Cu(Pf)(DPI)] + RfI	5.8 ± 0.11E-10	5.0E+27
[Cu(Pf)(DPI)] + BrPf	8.2 ± 0.10E-10	1.7E+27
[Cu(Pf)(Bipy)] + RfI	7.8 ± 0.14E-10	2.1E+27

Table 8. Results of diffusion experiments of different compounds in DMF at 273K.

Aggregate	MW_{det} (DOSY)	MW (calculated)
[Cu(Pf)(DPI)] + RfI	**783**	**777.8**
[Cu(Pf)(DPI)] + BrPf	**254**	**247.0**
[Cu(Pf)(Bipy)] + RfI	**336**	**326.9**
Rf-I	**327**	**326.9**
Pf-Br	**247**	**246.9**

Table 9. Results of MW in diffusion experiments and MW calculated in DMF at 273K.

In this case, as shown in Figure 28, the letter "**e**" corresponds to the mixture of **1-Pf** + Rf–Br. The correlation coincides with the molecular weight of the separately species in solution. On the other hand, the letter "**f**" corresponds to the mixture of [Cu(Pf)(bipy)] + Rf–I. Again, the relationship between molecular weight and diffusion coefficient (D) agrees with the molecular weights of the separately reactants. Orange line labeled as "**g**" represent the experimental value of ln(D) of Rf–I when measured in the presence of a threefold excess of (**1-Pf**) which correlates with the value of $\ln(Mw_{found}) = 6.66$ ($Mw_{found} = 783$). That means that in the presence of an excess of [Cu(Pf)(DPI)] the diffusion of Rf–I is that of a cluster {[Cu(Pf)(DPI)],Rf–I} ($Mw_{calcd} = 777.75$). This indicates that there is an association between both reagents forming an assembly that exists in a kinetically relevant concentration. This cluster can react with a second molecule of [Cu(Pf)(DPI)] to

activate the C–I bond. Similar behaviour has been proposed by Perego and co-workers in palladium catalysis. In that work a pre-association of the aryl iodide and the palladium complex has been hypothesized to explain the kinetic order of the reaction.[84]

If we carry out the computational calculations, the inclusion in the system of a second [Cu(Pf)(DPI)] (**1-Pf**) molecule substantially decreases the OA and RE barriers of this pathway, which are reduced to 19.9 and 9.1 kcal mol^{-1}, respectively (Figure 29).

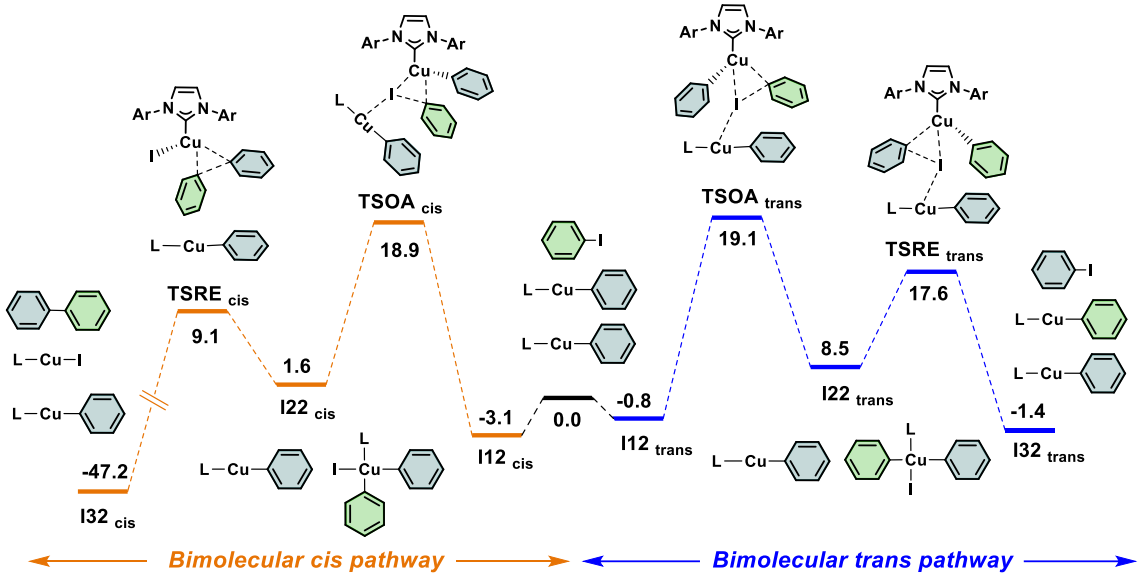

Figure 29 Calculated Gibbs energy profiles (kcal mol^{-1}) for the reaction between 2 [Cu(DPI)(Pf)] (**1-Pf**) and Rf–I. Color code: blue aryl = C_6F_5; green aryl = 3,5-$C_6F_3Cl_2$. (DFT at B3LYP-D3/BS2 level, SMD solvent model (DMF), 298 K).

The effect on the ***cis* pathway** is much smaller than on the ***trans* pathway**, the OA barrier being now 22.0 kcal mol^{-1}. This result reconciles computation with the experimental results, making ***trans* pathway** the most likely reaction way, with a barrier matching the experimental data (Calculated $\Delta G^{\ddagger}_{298}$ = 19.9 kcal mol^{-1} vs Experimental $\Delta G^{\ddagger}_{298}$ = 20.0 kcal mol^{-1}). Although the difference of 2 kcal mol^{-1} between the two transition states does not seem much, it implies a large difference in the reaction rate, since $k_1 = 10^{-2}$ s^{-1} would be the rate constant for the transition state of 19.9 kcal mol^{-1}, $k_1 = 5\times10^{-4}$ s^{-1} would represent the value for the transitional state of 22.0 kcal mol^{-1}. These results show that one reaction would be 20 times faster than the other, thus allowing us to obtain a result acceptable with the

experimental results. Differences between ***bimolecular cis pathway*** and ***bimolecular trans pathway*** can be explained by 2 different ways. First of all, the geometry of **TSOA$_{trans}$** is more favorable than **TSOA$_{cis}$** (Figure 30). The distance between the iodine atom and C_{ipso} is 2.46 Å, while in the case of the structure of the **TSOA$_{cis}$** it is 2.35 Å. This indicates that the bond that has to be broken during the transition state is longer. Furthermore, the bonds that have to be formed (C_{ipso}-Cu and I–Cu) are also shorter. Finally, the distance between the iodine atom and Cu(2) is almost 0.4 Å shorter in **TSOA$_{trans}$** than in **TSOA$_{cis}$**. For that reason, the electron density of the C–I bond in the transition state is more polarized than in the case of **TSOA$_{cis}$**, giving the geometric distortions that allow to have a lower energy process.

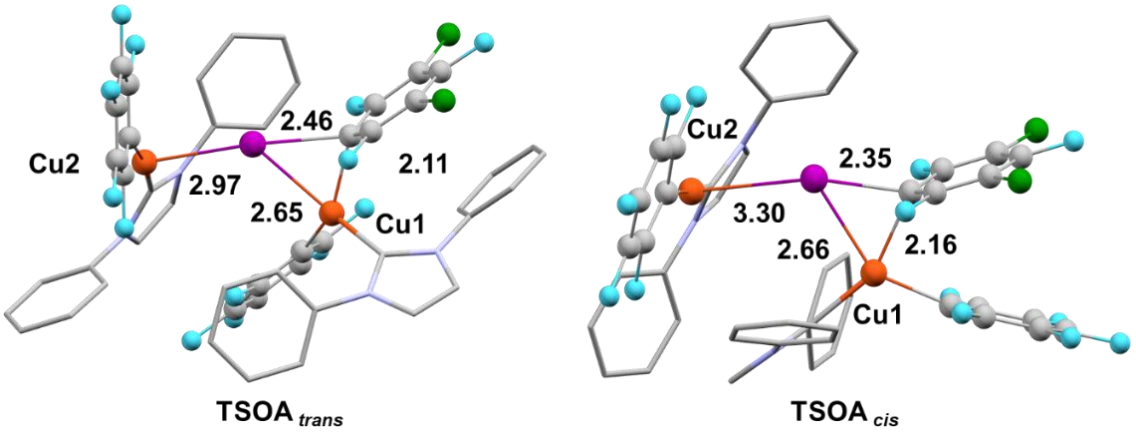

Figure 30. Calculated geometries for **TSOA$_{trans}$, TSOA$_{cis}$**. Selected distances in Å.

The surprising stability of the **TSOA$_{trans}$** compared to **TSOA$_{cis}$** can be understood using NBO (Natural Bond Orbital) analysis. Remarkably, significant donation from a (LP) I NBO orbital (55% s 45% p) to an empty (LP*) Cu(2) NBO orbital (100% p), involving a second order perturbation energy of 22 kcal mol^{-1} was identified in **TSOA$_{trans}$**. These values also suggest that the Cu(2) complex stabilizes the electron density that evolves at the iodine during the oxidative addition of Cu(1) to the C–I bond. Thus, Cu(2)–I interaction in the transition states is modifying the stereochemistry of the addition, favoring the formation of the aryl metathesis product.

Additionally, as shown in Figure 31, **TSRE$_{trans}$** has interaction between iodine atom and Cu(2), which means that it also has a lower energy. On the other hand, the

TSRE$_{cis}$ does not have any interaction between the transition state and the other **1-Pf** complex.

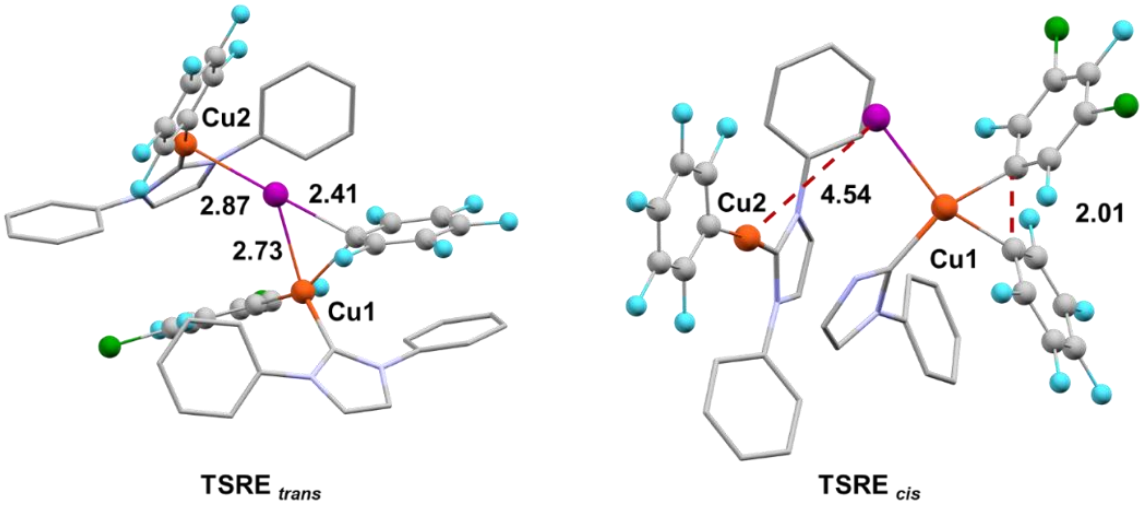

Figure 31. Calculated geometries for **TSRE$_{trans}$, TSRE$_{cis}$.** Selected distances in Å.

Moreover, the experimental points could be perfectly fit to the kinetic model shown in Scheme 10 using the COPASI software.[109] The association reaction is responsible of the afore mentioned complex, detected on diffusion experiments. The oxidative addition/reductive elimination kinetic analysis fits extremely well with de kinetic constants obtained by DFT calculation. The overall $\Delta G^{\ddagger}$ = 20 kcal mol^{-1}, just 0.1 kcal mol^{-1} higher than the experimental one.

Finally, the undesired hydrolysis product obtained due to the presence of traces of water, was also included in the kinetic analysis, with the final purpose of reproduce all the observed products. For kinetic simulations, a series of simplifications were made. The fluorinated aryls Rf and Pf are considered electronically identical, so the hydrolysis constants are considered virtually the same. In addition, the constants k_1/k_{-4} and k_4/k_{-1} are considered equal to simplify the system.

[109] Hoops, S.; Sahle, S.; Gauges, R.; Lee, C.; Pahle, J.; Simus, N.; Singhal, M.; Xu, L.; Mendes, P.; Kummer, U. COPASI—a COmplex PAthway SImulator. *Bioinformatics* **2006**, *22*, 3067–3074.

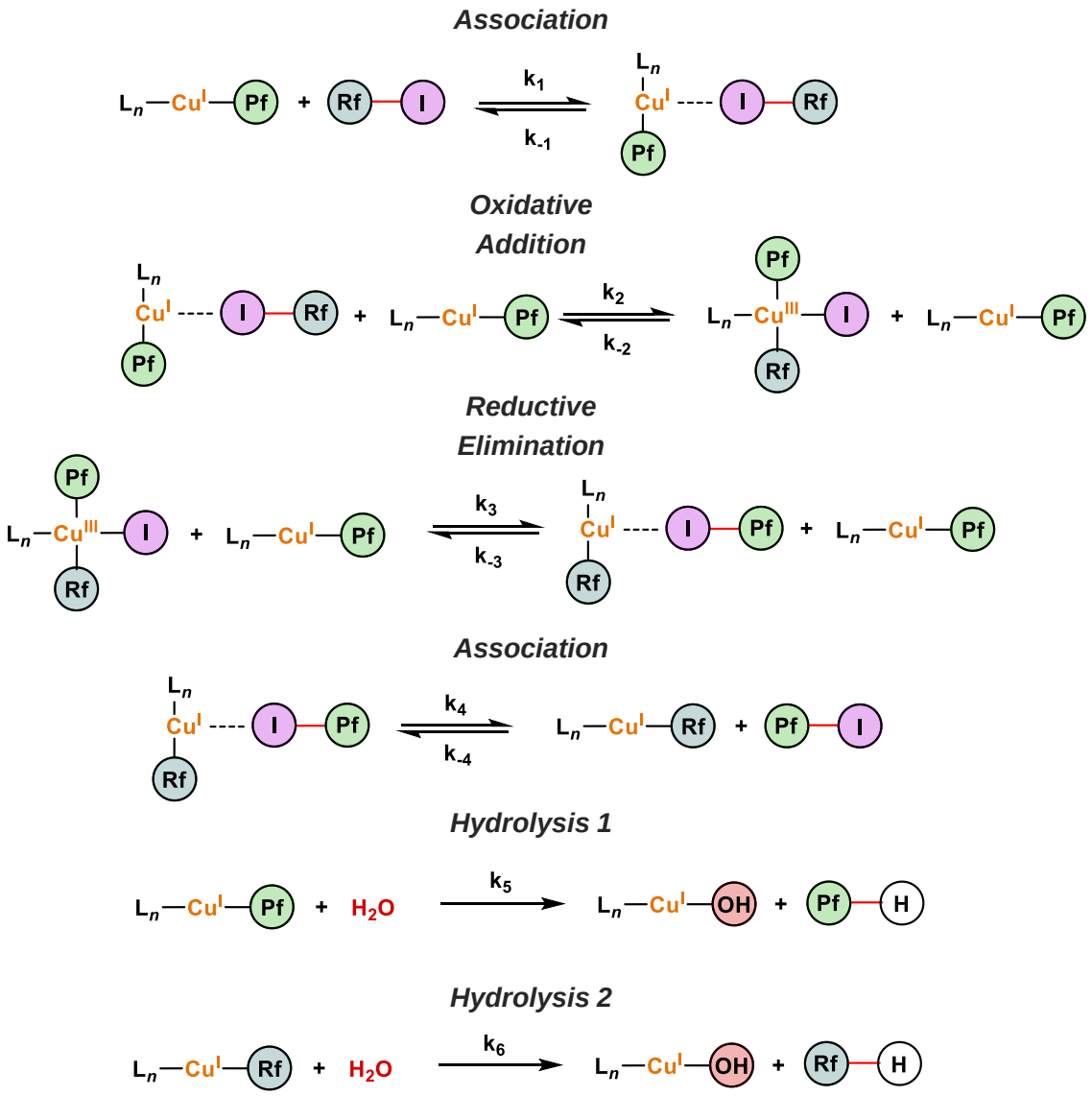

Scheme 10. Proposed reaction pathways for kinetic analysis on second kinetic order.

At this point, having studied in depth the oxidative addition of Rf–I, and seeing the great influence on the stereoselectivity that the iodine atom has, we considered extending the study to other halogens. As we had seen before, for the reaction with allyls, stereoselectivity changed between using allyl iodine or allyl bromine/chlorine. Unlike in the previous case, when aryl bromides are used, it is essential to heat the reaction to obtain product. In the oxidative addition with Rf–Br the reaction only provides the cross-coupling product Rf–Pf, and no traces of the metathesis product was detected by ^{19}F NMR. Kinetic studies show that it is a first-order reaction in copper complex (**1-Pf**) and a first-order reaction and also in Rf–Br.

All these results perfectly fit with the results of the diffusion experiments, where it was not observed pre-association between the two reagents in solution.

Finally, the results of the theoretical calculations (Figure 32) confirm what has been seen experimentally. The energy profile calculated for the second order reaction shows bigger energy deviations than the profile calculated for the first order reaction. This could be because the interactions between the halogen and the metal center are weaker, as they are farther away than in the case of the iodine atom. This would prevent the extra polarization of the bonds in the transition states, giving a higher energy than in the case with a single copper complex.

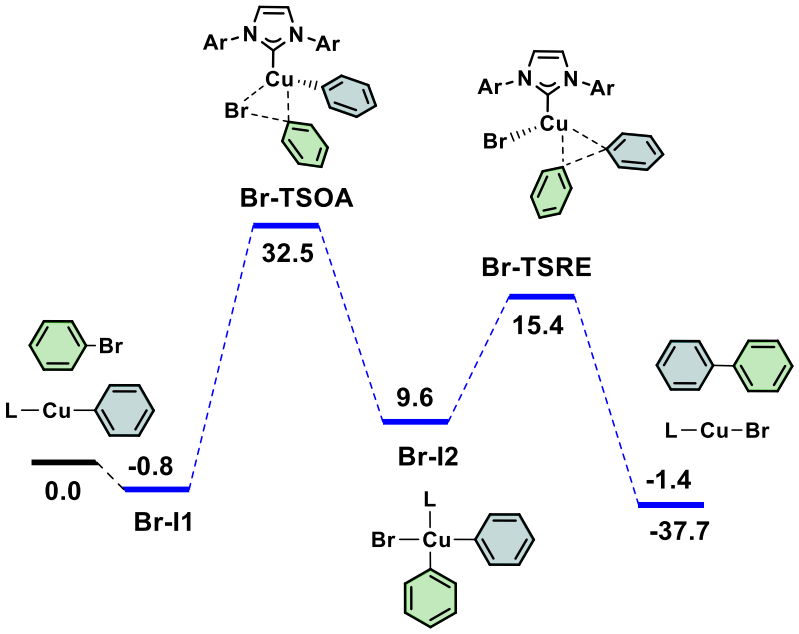

Figure 32. Calculated Gibbs energy profiles (kcal mol^{-1}) for the reaction between [Cu(Pf)(DPI)] (**1-Pf**) and Rf–Br. Color code: blue aryl = C_6F_5; green aryl = 3,5-$C_6F_3Cl_2$. (DFT at B3LYP-D3/BS2 level, SMD solvent model (DMF), 333 K).

2.3 Summary and conclusions

As conclusion of Chapter II, we can highlight that the reactivity and stereochemistry of the oxidative addition can be modified by the halogen or pseudo-halogen that were employed, and it is not necessary to change the mechanistic pathway. Besides, activation of the $C_6F_3Cl_2$–I bond by 14e$^-$ [Cu(Pf)(DPI)] complex occurs through the interaction of two copper complexes with one aryl iodide. This mode of activation does not require the formation of a copper dimer, it is based on the prior formation of an interaction of aryl iodide with a copper complex in a kinetically relevant concentration, which has been detected experimentally. This group reacts with a second copper complex, on which the oxidative addition occurs. The stabilization is efficient in the transition states of the C–I breaking (OA) and forming (RE) bonds, which is where the iodine atom has an increased anionic character. The stabilization of the transition state can be attributed to the polarized electron density of the iodine by the second copper confirmed by NBO analysis. The operation of this mechanisms has a dramatic effect in stereoselectivity of the reaction: since it leads to the *trans*-[CuI(C_6F_5)($C_6F_3Cl_2$)(DPI)] instead of the *cis* arrangement, no cross-coupling products are observed in this reaction conditions, but the metathesis of the halogen is produced instead.

The stabilization of transition states by a second copper does not operate with other halides as bromide due to the orbital overlap to generate a weak interaction between the bromine and the Cu^I which does not compensate the loss of entropy of this association in solution.

2.4 Experimental section

General information

General procedures and equipment have been described in the Experimental Section in Chapter I. [PdCl(Rf)(PPh_3)$_2$],[110] [Cu(Pf)(Bipy)],[111] [Pd(Rf)$_2$(PPh_3)$_2$],[112] [PdCl(Rf)(dppf)],[113] RfH,[114][Cu(Pf)(IPr)],[115] were prepared according to the described procedure.

[110]Minniti, D. Uncatalyzed Cis-Trans Isomerization of Bis(Pentafluorophenyl) Bis(Tetrahydrothiophene) Palladium(II) Complexes in Chloroform: Evidence for a Dissociative Mechanism. *Inorg. Chem.* **1994**, *33*, 2631–2634. DOI: 10.1021/ic00090a025

[111] Doshi, A.; Sundararaman, A.; Venkatasubbaiah, K.; Zakharov, L. N.; Rheingold, A. L.; Myahkostupov, M.; Piotrowiak, P.; Jäkle, F. Pentafluorophenyl Copper-Pyridine Complexes: Synthesis, Supramolecular Structures via Cuprophilic and π-Stacking Interactions, and Solid-State Luminescence. *Organometallics* **2012**, *31*, 1546–1558. DOI: 10.1021/om200989b

[112] Casado, A. L.; Casares, J. A.; Espinet, P. An Aryl Exchange Reaction with Full Retention of Configuration of the Complexes: Mechanism of the Aryl Exchange between [PdR$_2$L$_2$] Complexes in Chloroform (R = Pentahalophenyl, L = Thioether). *Organometallics* **1997**, *16*, 5730–5736. DOI: 10.1021/om970721f.

[113] Gallego, A. M.; Peñas-Defrutos, M. N.; Marcos-Ayuso, G.; Martin-Alvarez, J. M.; Martínez-Ilarduya, J. M.; Espinet, P. Experimental Study of Speciation and Mechanistic Implications When Using Chelating Ligands in Aryl-Alkynyl Stille Coupling. *Dalton Trans.* **2020**, *49*, 11336–11345. DOI: 10.1039/d0dt02335c

[114] Casares, J. A.; Espinet, P.; Martín-Alvarez, J. M.; Martínez-Ilarduya, J. M.; Salas, G. Stable Nickel Catalysts for Fast Norbornene Polymerization: Tuning Reactivity. *Eur. J. Inorg. Chem.* **2005**, *19*, 3825–3831. DOI: 10.1002/ejic.200500121

[115] Lesieur, M.; Lazreg, F.; Cazin, C. S. J. A Cooperative Pd–Cu System for Direct C–H Bond Arylation. *Chem. Commun.* **2014**, *50*, 8927–8929. DOI: 10.1039/c4cc03201b

Synthesis and characterization of compounds

1,3-Bisphenylimidazolium chloride DPI·HCl

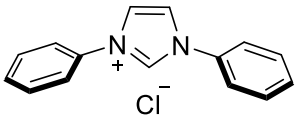

General procedure: Modified procedure from reference [116]

Aniline (1.17 mL, 12.86 mmol, 2.00 eq), 40% glyoxal in (0.73 mL, 6.43 mmol, 1.00 eq) and few drops of formic acid were introduced in a 10 mL Schlenk tube, and the mixture was stirred for 2 hours. Then a solution of paraformaldehyde in 4M hydrochloric acid in dioxane (1.00 eq) was introduced. The solution was stirred for 5 hours at room temperature. Then, ethyl acetate (5mL) was added, and the resulting suspension was filtrated. The solid was washed three times with ethyl acetate (5x3 mL) and then dried under vacuum to afford 1,3-bisphenylimidazolium chloride DPI·HCl (1.46 g, 6.43 mmol, 88%) as a light orange powder.

^{1}H NMR (499.73 MHz, DMSO-*d*$_6$) δ 10.45 (s, 1H), 8.62 (d, J = 1.4 Hz, 2H), 7.94 (d, J = 7.5 Hz, 4H), 7.70 (t, J = 7.7 Hz, 4H), 7.65 – 7.60 (m, 2H)
^{13}C NMR (125.67 MHz, DMSO-*d*$_6$) δ 134.9, 134.1, 130.1, 130.0, 129.6, 122.0, 121.8.
All the resonances of ^{1}H and ^{13}C NMR spectra were consistent with reported values.[116]

[116] Beillard, A.; Bantreil, X.; Métro, T. X.; Martinez, J.; Lamaty, F. A More Sustainable and Efficient Access to IMes·HCl and IPr·HCl by Ball-Milling. *Green Chem.* **2018**, *20*, 964–968. DOI: 10.1039/c7gc03539j

[Cu(C$_6$F$_5$)(DPI)] (1-Pf)

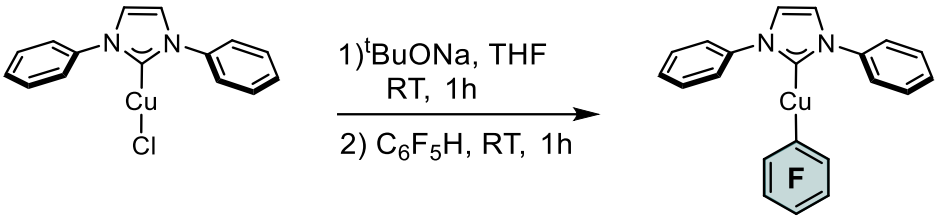

In the glovebox, to a suspension of [CuCl(DPI)] (504 mg, 1.57 mmol) in anhydrous THF (25 mL) was added sodium tert-butoxide (151 mg, 1.0 equiv). The mixture was stirred at room temperature for 1 h. Pentafluorobenzene (288 mg, 1.1 equiv) was subsequently added to the solution and stirred for another 1 h. The suspension was filtered and volatile materials were removed in vacuo. The residue was then washed with anhydrous n-hexane affording off-white solid [Cu(C$_6$F$_5$)(DPI)] (483 mg, 68%). Calcd. for $C_{21}H_{12}CuF_5N_2$ (M.W.= 450,88 g mol^{-1}): C, 55.94; H, 2.68; N 6.21; Found: C, 55.96; H, 2.69; N, 6.22.

All the resonances of ^{1}H and ^{13}C NMR spectra were consistent with reported values.

^{1}H NMR (499.73 MHz, DMF-*d*$_7$) δ 8.78 (t, $^3J_{HH}$ = 1.9 Hz, 2H), 8.23 – 8.19 (m, 4H), 7.75 – 7.62 (m, 6H).

^{19}F NMR (**470.17 MHz, DMF-*d*$_7$**) δ -110.0 (m, 2F), -160.9 (t, J = 19.5 Hz, 1F), -162.9 (m, 2F).

^{13}C NMR (150 MHz, DMF-*d*$_7$) δ 183.2, 139.1, 135.1, 134.3, 129.2, 121.4.

[Cu(DPI)(C$_6$F$_3$Cl$_2$)]

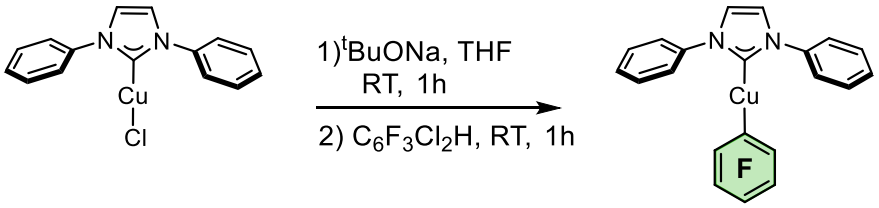

In the glovebox, to a suspension of [CuCl(DPI)] (504 mg, 1.57 mmol) in anhydrous THF (25 mL) was added sodium *tert*-butoxide (151 mg, 1.0 equiv.). The mixture was stirred at room temperature for 1 h. ($C_6HCl_2F_3$) (314 mg, 1.1 equiv.) was subsequently added to the solution and stirred for 1 h. The reaction mixture was filtered through a plug of celite and volatile materials were removed in vacuo. The residue was then washed with anhydrous n-hexane affording off-white solid [Cu(Rf)(DPI)] 446 mg, 72%). Calcd. for $C_{21}H_{13}Cl_2CuF_3N_2$ (M.W.= 484,79 g mol^{-1}): C, 52.03; H, 2.70; N 5.78; Found: C, 52.11; H, 2.72; N, 5.76.

^{1}H NMR (500 MHz, DMF-*d*$_7$) δ 8.81 (d, $^3J_{HH}$ = 1.7 Hz, 2H), 8.24 – 8.22 (m, 4H), 7.76 – 7.63 (m, 6H).

^{19}F NMR (470.17 MHz, DMF-*d*$_7$) δ -84.23 (s, 2F), -122.35 (s, 1F).

^{13}C NMR (150 MHz, DMF-*d*$_7$) δ 184.4, 138.5, 135.3, 134.6, 129.4, 121.7.

Reaction of [Cu(Pf)(DPI)] (Pf = C_6F_5) with allyl halides.

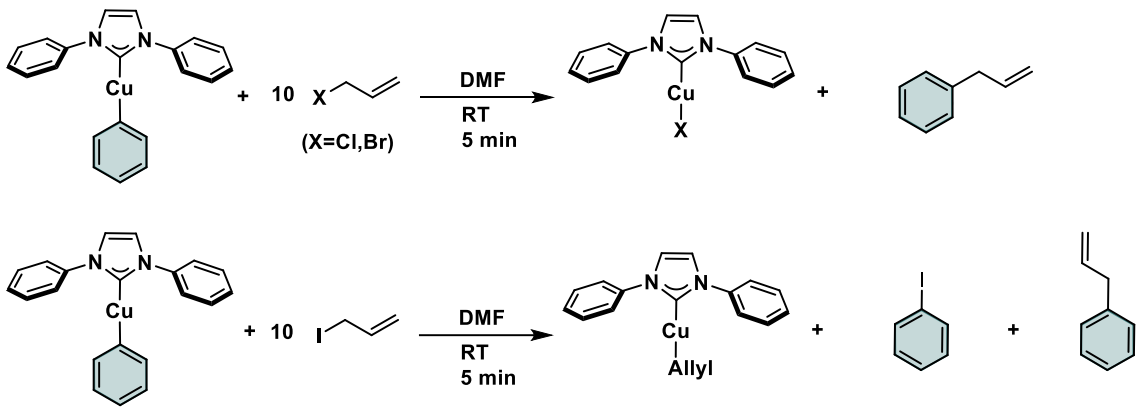

Scheme 11. Reaction between 1-Pf and allyl halides.

Weighted amounts of complex [Cu(Pf)(DPI)] (10.21 mg, 0.0125 mmol) and Allyl-X (X = Cl, Br, I) (0.0123 mmol) were added inside a screw cap NMR tube with the aid of a Schlenk NMR tube adaptor along with a flame sealed coaxial capillary containing acetone-d_6 to the lock the deuterium signal. The tube was cooled to 195 K in an isopropanol/N_2 (liq) bath and subsequently, 0.50 mL of dry DMF with dissolved trifluorotoluene as internal standard (0.0250 mol × L^{-1}) were added with a micro syringe. The tube was closed inside the adaptor and then taken out of the cool bath and mechanically shaken until total dissolution of the solids. The products were confirmed by NMR and GC–MS.

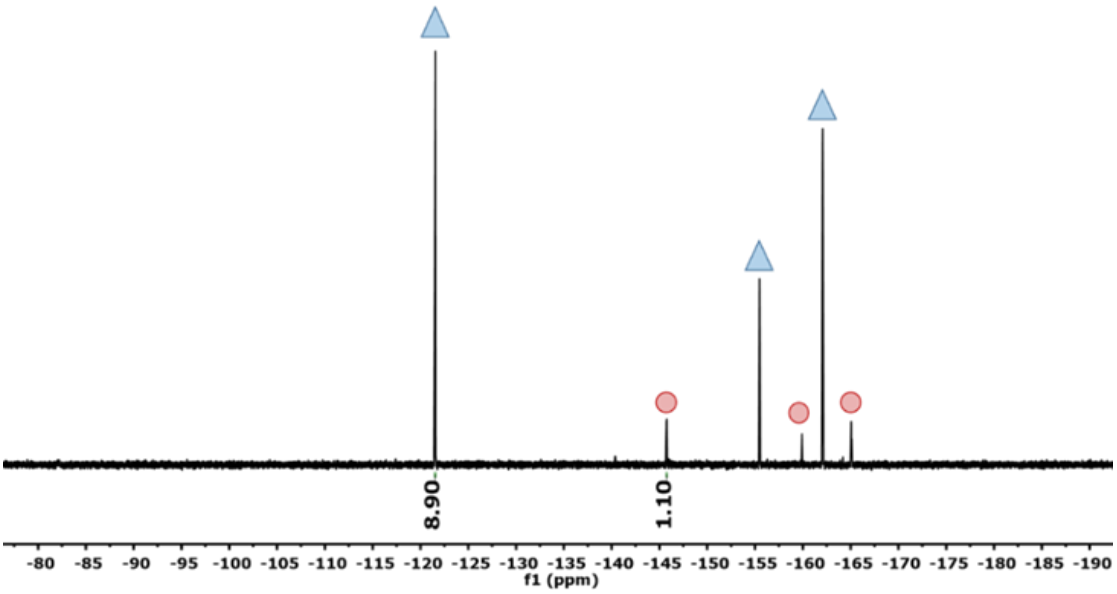

Figure 33. Final ^{19}F NMR (DMF/acetone-d_6) of **[Cu(Pf)(DPI)] + allyl iodide** (298K). Blue triangles represent the metathesis product Pf-I, and red dots represent the cross-coupling product Pf-Allyl.

Kinetic experiments

Weighted amounts of complex [Cu(Pf)(DPI)] **(1-Pf)** were added inside a screw cap NMR tube with the aid of a Schlenk NMR tube adaptor along with a flame sealed coaxial capillary containing acetone-d_6 to the lock deuterium signal. The tube was cooled to 195 K in an isopropanol bath and a weighted amount the allyl halide and a volume and DMF taken with a syringe. The tube was closed inside the adaptor and then, taken out of the cool bath, manually shaken until total dissolution of solids and transferred to the NMR probe, which had been preheated to the monitoring temperature.

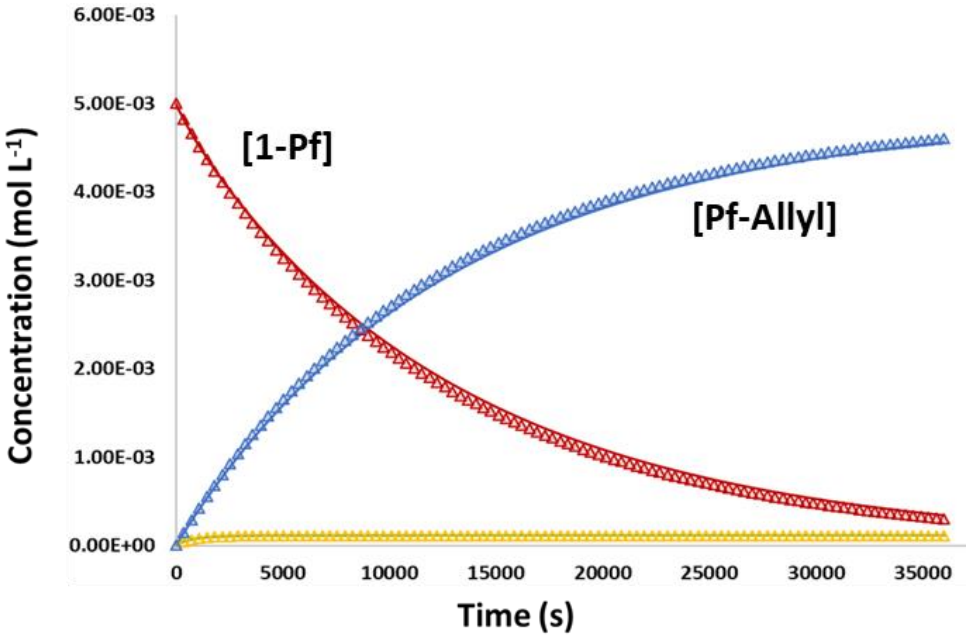

Figure 34. ^{19}F NMR monitoring of the reaction between [Cu(Pf)(DPI)] and Cl-Allyl (1:10) in dry DMF at 253 K. Lines represent kinetic fitting of data using COPASI software.

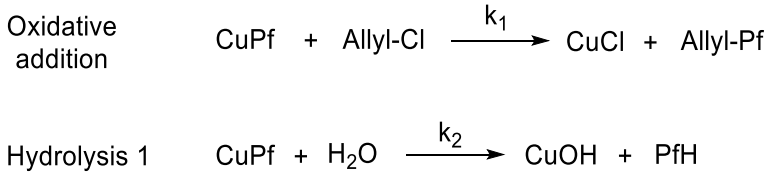

Scheme 12. Kinetic model proposed for Figure 34.

Traces of water have been included in the kinetic fit to maintain material balance.

Parameter	*Value s^{-1}; $M^{-1}{\cdot}s^{-1}$*	*Std. Deviation*
k_1	1.65E-3	6.5E-4
k_2	2.37E-1	3E-6

Table 10. Values of kinetic simulations constants.

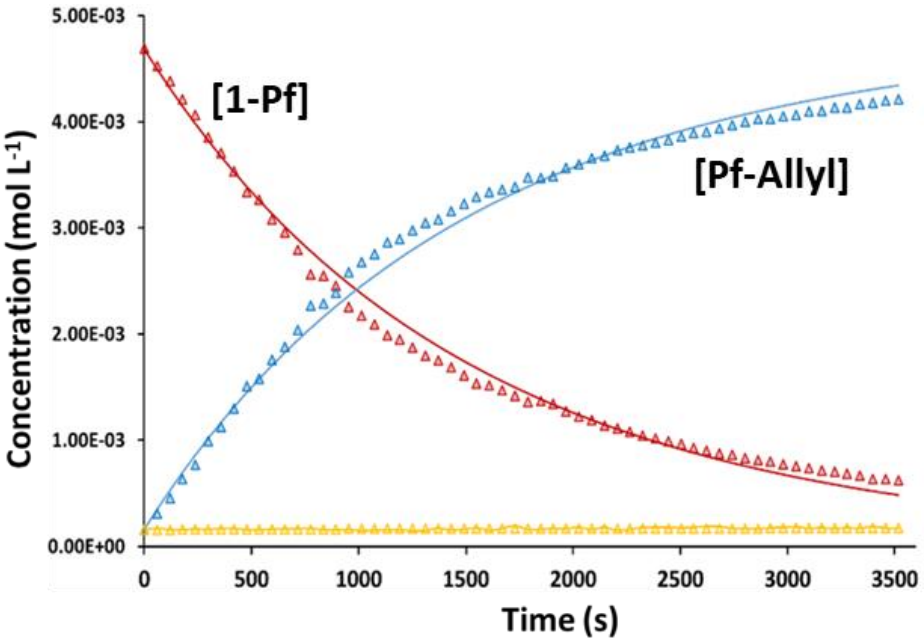

Figure 35. ^{19}F NMR monitoring of the reaction between [Cu(DPI)(Pf)] and Br-Allyl (1:10) in dry DMF at 253 K. Lines represent kinetic fitting of data using COPASI software

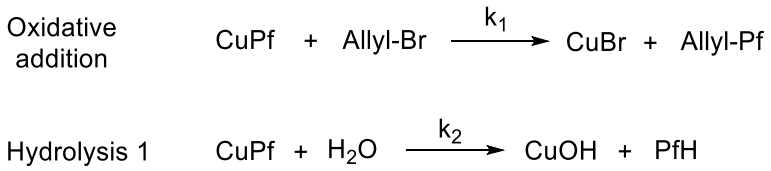

Scheme 13. Kinetic model proposed for Figure 35.

Parameter	*Value s^{-1}; $M^{-1}{\cdot}s^{-1}$*	*Std. Deviation*
k_1	1.51E-2	2.40E-4
k_2	3.12E-2	1.50E-5

Table 11. Values of kinetic simulations constants.

Reaction of [Cu(DPI)(Pf)] (Pf = C_6F_5) with Allyl p-toluenesulfonate.

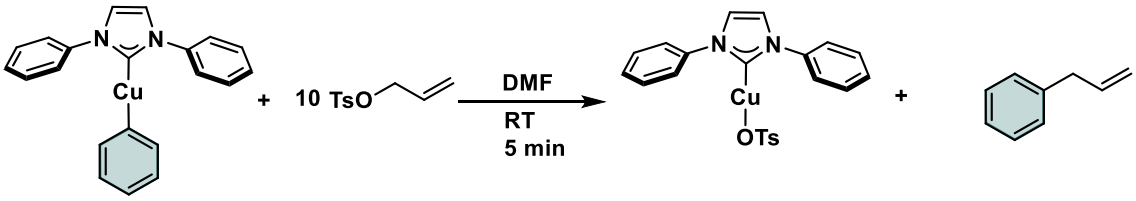

Scheme 14. Reaction between **1-Pf** and Allyl p-toluensulfonate

Complex [Cu(Pf)(DPI)] (10.0 mg) was added inside a screw cap NMR tube with the aid of a Schlenk NMR tube adaptor along with a flame sealed coaxial capillary containing acetone-d_6 to keep the lock signal. A weighted amount of Allyl p-toluensulfonate (10 Eq.), DMF (0.50 mL) were added. After 5 minutes, the reaction was finish and the product was recorded in ^{19}F NMR.

Kinetic experiments

Weighted amounts of complex [Cu(Pf)(DPI)] were added inside a screw cap NMR tube with the aid of a Schlenk NMR tube adaptor along with a flame sealed coaxial capillary containing acetone-d_6 to the lock deuterium signal. The tube was cooled to 195 K in an isopropanol/N_2 (liq) bath and a weighted amount the Allyl p-toluenesulfonate and a volume and DMF taken with a syringe. The tube was closed inside the adaptor and then, taken out of the cool bath, manually shaken until total dissolution of solids and transferred to the NMR probe, which had been preheated to the monitoring temperature. Kinetic constants summarized in Table 12.

Parameter	*Value s^{-1}; $M^{-1}\cdot s^{-1}$*	*Std. Deviation*
k_1	2.75E-4	3.25E-5
k_2	1.03E-1	2.99E-3

Table 12. Kinetic constants

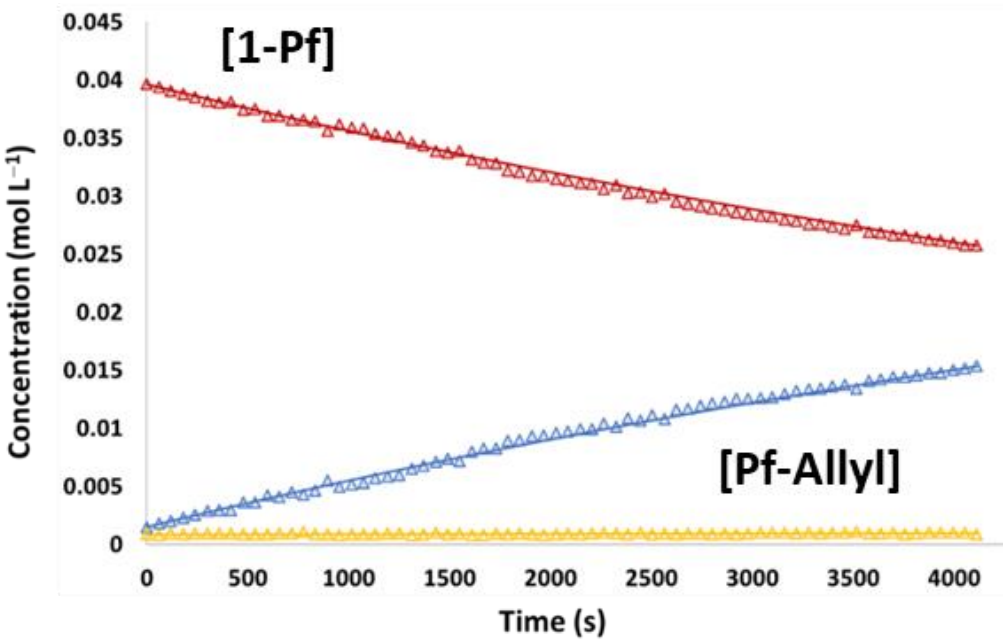

Figure 36. ^{19}F NMR monitoring of the reaction between [Cu(DPI)(Pf)] and TsO-Allyl (1:10) in dry DMF at 243 K. Lines represent kinetic fitting of data using COPASI software.

Under the same conditions, the reaction with allyl iodide lasts less than 5 minutes. Therefore, it is assumed to compare the constants of the oxidative addition step a simulated constant with the copasi software.

Parameter	Value s^{-1}; $M^{-1}{\cdot}s^{-1}$
k_1 (I-Allyl)	>3.0E-1
k_1 (Br-Allyl)	1.51E-2
k_1 (Cl-Allyl)	1.65E-3
k_1(OTs-Allyl)	2.75E-4

Table 13. Kinetic constants.

Reaction of [Cu(DPI)(Pf)] (Pf = C_6F_5) with Benzyl bromide.

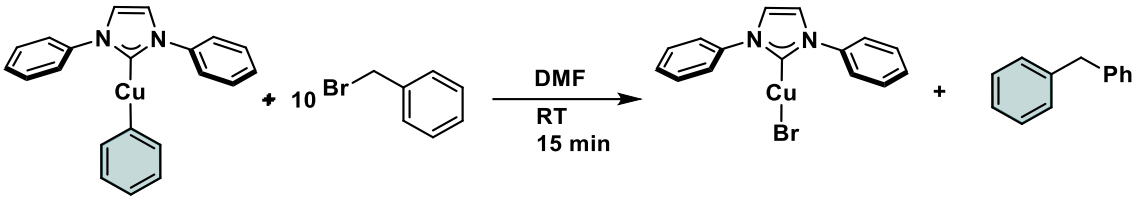

Scheme 15. Reaction between **1-Pf** and benzyl bromide.

Complex [Cu(Pf)(DPI)] (10.0 mg) was added inside a screw cap NMR tube with the aid of a Schlenk NMR tube adaptor along with a flame sealed coaxial capillary containing acetone-d_6 to keep the lock signal. A weighted amount of Benzyl bromide (10 Eq.), DMF (0.50 mL) were added. After 15 minutes, the reaction was finish (full conversion) and the product was recording in ^{19}F NMR. Spectra represented in Figure 37.

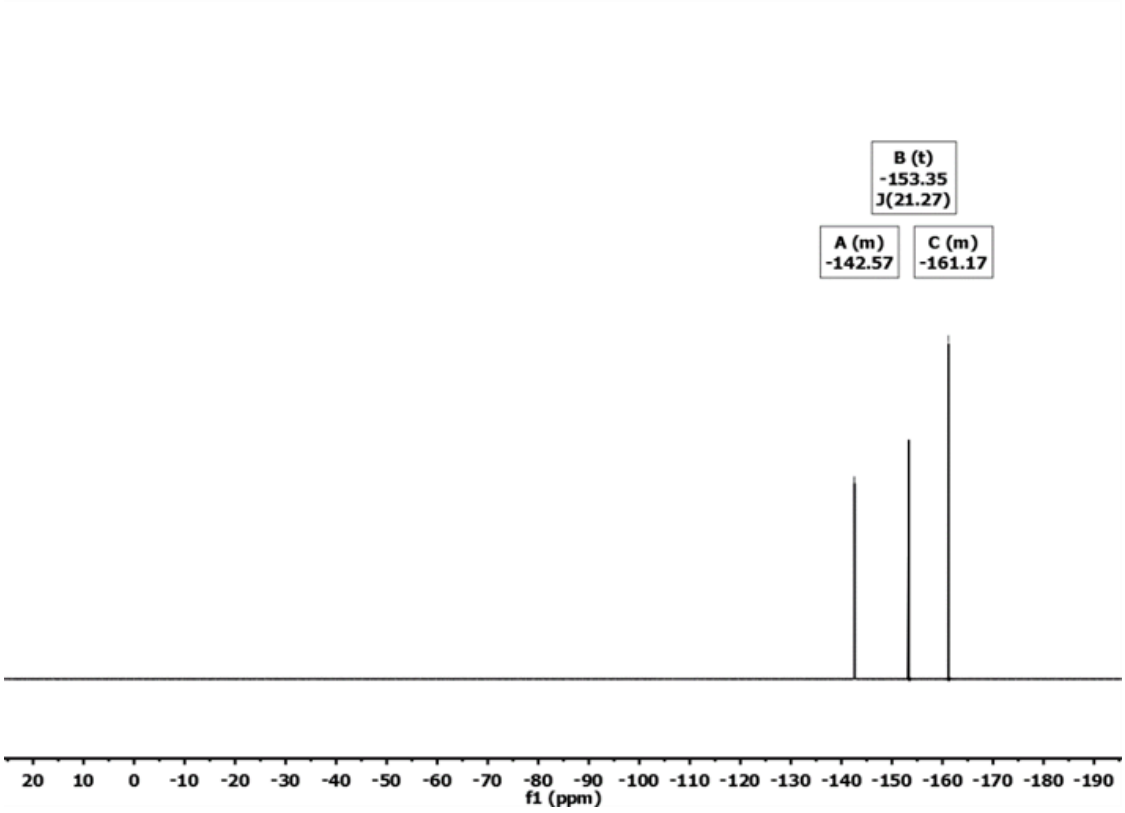

Figure 37. Final ^{19}F NMR (DMF/acetone-d_6) of **[Cu(Pf)(DPI)] + benzyl bromide** (298K). Full conversion to the cross-coupling product.

Kinetic data analysis

Determination of the kinetic order of reaction of compound [Cu(Pf)(DPI)] in oxidative addition reactions with Rf–I (Rf = $C_6F_3Cl_2$)

Weighted amounts of complex [Cu(Pf)(DPI)] **(1-Pf)** were added inside a screw cap NMR tube with the aid of a Schlenk NMR tube adaptor along with a flame sealed coaxial capillary containing acetone-d_6 to the lock deuterium signal. The tube was cooled to 195 K in an isopropanol bath and a weighted amount $C_6F_3Cl_2I$ (RfI) and a volume and DMF taken with a syringe. The tube was closed inside the adaptor and then, taken out of the cool bath, manually shaken until total dissolution of solids and transferred to the NMR probe, which had been preheated to the monitoring temperature (273 K). Data summarized in Table 14.

Exp.	Compound *[Cu(Pf)(DPI)]*	Rf-I	$[Cu(Pf)(DPI)]_0$ (mol L^{-1})	DMF (mL)
1	1.55 mg	26.30 mg	5.00E-4	0.5
2	6.82 mg	26.30 mg	2.20E-3	0.5
3	15.50 mg	26.30 mg	5.10E-3	0.5
4	25.10 mg	26.30 mg	6.58E-3	0.5
5	35.04 mg	26.30 mg	1.13E-2	0.5

Table 14. Amounts of reagents used in the monitoring experiments of the reaction of compound [Cu(DPI)(C_6F_5)] and $C_6F_3Cl_2I$.

Recording started after about 1 min used for the setup of the experiment, time zero for the measurements is taken at that moment. ^{19}F NMR spectra parameters are 1 scan, relaxation delay of 1 s, pulse angle of 90°. Spectra were collected every 58 s.

Order of reaction for compound [Cu(Pf)(DPI)] in the reaction of [Cu(Pf)(DPI)] and $C_6F_3Cl_2I$ was determined by initial rates method, measuring the linear rates for the formation of C_6F_5–I up to 15% of total conversion.

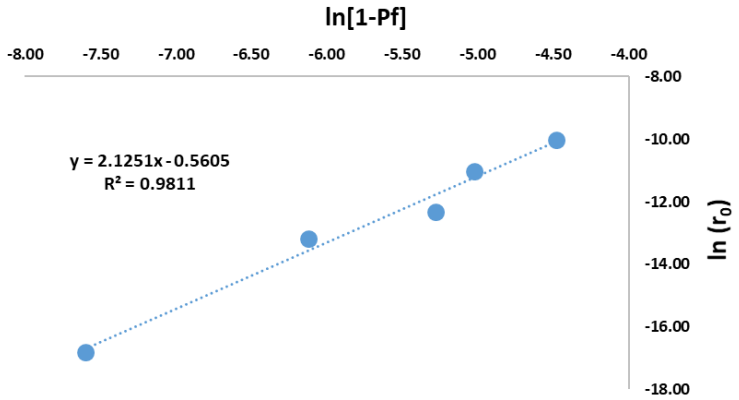

Figure 38. Correlation of the found initial reaction rates and initial concentrations of compound **[Cu(Pf)(DPI)]**.

r_0	**[1-Pf]** (mol L^{-1})	**ln(r0)**	**ln[1-Pf]**
4.47E-05	1.13E-02	-10.02	-4.48
1.61E-05	6.58E-03	-11.04	-5.02
4.40E-06	5.10E-03	-12.33	-5.28
1.90E-06	2.20E-03	-13.17	-6.12
5.00E-08	5.00E-04	-16.81	-7.60

Table 15. Correlation of the found initial reaction rates and initial concentrations of compound

Weighted amounts of compound **Rf-I** were added inside a screw cap NMR tube with the aid of a Schlenk NMR tube adaptor along with a flame sealed coaxial capillary containing acetone-d_6 to the lock deuterium signal. The tube was cooled to 195 K in an isopropanol bath and a weighted amount [Cu(Pf)(DPI)] and a volume and DMF taken with a syringe. The tube was closed inside the adaptor and then, taken out of the cool bath, manually shaken until total dissolution of solids and transferred to the NMR probe, which had been preheated to the monitoring temperature (273 K). Triflurotoluene was used as internal standard.

Exp.	Compound Rf-I	*[Cu(Pf)(DPI)]*	$[RfI]_0$(mol L^{-1})	DMF (mL)
1	0.79 mg	13.20 mg	4.80×10^{-4}	0.5
2	3.64 mg	13.20 mg	2.23×10^{-3}	0.5
3	8.32 mg	13.20 mg	5.09×10^{-3}	0.5
4	13.27 mg	13.20 mg	8.12×10^{-3}	0.5
5	18.14 mg	13.20 mg	1.11×10^{-2}	0.5

Table 16. Amounts of reagents used in the monitoring experiments of the reaction of compound [Cu(Pf)(DPI)] and $C_6F_3Cl_2I$.

Recording started after about 1 min used for the setup of the experiment, time zero for the measurements is taken at that moment. ^{19}F NMR spectra parameters are 1 scan, relaxation delay of 1 s, pulse angle of 90°. Spectra were collected every 58 s.

Order of reaction for compound Rf-I in the reaction of ***[Cu(DPI)(C_6F_5)]*** and Rf–I was determined by initial rates method, measuring the linear rates for the formation of Pf–I up to 15% of total conversion.

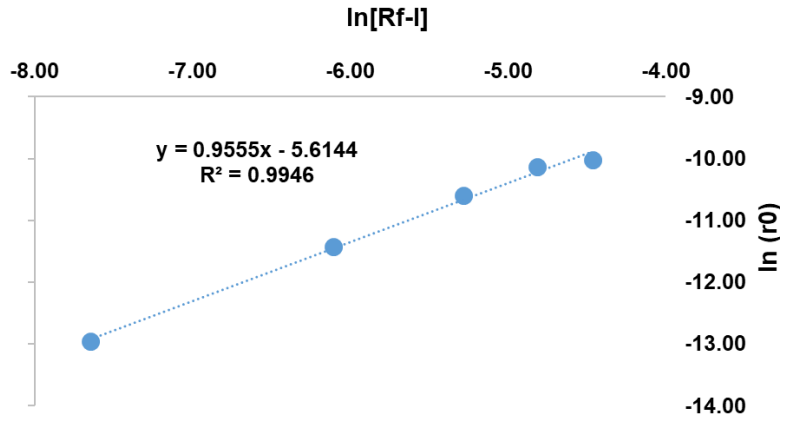

Figure 39. Correlation of the found initial reaction rates and initial concentrations of compound **Rf–I.**

r_0 (mol s^{-1})	[Rf-I] (mol L^{-1})	ln(r0)	ln[Rf-I]
4.47E-05	1.15E-02	-10.02	-4.46
3.99E-05	8.12E-03	-10.13	-4.81
2.51E-05	5.09E-03	-10.59	-5.28
1.09E-05	2.23E-03	-11.43	-6.11
2.36E-06	4.79E-04	-12.96	-7.64

Table 17. Amounts of reagents used in the monitoring experiments of the reaction of compound [Cu(Pf)(DPI)] and $C_6F_3Cl_2I$ (Rf-I).

Determination of the kinetic order of reaction of compound [Cu(Pf)(DPI)] in oxidative addition reactions with Rf-Br (Rf = $C_6F_3Cl_2$)

Weighted amounts of complex [Cu(Pf)(DPI)] were added inside a screw cap NMR tube with the aid of a Schlenk NMR tube adaptor along with a flame sealed coaxial capillary containing acetone-d_6 to the lock deuterium signal. The tube was cooled to 273 K in an isopropanol bath and a weighted amount **Rf–Br** and a volume and DMF taken with a syringe. The tube was closed inside the adaptor and then, taken out of the cool bath, manually shaken until total dissolution of solids, and transferred to the NMR probe, which had been preheated to the monitoring temperature (323 K). Triflurotoluene was used as internal standard.

Exp.	Compound [Cu(Pf)(DPI)]	Rf-Br	$[Cu(Pf)(DPI)]_0$ (mol L^{-1})	DMF (mL)
1	1.00 mg	26.30 mg	4.21E-4	0.5
2	1.38 mg	26.30 mg	6.13E-4	0.5
3	4.08 mg	26.30 mg	1.81E-3	0.5
4	7.19 mg	26.30 mg	3.19E-3	0.5
5	32.01 mg	26.30 mg	1.42E-2	0.5

Table 18. Amounts of reagents used in the monitoring experiments of the reaction of compound [Cu(Pf)(DPI)] and $C_6F_3Cl_2I$.

Recording started after about 1 min used for the setup of the experiment, time zero for the measurements is taken at that moment. ^{19}F NMR spectra parameters are 1 scan, relaxation delay of 1 s, pulse angle of 90°. Spectra were collected every 58 s.

Order of reaction for compound ***[Cu(Pf)(DPI)]*** in the reaction of ***[Cu(Pf)(DPI)]*** and Rf-I was determined by initial rates method, measuring the linear rates for the formation of Pf–Rf up to 15% of total conversion.

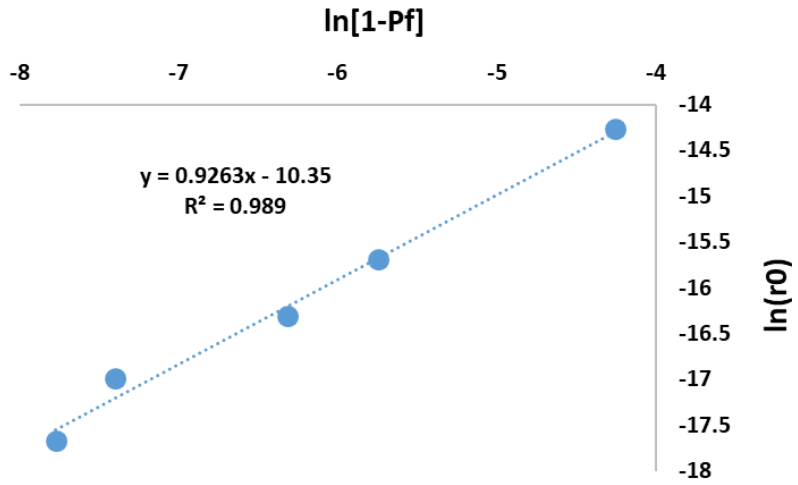

Figure 40. Correlation of the found initial reaction rates and initial concentrations of compound [Cu(Pf)(DPI)] with Rf-Br.

r_0	**[1-Pf]** (mol L^{-1})	**ln(r0)**	**ln[1-Pf]**
6.42E-07	1.42E-02	-1.43E+01	-4.25E+00
1.53E-07	3.19E-03	-1.57E+01	-5.75E+00
8.30E-08	1.81E-03	-1.63E+01	-6.31E+00
4.20E-08	6.13E-04	-1.70E+01	-7.40E+00
2.11E-08	4.21E-04	-1.77E+01	-7.77E+00

Table 19. Amounts of reagents used in the monitoring experiments of the reaction of compound [Cu(Pf)(DPI)].

Kinetic models used for non-linear fitting of the concentration / time data for the reaction between [Cu(Pf)(DPI)] and Rf–I (Rf = $C_6Cl_2F_3$)

Complex [Cu(Pf)(DPI)] reacts with $C_6Cl_2F_3I$ in dry DMF at 298 K producing the aryl methatesis product C_6F_5–I and the complex [Cu(Rf)(DPI)], and residual amounts of the hydrolysis products C_6F_5H and $C_6Cl_2F_3H$. (Pf = C_6F_5, Rf = $C_6F_3Cl_2$).
A 500 MHz NMR spectrometer was preheated to the appropriate reaction temperature. Shimming and 90° pulse calibration were performed according to the ^{19}F signals of a dummy sample (500 µL of dry DMF, Trifluorotoluene was used as internal standard). The cold sample was then quickly warmed to room temperature and transferred to the NMR. After letting the sample thermally equilibrate for ~30 s, single-scan ^{19}F NMR spectra were collected. (Figure 26)

Kinetic model

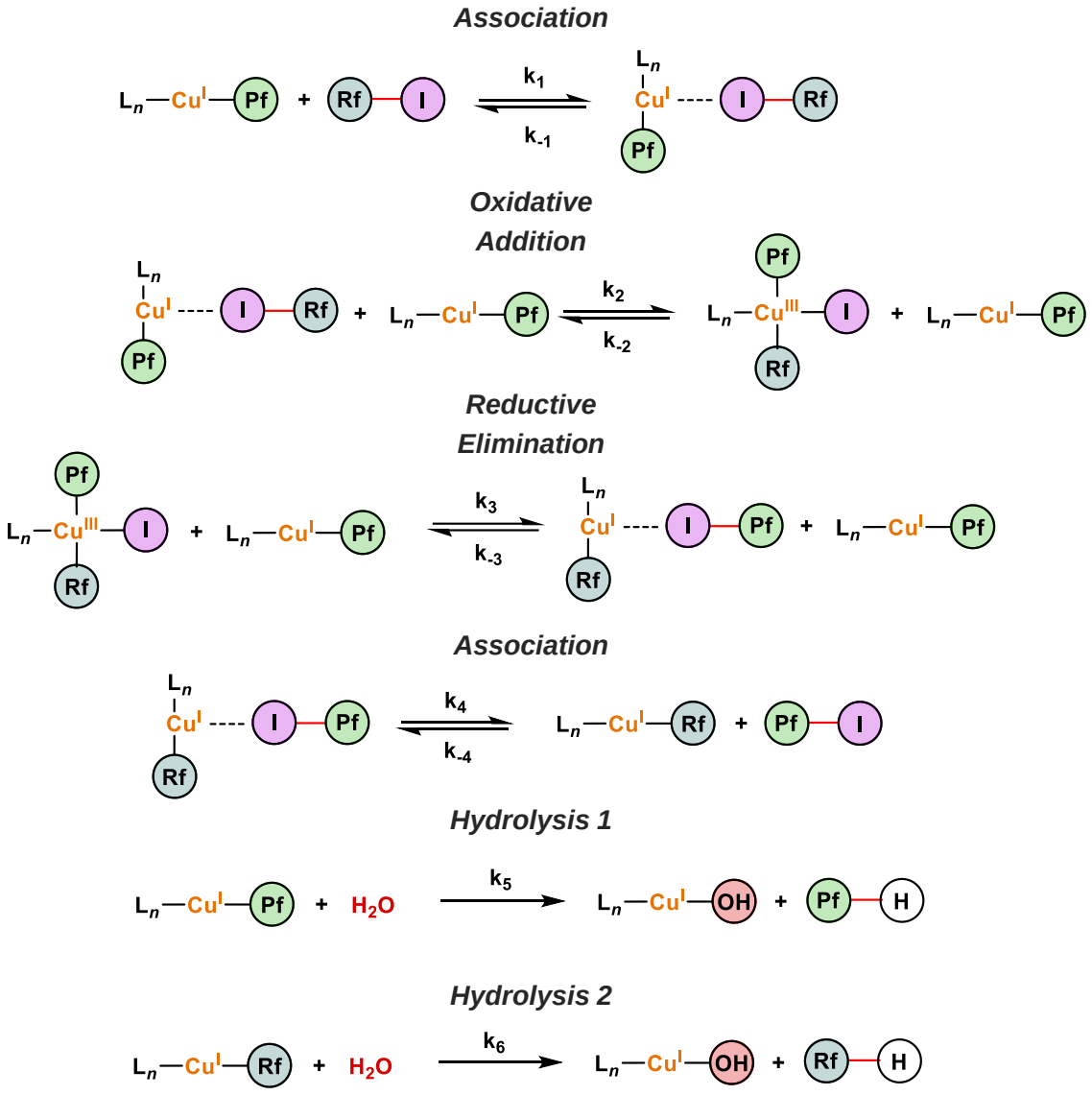

Figure 41. Kinetic equations for the fitting.

For kinetic simulations, a series of simplifications are made. The fluorinated aryls Rf and Pf are considered electronically identical, so the hydrolysis constants are considered virtually the same. In addition, the constants k_1/k_{-4} and k_4/k_{-1} are considered equal to simplify the system. Kinetic constants and the standard desviations are summarized in Table 20.

Parameter	Value s^{-1}; $M^{-1} \cdot s^{-1}$	Std. Deviation
k_1	49.95	6.9E+03
k_{-1}	1000	3.5E+02
k_2	0.01	2.0E-02
k_{-2}	1.21E-06	6.2E-06
k_3	0.01	1.4E-03
k_{-3}	1.32e-6	2.5E-03
k_4	1000	6.9E+03
k_{-4}	49.95	3.5E+02
k_5	1.65 e-3	3.3E-06
k_6	1.88 e-3	8.0E-06

Table 20. Values of kinetic simulations constants.

NMR DOSY – diffusion experiments

NMR experiments were recorded with a Variant spectrometer (11.7 T). All spectra were acquired in a 5 mm observe probehead at 273.15 K in 5 mm tubes.

All DOSY experiments were performed using DOSY Bipolar Pulse Pair Simulated Echo with convection compensation (dbppste_cc) pulse sequence. The total diffusion-encoding pulse duration δ and the diffusion delay Δ were optimized in order to obtain a 1 - 5% residual signal with the maximum gradient strength. Typically, in each NMR experiment ''dbppste_cc'' using 20 spectra on 16 K data points were collected, the value of d was of 1.0 ms duration, the diffusion delay (D) was set to 50 ms in all experiments and relaxation time (t1) between acquisition was set to 2 s. The experiments were performed without sample spinning. Resonance frequency [MHz]: 470.17 Fitted function: $f(x) = Io*\exp(-D*x^2*\gamma^2*\delta^2(\Delta-\delta/3)*10^4$

Used γ: 26752 rad/(s*Gauss) used δ: 0.0017200 s used Δ: 0.099900 s. Used gradient strength: variable. Random error estimation of data: RMS per spectrum (or trace/plane) Systematic error estimation of data: worst case per peak scenario

Fit parameter Error estimation method: from fit using arbitrary uncertainties confidence level: 95 % Dosy experiments were processed in NMR Varian Software. For the calibration line, different tubes were charged with similar quantities of the standard substances (0.0199 mmol) in dry DMF (0.5 mL). When the substance got dissolved, the sample was placed into the NMR probe thermostated at 273.15 K. An empirical relation between diffusion coefficient and molecular weight was established and its expressed as: $D = K \cdot M_W^{\alpha}$ where K is a molecule-dependent constant and α is a parameter that depends highly on the particle shape.[45–49] This equation was transformed into a linear equation in order to obtain the parameter α.

$$\mathbf{\ln D = \ln K + \alpha \cdot \ln M_W}$$

Weighted amounts of $C_6F_3Cl_2$–I ($4.2 \cdot 10^{-2}$ M) and [Cu(Pf)(DPI)] (**1-Pf**) ($4.2 \cdot 10^{-2}$ M) were added inside a screw cap NMR tube with the aid of a Schlenk NMR tube adaptor along with a flame sealed coaxial capillary containing acetone-d_6 to the lock deuterium signal. The tube was cooled to 273 K in an isopropanol bath and a volume and DMF taken with a syringe. The tube was closed inside the adaptor and then, taken out of the cool bath, manually shaken until total dissolution of solids and transferred to the NMR probe, which had been preheated to the monitoring temperature (273 K). C_6F_6 was used as internal standard, as we can see in Figure 42.

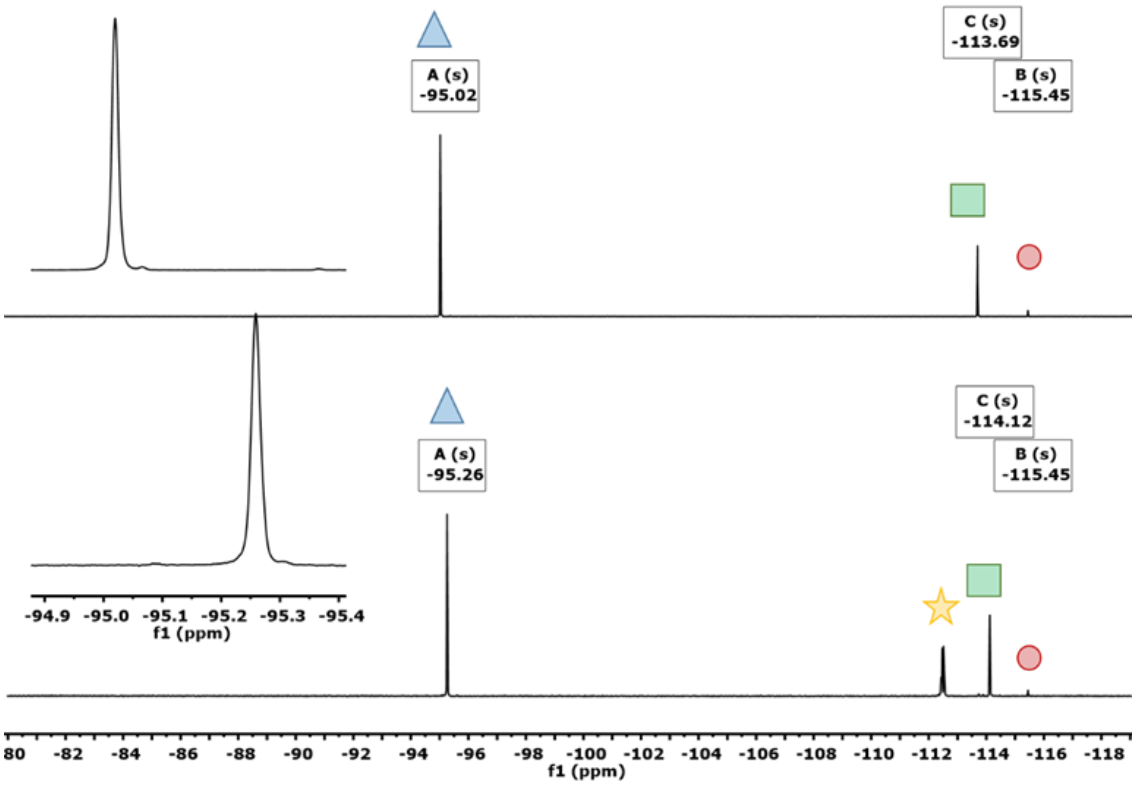

Figure 42. ^{19}F NMR chemical shifts for the reactants 1-Pf and Rf–I.

First spectra (Figure 43) represents the ^{19}F NMR spectra of $C_6F_3Cl_2$–I (blue triangles F_{ortho} and green square F_{para}) and C_6F_6 (red circle, internal standar) in DMF at 273 K. Second one represents the ^{19}F NMR of $C_6F_3Cl_2$–I (blue triangles F_{ortho} and green square F_{para}) with [Cu(Pf)(DPI)] (yellow star) and C_6F_6 (red circle, internal standar) in DMF at 273 K.

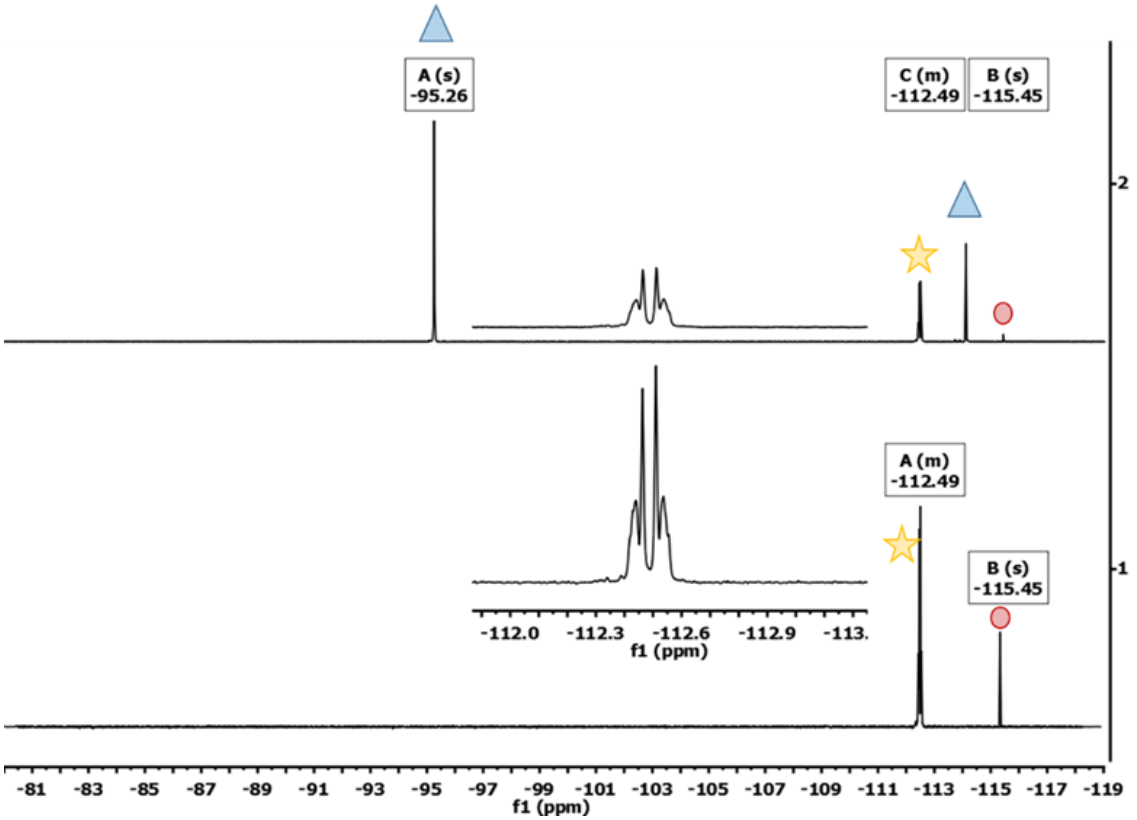

Figure 43. First spectra represents the ^{19}F NMR spectra of Rf–I (blue triangles F_{ortho} and F_{para}) , C_6F_6 (red circle, internal standar) and [Cu(Pf)(DPI)] (yellow star) in DMF at 273 K. Second one represents the ^{19}F NMR of [Cu(Pf)(DPI)] (yellow star) and C_6F_6 (red circle, internal standar) in DMF at 273 K

Computational section

Theoretical calculations were performed at DFT level of theory using Gaussian16 software.[117] The structures of all the intermediates and transition states were optimized in tetrahydrofuran solvent (DMF, ε= 37.219) with the SMD continuum model using the B3LYP functional combined with the Grimme's D3 correction for dispersion. Basis set BS1 was used for the optimizations. BS1 includes the 6-31G(d,p) basis set for the main group elements, excluding iodine, and the scalar relativistic Stuttgart-Dresden SDD pseudopotential and its associated double-ζ basis set, complemented with a set of polarization functions, for the copper (*f* polarization functions) and iodine (*d* polarization functions) atoms. Frequency calculations were carried out for all the optimized geometries in order to characterize the stationary points as either minima or transition states. Gibbs energies in DMF were calculated at 298.15 K adding to the potential energies in DMF, obtained with single point calculations using an extended basis set (BS2) at the BS1 optimized geometries, the thermal and entropic corrections obtained with BS1. BS2 consists in the def2-TZVP basis set for the main group elements, and the quadruple-ζ def2-QZVP basis set for Cu. A correction of 1.9 kcal mol^{-1} was applied to all Gibbs values to change the standard state from the gas phase (1 atm) to solution (1 M) at 298.15 K. In this way, all the energy values in the energy profiles are Gibbs energies in THF solution calculated using the formula:

$$G = E(BS2) + G(BS1) - E(BS1) + \Delta G^{1atm \rightarrow 1M}$$

where $\Delta G^{1atm \rightarrow 1M}$ = 1.9 kcal mol^{-1} is the Gibbs energy change for compression of 1 mol of an ideal gas from 1 atm to the 1 M solution phase standard state. NBO analysis was performed using NBO program.[118]

---

[117] Gaussian 16, Revision C.01, M. J. Frisch, G. W. Trucks, H. B. Schlegel, G. E. Scuseria, M. A. Robb, J. R. Cheeseman, G. Scalmani, V. Barone, G. A. Petersson, H. Nakatsuji, X. Li, M. Caricato, A. V. Marenich, J. Bloino, B. G. Janesko, R. Gomperts, B. Mennucci, H. P. Hratchian, J. V. Ortiz, A. F. Izmaylov, J. L. Sonnenberg, D. Williams-Young, F. Ding, F. Lipparini, F. Egidi, J. Goings, B. Peng, A. Petrone, T. Henderson, D. Ranasinghe, V. G. Zakrzewski, J. Gao, N. Rega, G. Zheng, W. Liang, M. Hada, M. Ehara, K. Toyota, R. Fukuda, J. Hasegawa, M. Ishida, T. Nakajima, Y. Honda, O. Kitao, H. Nakai, T. Vreven, K. Throssell, J. A. Montgomery, Jr., J. E. Peralta, F. Ogliaro, M. J. Bearpark, J. J. Heyd, E. N. Brothers, K. N. Kudin, V. N. Staroverov, T. A. Keith, R. Kobayashi, J. Normand, K. Raghavachari, A. P. Rendell, J. C. Burant, S. S. Iyengar, J. Tomasi, M. Cossi, J. M. Millam, M. Klene, C. Adamo, R. Cammi, J. W. Ochterski, R. L. Martin, K. Morokuma, O. Farkas, J. B. Foresman, and D. J. Fox, Gaussian, Inc., Wallingford CT, **2016**.

[118] NBO Version 3.1, E. D. Glendening, A. E. Reed, J. E. Carpenter, and F. Weinhold.

CHAPTER III: Copper-catalysed radical photo-decarboxylative cross-coupling of fluoroaryl carboxylates and fluoroaryl halides under mild conditions.

3.1 Introduction

Cross-coupling reactions, particularly those between halide electrophiles and organometallic nucleophiles under transition metal catalysis, are widely used to produce more complex molecules in industrial and pharmaceutical chemistry, especially in the design of new and effective drugs.[119,120] For these reasons, transition metal–catalysed arene functionalization is an important challenge in organic and organometallic chemistry.[121] Traditionally, bimetallic catalysis is the most powerful methodology for this type of couplings. In these reactions, two transition metals (TM) or a transition metal and other element cooperates to generate the new molecule.[122, 123]

New synthetic protocols are being developed nowadays for the formation of these same products using more accessible reagents.[124,125] For example, the bimetallic catalysis using Pd/Cu systems for cross-coupling, using the copper catalytic cycle for the C–H functionalization (Chapter I). For that, aryl carboxylic acids represent attractive aryl precursors, because they are abundant, structurally diverse, and accessible. The aryl carboxylic acid functionalization was explored by Gooßen et al. in 2006.[126,127,128] The copper(I) halide was able to generate the

---

[119] Pérez Sestelo, J.; Sarandeses, L. A. Advances in Cross-Coupling Reactions. *Molecules* **2020**, *25*, 23–26. DOI: 10.3390/molecules25194500.

[120] de Meijere, A.; Diederich, F. Metal-Catalyzed Cross-Coupling Reactions Eds.; Wiley, **2004**. ISBN:9783527619535 DOI: 10.1002/9783527619535.

[121] Ajitha, M. J.; Pary, F.; Nelson, T. L.; Musaev, D. G. Unveiling the Role of Base and Additive in the Ullmann-Type of Arene-Aryl C-C Coupling Reaction. *ACS Catal.* **2018**, *8*, 4829–4837. DOI: 10.1021/ACSCATAL.8B00837

[122] Pye, D. R.; Mankad, N. P. Bimetallic Catalysis for C–C and C–X Coupling Reactions. *Chem. Sci.* **2017**, *8*, 1671–2466. DOI: 10.1039/c6sc05556g

[123] Pérez-Temprano, M. H.; Casares, J. A.; Espinet, P. Bimetallic Catalysis Using Transition and Group 11 Metals: An Emerging Tool for C–C Coupling and Other Reactions. *Eur. J. Chem.* **2012**, *18*, 1864–1884. DOI: 10.1002/CHEM.201102888.

[124] Schwarz, J.; König, B. Decarboxylative Reactions with and without Light-a Comparison. *Green Chem*., **2018**, *20*, 323-361. DOI: 10.1039/c7gc02949g.

[125] Beaudelot, J.; Oger, S.; Peruško, S.; Phan, T. -A.; Teunens, T.; Moucheron, C.; Evano, G. Photoactive Copper Complexes: Properties and Applications. *Chem. Rev.* **2022**, *122*, 16365–16609. DOI: 10.1021/acs.chemrev.2c00033

[126] Gooßen, L. J.; Deng, G.; Levy, L. M. Synthesis of Biaryls via Catalytic Decarboxylative Coupling. *Science* **2006**, *313*, 662–664. DOI: 10.1126/science.1128684.

[127] Fromm, A.; van Wüllen, C.; Hackenberger, D.; Gooßen, L. J. Mechanism of Cu/Pd-Catalyzed Decarboxylative Cross-Couplings: A DFT Investigation. *J. Am. Chem. Soc.* **2014**, *136*, 10007–10023. DOI: 10.1021/JA503295X.

[128] Gooßen, L. J.; Rodríguez, N.; Linder, C.; Lange, P. P.; Fromm, A. Comparative Study of Copper- and Silver-Catalyzed Protodecarboxylations of Carboxylic Acids. *Chem. Cat. Chem.* **2010**, *2*, 430–442. DOI: 10.1002/cctc.200900277.

decarboxylation of the carboxylic acid and transmetalate the organic moiety to the Pd^{II} complex, as we can see in Figure 44.

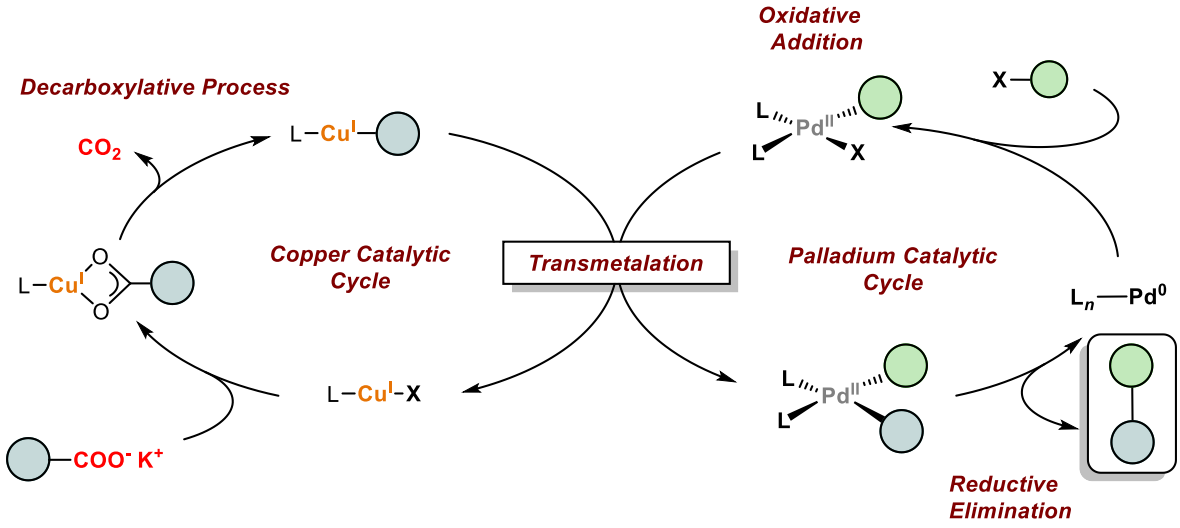

Figure 44. Bimetallic catalytic cycle proposed by Gooßen *et. al.*

In contrast to traditional cross-couplings, which require the prior preparation of organometallic reagents, the use a copper catalyst to generate the carbon nucleophiles in situ, *via* decarboxylation of carboxylic acids avoid additional synthetic steps. The disadvantage of this process is that it requires harsh reaction conditions for the generation of the Cu–C bond (up to 100 °C in all cases).

More recently, in 2009, Liu *et al*. reported the first, copper-only systems that catalyze the decarboxylative coupling of potassium fluoro-benzoates with aryl halides.[129] The new reactions allow to elude the use of expensive fluoro-aryl organometallics reagents ($Zn(C_6F_5)_2$, $Mg(C_6F_5)$ or $Ag(C_6F_5)$) in the synthesis of fluoro-biaryls. Therefore, the reaction reported herein represent a novel type of copper-catalyzed cross-coupling reactions and eliminates the palladium catalyst used by Gooßen in 2006, but high temperatures were also needed (Scheme 16).

[129] Shang, R.; Fu, Y.; Wang, Y.; Xu, Q.; Yu, H. Z.; Liu, L. Copper-Catalyzed Decarboxylase Cross-Coupling of Potassium Polyfluorobenzoates with Aryl Iodides and Bromides. *Angew. Chem. Int. Ed.* **2009**, *48*, 9350–9354. DOI: 10.1002/anie.200904916.

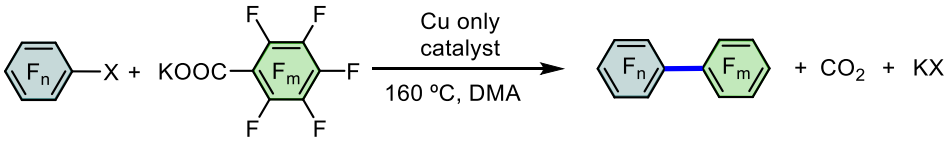

Scheme 16. General reaction scheme for the synthesis of high fluorinated biaryls proposed by Liu.

Interestingly, DFT calculations were used to compare the two plausible mechanisms. As we can see in Figure 45, in pathway A, the initial copper(I) complex reacts with perfluorobenzoate to form [Cu(OCOC$_6$F$_5$)(Phen)], which then undergoes a decarboxylation process via four-membered-ring transition state which has an energy barrier of 20.3 kcal mol^{-1}. On the other hand, in pathway B, oxidative addition takes places first on the Cu(I) complex. After oxidative addition the resulting copper(III) species is pentacoordinate and therefore, decarboxylation at copper(III) has to pass through a hexacoordinated transition state. As a result, the energy barrier for decarboxylation is calculated to be 51.1 kcal mol^{-1}, proposing that decarboxylation occurs on Cu(I) and not on Cu(III).

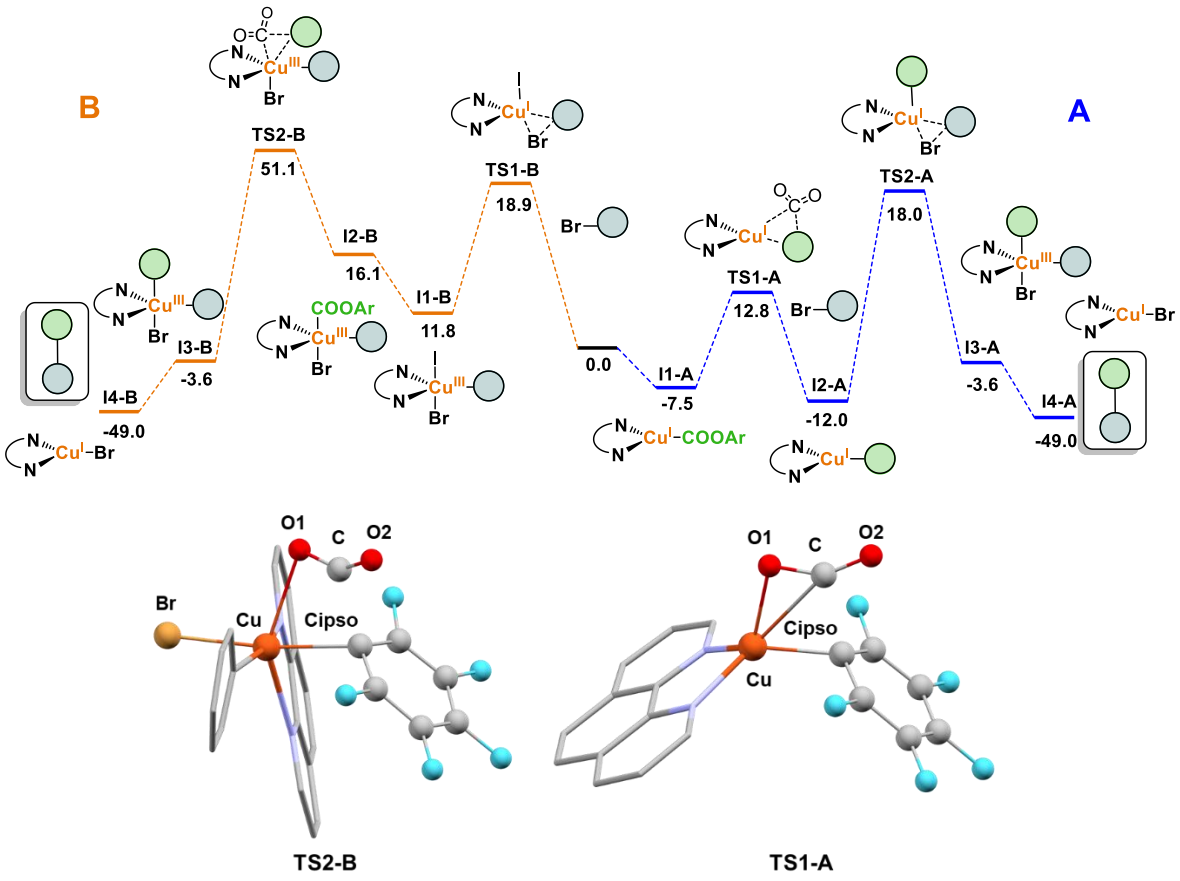

Figure 45. Energy profile of the proposed mechanism. Data in kcal mol^{-1}. TS2-B and TS1-A are also represented.

Thermal decarboxylation is not the only pathway to obtain this kind of transformation. The decarboxylation of carboxylic acids under UV-light irradiation in presence of Cu(II) salts has been known for 50 years,[130] but it was not until 2021 when the first synthetic methodologies exploiting this reactivity emerged. This new methodology is very important to improve the main disadvantage of these processes described above, which is the high temperature.

The challenging decarboxylation of aryl carboxylic acids was first unveiled by Ritter and coworkers, who reported a method for the decarboxylative fluorination aryl carboxylic acids using stoichiometric or over-stoichiometric mixture of copper(I) and copper(II) and fluoride salts, represented in Scheme 17.[131]

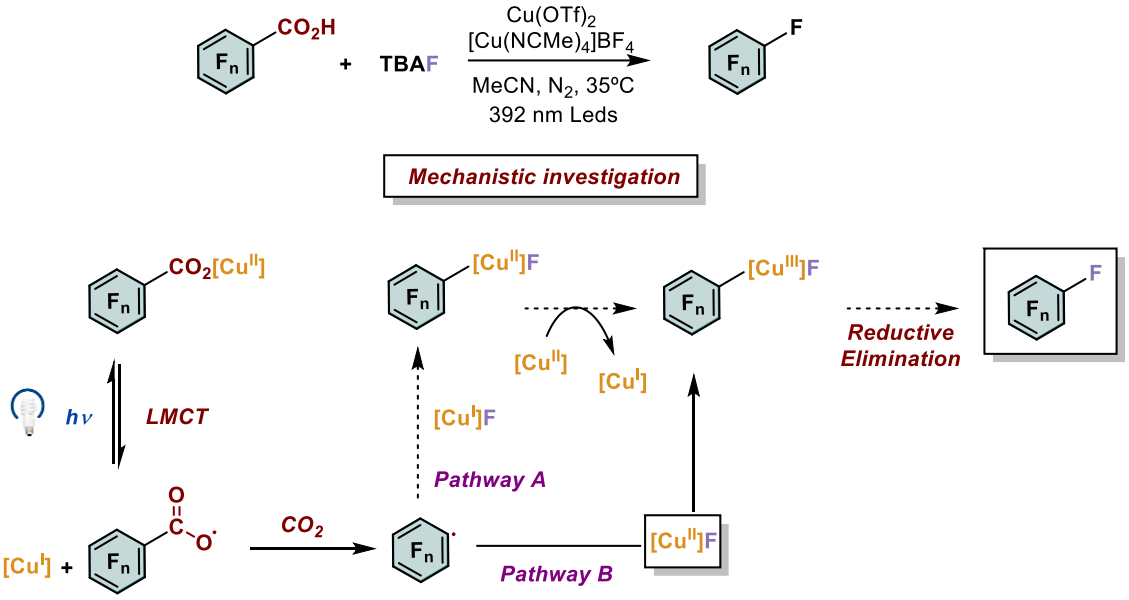

Scheme 17. Mechanistic proposed by Ritter for the fluorination of aryl carboxylic acids. [131]

The irreversible decarboxylation of the ArCOO• radical generated after Cu–O bond homolysis is allowed to proceed efficiently due to the photoinduced Ligand To Metal Charge Transfer (***LMCT***) step. These phenomena imply an electronic-transfer situation from one molecular orbital (MO) of the ligand to another MO of the metal, and results in the reduction of the metal center and the generation of a radical

[130] J. Y. Morimoto; B. A. DeGraff, J. Photochemistry of the copper(II)-Malonate System. *J. Phys. Chem.* **1972**, *76*, 1387–1388. DOI: 10.1021/j100653a029.

[131] Xu, P.; López-Rojas, P.; Ritter, T. Radical Decarboxylative Carbometalation of Benzoic Acids: A Solution to Aromatic Decarboxylative Fluorination. *J. Am. Chem. Soc.* **2021**, *143*, 5349–5354. DOI: 10.1021/jacs.1c02490.

organic moiety. This behaviour is characteristic of metals such as Cu(II), Ni(III) or Fe(III).

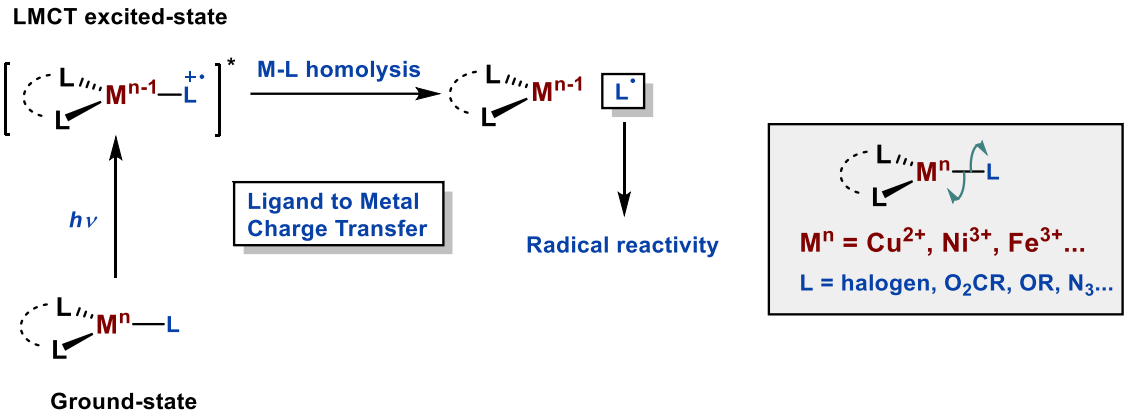

Scheme 18. Simplified representation of the LMCT process proposed by F.Juliá.[132]

The resultant aryl radical can be then efficiently trapped by [Cu^{I}–F] leading to the desired aryl fluoride products, taking advantage of the ability of the putative [Cu^{II}(Ar)F] intermediates, witch reacts with another Cu(II), generating the putative [Cu^{III}(Ar)F] in a single electron process *via* charge transfer between two copper organometallic complexes that undergo C–F reductive elimination. Additionally, the use of a Cu(I) over-stoichiometric reagent benefits the ratio of products/by-products, probably due to the possibility of electron transfer between different oxidation states. This outcome is rationalized by the higher tendency of Cu(I) to capture aryl radicals in comparison to Cu(II) complexes, that further contributes to reduce competitive HAT (Hydrogen Atom Transfer) pathways which leads to undesired byproducts (hydrolysis product), detected by experiments with deuterated solvents. This protocol demonstrates the effective synergy between Cu(I) and Cu(II) salts to generate species that can undergo reductive elimination. However, the decarboxylation reaction from the Cu(II) complex is proposed, and the Cu(I) complex being the radical acceptor. On the other hand, mechanistic details are not very concrete, especially the formation of the Cu(III) complex that undergoes the reductive elimination step and over-stoichiometric copper salts are also mandatory.

[132] Juliá, F. Ligand-to-Metal Charge Transfer (LMCT) Photochemistry at 3d-Metal Complexes: An Emerging Tool for Sustainable Organic Synthesis. *Chem. Cat. Chem*. **2022,** *14*. DOI: 10.1002/cctc.202200916.

In 2022, Reiser et al.[133] published the photocatalyzed decarboxylation. They have developed an efficient protocol for the Cu(II) photocatalyzed oxidative decarboxylation of phenylacetic acids to the corresponding aldehydes or ketones with oxygen as external oxidant (Equation 7). The light-induced homolysis of a Cu(II) carboxylate is suggested to be the key step in the decarboxylation process via LMCT. Upon Cu(II)-carboxylate homolysis and decarboxylation, the resulting radical is efficiently captured by oxygen and the resulting Cu(I) complex which delivers aldehydes or ketones and recovering the Cu(II) reactant, closing the catalytic cycle. Isolated intermediates demonstrate that the protodecarboxylation takes place in copper(II) species. Furthermore, the radical trap in this case was effective, demonstrating the existence of a radical organic moiety.

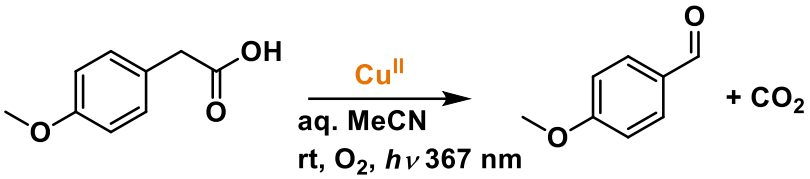

Equation 7. Cu(II) photocatalyzed oxidative decarboxylation of phenylacetic acids to the corresponding aldehydes or ketones with oxygen as external oxidant.

This protocol uses copper catalysts to generate the carbon nucleophiles in situ, *via* photo-decarboxylation was immediately used for different chemical reactions and transformations. Very recently, MacMillan, in 2022, publish *''Decarboxylative Borylation and Cross-Coupling of (Hetero)aryl Acids Enabled by Copper Charge Transfer Catalysis''* and *''A Unified Approach to Decarboxylative Halogenation of (Hetero)aryl Carboxylic acids''* represented in Figure 46.[134,135] In the first research, they generated in situ Ar–Bpin species using Ar–COOH and B_2Pin_2 as reagents, and the use of external oxidant is mandatory to close the catalytic cycle. For this

[133] Reichle, A.; Sterzel, H.; Kreitmeier, P.; Fayad, R.; Castellano, F. N.; Rehbein, J.; Reiser, O. Copper(II)-Photocatalyzed Decarboxylative Oxygenation of Carboxylic Acids. *Chem. Commun.* **2022**, *58*, 4456–4459. DOI: 10.1039/d2cc00570k.

[134] Chen, T. Q.; Pedersen, P. S.; Dow, N. W.; Fayad, R.; Hauke, C. E.; Rosko, M. C.; Danilov, E. O.; Blakemore, D. C.; Dechert-Schmitt, A. M.; Knauber, T.; Castellano, F. N.; Macmillan, D. W. C. A Unified Approach to Decarboxylative Halogenation of (Hetero)Aryl Carboxylic Acids. *J. Am. Chem. Soc.* **2022,** *144*, 8296–8305. DOI: 10.1021/jacs.2c02392.

[135] Dow, N. W.; Pedersen, P. S.; Chen, T. Q.; Blakemore, D. C.; Dechert-Schmitt, A. M.; Knauber, T.; Macmillan, D. W. C. Decarboxylative Borylation and Cross-Coupling of (Hetero)Aryl Acids Enabled by Copper Charge Transfer Catalysis. *J. Am. Chem. Soc.* **2022**, *144*, 6163–6172. DOI: 10.1021/jacs.2c01630.

activation, they proposed a LMCT in a copper (II) species (Figure 46). The successful design of a copper-catalysed LMCT decarboxylative borylation methodology allowed them to generate an important reactive in traditional palladium catalysis, and its combination with palladium-catalysed Suzuki–Miyaura coupling for one-pot decarboxylative cross-couplings of diverse (hetero)aryl carboxylic acids to synthetize several organic molecules.

The mechanistic proposal started with a Cu(II) carboxylate, which in presence of blue light, undergoes homolytic rupture in a LMCT process (in the same way that the Ar–CO_2 activation proposed by Ritter). The aryl carboxylate suffers a decarboxylative reaction, generating an aryl radical and CO_2, which can react with the boron salt to generate de Aryl–Bpin product. The copper(I) complex resulting in the homolytic rupture reacts with another carboxylic acid and with an external oxidant, regenerating the Cu(II) carboxylate (Figure 46).

On the other hand, in ''*A Unified Approach to Decarboxylative Halogenation of (Hetero)aryl Carboxylic Acids*'' they used the photo-decarboxylation to synthetize different aryl halides. This methodology exploits the diverse reactivity of aryl radicals generated via an LMCT mechanism previously reported. In this case, the mechanistic investigation shed light on the nature of the charge transfer process and the behaviour of the radicals. The unequivocal detection of the Ar-$CO_2^{\bullet}$ radical using ultrafast transient absorption spectroscopy allows them to support the homolytic rupture proposed in both works.

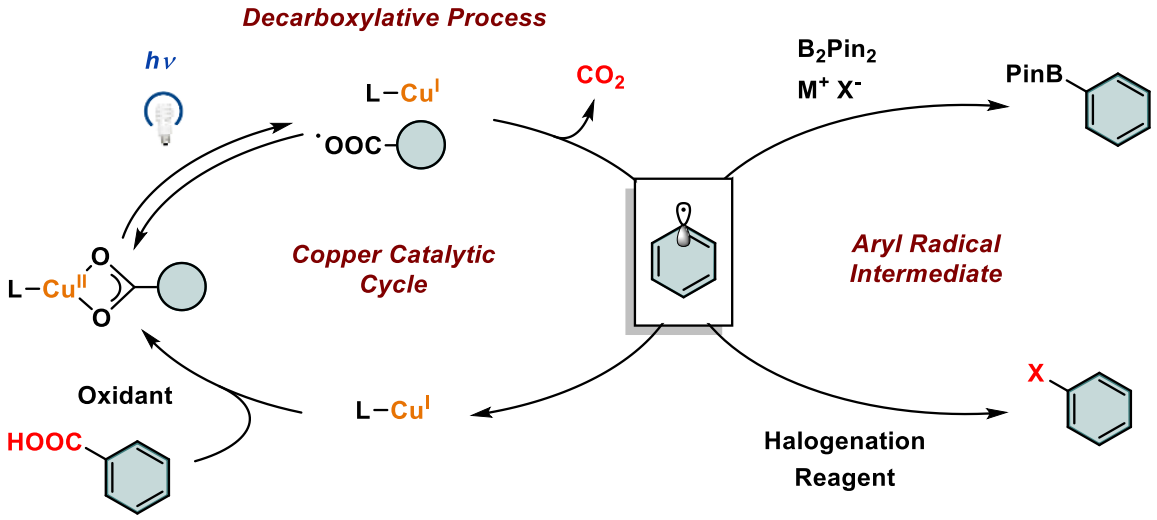

Figure 46 Copper catalytic cycle for the decarboxylation of aryl carboxylic acids proposed by MacMillan et al.

Both works allow to synthesize different products with high interest by reacting the radical formed with another reactive. In agreement with the other works, copper complexes in oxidation state one and two coexist in the reaction, in the same way of the mechanism offered by Ritter et al.

Particularly interesting is the other Ritter's *et al.* work, published in 2021 for the synthesis of phenols from carboxylic acids.[136] Radical decarboxylative carbometalation enabled by LMCT in copper benzoates provides the first hydroxylation of benzoic acids under mild conditions, as we can see in Equation 8.

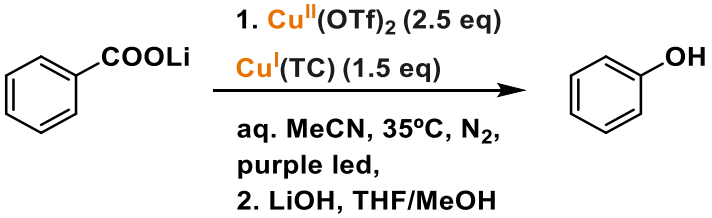

Equation 8. Synthesis of phenols from carboxylic acids proposed by Ritter et al. Copper(I) thiophene-2-carboxylate was represented as Cu^{I}(TC). Copper(II) trifluoromethanesulfonate was represented as $Cu^{II}(OTf)_2$.

The extent of the reaction using the protocol with LMCT decarboxylative carbometalation to obtain C–O bond formation beyond the initially discovered C–X

[136] Su, W.; Xu, P.; Ritter, T. Decarboxylative Hydroxylation of Benzoic Acids. *Angew. Chem. Int. Ed.* **2021**, *60*, 24012–24017. DOI: 10.1002/anie.202108971.

(X=halogen) bond formation establishes the utility and power of the photo-decarboxylative reactions in the present and near future. Furthermore, the mechanisms operating in these reactions were not studied. Again, the formation of the aryl radical by LMCT process was proposed. Reaction between [(Ln)Cu(OCOAr)], the aryl radical and again the reaction between another Cu species generates the copper(III) complex that undergoes reductive elimination to obtain the corresponding ester (Scheme 19). Finally, the hydrolysis reaction using LiOH generated the desired phenol. It is important to note that this methodology does not provide the hydroxylation product using catalytic conditions.

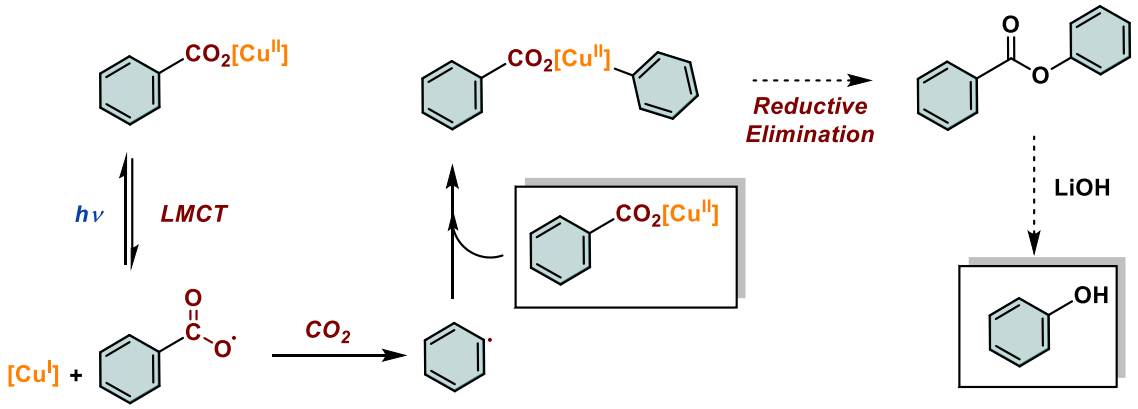

Scheme 19. Mechanistic proposal for the Synthesis of phenols from carboxylic acids proposed by Ritter et al.

This aryl carboxylic acids transformation has proven to be extremely efficient in generating Cu(I)–Ar complexes. Furthermore, several reactions can be performed using the classical doble-electron oxidative addition/reductive elimination, radical oxidative addition, or an electrophilic substitution (see Chapter II for detailed information). In this area, copper catalysis has long been considered one of the best platforms due to the propensity of high-valent copper to undergo an extremely fast reductive elimination with a wide variety of coupling fragments, used in some photo–decarboxylation protocols, as we previously commented.[137,138,139] This

[137] El-Hage, F.; Pospech, J. Copper-Catalyzed Decarboxylative Coupling. **2020**, 309–328 ISBN: 9783527826445. DOI: 10.1002/9783527826445.CH14.

[138] Evano, G.; Blanchard, N.; Toumi, M. Copper-Mediated Coupling Reactions and Their Applications in Natural Products and Designed Biomolecules Synthesis. *Chem. Rev.* **2008**, *108*, 3054–3131 DOI: 10.1021/cr8002505.

[139] Trammell, R.; Rajabimoghadam, K.; Garcia-Bosch, I. Copper-Promoted Functionalization of Organic Molecules: From Biologically Relevant Cu/O_2 Model Systems to Organometallic Transformations. *Chem. Rev.* **2019**, *119*, 2954–3031. DOI: 10.1021/acs.chemrev.8b00368.

allows to generate more challenging couplings, which metals such as Ni or Pd are not able to produce at room temperature.[140] However, the sluggish nature of oxidative addition has limited copper's capacity to broadly facilitate haloarene coupling protocols. Furthermore, there are no C–C cross-coupling reactions until this moment, leaving the most important field within classical copper chemistry unexplored using the photo-decarboxylation system.

With all these resources in our hands, we set out to create a catalytic system that would unite the best of both worlds:

1) The photochemical activation of carboxylic acids to generate a Cu–Ar species.
2) Use the easy reductive elimination of Cu(III) organometallic complexes to form high fluorinated biaryls, where metals such as Pd or Ni are not able to act at room temperature.[141,142,143]
3) Create the first cross-coupling system for C–C bond formation using this protocol.

[140] Gioria, E.; del Pozo, J.; Martínez-Ilarduya, J. M.; Espinet, P. Promoting Difficult Carbon–Carbon Couplings: Which Ligand Does Best? *Angew. Chem. Int. Ed.* **2016**, *55*, 13276–13280. DOI: 10.1002/ANIE.201607089.
[141] Budiman, Y. P.; Jayaraman, A.; Friedrich, A.; Kerner, F.; Radius, U.; Marder, T. B. Palladium-Catalyzed Homocoupling of Highly Fluorinated Arylboronates: Studies of the Influence of Strongly vs Weakly Coordinating Solvents on the Reductive Elimination Process. *J. Am. Chem. Soc.* **2020**, *142*, 6036–6050. DOI: 10.1021/JACS.9B11871/.
[142] Ponce-De-León, J.; Espinet, P. Selective Synthesis of Fluorinated Biaryls by [MCl_2(PhPEWO-F)] (M = Ni, Pd) Catalysed Negishi Cross-Coupling. *Chem. Commun.* **2021**, *57*, 10875. DOI: 10.1039/d1cc04915a.
[143] Bulfield, D.; Huber, S. M. Synthesis of Polyflourinated Biphenyls; Pushing the Boundaries of Suzuki-Miyaura Cross Coupling with Electron-Poor Substrates. *J. Org. Chem.* **2017**, *82*, 13188–13203. DOI: 10.1021/ACS.JOC.7B02267.

3.2 Results and discussion

Inspired by these precedents we envisioned the in situ photogeneration of highly fluorinated copper intermediates that could enter in a cross-coupling catalytic cycle with a fluorinated aryl halides to release the asymmetrical or symmetrical fluorinated product. We chose the pentafluoro benzoic acid (C_6F_5COOH) as fluorinated carboxylic acid which, under irradiation of light (440 nm) in the presence of $[Cu(CH_3CN)_4]BF_4$ completely decarboxylate one hour to give C_6F_5H (see Experimental section). Unfortunately, under the same conditions, the reaction between 4-C_6H_4F−I and C_6F_5COOH produced only C_6F_5H as the only new organic product in the system (Table 21 entry 1), suggesting the interference of the protonolysis reaction on copper intermediates. The alternative use of fluorinated carboxylates (instead of the acid) allows the formation of the desired product in a 10 % or 20 % of yield depending on the copper salt used (entries 2 and 3 of Table 21). The choice of the solvent is critical. DMA (DMA: N,N-dimethylacetamide) has shown to be the best solvent for this reactivity leading to a 96 % of yield for the desired product using simple 1,10-phenantroline as ligand (entry 4, Table 21, Figure 47), probably because of its capability of dissolving carboxylate salts.

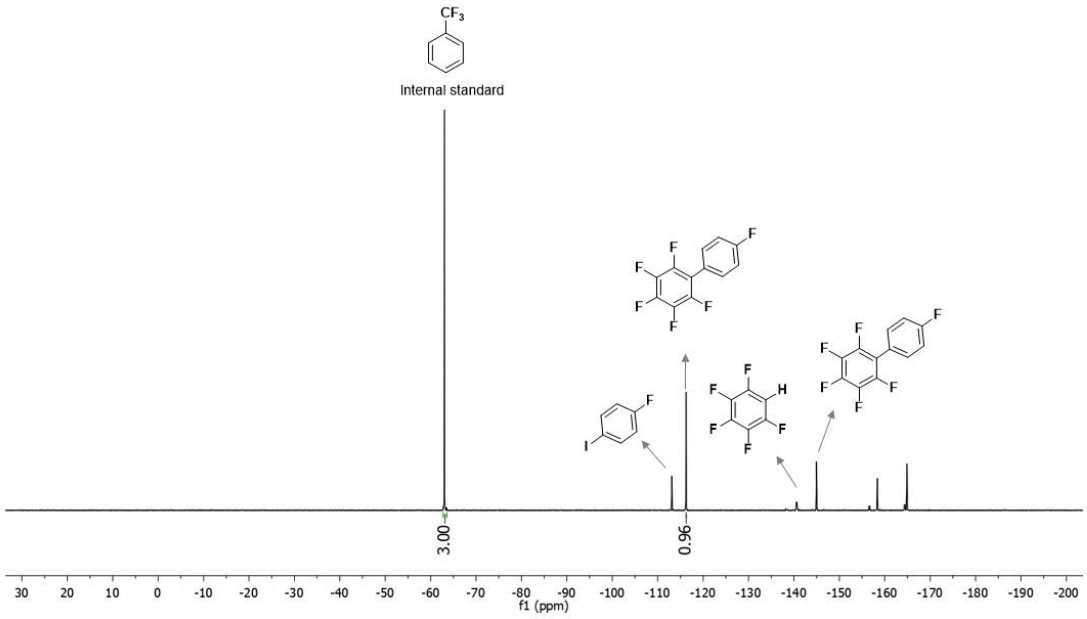

Figure 47. ^{19}F NMR of the resulting mixtures for entry 4.

Other solvents such as toluene, THF or acetonitrile does not provide the desired product.[144,145,146] The use of other ligands (Table 21, entries 5-7) has also been assayed but none of them improved the previously optimized conditions.[147] The use of other ligands (Table 21, entries 5-7) has also been tested but none of them improved the previously optimized conditions.

Table 21. Optimization conditions for the reaction:

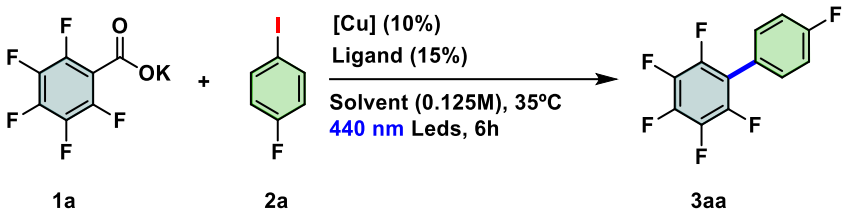

Entry	[Cu]	Solvent	L	**Yield**
1[a]	$[Cu(CH_3CN)_4]BF_4$	MeCN	Phen	**0 %**
2[b]	$[Cu(CH_3CN)_4]BF_4$	MeCN	Phen	**10 %**
3[b]	CuI	MeCN	Phen	**20 %**
4[b]	CuI	DMA	Phen	**96 %**
5[b]	CuI	DMA	dtbbpy	**51 %**
6[b]	CuI	DMA	dmphen	**32 %**
7[b]	CuI	DMA	Xantphos	**20 %**
8[b]	CuI	THF	Phen	**0 %**
9[b]	CuI	Toluene	Phen	**0 %**
10[b]	CuI	^tBuOH	Phen	**0 %**
11[b]	CuI	DMF	Phen	**70 %**

144 Armaroli, N. Photoactive Mono- and Polynuclear Cu(I)-Phenanthrolines. A Viable Alternative to Ru(II)-Polypyridines? *Chem. Soc. Rev.* **2001**, *30*, 113–124. DOI: 10.1039/b000703j.

145 Lavie-Cambot, A.; Cantuel, M.; Leydet, Y.; Jonusauskas, G.; Bassani, D. M.; McClenaghan, N. D. Improving the Photophysical Properties of Copper(I) Bis(Phenanthroline) Complexes. *Coord. Chem. Rev.* **2008**, *252*, 2572–2584. DOI: 10.1016/j.ccr.2008.03.013.

146 Blaskie, M. W.; Mcmillin, D. R. Photostudies of copper(I) systems. 6. Room-temperature emission and quenching studies of bis(2,9-dimethyl-1,10-phenanthroline) copper(I). *Inorg. Chem*. **1980**, *19*, 3519–3522. DOI: 10.1021/ic50213a062.

147 Ponce-de-León, J.; Marcos-Ayuso, G.; Casares, J. A.; Espinet, P. Pd/Cu Bimetallic Catalysis to Access Highly Fluorinated Biaryls from Aryl Halides and Fluorinated Arenes. *Chem. Commun.* **2022**, *58*, 3146–3149. DOI: 10.1039/d2cc00141a.

Reaction Conditions: a) C_6F_5COOH (0.25 mmol), ArF-I (0.375 mmol), [Cu] (10 mol%) and solvent (2 mL). 6h, 35 C b) C_6F_5COOK used as substrate instead of C_6F_5COOH, 6h, 35 °C. Yield determined by ^{19}F-NMR.

Control experiments showed no conversion in the absence of light irradiation, copper catalyst, and just 10% of the product was observed in the absence of ligand, summarized in Table 22.

Table 22. Control experiments.

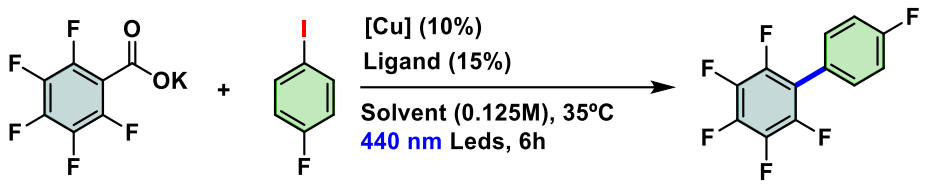

1a 2a 3aa

Entry	Conditions	**3aa** (%)[a]	**C_6F_5-H/$C_6F_5C_6F_5$** (%)[a]	**S.M** (%)
1	Standard	96	4/0	n.d
2	No Cu	n.d	n.d	>99
3	No Ligand	10	n.d	90
4	No Light	n.d	n.d	>99

Standard conditions: **1a** (0.250 mmol), **2a** (0.375 mmol), CuI (0.025 0mmol, 10 %), Phenantroline (0.0375 mmol), DMA (2 mL), 35 °C, 6 h, 440 nm Leds. [a] Yield determined by ^{19}F NMR.

Although the yields are referred to aryl iodide (due to the low solubility of the carboxylate), it is necessary to differentiate the cases in which the reaction of the carboxylate with the copper complex and light is observed, giving the hydrolysis product, or when the carboxylate does not react either, due to the absence of one of these reagents. These results allow us to determine which step is failing in the optimization process.

The scope of this methodology was explored (chart 1). In all cases, the consumption of the starting benzoate is complete to give C_6F_5–R, C_6F_5–C_6F_5 and C_6F_5H as only products. Thus, the coupling of C_6F_5COOK with C_6F_5I generates de desired product in a 95 % of yield in 6 h at 35 °C. This result contrasts with the palladium catalysed C_6F_5–C_6F_5 coupling,[140] for which the high stability of the

[$Pd(C_6F_5)_2L_n$] intermediate prevents the easy reductive elimination step making of this one of the most difficult Pd-catalysed couplings. Furthermore, the 95 % of yield in 6 h at 35 °C is quite higher than in the Pd/Cu bimetallic system (67% with standard conditions, Chapter I)[147] When the aryl halide has less fluorine atoms, the yield decreases to 85-90 %. In this way, when non-fluorinated aryls were used (**3ak** and **3al**) the yields dropped down to 52 and 27 % respectively. It is well known that the oxidative addition of non-fluorinated aryl halides is energetically more difficult than in the case of high fluorinated ones. These results agree with the catalytic yields for the non-fluorinated aryls if the oxidative addition is a step inside the catalytic cycle, and more determinant if this process is the rate determining step.

The methodology allows the use of aryl bromides as coupling partners obtaining in all cases competitive yields (**3ac-Br**, **3ai-Br** and **3ae-Br**) although more reaction time is needed. As we commented in Chapter I and Chapter II, the oxidative addition with aryl bromides is more difficult than the aryl iodides one. The use of fluorinated anilines is not productive under these reaction conditions (**3am**) perhaps due to the coordination of the aniline on the metal core blocking further reactivity.

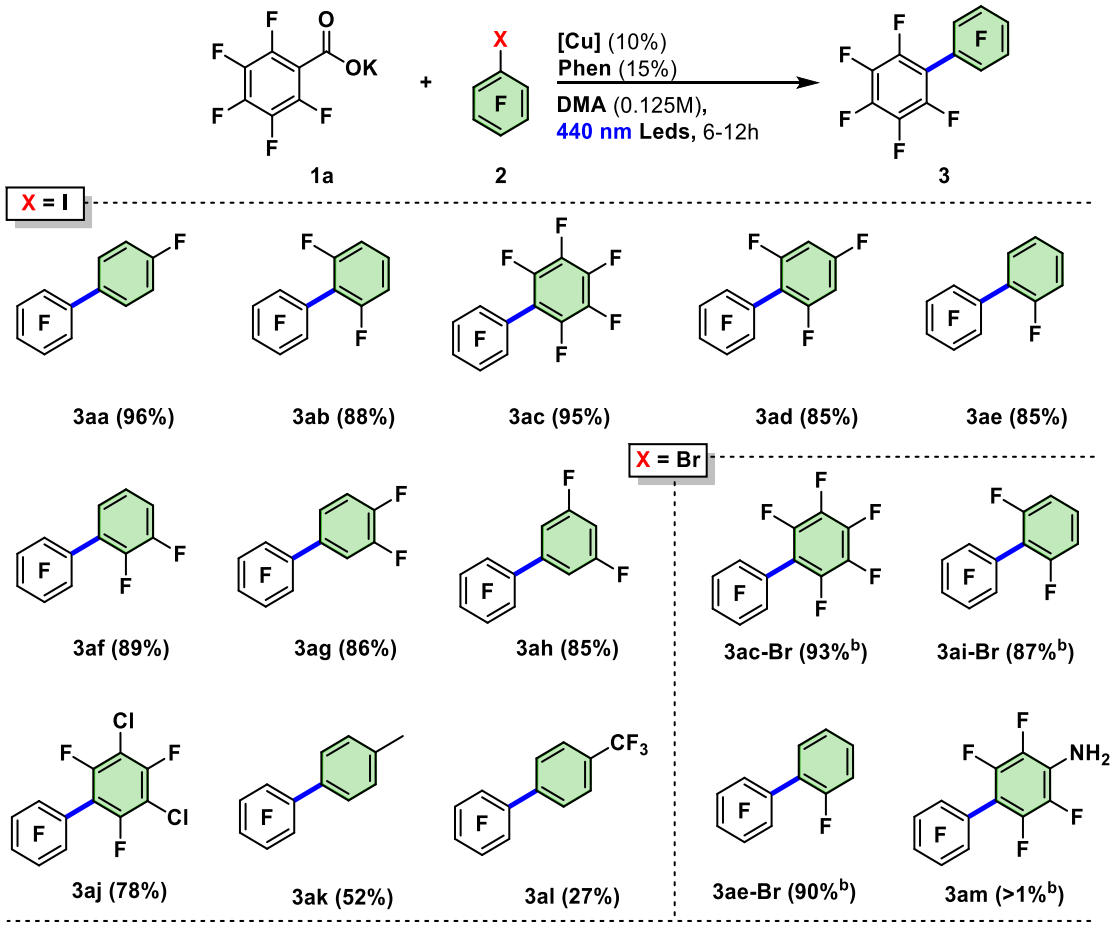

Chart 1. Reaction Conditions: C_6F_5COOK (0.25 mmol), ArF-I (0.375 mmol), [CuI] (0.025 mmol, 10 mol%), 1,10-phenantroline (0.0375 mmol, 12 mol%) and solvent (2 mL), 6h. b) C_6F_5COOK (0.25 mmol), ArF-Br (0.375 mmol), [Cu] (0.025 mmol, 10 mol%) and solvent (2 mL), 12h, 35 °C.

The reaction works with partially fluorinated aryl iodides bearing different functional groups such alkyls (**3ap**), ethers (**3aq**) or nitriles (**3ar**) in good to excellent yields, as we can see in Chart 2. The use of iodo cyclohexane does not afford any product. This confirms the no existence of a XAT (Halogen-Atom Transfer) process or another type of halogen activation.

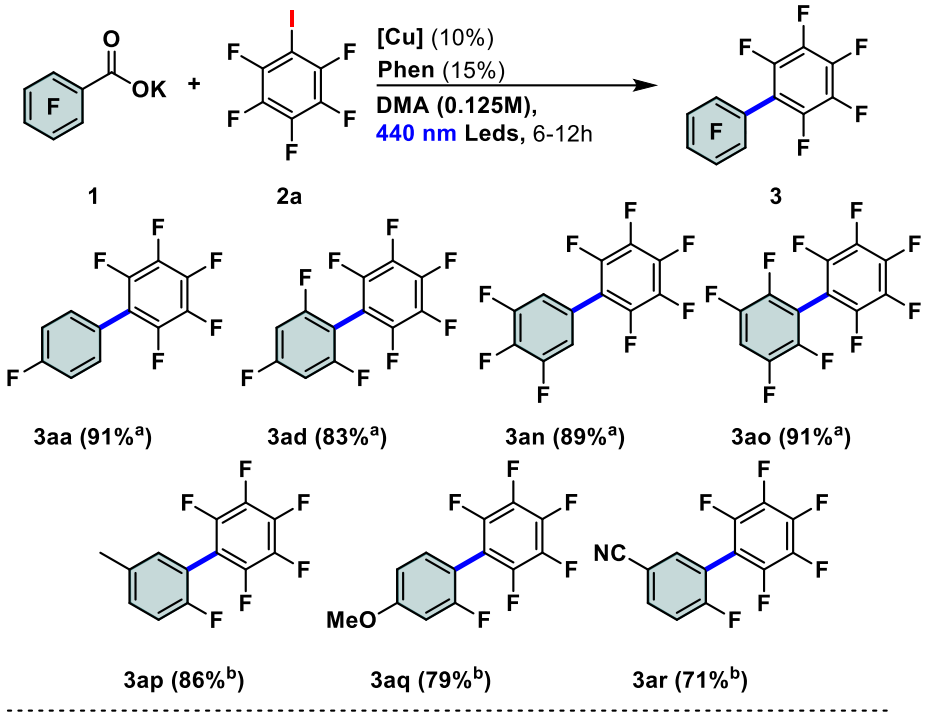

Chart 2. Reaction Conditions: ArF-COOK (0.125 mmol), C_6F_5-I (0.185 mmol), [CuI] (10 mol%) 1,10-phenantroline (12 mol %) and solvent (2 mL). a) 6 h of irradiation at 35 ˚C. b) 12 h of irradiation a 35 ˚C.

The good experimental results make us want to go deeper into this type of reaction, elaborating a mechanistic proposal that will help us to understand what happens inside the catalytic cycle. This part can become fundamental to improve in future research the process of the optimization conditions.

Mechanistic investigation

To study mechanistically in depth this reaction, different techniques were used to measure the different stages, and try to shed some light on their nature.

First, the photodecarboxylation evolves to the excision of a CO_2 molecule which has been detected by in situ IR spectroscopy, using the catalytic standard conditions, as we can see in Figure 48.

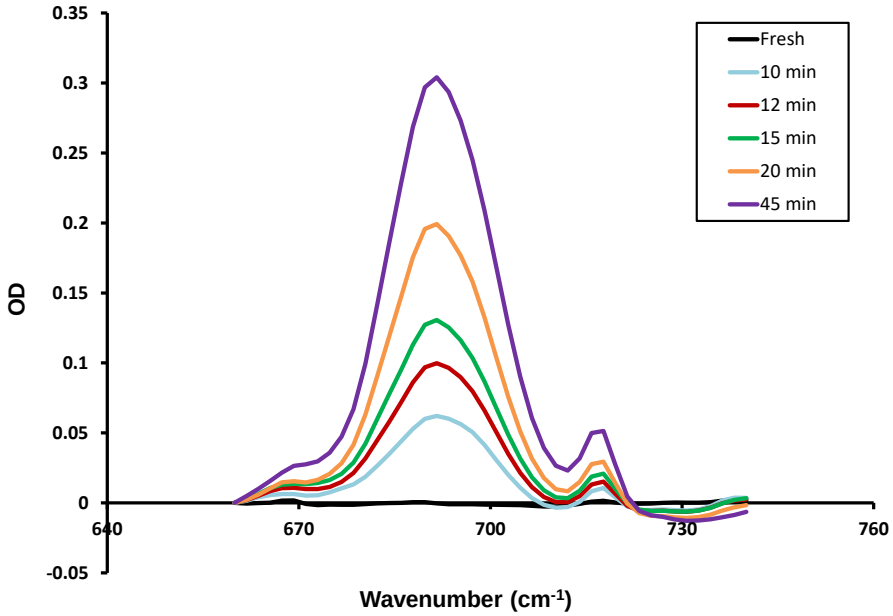

Figure 48 Solution-phase IR spectra (O-C-O bending) of the reaction between CuI (48 mg, 0.250 mmol), Phenantroline (68 mg, 0.375 mmol) and potassium pentafluorobenzoate **1a** (0.250 mmol) in DMA (4mL) at 298K.

The appearance of CO_2 in the solution demonstrates that photo-decarboxylation is taking place, and that it is not another process that governs the disappearance of the carboxylate group.

As mentioned in the introduction, all mechanistic proposals propose photo-decarboxylation by an LMCT process from an organometallic Cu(II) species. In some of these cases, including ours, Cu(I) salts are used as precatalysts, but external oxidants are used, unlike in this research. In contrast with that, combination of Cu(I) and Cu(II) salts are also used. [131,136]

Therefore, we set out to determine which is the active species in the photo-decarboxylation process. For that, we test both possible catalysts.
The complex $[Cu^{II}(OCO\text{-}p\text{-}C_6H_4F)_2(Phen)(OH_2)]$ could be prepared and isolated for the experiment and was characterized by X-ray diffraction, as we can see in Figure 49.

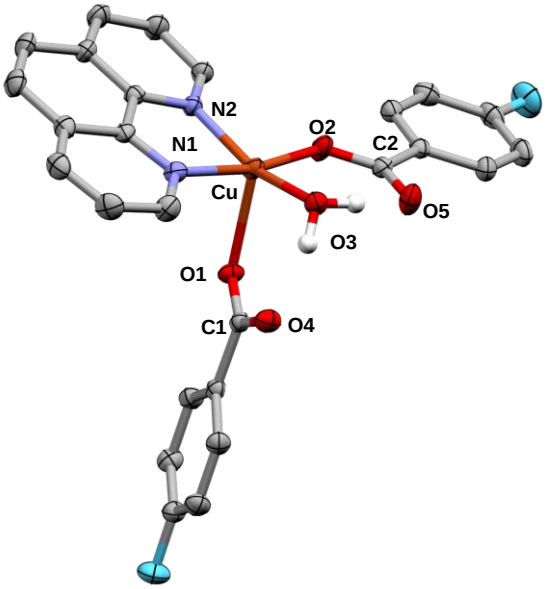

Figure 49. Xray-diffraction of $[Cu^{II}(OCO\text{-}p\text{-}C_6H_4F)_2(Phen)(OH_2)]$.

On the contrary, the complex $[Cu^{I}(OCO\text{-}p\text{-}C_6H_4F)(Phen)]$ was prepared in situ for the experiment, but due to its high reactivity it could not be isolated. The experiment was carried out by ^{19}F NMR. The Cu(I) complex in dry DMA solution and under N_2 atmosphere, does not show any change under blue light, i.e., no photodecarboxylation scavenging species are seen. On the other hand, the Cu(II) complex shows a high reactivity to blue light, generating the C_6H_5F species, a hydrolysis product of the hypothetical intermediate $[Cu(C_6H_4F)(Phen)]$, formed by reaction with residual water or by a HAT process with the solvent. [131, 136]

Different reaction pathways could be proposed accounting for these results. It may be that we have a species that is oxidizing our system, generating Cu(II) in the media, which is the cause of decarboxylation reaction. Another option is that Cu(II) species are introduced from the reactants or that there are uncontrollable oxidations due to the residual ppm of O_2 in the solvent.

Recently, our research group has published aryl exchange reactions between Cu(III) complexes and Cu(I) complexes by electronic transfers in systems with bipyridine ligands, using fluorinated aryls.[148] This leads us to propose different

[148] Lozano-Lavilla, O.; Gómez-Orellana, P.; Lledós, A.; Casares, J. A. Transmetalation Reactions Triggered by Electron Transfer between Organocopper Complexes. *Inor. Chem.* **2022**, *18*, 11633–11639. DOI: 10.1021/acs.inorgchem.1c01595.

reaction pathways for the formation of the active species in the decarboxylation process using different oxidation states of the catalyst.

Starting from Cu(I), it is possible to propose two oxidative addition processes, using both reactants involved in the equilibrium, since we know that none of the two reactants undergoes any modification under blue light. On the other hand, oxidative addition onto the Cu(I) complex with the carboxylate is more plausible due to the fast ligand substitution to generate the corresponding salt (Scheme 20).

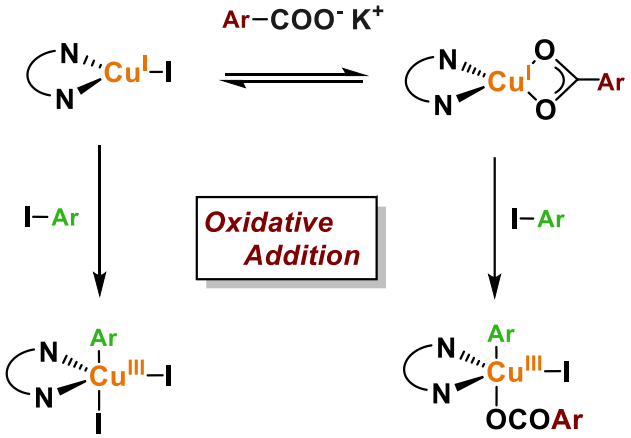

Scheme 20. Possible oxidative addition pathways between reactants.

Then, the reaction of any of these Cu(III) with one of the Cu(I) complexes, which is in high concentration, would generate a redox reaction, generating Cu(II) species that can enter the catalytic cycle, undergoing a decarboxylation process (Scheme 21).

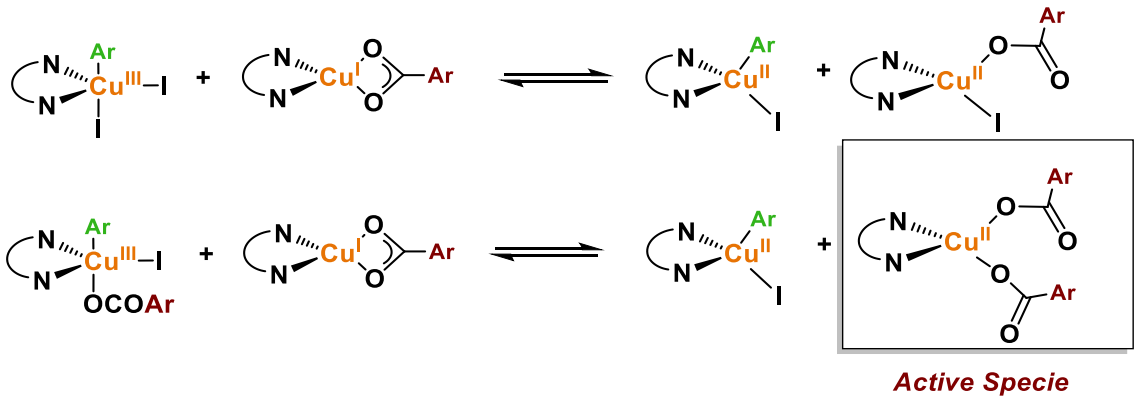

Scheme 21. Possible formation of the active specie pathway.

This mechanism provides a reasonable pathway for the formation of Cu(II) carboxylates which, accordingly with the literature, are necessary for the decarboxylation step. The other part of the catalytic cycle would be the oxidative addition of aryl iodide to [Cu(Ar)(Phen)]. This process is well known and can be monitored by ^{19}F NMR, stoichiometric tests and DFT calculations can be performed. First of all, it is necessary to determine if the oxidative addition modifies its reaction rate in the presence of blue led, that is, if the oxidative addition step is a photocatalyzed process. For this purpose, a low-temperature experiment is carried out, where two reactions are measured, one under blue led, and one without light, of the oxidative addition step. The reaction between [Cu(Pf)(phen)] and 10 RfI in dry DMA at 283 K. ($[Cu]_0$= 5.0 x 10^{-3} mol L^{-1};$[RfI]_0$= 5.1 x 10^{-2} mol L^{-1}) was measured with and without blue leds. In both cases, no consumption of the starting materials was detected, demonstrating that the oxidative addition cannot be carried out at low temperatures. Furthermore, if the reaction was carried out at 308 K (catalytic conditions), with and without blue leds, the formation of the cross-coupling product was measured by ^{19}F NMR. As we can see in Figure 50, the reaction under blue led is faster than the reaction without it, but not enough to consider a light promoted oxidative addition process. For this reason, the oxidative addition step is not a photocatalyzed process in this system.

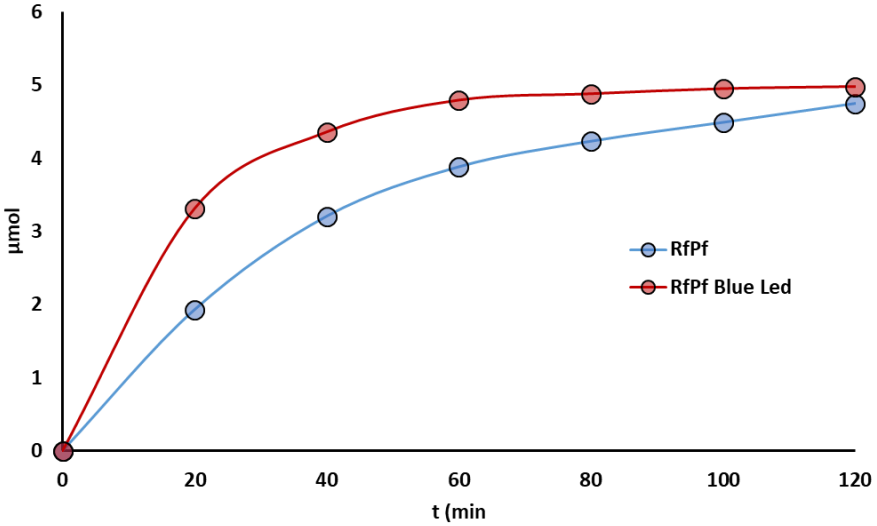

Figure 50 ^{19}F NMR monitoring of the reaction between [Cu(Pf)(phen)] and 10 RfI in dry DMA at 308 K. $[Cu]_0$= 5.0 x 10^{-3} mol L^{-1};$[RfI]_0$= 5.1 x 10^{-2} mol L^{-1} (Blue dots), reaction between [Cu(Pf)(phen)] and 10 RfI in dry DMA at 308 K under Blue Led (440 nm). $[Cu]_0$= 5.0 x 10^{-3} mol L^{-1}; $[RfI]_0$= 5.1 x 10^{-2} mol L^{-1} (Red dots).

These two experiments allow us to conclude that the oxidative addition step is a concerted process and that it does not suffer any significant alterations under blue led.

In Figure 51, the reaction rate between the [Cu(Pf)(Phen)] complex and $C_6F_3Cl_2$–I is represented. As we can see, it is a relatively fast reaction at room temperature.

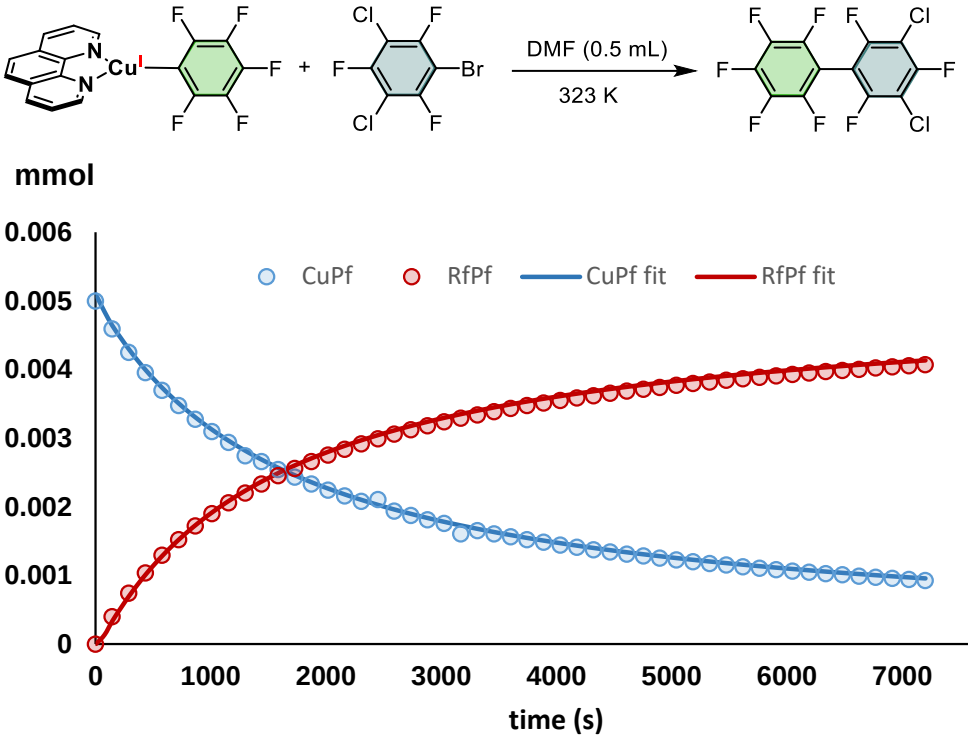

Figure 51. ^{19}F NMR monitoring of the reaction between [Cu(Pf)(Phen)] (0.005 mmol) and Rf-Br (0.0051 mmol) in dry DMA (0.5 mL) at 323 K.

Using copasi software with a simple kinetic model of two elementary reactions (shown in Figure 52), which would be oxidative addition and reductive elimination, we can fit the experimental data (representation in experimental section).

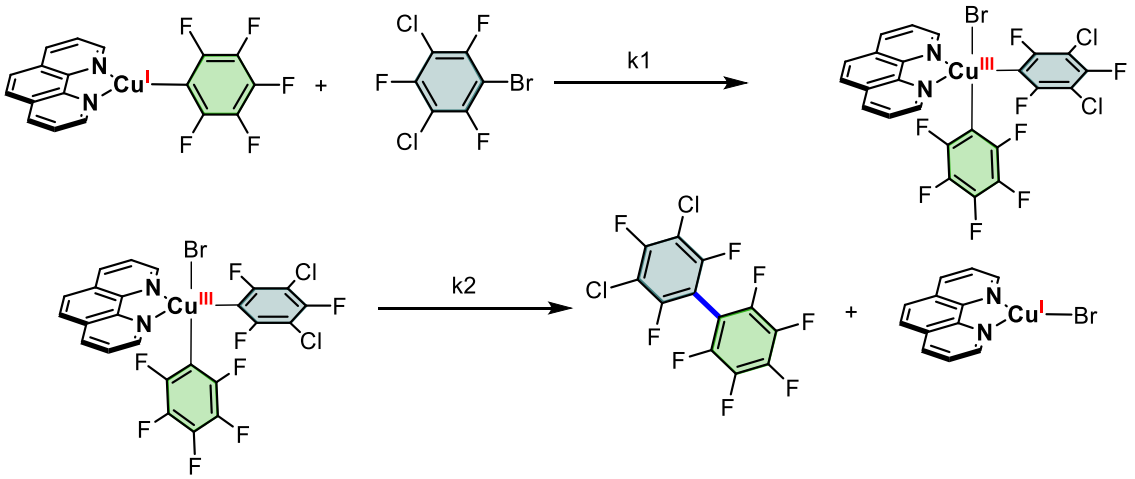

Figure 52. Kinetic model used for the non-linear fitting shown in. **Figure 51.**

Using the same methodology employed in other chapters, we can aim the kinetic values. For the oxidative addition step, we obtain k_1 = 1.20 x 10^{-1} ± 6 x 10^{-4} s^{-1}, and k_2 =fast, verifying a relatively slow oxidative addition step at 323 K and a fast reductive elimination.

To explain the discrepancies that we observed in the reactivity of the different aryl iodides in the catalytic reactions, the competitive reaction between [Cu(Pf)(Phen)] + Pf–I + Ph–I was tested under catalytic conditions. Analyzing the differences in the bond dissociation energy, the C–I (Pf) bond energy is higher than the C–I (Ph) one, which implies that the homolytic rupture produced by light should give as a majority product the Pf–Ph heterocoupling in the case of a photochemically activated process. On the other hand, the formation of Pf–Pf homocoupling would be due to a process of oxidative addition and traditional reductive elimination, considering the higher reaction rate of Pf–I *vs* Ph–I due to the electronic differences in the aromatic ring.

As we can observe in the spectrum, the formation of the Pf–Pf product is the majority (81%) compared to the formation of Pf–Ph, which explains that the oxidative addition is much faster for the highly fluorinated aryls. This would explain the difference in catalysis yields, assuming that oxidative addition is the rate limiting step. This result implies that the C–I activation is not a radical process (Figure 53).

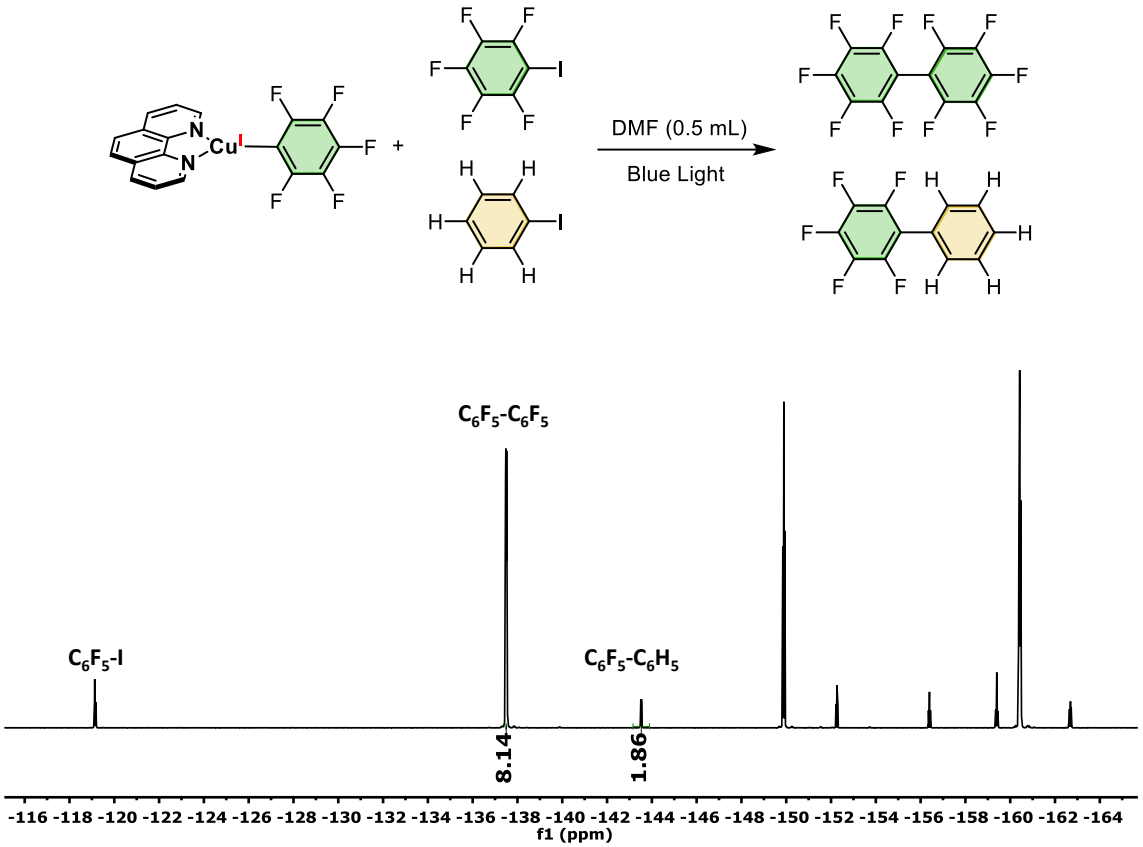

Figure 53. ^{19}F NMR of the final mixture products.

Furthermore, oxidative radical decarboxylation has been studied from the copper carboxylate complex, which benefits from the lower activation barrier of about 8–9 kcal/mol for CO_2 extrusion to afford aryl radicals.[131] This information leaves the oxidative addition step as the most likely hypothesis to be the rate limiting stage. DFT calculations show an activation barrier of 21.8 kcal mol^{-1} for this process when I–C_6F_5 is used as the aryl iodide. Furthermore, it is well known that the reductive elimination step in Cu(III) species is fast at room temperature.

With all this information, we can design the following mechanistic proposal: As mentioned above, is to determine the reaction that generates the active species (Scheme 22).

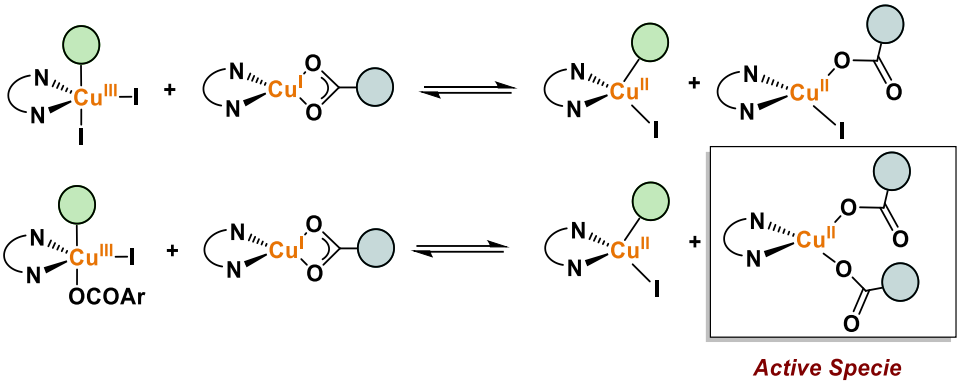

Scheme 22. Proposed mechanism of the formation of the active specie for the decarboxylation process.

Once we have the active species, which undergoes photochemical decarboxylation, we can propose the rest of the catalytic cycle, up to the formation of the product and the regeneration of the catalyst, represented in Figure 54.

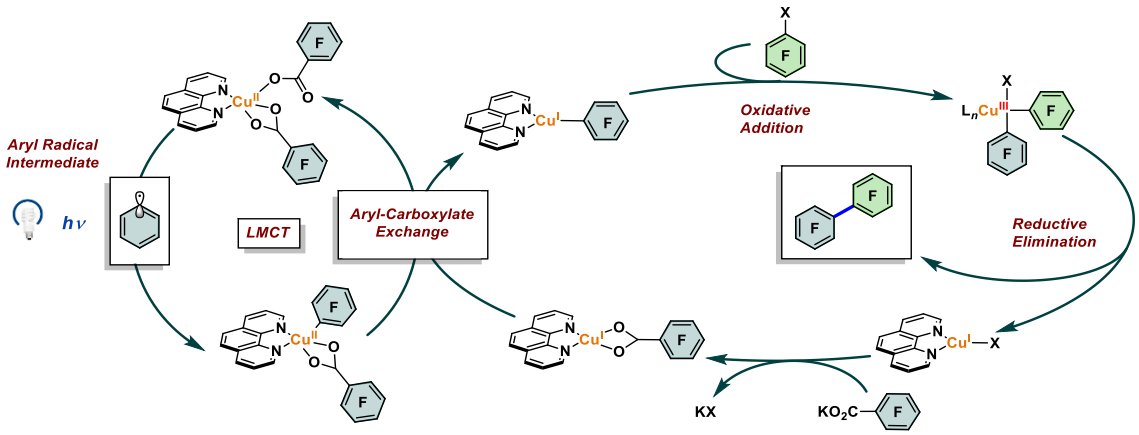

Figure 54. Proposed catalytic cycle for the formation of high fluorinated biaryls.

Once the active species is formed and undergoes the decarboxylation step by means of an LMCT process, a Cu(II) complex is formed with a coordinated carboxylate and aryl. This complex reacts by means of an aryl-carboxylate exchange step with the complex [Cu(OCOAr)(Phen)] (majority in solution). In this way, the Cu–Ar complex is generated, which is necessary for the oxidative addition stage to occur. It is at this moment when the Cu(I) complex reacts with the aryl iodide to formally generate the Cu(III) complex, which undergoes a reductive elimination step, giving the desired product and regenerating the precatalyst. Due to the great relevance of this type of reaction today, in-depth investigation of the reaction mechanism is ongoing.

3.3 Summary and conclusions

In conclusion we present a novel and modern methodology for the formation of fluorinated and highly fluorinated biaryl from the abundant and bench stable benzoates. Focused on the methodology, we perform the fluorinated and highly fluorinated symmetrical and unsymmetrical biaryls under mild conditions using a copper catalytic system. The use of stoichiometric salts, long reaction times or non-abundant metals are also removed.

On the other hand, this photochemical methodology is the first example of C–C cross-coupling reaction using a photodecarboxylation via LMCT using copper as catalyst. This innovative reaction opens the door to several coupling processes using carboxylic acids/carboxylates as a source of reagents for the formation of the most important bonds for generating building blocks.

Some features of the mechanism are particularly relevant: i) the photochemical activation could operate in two consecutive steps of the catalytic cycle, and ii) the photochemical Ar–COO cleavage leads primarily to the Cu–Ar instead of the Cu–I bond. These contributions, together with those described above, allow us to be a little closer to a complete understanding of the mechanism of this type of reaction.

3.4 Experimental section

General experimental section

General procedures and equipment have been described in the Experimental Section in Chapter I.

Anhydrous, oxygen-free, N,N-Dimethylformamide, amine free, 99.9% obtained by Alfa Aesar Solvents for experiments in an inert atmosphere were stored into flame-dried Schlenk flasks over freshly activated 3 or 4 Å molecular sieves.[149] Commercially available chemicals were purchased from Sigma Aldrich, Alfa Aesar, Fluorochem, Acros Organics and BLDPharm and were used without further purification. Ligands were purchased from BLDPharm and Sigma Aldrich. [Cu(Pf)(Phen)] was synthesized as previously reported.[150]

Some high fluorinated potassium benzoates were synthesized as previously reported. [129]

Flash chromatography was carried out using silica gel (230-240 mesh). Chemical yields refer to pure isolated substances or determined by ^{19}F-NMR.
IR spectra in solution were measured with a ReactIR (Metler-Toledo) spectrometer with DiComp Fiberto-Sentinel sensor, collecting from 650 cm^{-1} to 1600 cm^{-1}.

Photoreactor setup: The Integrated Photoreactor is used for reaction irradiation. For all the experiments, 440 nm LED modules were used. LED intensity for irradiation is generally 100% at 1.5 cm from the reaction, 12V Blue LED Strips (60 LEDs per meter). The reaction temperature is thermostatically controlled at (~35° C) under this setting.

For the mechanistic studies, a Kessil lamp based photoreactor was used (PR160L with a wavelength of 440 nm). In this case, reaction vessels were put at 6 cm from the light source to ensure an average intensity of 137 mW/cm^2 in a reproducible manner. Temperature was controlled with a thermostatized flow of compressed air.

---

[149] Kieboom, A. P. G. Purification of Laboratory Chemicals, 3rd Edition. D.D. Perrin and W. L. F. Armarego. Pergamon Press, Oxfor. ISBN 0-08-034715-0, Hardcover, **2010**, *107*, 685–685. DOI: 10.1002/recl.19881071209.
[150] Do, H.-Q.; Khan, R. M. K.; Daugulis, O. A General Method for Copper-Catalyzed Arylation of Arene C-H Bonds. *J. Am. Chem. Soc*. **2008**, *130*, 15185–15192. DOI: 10.1021/ja805688p.

HRMS (EI) were performed with a MALDI Bruker Autoflex at the LTI facilities of Valladolid University (Spain).

Synthesis of potassium perfluorobenzoates

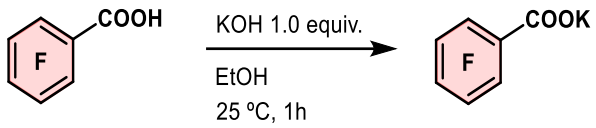

A 100ml schlenk was charged with the carboxylic acid (20.0 mmol) and ethanol (20ml). To this, a solution of potassium hydroxide (20 mmol) in ethanol (15 ml) was added. After completion of addition, the reaction mixture was stirred for another 1h at room temperature. A gradual formation of a white precipitate was observed. After removing the ethanol solvent by evaporation under vacuum, 20 ml of diethyl ether was added. The resulting withe solid was collected by filtration, washed with ethanol (5ml x 3) and diethyl ether (10 ml x 2), transferred to a round-bottomed flask and dried under vacuum at 50°C for 1 h to provide the corresponding potassium salts in 95-99% yields.

This methodology has been modified from that previously described in the literature.[129] The ^{19}F chemical shifts previously described confirm the desired products.

Potassium pentafluorobenzoate (1a)

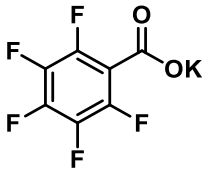

Following general procedure with pentafluorobenzoic acid. The product was obtained as a white solid (99%).

$^{13}C\{^{1}H\}$ NMR (125.67 MHz, Deuterium Oxide) δ 165.4, 144.5 – 141.3 (m), 142.5 – 139.4 (m), 139.0 – 135.8 (m), 114.5 (t, J = 225 Hz).

^{19}F NMR (470 MHz, Deuterium Oxide) δ -143.82 – -144.60 (m, 2F), -155.82 (t, J = 20 Hz, 1F), -161.05 – -163.60 (m, 2F).

Potassium tetrafluorobenzoate (1b)

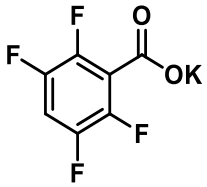

Following general procedure with 2,3,5,6-tetrafluorobenzoic acid. The product was obtained as a white solid (98%).

^{1}H NMR (500 MHz, Deuterium Oxide) δ 7.20 (tt, J = 10.1, 8 Hz, 1H)

^{13}C{^{1}H} NMR (101 MHz, Deuterium Oxide) δ 165.7, 147.1 – 144.2 (m), 142.4 (dddd, J = 246, 15, 7, 4 Hz), 118.8 (t, J = 21 Hz), 106.1 (t, J = 23 Hz).

^{19}F NMR (470 MHz, Deuterium Oxide) δ -139.05 – -139.17 (m, 2F), -144.25 – -144.38 (m, 2F).

Potassium 2,4,6-trifluorobenzoate (1c)

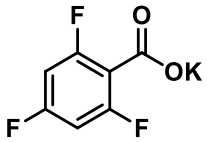

Following general procedure with 2,4,6-trifluorobenzoic acid. The product was obtained as a white solid (99%).

^{1}H NMR (500 MHz, Deuterium Oxide) δ 6.78 – 6.71 (m, 1H).

^{13}C{^{1}H} NMR (101 MHz, Deuterium Oxide) δ 167.7, 162.4 (dt, J = 248, 15 Hz), 159.3 (ddd, J = 248, 15, 11 Hz), 112.6 (t, J = 23 Hz), 101.4 – 99.7 (m).

^{19}F NMR (470 MHz, Deuterium Oxide) δ -107.25 – -107.63 (m, 2F), -112.06 (dd, J = 8, 6 Hz, 1F).

Potassium 3,4,5-trifluorobenzoate (1d)

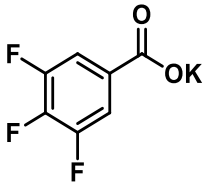

Following general procedure with 2,4,6-trifluorobenzoic acid. The product was obtained as a white solid (95%).

^{1}H NMR (500 MHz, Deuterium Oxide) δ 7.43 – 7.30 (m, 2H).

^{13}C{^{1}H} NMR (125.67 MHz, Deuterium Oxide) δ 171.6, 150.3 (ddd, J = 248, 10, 3 Hz), 141.4 (dt, J = 252.4, 15.7 Hz), 132.4, 113.6 – 113.0 (m).

^{19}F NMR (470 MHz, Deuterium Oxide) δ -135.16 – -135.31 (m, 1F), -157.88 (tt, J = 20, 6 Hz, 2F).

Potassium 2-fluoro-4-methyl-benzoate (1e)

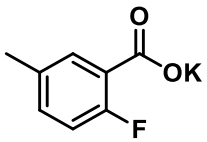

Following general procedure with 2,4,6-trifluorobenzoic acid. The product was obtained as a white solid (97%).

^{1}H NMR (500 MHz, Deuterium Oxide) δ 7.32 – 7.23 (m, 1H), 7.13 (ddd, J = 7, 5, 2 Hz, 1H), 6.91 (dd, J = 10.7, 8.5 Hz, 1H), 2.17 (s, 1H).

^{13}C{^{1}H} NMR (125.67 MHz, Deuterium Oxide) δ 173.4, 158.0 (d, J = 245 Hz), 134.0 (d, J = 3 Hz), 132.1 (d, J = 8 Hz), 130.6 – 129.7 (m), 125.2 (d, J = 14 Hz), 115.8 (d, J = 22 Hz), 19.7.

^{19}F NMR (470 MHz, Deuterium Oxide) δ -121.39 (dt, J = 11, 5 Hz, 1F).

Potassium 2-fluoro-4-methoxy-benzoate (1f)

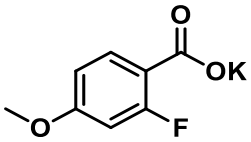

Following general procedure with 2,4,6-trifluorobenzoic acid. The product was obtained as a white solid (97%).

^{1}H NMR (500 MHz, Deuterium Oxide) δ 7.50 (t, J = 8 Hz, 1H), 6.69 – 6.57 (m, 2H), 3.71 (s, 3H).

^{13}C{^{1}H} NMR (125.67 MHz Deuterium Oxide) 175.3, 164.4 (d, J = 11 Hz), 164.1 (d, J = 250 Hz), 134.4 (d, J = 4 Hz), 120.1 (d, J = 12 Hz), 112.3, 104.5 (d, J = 27 Hz), 58.2.

^{19}F NMR (470 MHz, Deuterium Oxide) δ -112.00 – -112.08 (m, 1F).

Potassium 5-cyano-2-fluorobenzoate (1g)

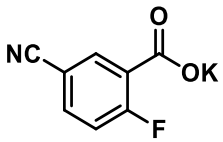

Following general procedure with 2,4,6-trifluorobenzoic acid. The product was obtained as a white solid (97%).

^{1}H NMR (500 MHz, Deuterium Oxide) δ 7.86 (dd, J = 6, 2 Hz, 1H), 7.68 (ddd, J = 9, 5, 2 Hz, 1H), 7.17 (dd, J = 10, 9 Hz, 1H).

^{19}F NMR (470 MHz, Deuterium Oxide) δ -105.77 (ddd, J = 10, 6, 4 Hz, 1F).

Optimization of catalytic conditions

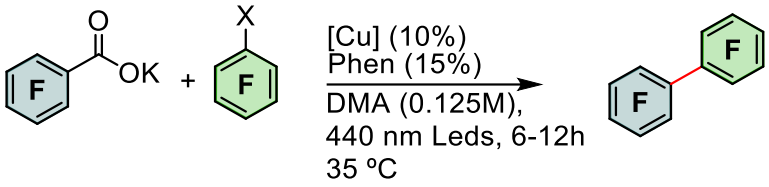

Screening reactions were conducted on a 0.250 mmol scale of Potassium pentafluorobenzoate (**1a**) in 2.0 mL of solvent (0.125 M). CuI (0.025 mmol) and ligand (0.0375 mmol) were added to a flame-dried screwed-capped Schlenk flask with a magnetic stirrer. Then, the corresponding aryl iodide, 4-Fluoroiodobenzene (**3a**, 0.375 mmol) and solvent (2 mL) were added to the flask. The Schlenk was placed in a photo-reactor and stirred for 6 hours. Then, it was taken out of the reactor, cooled to room temperature, and an aliquot was checked by ^{19}F NMR. **3aa** was obtained in 94 % isolated yield employing the standard conditions (6h, 35 °C) stated in the image.

When the reaction was carried out in the absence of the catalyst or light, only traces of coupling product were observed, as we can see in Table 23.

Control experiments

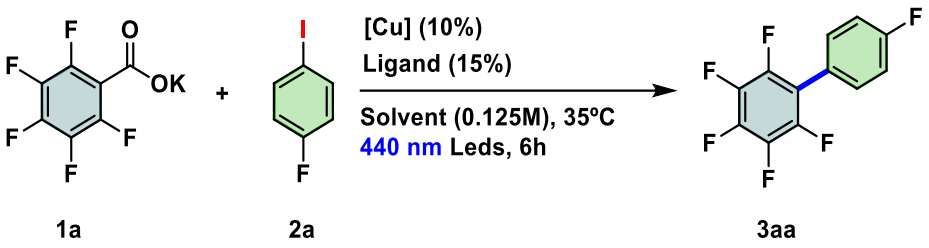

Entry	Conditions	**3aa** (%)[a]	**Pf-H/Pf-Pf** (%)[a]	**S.M(%)**
1	Standard	97 (94)	3/0	n.d
2	No Cu	n.d	n.d	>99
3	No Ligand	10	n.d	90
4	No Light	n.d	n.d	>99

Table 23. Standard conditions: **1a** (0.250 mmol), **2a** (0.375 mmol), CuI (10 %), Phenantroline (0.0375 mmol), DMA (2 mL), 35 °C, 6 h,440 nm Leds. [a] Yield determined by ^{19}F NMR. Isolated Yield in parenthesis.

Variation of the aryl halide

Employing an aryl bromide (**2a-Br**) gave the product in a similar yield (Table 24, entry 1). However, when an aryl chloride (**2a-Cl**) was used the product was not detected (entry 2).

Entry	Aryl halide	**3aa** (%)[a]	**Pf-H/Pf-Pf** (%)[a]	**S.M(%)**
1[b]	Aryl bromide	92	8/0	n.d
2	Aryl chloride	n.d	n.d	>99
3	Aryl iodide	97	3/0	n.d

Table 24. Standard conditions: **1a** (0.250 mmol), **aryl halide** (0.375 mmol), CuI (10 %), Phen (0.0375 mmol), DMA (2 mL), 35 °C, 6 h,440 nm Leds. [a] Yield determined by ^{19}F NMR.[b] Reaction time 12h.

Variation of the copper ligand

Screening reactions were conducted on a 0.250 mmol scale of Potassium pentafluorobenzoate (**1a**) in 2.0 mL of solvent (0.125 M). CuI (0.025 mmol) and ligand (0.0375 mmol) were added to a flame-dried screwed-capped Schlenk flask

with a magnetic stirrer. Then, the corresponding aryl iodide, 4-Fluoroiodobenzene (**3a**, 0.375 mmol) and solvent (2 mL) were added to the flask. The Schlenk was placed in a photo-reactor and stirred for 6 hours. Then, it was taken out of the reactor, cooled to room temperature, and an aliquot was checked by ^{19}F NMR, represented in Table 25.

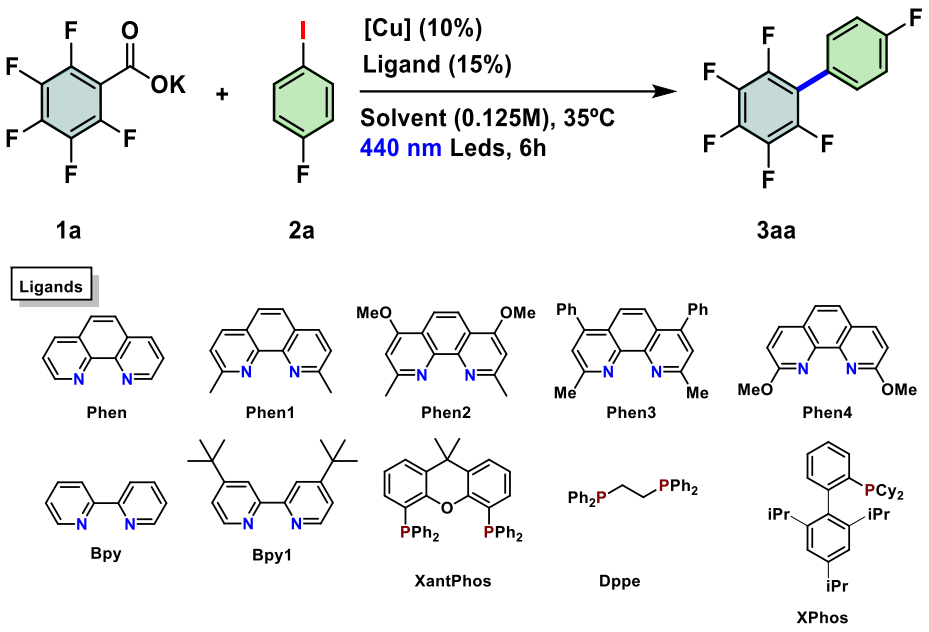

Entry	Ligand	**3aa** (%)[a]	**Pf-H/Pf-Pf** (%)[a]	**S.M(%)**
1	Phen	97	3/0	n.d
2	Phen1	32	68/0	n.d
3	Phen2	2	97/1	n.d
4	Phen3	n.d	95/5	n.d
5	Phen4	n.d	93/7	n.d
6	Bipy	10	50/18	22
7	Bipy1	51	36/13	n.d
8	XantPhos	20	44/26	10
9	Dppe	1	44/33	22
10	XPhos	15	27/58	n.d

Table 25. Standard conditions: **1a** (0.250 mmol), **2a** (0.375 mmol), CuI (10 %), Ligand (0.0375 mmol), DMA (2 mL), 35 °C, 6 h,440 nm Leds. [a] Yield determined by ^{19}F NMR.

Solvent Screening

Different solvents where tested as we can see in Table 26.

Entry	Conditions	**3aa** (%)[a]	**4/5** (%)[a]	**S.M**(%)
1	THF	n.d	n.d	>99
2	Toluene	n.d	n.d	>99
3	Acetonitrile	30	35/30	5
4	DMF	70	30/0	n.d
5	^{t}BuOH	n.d	n.d	>99

Table 26. Standard conditions: **1a** (0.250 mmol), **2a** (0.375 mmol), CuI (10 %), Phen (0.0375 mmol), Solvent (2 mL), 35 °C, 6 h,440 nm Leds. [a] Yield determined by ^{19}F NMR.

Light Screening

Different lights were tested as we can see in Table 27.

Entry	Conditions	**3aa** (%)[a]	**4/5** (%)[a]	**S.M**(%)
1	440 nm	96	4/0	n.d
2	Blue Strips	96	4/0	n.d

Table 27. Standard conditions: **1a** (0.250 mmol), **2a** (0.375 mmol), CuI (10 %), Phenantroline (0.0375 mmol), DMA (2 mL), 35 °C, 6 h. [a] Yield determined by ^{19}F NMR.

General procedure for catalysis

To a flame-dried screwed-capped Schlenk flask with a magnetic stirrer, CuI (4.8 mg, 0.0250 mmol), Phenantroline (6.8 mg, 0.0375 mmol) and the corresponding benzoate (0.250 mmol) were added. Then, the corresponding aryl iodide or bromide (0.375 mmol), and dry DMA (2 mL) were added to the flask. The Schlenk was placed in a photo-reactor and stirred for 6-12 hours. Then, the flask was taken out of the reactor and 5 mL of aqueous saturated NH_4Cl solution were added. The aqueous layer was extracted with Et_2O (3 x 3 mL). The organic fraction was dried over $MgSO_4$ and filtered through a short path of silica gel. The colored solution was concentrated and the residue was purified by flash column chromatography in silica gel. All compounds are summarized in Figure 55.

Stoichiometric and mechanistic studies.

Decarboxylation experiments

To a flame-dried screwed-capped NMR tube, CuI (4.8 mg, 0.0250 mmol), phen (4.5 mg, 0.0250 mmol) and the corresponding benzoate (0.0250 mmol) were added. Then, 500 µL of DMA was added. After addition of the solvent, the formation of [CuI(Phen)] was confirmed due to the solubility of the CuI and the solution turned to dark red colour. The NMR tube was placed in the photo-reactor during 1h. After that time, ^{19}F NMR was measured and represented in Figure 55.

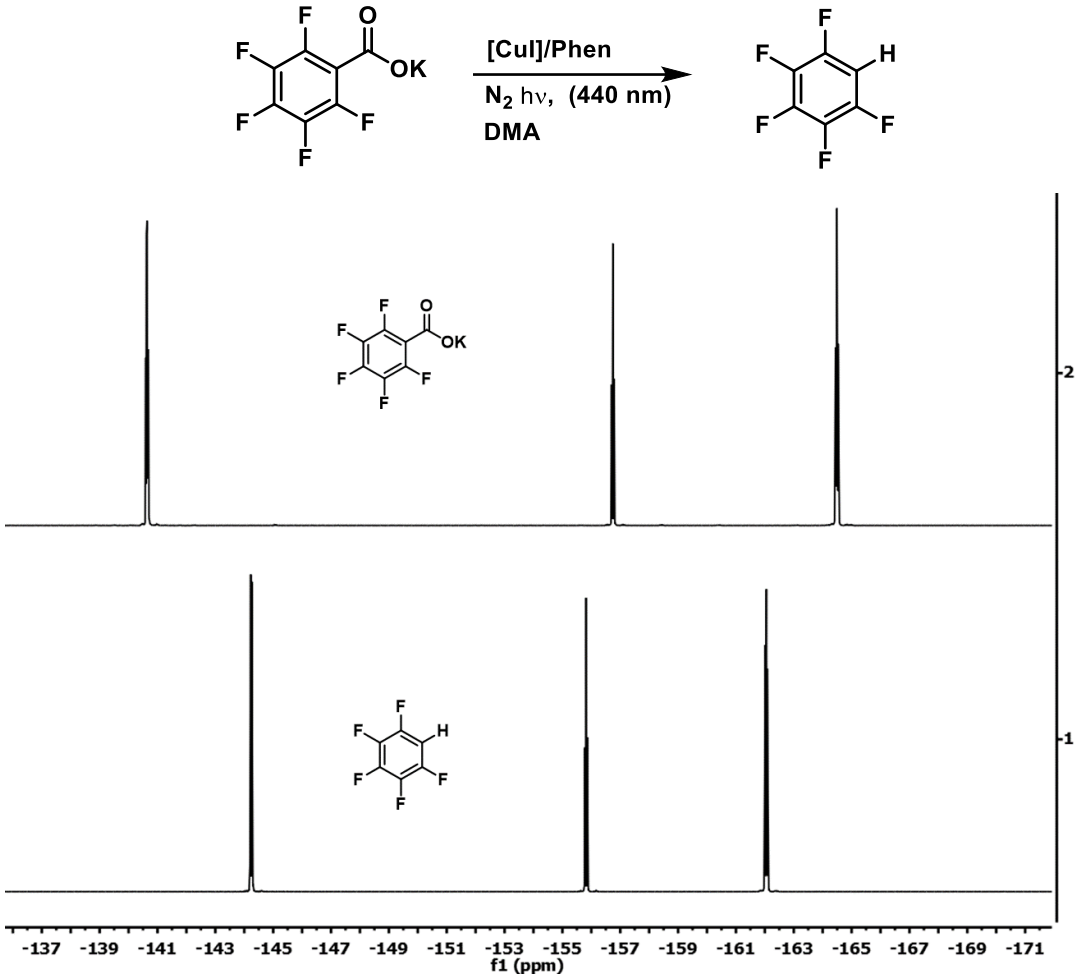

Figure 55 ^{19}F NMR of the reaction between CuI (4.8 mg, 0.0250 mmol), Phenantroline (4.5 mg, 0.0250 mmol) and potassium pentafluoro-benzoate **1a** (0.0250 mmol) in DMA after 1 hour of irradiation.

IR experiments

Infrared measurements were made as follows: To a flame-dried screwed-capped Schlenk flask with a magnetic stirrer, CuI (48 mg, 0.250 mmol), phenantroline (68 mg, 0.375 mmol) and potassium pentafluorobenzoate (0.250 mmol) were added. DMA (4 mL) were added to the flask. IR spectra showing the emergence of an absorbance band at 685 cm^{-1} growing with irradiation time. This band is assigned to the proposed CO_2 bending upon decarboxylation of potassium pentafluorobenzoate **1a** (see Fig 48, page 162).

Catalysis products

2,3,4,4',5,6-hexafluoro-1,1'-biphenyl (3aa)

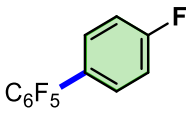

Following general procedure with 1-bromo/iodo-4-fluorobenzene. The product was obtained as a white solid after column chromatography employing *n*-pentane as eluent.

HRMS (EI) Calculated for $C_{12}H_4F_6$ $[M]^+$: 262.0217. Experimental $[M]^+$: 262.0215.

^{1}H NMR (499.72 MHz, Chloroform-*d*) 7.41 (m, 2H), 7.23 – 7.14 (m, 2H).

^{13}C{^{1}H} NMR (125.67 MHz, Chloroform-*d*) δ 163.1, 144.1, 141.8 – 139.2, 139.0 – 136.4, 122.2, 115.9.

^{19}F NMR (470.17 MHz, Chloroform-*d*) δ -106.38 – -116.03 (m), -143.36 (dd, J = 23, 8 Hz), -155.25 (t, J = 21 Hz), -159.60 – -164.15 (m).

2,2',3,4,5,6,6'-heptafluoro-1,1'-biphenyl (3ab)

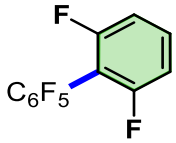

Following general procedure with 2-bromo/iodo-1,3-difluorobenzene. The product was obtained as a white liquid after column chromatography employing *n*-pentane as eluent.

HRMS (EI) Calculated for $C_{12}H_3F_7$ $[M]^+$: 280.0123. Experimental $[M]^+$: 280.0116.

^{1}H NMR (499.72 MHz, Chloroform-*d*) δ 7.51 – 7.45 (m, 1H), 7.10 – 7.04 (m, 2H).

^{13}C{^{1}H} NMR (125.67 MHz, Chloroform-*d*) δ 160.2 (dd, J = 252, 6 Hz), 147.9 – 146.4 (m), 146.2 – 144.5 (m), 143.1 (dt, J = 16, 4 Hz), 131.9 (t, J = 10 Hz), 112.4 – 111.1 (m). C_{ipso} not observed.

^{19}F NMR (470.17 MHz, Chloroform-*d*) δ -105.97 – -112.87 (m), -136.60 – -140.58 (m), -152.60 (t, J = 21 Hz), -161.81 (td, J = 20, 6 Hz).

Perfluoro-1,1'-biphenyl (3ac)

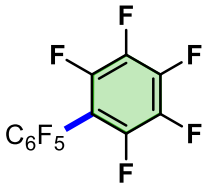

Following general procedure with bromopentafluorobenzene or iodopentafluorobenzene. The product was obtained as a white solid after column chromatography employing *n*-pentane as eluent.

HRMS (EI) Calculated for $C_{12}F_{10}$ $[M]^+$: 333.9840. Experimental $[M]^+$: 333.9837.

$^{13}C\{^1H\}$ NMR (125.67 MHz, Chloroform-*d*) δ 146.0 – 142.9 (m), 144.1 – 140.6 (m), 139.61 – 136.2 (m), 101.4 (t, J = 16 Hz).

^{19}F NMR (376.21 MHz, Chloroform-*d*) δ -137.18 – -137.73 (m), -149.81 (t, J = 21 Hz), -160.26 – -160.45 (m).

2,2',3,4,4',5,6,6'-octafluoro-1,1'-biphenyl (3ad)

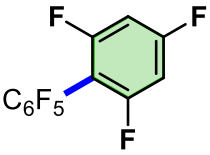

Following general procedure with 2-bromo-1,3,5-trifluorobenzene or potassium 2,4,6-trifluorobenzoate. The product was obtained as a white volatile liquid after column chromatography employing *n*-pentane as eluent.

HRMS (EI) Calculated for $C_{12}H_2F_8$ $[M]^+$: 298.0029. Experimental $[M]^+$: 298.0036.

^1H NMR (499.72 MHz, Chloroform-*d*) δ 6.87 – 6.82 (m, 2H).

$^{13}C\{^1H\}$ NMR (125.67 MHz, Chloroform-*d*) δ 164.0 (dt, J = 253, 15 Hz), 160.6 (ddd, J = 253, 15, 9 Hz), 144.6 (dddt, J = 250, 11, 7, 4 Hz), 141.8 (dtt, J = 256, 13, 5 Hz), 139.1 – 136.3 (m), 103.4 (td, J = 18.0 Hz), 100.8 (d, J = 3 Hz), 100.6 (d, J = 3 Hz).

^{19}F NMR (470.17 MHz, Chloroform-*d*) δ -104.03 (t, J = 8 Hz), -107.03 – -107.11 (m), -138.02 – -138.20 (m), -152.16 – -152.29 (m), -161.62 – -161.76 (m).

2,2',3,4,5,6-hexafluoro-1,1'-biphenyl (3ae)

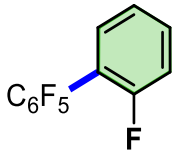

Following general procedure with 1-bromo/iodo-2-fluorobenzene. The product was obtained as a white volatile liquid after column chromatography employing *n*-pentane as eluent.

HRMS (EI) Calculated for $C_{12}H_4F_6$ $[M]^+$: 262.0217. Experimental $[M]^+$: 262.0221.

^{1}H NMR (499.72 MHz, Chloroform-*d*) δ 7.52 – 7.45 (m, 1H), 7.40 – 7.32 (m, 1H), 7.28 (td, J = 7, 1 Hz, 1H), 7.27 – 7.20 (m, 1H).

^{13}C{^{1}H} NMR (125.67 MHz, Chloroform-*d*) δ 159.9 (d, J = 250 Hz), 145.8 – 142.9 (m), 142.5 – 139.5 (m), 139.2 – 136.2 (m), 131.9, 131.6 (d, J = 8 Hz), 124.3 (d, J =.6 Hz), 116.1 (d, J = 21 Hz).

2,2',3,3',4,5,6-heptafluoro-1,1'-biphenyl (3af)

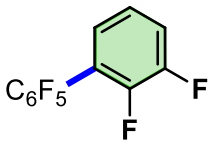

Following general procedure with 1-iodo-2,3-difluorobenzene. The product was obtained as a white volatile liquid after column chromatography employing *n*-pentane as eluent.

HRMS (EI) Calculated for $C_{12}H_3F_7$ $[M]^+$: 280.0123. Experimental $[M]^+$: 280.0127.

^{1}H NMR (499.72 MHz, Chloroform-*d*) δ 7.38 – 7.26 (m, 1H), 7.27 – 7.19 (m, 1H), 7.16 – 7.07 (m, 1H).

^{13}C{^{1}H} NMR (125.67 MHz, Chloroform-*d*) δ 152.3 – 149.6 (m), 147.0 (d, J = 13.2 Hz), 144.3 (dddt, J = 250, 11, 7, 3 Hz), 142.8 – 139.9 (m), 139.3 – 136.2 (m), 126.6 (d, J = 3 Hz), 124 (dd, J =7, 4 Hz), 118.8 (d, J = 17 Hz), 116.3 (d, J = 12 Hz), 108.9 (tt, J = 18, 3 Hz).

^{19}F NMR (470.17 MHz, Chloroform-*d*) δ -136.33 – -136.48 (m), -136.94 – -137.13 (m), -153.10 (t, J = 20.8 Hz), -161.55 – -161.70 (m).

2,3,3',4,4',5,6-heptafluoro-1,1'-biphenyl (3ag)

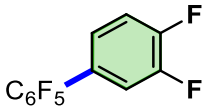

Following general procedure with 4-iodo-1,2-difluorobenzene. The product was obtained as a white solid after column chromatography employing *n*-pentane as eluent.

HRMS (EI) Calculated for $C_{12}H_3F_7$ $[M]^+$: 280.0123. Experimental $[M]^+$: 280.0128.

^{1}H NMR (499.72 MHz, Chloroform-*d*) δ 7.34 – 7.26 (m, 2H), 7.23 – 7.14 (m, 1H).

^{13}C{^{1}H} NMR (125.67 MHz, Chloroform-*d*) δ 151.61 (dd, J = 74.6, 12.3 Hz), 149.62 (dd, J = 72, 12 Hz), 145.52 – 142.55 (m), 142.17 – 139.56 (m), 139.25 – 136.41 (m), 126.73 (dq, J = 6, 2 Hz), 122.93 (d, J = 6 Hz), 119.49 (d, J = 18 Hz), 117.83 (d, J = 17 Hz), 113.91 (t, J = 14 Hz)

^{19}F NMR (470.17 MHz, Chloroform-*d*) -135.55 – -135.83 (m), -136.26 – -136.46 (m), -143.07 (dd, J = 22, 8 Hz), -154.13 (t, J = 20 Hz), -161.40 – -161.62 (m).

2,3,3',4,5,5',6-heptafluoro-1,1'-biphenyl (3ah)

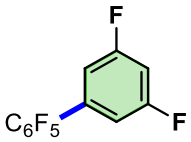

Following general procedure with 1-iodo-3,5-difluorobenzene. The product was obtained as a white solid after column chromatography employing *n*-pentane as eluent.

HRMS (EI) Calculated for $C_{12}H_3F_7$ $[M]^+$: 280.0123. Experimental $[M]^+$: 280.0126.

^{1}H NMR (499.72 MHz, Chloroform-*d*) δ 7.02 – 6.95 (m, 2H), 6.93 (tt, J = 8, 2 Hz, H).

^{13}C{^{1}H} NMR (125.67 MHz, Chloroform-*d*) δ 162.9 (dd, J = 249.9, 12.9 Hz), 145.0, 142.30 – 139.61 (m), 139.2 – 136.6 (m), 129.0, 113.6 – 113.4 (m), 113.4 – 113.2 (m), 105.0 (t, J = 25.0 Hz).

^{19}F NMR (470.17 MHz, Chloroform-*d*) δ -103.59 – -112.22 (m), -140.09 – -145.25 (m), -153.35 (t, J = 21.0 Hz), -159.05 – -162.86 (m).

3,5-dichloro-2,2',3',4,4',5',6,6'-octafluoro-1,1'-biphenyl (3aj)

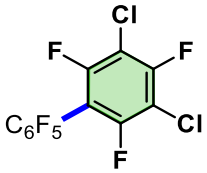

Following general procedure with 1,3-dichloro-2,4,6-trifluoro-5-iodobenzene. The product was obtained as a white solid after column chromatography employing *n*-pentane as eluent.

HRMS (EI) Calculated for $C_{12}Cl_2F_8$ $[M]^+$: 365.9249. Experimental $[M]^+$: 365.9255.

^{19}F NMR (470.17 MHz, Chloroform-*d*) δ -106.72 (t, J = 3.6 Hz), -110.40 (td, J = 8, 3 Hz), -137.35 (dddd, J = 23, 11, 6, 3 Hz), -149.99 (tt, J = 21, 3. Hz), -160.32 – -160.49 (m).

^{13}C{^{1}H} NMR (100.56 MHz, Chloroform-*d*) δ156.5 (d, J = 229.5 Hz), 153.6, 145.5, 137.8 (d, J = 254.2 Hz), 108.2, 102.1, 67.0.

2,3,4,5,6-pentafluoro-4'-methyl-1,1'-biphenyl (3ak)

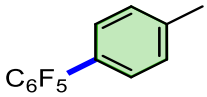

Following general procedure with 4-iodotoluene. The product was obtained as a white solid after column chromatography employing*n*-pentane as eluent.

HRMS (EI) Calculated for $C_{13}H_7F_5$ $[M]^+$: 258.0468. Experimental $[M]^+$: 258.0463.

^{1}H NMR (499.72 MHz, Chloroform-*d*) δ 7.28 (s, 4H), 2.40 (s, 3H).

^{13}C{^{1}H} NMR (100.56 MHz, Chloroform-*d*) δ 145.68 – 142.39 (m), 141.83 – 140.89 (m), 139.40, 139.24 – 136.30 (m), 129.96, 129.44, 123.35, 117.79 – 114.13 (m), 21.31 (s).

^{19}F NMR (470.17 MHz, Chloroform-*d*) δ -143.42 (dd, J = 23, 7 Hz), -156.21 (t, J = 20 Hz), -162.52 (ddd, J = 23, 20, 8 Hz).

2,3,4,5,6-pentafluoro-4'-(trifluoromethyl)-1,1'-biphenyl (3al)

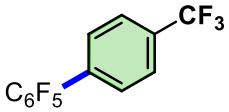

Following general procedure with 4-iodo-benzotrifluoride. The product was obtained as a white solid after column chromatography employing *n*-pentane as eluent.

HRMS (EI) Calculated for $C_{13}H_4F_8$ $[M]^+$: 312.0185. Experimental $[M]^+$: 312.0190.

^{1}H NMR (499.72 MHz, Chloroform-*d*) δ7.77 (d, J = 9 Hz, 2H), 7.56 (d, J = 7 Hz, 2H).

^{13}C{^{1}H} NMR (125.67 MHz, Chloroform-*d*) δ 144.11 (dddt, J = 249, 11, 7, 4 Hz), 142.33 – 139.60 (m), 139.20 – 136.54 (m), 131.45 (q, J = 33 Hz), 130.71 – 130.57 (m), 130.09, 125.71 (q, J = 4 Hz), 124.83, 122.66, 114.81 – 114.22 (m).

^{19}F NMR (470.17 MHz, Chloroform-*d*) δ -62.99 (3F, s), -142.86 – -143.09 (2F, m), -153.78 (1F, t, J = 21 Hz), -160.41 – -163.88 (2F, m).

2,3,3',4,4',5,5',6-octafluoro-1,1'-biphenyl (3an)

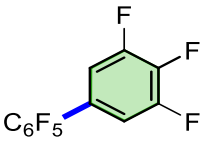

Following general procedure with Iodo 3,4,5-trifluorobenzene. The product was obtained as a white solid after column chromatography employing *n*-pentane as eluent.

HRMS (EI) Calculated for $C_{12}H_2F_8$ $[M]^+$: 298.0029. Experimental $[M]^+$: 298.0025.

^{1}H NMR (499.72 MHz, Chloroform-*d*) δ 7.09 (t, *J* = 6.9 Hz, 2H).

^{13}C{^{1}H} NMR (125.67 MHz, Chloroform-*d*) δ 151.3 (ddd, J = 251, 10, 4 Hz), 144.0 (dddt, J = 249, 11, 7, 4 Hz), 141.4 (t, J = 15 Hz), 142.4 – 139.8 (m), 139.17 – 136.8 (m), 122.2 – 121.7 (m), 114.8 (ddt, J = 17, 2, 2 Hz), 113.2 – 112.8 (m).

^{19}F NMR (470.17 MHz, Chloroform-*d*) δ -131.95 – -133.87 (m), -142.14 – -143.95 (m), -152.45 – -155.49 (m), -156.18 – -159.02 (m), -160.14 – -162.64 (m).

2,2',3,3',4,5,5',6,6'-nonafluoro-1,1'-biphenyl (3ap)

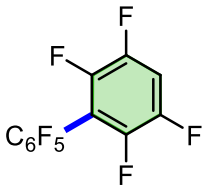

Following general procedure with Iodo 2,3,5,6-tetrafluorobenzene. The product was obtained as a white solid after column chromatography employing *n*-pentane as eluent.

^{1}H NMR (499.72 MHz, Chloroform-*d*) δ 7.13–7.02 (m).

^{13}C{^{1}H} NMR (125.67 MHz, Chloroform-*d*) δ 147.6 (m), 145.8 (m), 144.3 (m), 142.3 (m), 139.5 (m), 108.1 (tt, $^{2}J_{CF}$ = 97 Hz, $^{3}J_{CF}$ = 5 Hz).

^{19}F NMR (470.17 MHz, Chloroform-*d*) δ −137.4 (m, 4F), −138.2 (m, 2F), −150.2 (t, 1F), −160.5 (m, 2F).

2,2',3,4,5,6-hexafluoro-5'-methyl-1,1'-biphenyl (3ao)

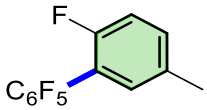

Following general procedure with 1-fluoro-2-iodo-4-methylbenzene. The product was obtained as a white solid after column chromatography employing *n*-pentane as eluent.

^{1}H NMR (499.72 MHz, Chloroform-*d*) δ 7.17 (d, J = 8 Hz, 1H), 7.15 (d, J = 8 Hz, 1H), 7.04 (dd, J = 10, 8 Hz, 2H), 4.65 (s, 3H).

^{19}F NMR (470.17 MHz, Chloroform-*d*) δ -136.07 – -137.12 (1F, m), -141.01 – -141.56 (2F, m), -154.29 (1F, t, J = 21 Hz), -161.78 – -162.07 (2F, m).

^{13}C{^{1}H} NMR (125.67 MHz, Chloroform-*d*) δ 150.6 (dd, J = 251.2, 12.4 Hz), 148.2 (dd, J = 247, 13 Hz), 144.0 (dddt, J = 247, 11., 7, 4 Hz), 142.4 – 139.8 (m), 139.0 – 136.4 (m), 134.8 (dd, J = 6, 4 Hz), 121.8 (ddd, J = 6, 4, 2 Hz), 119.4 (d, J = 18 Hz), 119.1 (d, J = 17 Hz), 113.5 (td, J = 19, 4 Hz), 18.9.

2,2',3,4,5,6-hexafluoro-5'-methyl-1,1'-biphenyl (3aq)

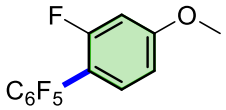

Following general procedure with 2-fluoro-1-iodo-4-methoxybenzene. The product was obtained as a white solid after column chromatography employing *n*-pentane as eluent.

^{1}H NMR (499.72 MHz, Chloroform-*d*) δ 7.44 (tt, J = 8, 6 Hz, 1H), 7.20 – 6.83 (m, 2H), 4.15 (s, 3H).

^{19}F NMR (470.17 MHz, Chloroform-*d*) δ -104.68 – -114.33 (1F, m), -141.66 (2F, dd, J = 23, 8 Hz), -153.55 (1F, t, J = 21 Hz), -157.90 – -162.45 (2F, m).

^{13}C{^{1}H} NMR (125.67 MHz, Chloroform-*d*) δ 160.4 (dd, J = 252, 6 Hz), 144.7 (dddd, J = 248, 12, 8, 4 Hz), 142.6 – 139.6 (m), 139.0 (tt, J = 12, 4 Hz), 131.6 (t, J = 10 Hz), 112.1 – 111.1 (m), 105.2 – 104.3 (m), 102.1 (t, J = 19 Hz), 62.0 (td, J = 4, 2 H).

CHAPTER IV: Copper catalyzed synthesis of highly fluorinated aryl-iron(II) complexes. Detailed study of the transmetalation step.

4.1 Introduction

Transition metal (TM) catalysed reactions play an important role in modern chemistry and organic synthesis due to their versatility to modify many functional groups, their efficiency, and their tolerance to harsh reaction conditions.[151,152] Although traditionally the most used metals for this type of reactions have been Pd and Rh,[153] nowadays the trend is to use more abundant transition metals such as Cu or Fe.[154,155,156,157] In contrast to precious metals, iron and copper are inexpensive and readily available, which will benefit their large-scale application in the chemical industry.

Currently, bimetallic co-catalysis is growing as a complement to traditional single metal catalysis because the synergy between the two metals can generate an impossible reactivity for monometallic reaction. In this field many bimetallic systems such as Pd/Cu, Pd/Ni or Fe/Cu are being developed, which prove to be extremely efficient in different transformations. Special interest is the Fe/Cu catalytic system, where both metals are uncommon in traditional bimetallic catalytic systems.[158,159] Although the combination of these two metals seems unusual, they show a great synergy between them, and are capable of performing a large number of transformations.[160] For this reason, they represent a bimetallic system in full

---

151 Negishi, E. I. Magical Power of Transition Metals: Past, Present, and Future (Nobel Lecture). *Angew. Chem. Int. Ed.* **2011**, *50*, 6738–6764. DOI: 10.1002/anie.201101380.

152 Pérez-Temprano, M. H.; Casares, J. A.; Espinet, P. Bimetallic Catalysis Using Transition and Group 11 Metals: An Emerging Tool for C-C Coupling and Other Reactions. *Eur. J. Chem.* **2012**, *18*, 1864–1884. DOI: 10.1002/CHEM.201102888.

153 Kim, U. Bin; Jung, D. J.; Jeon, H. J.; Rathwell, K.; Lee, S. G. Synergistic Dual Transition Metal Catalysis. *Chem. Rev.* **2020**, *120*, 13382–13433. DOI: 10.1021/acs.chemrev.0c00245.

154 Bauer, I.; Knölker, H. J. Iron Catalysis in Organic Synthesis. *Chem. Rev.* **2015**, *115*, 3170–3387. DOI: 10.1021/cr500425u.

155 Wei, D.; Darcel, C. Iron Catalysis in Reduction and Hydrometalation Reactions. *Chem. Rev*. **2019**, *119*, 2550–2610. DOI: 10.1021/jacs.3c01091.

156 Lazreg, F.; Nahra, F.; Cazin, C. S. J. Copper-NHC Complexes in Catalysis. *Coor. Chem. Rev.* **2015**, *15*, *293*, 48–79. DOI: 10.1016/j.ccr.2014.12.019.

157 Pye, D. R.; Mankad, N. P. Bimetallic Catalysis for C–C and C–X Coupling Reactions. *Chem. Sci.* **2017**, *8*, 1671–2466. DOI: 10.1039/c6sc05556g.

158 Wu, Y.; Huo, X.; Zhang, W. Synergistic Pd/Cu Catalysis in Organic Synthesis. *Eur. J. Chem.* **2020**, *26*, 4895–4916. DOI: 10.1002/chem.201904495.

159 Huo, L.; Shi, L.; Fu, J. Iron–Copper Dual Catalysis Enabling C–C and C–X (X=N, B, P, S, Sn) Bond Formation. *Eur. J. Org. Chem.* **2022**, *30,* 1–16. DOI: 10.1002/ejoc.202200454.

160 Mao, J.; Xie, G.; Wu, M.; Guo, J.; Ji, S. Ligand-Free Iron/Copper Cocatalyzed Alkynylation Coupling Reactions. *Adv. Synth. Catal.* **2008**, *350*, 2477–2482. DOI: 10.1002/adsc.200800517.

exploration, many reactions have been optimized, but there are few mechanistic studies with this bimetallic system.

One of the iconic reactions of the Pd/Cu bimetallic system is the Sonogashira reaction,[161,162] and Pd can be easily suppressed by an iron salt. In 2008, Mao and co-workers published the first case of Sonogashira reaction using the Fe/Cu system.[160]

In this work they develop a bimetallic system using $Fe(acac)_3$ and CuI in the absence of external ligands. As in the traditional Sonogashira reaction, the combination of an acetylene and a copper salt, in the presence of base, generates the corresponding copper acetylide, which transfers the organic moiety to the Fe complex, which will carry out the oxidative addition reactions of aryl halides followed by the subsequent reductive elimination. This reaction shows very high yields in most cases, but use harsh reaction conditions (140°C, DMSO, 24h) is mandatory. In addition, to extend the applicability of these system, C–O or C–S bond forming reactions are successfully carried out under the same conditions.

More recently than Mao's research, in in 2014, the first Fe/Cu system for aryl borylation was published.[163] In that work, a bimetallic catalysis is presented in which, the copper salt catalyzed the C–H activation of Bpin–H in the presence of base (Figure 56). As in the previous example, the boron derivative coordinated to the Cu atom is transmetalated to the Fe complex, which undergoes the oxidative addition and reductive elimination processes, generating the corresponding Ar–Bpin.

---

161 Chinchilla, R.; Nájera, C. N. Recent Advances in Sonogashira Reactions. *Chem. Soc. Rev.* **2011**, *12*, 5084–5121. DOI: 10.1039/c1cs15071e.

162 Chinchilla, R.; Nájera, C. The Sonogashira Reaction: A Booming Methodology in Synthetic Organic Chemistry. *Chem. Rev*. **2007**, *107*, 874–922. DOI: 10.1021/cr050992x.

163 Labre, F.; Gimbert, Y.; Bannwarth, P.; Olivero, S.; Duñach, E.; Chavant, P. Y.; Dun, E.; Chavant, P. Y. Application of Cooperative Iron/Copper Catalysis to a Palladium-Free Borylation of Aryl Bromides with Pinacolborane. *Org. Lett.* **2014**, *16*, 2366–2369. DOI: 10.1021/ol500675q.

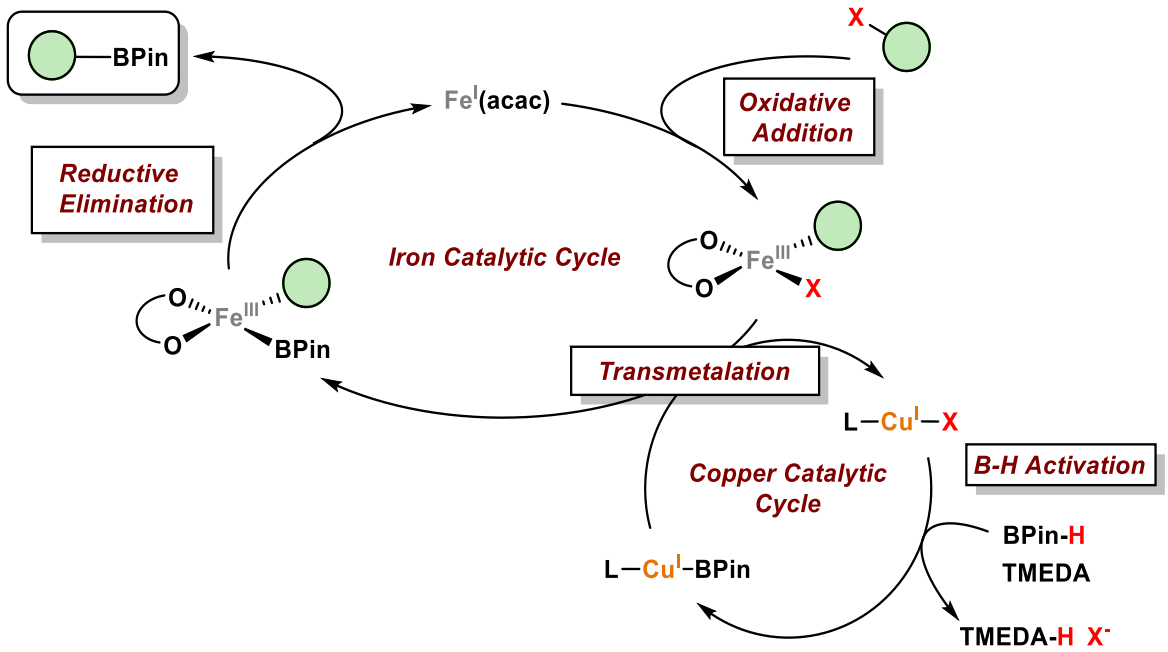

Figure 56. Bimetallic catalytic cycle proposed for the borylation of aryls using Fe(acac)/Cu system. Green circles represent a generic aryl.

In these two examples of Fe/Cu bimetallic catalysis we have seen that as in most of the Pd/Cu catalytic systems, the copper complex always has the same function, the activation of an X–H bond (X=C, B).[164,165] It is therefore essential to study this step-in depth when designing a bimetallic catalysis where Cu complex is involved. As in most cases, to activate a C–H or B–H bond, several factors must be taken into account, the most important are the acidity of the proton to be activated, the base used, whether it is coordinated to the metal center or not, the ligand on the Cu complex or the speciation and nature of the complex in solution.[166]

Copper Catalytic Cycle

I) Proton acidity

Experimental studies have indicated that the acidity of the cleaved C–H bond plays a crucial role in the cross-coupling reactions. For example, it has been found that the reactivity order of the C–H bonds at the 2-position of benzoxazole,

[164] Guo, X.-X. Copper-Catalyzed C-H Activation - Copper Catalysis in Organic Synthesis, Chapter 15. ISBN: 9783527826445 **2020**.
[165] Waltz, K. M.; Muhoro, C. N.; Hartwig, J. F. C–H Activation and Functionalization of Unsaturated Hydrocarbons by Transition-Metal Boryl Complexes. *Organometallics* **1999**, *18*, 3383–3393. DOI: 10.1021/om990113v.
[166] Yoshizumi, T.; Tsurugi, H.; Satoh, T.; Miura, M. Copper-Mediated Direct Arylation of Benzoazoles with Aryl Iodides. *Tetrahedron Lett.* **2008**, *49*, 1598–1600. DOI: 10.1016/j.tetlet.2008.01.042.

benzothiazole, and benzimidazole follows their acidity order in the copper-mediated arylation when 1 equivalent of CuI was used.[166]

To understand how C–H activation works in copper catalytic systems, Lin and co-workers presented in 2012 an extensive study of this phenomenon, studying computationally many of these variables.[167] In this work they show an aryl or aryl-heterocycle coupling that proceeds through C–H activation, followed by oxidative addition and reductive elimination steps, and analyse the energies of all the processes, especially of the C–H bond activation under different conditions. To discuss how the C–H activation varies in this process, we will discuss the following energy profile with many substrates, as shown in Figure 57.

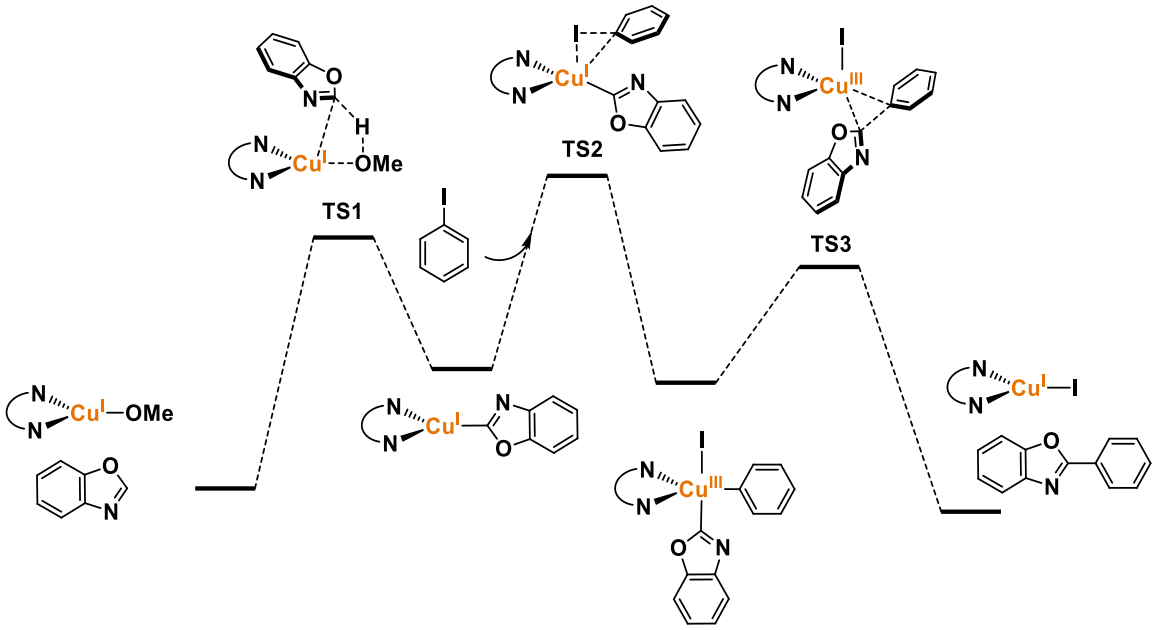

Figure 57. Energy profile proposed for the [(phen)Cu–OMe] catalyzed cross-coupling of benzoxazole with phenyl iodide.

In order to get a better understanding of this behaviour, the authors studied several substrates which have different pK_a values of the relevant C–H bonds by calculating their reaction energy profiles on the basis of the mechanism shown in Figure 57. The pK_a values of the relevant C–H bonds of these substrates in DMSO can

[167] Wang, M.; Fan, T.; Lin, Z. DFT Studies on Copper-Catalyzed Arylation of Aromatic C–H Bonds. *Organometallics* **2012**, *31*, 560–569. DOI: 10.1021/om2007612.

be found in the literature and are summarized in Figure 58 for better understanding.[168,169]

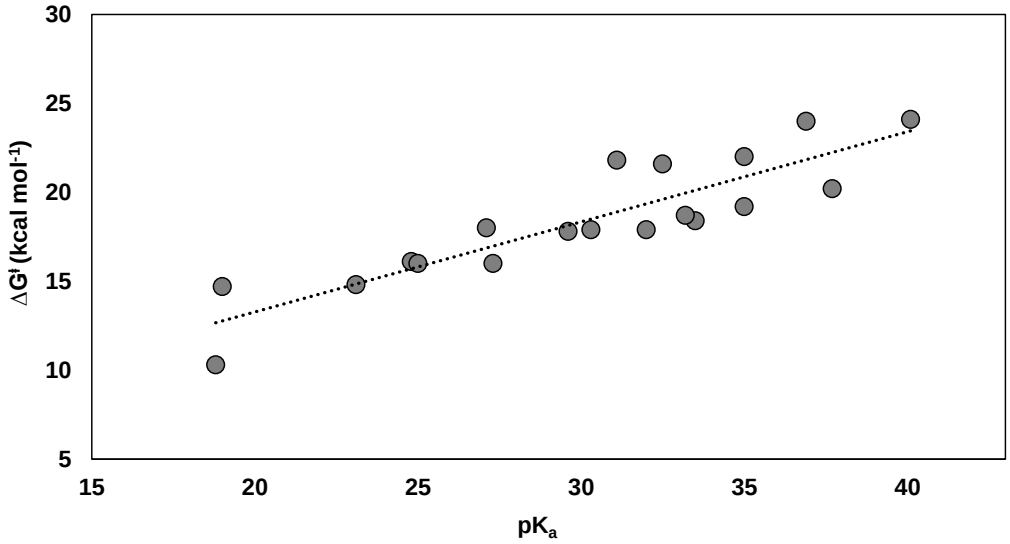

Figure 58. Correlation between the pKa values of relevant C–H bonds and the energy of the C–H activation.[167]

As we can see in the data collected in Figure 58, there is a direct correlation between the acidity of the proton to be activated and the total energy of that process. This implies that with more acidic substrates, the reaction will be faster within the same system. If what we are interested in the overall energy, it will be necessary to compare the C–H activation energy with the rest of the steps, especially with the oxidative addition, which is normally the highest energy process in copper-catalyzed cross-coupling reactions, which is in agreement with the experimental results.[166]

II) Importance of the base

The election of the base to achieve copper-catalysed C–H activation, understanding the different behaviour they may have with the metal center is mandatory. For example, bases such as $^{t}BuO^{-}$, MeO^{-}, or different carbonates are salts that are able to coordinate to the metal center, modifying its basicity. In contrast,

[168] Shen, K.; Fu, Y.; Li, J. N.; Liu, L.; Guo, Q. X. What Are the PKa Values of C-H Bonds in Aromatic Heterocyclic Compounds in DMSO? *Tetrahedron Lett.* **2007**, *63*, 1568–1576. DOI: 10.1016/j.tet.2006.12.032.
[169] Bordwell, F. G. Equilibrium Acidities in Dimethyl Sulfoxide Solution. *Acc. Chem. Res.* **1988**, *21*, 456–463. DOI: 10.1021/ar00156a004.

salts such as K_3PO_4 or some amines are non-coordinating bases, *i.e.*, they behave like a common salt in solution. This may not seem very important, but it is vital in understanding why some bases work in certain systems and why others do not.

Alkoxy-derivates such as $^tBuO^-$ or MeO^- are among the most widely used bases in copper chemistry nowadays. They have become very popular in catalytic reactions involving activation of a C–H, C–B or B–H bond due to the process involved. Concerted metalation–deprotonation (CMD) process,[170,171] occurs via the four-membered transition state TS to generate a MeOH or ^{t}BuOH molecule and form the aryl-copper organometallic complex, represented in Figure 59. This mechanism was proposed in several C–H activation investigations using NaO^{t}Bu,[171] NaOMe,[166,167] or K_2CO_3.[172]

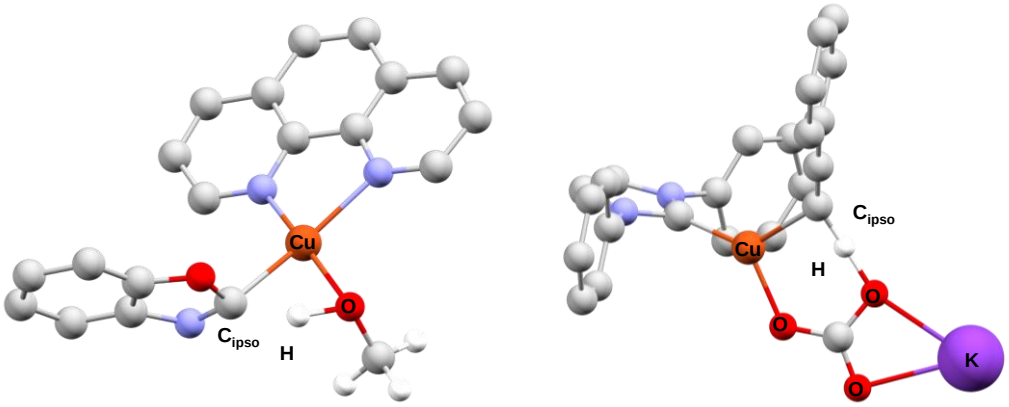

Figure 59. Representation of two different C–H activation Transition States. Left = C–H activation using $^-$OMe as base. Right = C–H activation using KCO_3^- as base.

On the contrary, all reactions using amines as base, such as NEt_3, TMEDA and others, are proposed as mechanisms where the base does not interact with the metal center when the transition state is based on the activation of the C–H bond, as we can see in Figure 60.

[170] Xie, W.; Chang, S. [Cu(NHC)]-Catalyzed C–H Allylation and Alkenylation of Both Electron-Deficient and Electron-Rich (Hetero)Arenes with Allyl Halides. *Angew. Chem. Int. Ed.* **2016**, *55*, 1876–1880. DOI: 10.1002/anie.201510180.

[171] Xie, W.; Heo, J.; Kim, D.; Chang, S. Copper-Catalyzed Direct C-H Alkylation of Polyfluoroarenes by Using Hydrocarbons as an Alkylating Source. *J. Am. Chem. Soc.* **2020**, *142*, 7487–7496. DOI: 10.1021/jacs.0c00169.

[172] Yuan, R.; Lin, Z. Mechanism for the Carboxylative Coupling Reaction of a Terminal Alkyne, CO_2, and an Allylic Chloride Catalyzed by the Cu(I) Complex: A DFT Study. *ACS Catal.* **2014**, *4*, 4466–4473. DOI: 10.1021/cs5011184.

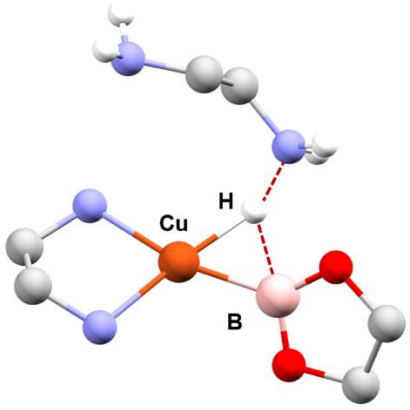

Figure 60. Transition State for the B–H activation TMEDA as a ligand and base.

III) Speciation in solution

It is well known that organometallic Cu(I) complexes of the type [L–Cu–OMe] (L = monodentate or bidentate ligands) and their derivatives are in fast equilibrium with the cationic species $[L–Cu–L]^+$ and the anionic species $[MeO–Cu–OMe]^-$. Therefore, it is important to take this behaviour into account when performing an in-depth study.[173]

The authors analysed the differences between the neutral and anionic species as in the case of the proton acidity study, and they observe some interesting data.[167] The transition state proposed for this process is concerted metalation-deprotonation (CMD) process. Interestingly, the same trend as in the neutral pathway is observed, there is a strong correlation between proton acidity and C–H activation rate. As we can see in Equation 9, the C–H activation energy using the anionic $[MeO–Cu–OMe]^-$ complex are higher in energy than using the neutral species [L–Cu–OMe] for the arenes with the highest pKa.

[173] Kalkman, E. D.; Mormino, M. G.; Hartwig, J. F. Unusual Electronic Effects of Ancillary Ligands on the Perfluoroalkylation of Aryl Iodides and Bromides Mediated by Copper(I) Pentafluoroethyl Complexes of Substituted Bipyridines. *J. Am. Chem. Soc.* **2019**, *49*, 19458–19465. DOI: 10.1021/jacs.9b10540.

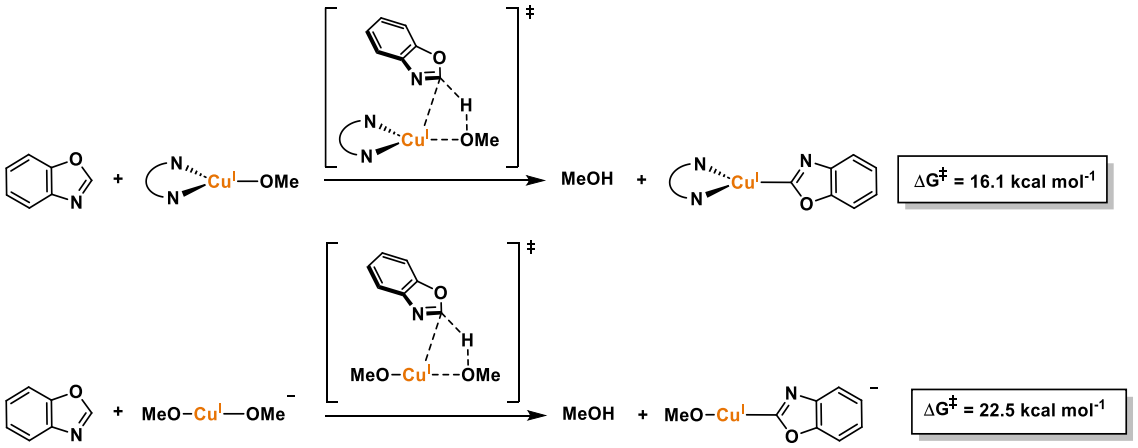

Equation 9. Different pathways for the C–H activation step depending on the nature of the catalyst.

Furthermore, for compounds with the lowest pKa, the C–H activation energy using the anionic $[MeO–Cu–OMe]^-$ complex are lower in energy than using the neutral species [L–Cu–OMe]. This process has a possible explanation, the OMe group is smaller than practically any ligand, which makes the arene approach easier and facilitates the C–H activation process making the involved transition state less energetic. Additionally, $[MeO–Cu–OMe]^-$could be more basic than the neutral specie. Although it is well known that the equilibrium between the anionic complex $[MeO\text{-}Cu\text{-}OMe]^-$ and the neutral species [L-Cu-OMe] is strongly shifted towards the neutral organometallic complex, it is important to keep in mind that these species coexist in solution, and have different reaction rates, which may change the outcome of the mechanistic investigations, as the authors comment.[167]

IV) ***Ligand effect***

In the C–H activation process, the active species [Cu(OMe)L] has a neutral ligand coordinated to the Cu center. Authors compared the C–H activation of N-methylpyrrole with three common ligands with different coordination and electronic properties,[167] such us 1,10-phenantroline, N-methyl-pyrrolidine-2-carboxamide and DMEDA. To understand the difference in the relative energies of the transition states, we compared the optimized structures TS1, TS2, and TS3, as we can see in Figure 61.

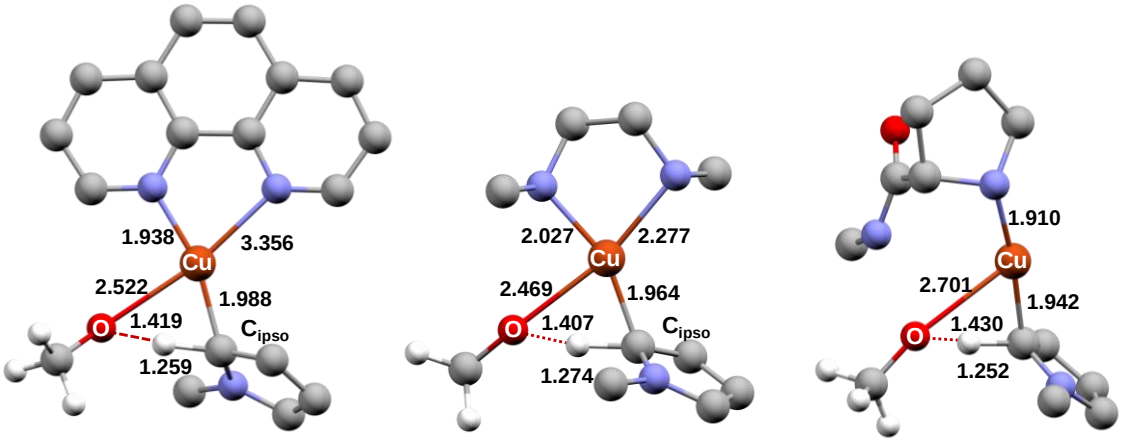

Figure 61. Comparison of the transition sates of the C–H activation of N-methylpyrrole with three common ligands with different coordination and electronic properties, such us 1,10-phenantroline, N-methyl-pyrrolidine-2-carboxamide and DMEDA.[161]

As we can see in the transition states of the figure, the Cu–C distance follows a clear trend, and we can observe that the distance is decreasing for the case of the monocoordinating ligand, being the largest Cu–C distance for the case of phenanthroline (1.988 Å). On the other hand, the Cu–N distances are also clearly different, suggesting a higher electronic ligand contribution in the cases where the bond is shorter, especially for the N-methyl-pyrrolidine-2-carboxamide ligand (1.910 Å).[161]

Finally, the other bond that has been modifying in the transition state would be Cu–O, where it can also be clearly observed how the case of the N-methyl-pyrrolidine-2-carboxamide ligand is much longer than in the other two cases.

Another important variable, which depends directly on the ligand, is the geometry of the complex. It is well known that linear complexes of the [(NHC)Cu(OR)] type are extremely efficient in the C–H activation of acidic protons. Thus, it has become the general process of synthesis of a large number of aryl–Cu, acetylene–Cu or heterocycle–Cu complexes.[174] For this reason, the transition state, shown on the right of the Figure 61, is the one with the lowest activation energy. As we can see, thanks to its linear coordination, the bond that is broken (Cu–O) is the longest of the three examples. The possibility to modify the geometry with a partial

[174] Xie, W.; Yoon, J. H.; Chang, S. (NHC)Cu-Catalyzed Mild C-H Amidation of (Hetero)Arenes with Deprotectable Carbamates: Scope and Mechanistic Studies. *J. Am. Chem. Soc.* **2016**, *138*, 12605–12614. DOI: 10.1021/jacs.6b07486.

dissociation of ligand suggest a reduction in the activation energy.[161] On the other hand, the new bond formed (Cu–C) is also the shortest (1.942 Å) of the three examples, which results in a stabilization of the transition state, being 17.6 kcal mol^{-1}. If we now compare the other two transition states (placed on the left and in the center on Figure 61, we do not observe significant differences in the distances involved in the transition state. Since there are little difference in the distances involved in the transition states, the activation energies for the C–H activation are quite similar (20 kcal mol^{-1} for the phenanthroline complex and 19 kcal mol^{-1} for the complex with DMEDA).

Another interesting analysis is to understand how the C–H activation depends on the charge of the ligand. Chan and co-workers reported the coupling of fluoroarenes with alkanes by means of double C–H activation, one catalysed by copper and the other by radical activation (Commented in Chapter II, Figure 24).[171] For this purpose, they employed an anionic chelating N,N-donor ligand. The activation barrier of the C–H bond of tetrafluoroanisole rises to 26 kcal mol^{-1}, while in the previous examples, the pentafluorobenzene is approximately 10 kcal mol^{-1} less for neutral ligands.[170,174] These means that the use of anionic ligands disfavoured the C–H activation process.

Iron Catalytic Cycle

Nowadays, it is very common to find organic reactions catalysed by iron complexes, and traditionally, the most used and therefore most studied complexes are Fe^{II} derivatives of the type [Fe(Cp)Ar(CO)$_2$]. Some of its most important uses are the arylation of styrene,[175] the borylation of aryls or the synthesis of ketones.[176] Organoiron complexes bearing a dicarbonylcyclopentadienyl moiety [Fe(Cp)Ar(CO)$_2$] are utilized as useful organometallic reagents in organic and synthetic chemistry.[169] One of the groups that have done the most research in this field is the group of Oshima. Over the years, they have developed different methods

[175] Yasuda, S.; Yorimitsu, H.; Oshima, K. Arylation of Styrenes with Aryliron Complexes [CpFe(CO)$_2$Ar]. *Organometallics* **2010**, *29*, 2634–2636. DOI: 10.1021/om1001952.

[176] Yasuda, S.; Yorimitsu, H.; Oshima, K. Use of Aryliron Complexes [CpFe(CO)$_2$Ar] as Arylcarbonyl Cation Equivalents in the Reactions with Organolithium Reagents To Yield Ketones. *Organometallics* **2009**, *28*, 4872–4875. DOI: 10.1021/om900558a.

for their synthesis. First, in 2008, Oshima and coworkers published the synthesis of aryl-iron derivatives catalysed by Pd and Grignard reagents.[177] For this, they use $Pd(OAc)_2$ as catalyst, the iron(II) derivative $[Fe(Cp)I(CO)_2]$ and an excess of ArMgBr under mild conditions, shown in Figure 62.

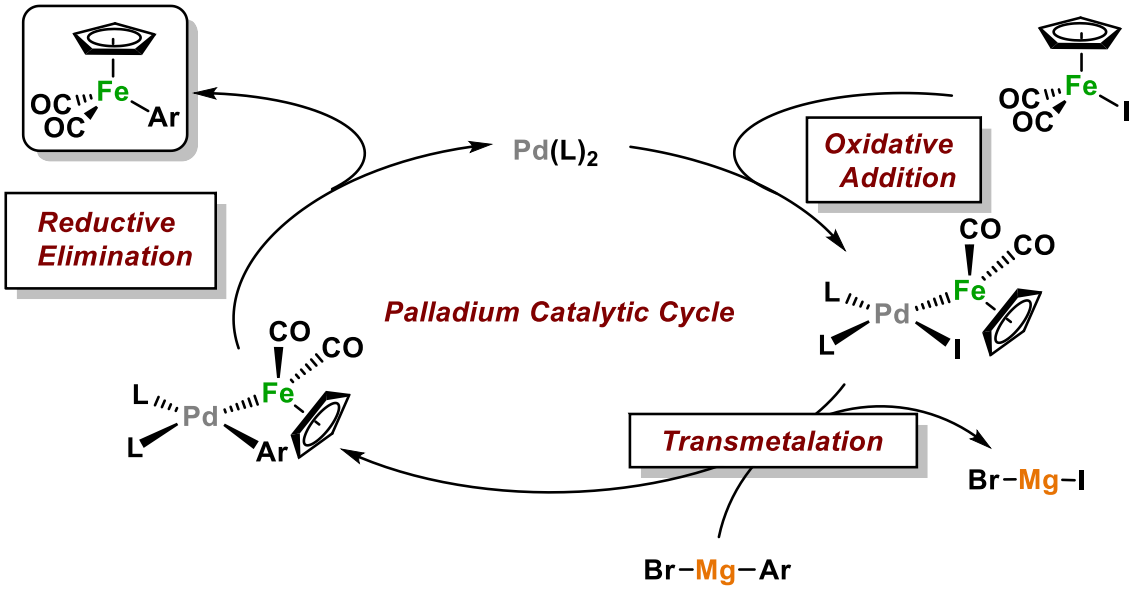

Figure 62. Mechanism for the synthesis of aryl-iron complexes using Pd/Mg catalysis proposed by Oshima et al.

This method allows the isolation in moderate yields of arylated Fe^{II} derivatives for subsequent use in cross-coupling reactions. This reaction cannot be carried out without the palladium organometallic complex because the substitution with Grignard reagents is not effective enough. For the mechanism, they proposed a similar mechanism to the conventional cross-coupling reaction with this complexes,[178,179] which consists of oxidative addition of $[Fe(Cp)I(CO)_2]$ to palladium that generates $[Cp(CO)_2Fe–Pd–I]$, transmetalation with arylmagnesium bromide, and reductive elimination that undergoes the C–iron bond. Another example, published by Ustynyuk et al. in 2020, proposed the formation of acetylene-iron bond

[177] Yasuda, S.; Yorimitsu, H.; Oshima, K. Synthesis of Aryliron Complexes by Palladium-Catalyzed Transmetalation between $[CpFe(CO)_2I]$ and Aryl Grignard Reagents and Their Chemistry Directed toward Organic Synthesis. *Organometallics* **2008**, *27*, 4025–4027. DOI: 10.1021/OM800560M.

[178] Ricci, A.; Angelucci, F.; Bassetti, M.; lo Sterzo, C. Mechanism of the Palladium-Catalyzed Metal-Carbon Bond Formation. A Dual Pathway for the Transmetalation Step. *J. Am. Chem. Soc.* **2002**, *124*, 1060–1071. DOI: 10.1021/ja011644p.

[179] Verpekin, V; Semeikin, O. v.; Vasiliev, A. D.; Kondrasenko, A. A.; Belousov, Y. A.; Ustynyuk, N. A. Catalyzed M–C Coupling Reactions in the Synthesis of σ-(Pyridylethynyl)Dicarbonylcyclopentadienyliron Complexes. *RSC Adv.* **2020**, *10*, 17014–17025. DOI: 10.1039/D0RA02333G.

using multimetallic catalysis. As we can see in Figure 63, the copper catalyst activates the C–H bond. After this step, a transmetalation reaction occurs to the Pd complexes. This complex undergoes reductive elimination to obtain the Fe(II) desired product.

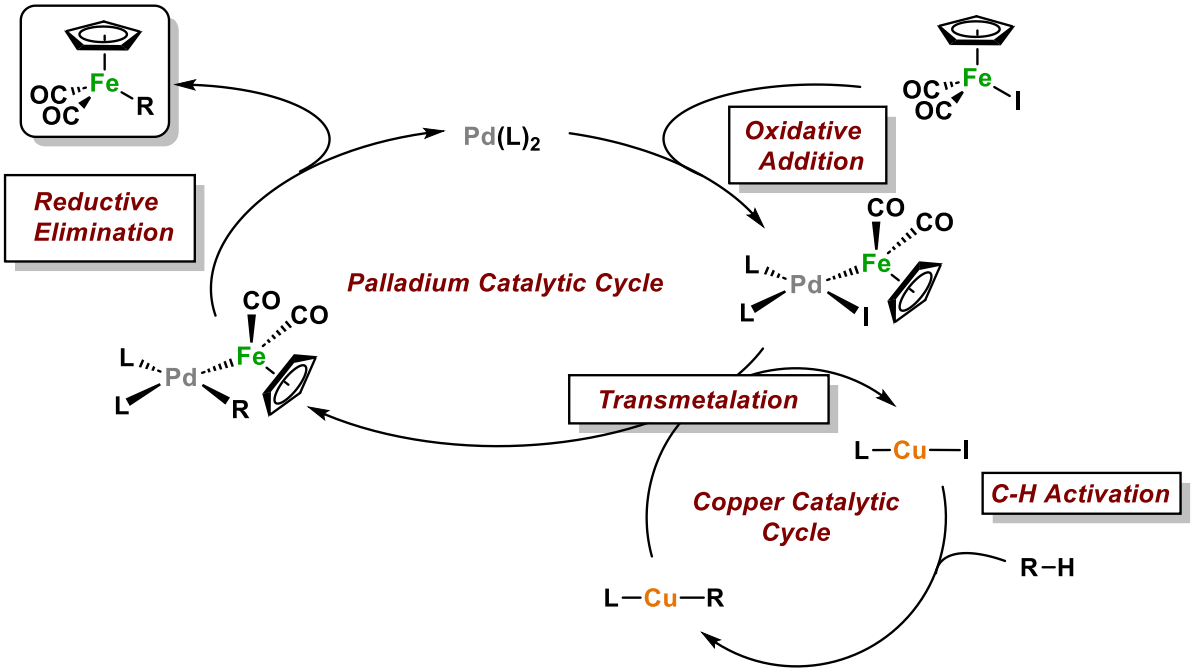

Figure 63. Mechanism for the synthesis of Acetylene-iron complexes using Pd/Cu catalysis proposed by Ustynyuk et al.

The following year, they published the synthesis of aryliron complexes $[Fe(Cp)Ar(CO)_2]$ by catalysis with Pd by reaction of $[Fe(Cp)I(CO)_2]$ with aryl-zinc, aryl-boron, or aryl-indium reagents.[180] In that work the catalysis by transmetalation to Pd complexes of different transmetalating agents, such as boronic acid derivatives, Zn or In and Al derivatives, is detailed. The palladium-catalysed arylation of $[Fe(Cp)I(CO)_2]$ with arylzinc or arylboron reagents offers an efficient method for the synthesis of various iron complexes (Equation 10). Triphenylindium transfers the phenyl groups under palladium catalysis to arylate $[Fe(Cp)I(CO)_2]$, but the aluminum derivate does not generate the product in good yield.

[180] Yasuda, S.; Asada, Y.; Yorimitsu, H.; Oshima, K. Synthesis of Aryliron Complexes $[CpFe(CO)_2Ar]$ by Palladium-Catalyzed Reactions of $[CpFe(CO)_2I]$ with Arylzinc, Boron, or Indium Reagents. *Materials* **2009**, *2*, 978–991. DOI: 10.3390/MA2030978.

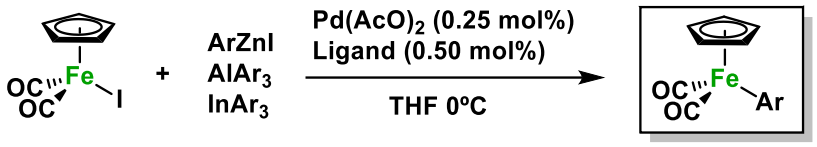

Equation 10. Palladium-catalysed arylation of [Fe(Cp)I(CO)$_2$] with arylzinc, aryl-aluminium or aryl-indium reagents.

Oshima and co-workers published a new method for the synthesis of [Fe(Cp)Ar(CO)$_2$]-type complexes using a copper-containing system employing organo-tin derivatives, as we can see in Equation 11.

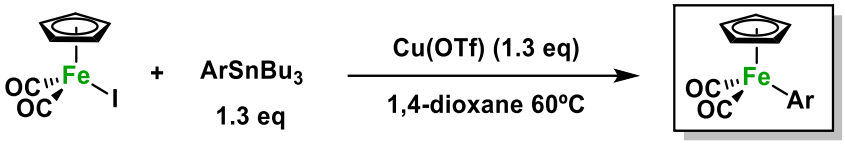

Equation 11. Copper-catalysed arylation of [Fe(Cp)I(CO)$_2$] with aryl-tin reagents.

Transmetalation between [Fe(Cp)I(CO)$_2$] and aryl tin reagents in the presence of copper salts yields the corresponding aryliron complexes [Fe(Cp)Ar(CO)$_2$]. This method employs the copper salt Cu(OTf) and organo-tin derivatives of the type R–SnBu$_3$ in 1,4-dioxane at 60°C for one hour. The advantages of this method with respect to those previously described are that it does not require precious metals such as palladium and that it has greater tolerance to functional groups, due to lower reactivity compared to Zn or Al derivatives. On the other hand, these systems have some disadvantages. The first and most important one is that it always requires one or more metals to be in excess of Fe complex, preventing the development of an efficient catalytic system.

Practically at the same time, Hashmi's research group published the synthesis of [Fe(Cp)(R)(CO)$_2$] (R=aryl, alkynyl, alkyl) type complexes by transmetalation from Au^{I} complexes.[181] They demonstrated that the transmetalation of linear complexes of [Au(R)(PPh$_3$)] with [Fe(Cp)I(CO)$_2$] is fast and effective at room temperature, generating the desired Fe^{II} complex. In this work a varied scope was presented by

[181] Hashmi, A. S. K.; Molinari, L. Effective Transmetalation from Gold to Iron or Ruthenium. *Organometallics* **2011**, *30*, 3457–3460. DOI: 10.1021/om200360q.

the authors, where a large number of aryls with different functional groups can be found, and all of the aryl-iron complexes were obtained in good to excellent yields. In this case, large differences in the reaction rate are observed in the transmetalation of Au^{I} complexes to the different halogenated derivatives $[Fe(Cp)(X)(CO)_2]$ (X=Cl < Br < I). On the other hand, good yields are also reported for the transmetalation of the methyl or acetylene groups.

Furthermore, they are able to prepare a catalytic system with a gold complex (5%) with a carbene ligand, phenylacetylene and NEt_3 as base, reporting an almost quantitative yield at 60 °C (as we can see in Equation 12).

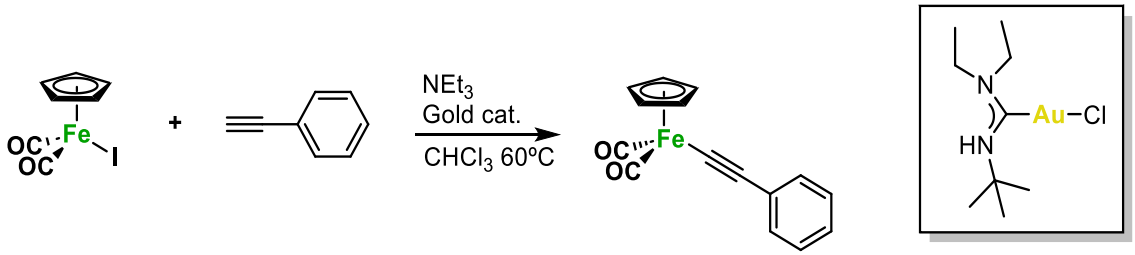

Equation 12. Gold-Catalysed Formation of Organoiron acetylene.

To further emphasize the synthetic advantages of this protocol, the authors decided to test the coupling reaction of the acetylene-iron derivate with 3-bromo-2-methylpropene, which had been found by Oshima and co-workers to be a good coupling partner.[175] The conversion was conducted as a one pot reaction with sequential transformations: gold-catalysed formation of the iron derivate, followed by a C–C bond formation reaction with 3-bromo-2-methylpropene under UV irradiation, as we can see in Equation 13. The Csp–Csp^3 coupling product could be isolated in moderated yields.

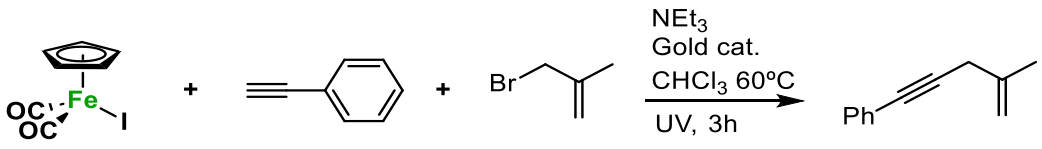

Equation 13. One-Pot sp–sp3 cross-coupling reaction using gold as catalyst.

They monitored the transmetalation reaction between $[Fe(Cp)(X)(CO)_2]$ (X=Cl, Br, I). and $[Au(C_6H_4NO_2)(PPh_3)]$ using ^{31}P NMR. They concluded that the thermodynamics of the reaction is relevant in the case of this transmetalation,

observing the reaction rate when they use different halides (formation of Au–X bonds). However, in some cases an induction period can be observed in the manuscript, but the explanation is not discussed.

For this behavior, it is well known that complexes of the type $[FeCp(X)(CO)_2]$ (X=Cl, Br, I) or $[Fe(Cp)(R)(CO)_2]$ (R=aryl, alkynyl, alkyl) can undergo ligand substitution reactions by displacement of one of the carbonyl groups, not proposed by Hashmi and co-workers. Therefore, an equilibrium of coordination and non-coordination of one of these carbonyl groups, facilitating the possibility of substitution by relatively donor groups, such as phosphine ligands. Although this is a process that occurs without any external reagent, and it is well known until decades, there are several ways to displace it thus enabling a better substitution, or even a transmetalation process. As discussed earlier in the reaction of Hashmi and co-workers, UV irradiation is one of the most common ways of shifting this equilibrium.[182,183,184]

With all the information gathered in this introduction, we set ourselves the objective of an in-depth study of the transmetalation step between complexes of the type $[Fe(Cp)I(CO)_2]$ and organometallic Cu(I) complexes with high-fluorinated aryls. This study is of vital importance due to the growing number of catalytic research that are currently being developed using these two metals, and whose transmetalation step is unknown.

---

[182] Albers, M. O.; Coville, N. J. Reagent and Catalyst Induced Substitution Reactions of Metal Carbonyl Complexes. *Coord. Chem. Rev.* **1984**, *53*, 227–259. DOI: 10.1016/0010-8545(84)85009-2.

[183] Ishio, M.; Terashima, T.; Ouchi, M.; Sawamoto, M. Carbonyl-Phosphine Heteroligation for Pentamethylcyclopentadienyl (Cp*)-Iron Complexes: Highly Active and Versatile Catalysts for Living Radical Polymerization. *Macromolecules* **2010**, *43*, 920–926. DOI: 10.1021/MA9022247

[184] Blaha, J. P.; Wrighton, M. S. Relative Importance of Dissociative Loss of Carbon Monoxide and Formation of Benzyl Radicals from Photoexcitation of $[CpFe(CO)_2(1\text{-}CH_2C_6H_5)$ and Evidence for Reaction of Carbon Monoxide with 17-Electron Radicals. *J. Am. Chem. Soc.* **1985**, *107*, 2694–2702. DOI: 10.1021/ja00295a023.

4.2 Results and discussion

To begin our study, the main challenge is to concentrate on the two fundamental steps of this catalytic cycle, which are the C–H activation of high fluorinated arenes, and the transmetalation between the Cu^{I} and the Fe^{II} organometallic complexes. First of all, it was tested whether the transmetalation step between a $Cu–Ar^{F}$ and an Fe^{II} complex occurred, or, in other words, to check if the thermodynamics of the whole system is favourable, as we shown in Scheme 23. Copper complexes of the type $[Cu(C_6F_5)(L)]$, which have already been used in this doctoral thesis with good results, and Fe^{II} complexes of the type $[Fe(Cp)X(CO)_2]$ (X=Cl, Br, I) were used. For this purpose, all Fe^{II} halides derivates were synthesized using the methodology used in the literature for X=Cl, Br and I. Once the Fe^{II} complexes were synthesized, the transmetalation reaction was tested with two different Cu^{I} complexes, the complex with a carbene ligand $[Cu(C_6F_5)(IPr)]$ (IPr = 1,3-Bis-(2,6-diisopropylphenyl)imidazol) and the trigonal-planar $[Cu(C_6F_5)(bipy)]$.[185]

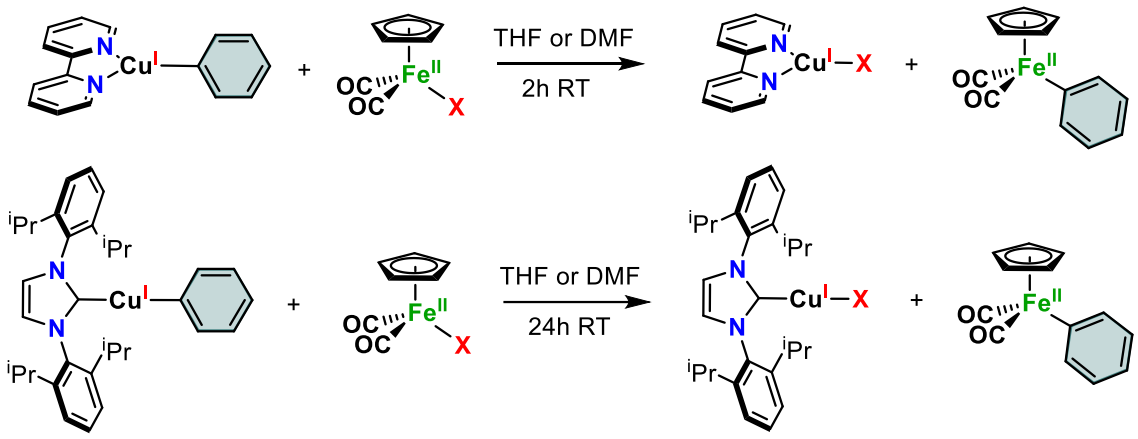

Scheme 23. General reaction for the synthesis of high-fluorinated aryl-iron complexes. Blue aryls represent pentafluorophenyl group.

The reaction with both complexes proved to be really effective, generating the desired product $[Fe(Cp)(C_6F_5)(CO)_2]$ in practically quantitative yield using the iodine derivative. Due to its relative stability, in the case of bipy ligand, undesired reactions, such as hydrolysis, generated the corresponding arene C_6F_5H in very low

[185] Lozano-Lavilla, O.; Gómez-Orellana, P.; Lledós, A.; Casares, J. A. Transmetalation Reactions Triggered by Electron Transfer between Organocopper Complexes. *Inorg. Chem.* **2021**, *15*, 11633–11639. DOI: 10.1021/acs.inorgchem.1c01595.

concentration. On the other hand, the complex [Fe(Cp)(C_6F_5)$(CO)_2$] is stable to oxygen and water. Although both copper complexes proved to be effective in the transmetalation process, [Cu(C_6F_5)(bipy)] demonstrated to be much faster, generating the desired product in just two hours at room temperature, compared to the other complex with carbene ligand, which needed 24 hours to give the final product in quantitative yield. These behaviour can be explained due to the steric hindrance of the IPr ligand, or because the 16 e^- copper (I) complex with bipy ligand is better nucleophile than the linear 14 e^- [Cu(C_6F_5)(IPr)] Additionally, it is observed that the reaction is faster when X = I > Br > Cl was used, as previously described in other cases.[181]

This showed that the thermodynamics of the reaction was favourable, but there was a large difference in the activation energy of the process between both ligands, being the transmetalation barrier much higher for the case of the IPr ligand, either by steric control, electronic and geometrical differences (linear vs. trigonal-planar geometry) or different reaction pathways. As we have commented in the introduction, there are several problems in the methods described for the synthesis of [Fe(Cp)(Ar^F)$(CO)_2$] complexes, which are :

I) There are few examples of effective catalytic systems, and in the case of the work of Hashmi *et al.* it has not been tested with fluorinated aryls.[175]

II) II) The mechanism of transmetalation in these systems is unknown, preventing to improve the Cu/Fe catalysis in an effective and definitive pathway.

Therefore, we examined the possibility of found a catalytic system to obtain high fluorinated-iron (II) complexes using a C–H functionalization process catalysed by copper complexes. Complex [CuI(bipy)] (**1**) will be used in catalytic amounts, NaO^tBu as base and Ar^F–H and [Fe(Cp)I$(CO)_2$] (**2**) as coupling partners, as we can see in Table 28.

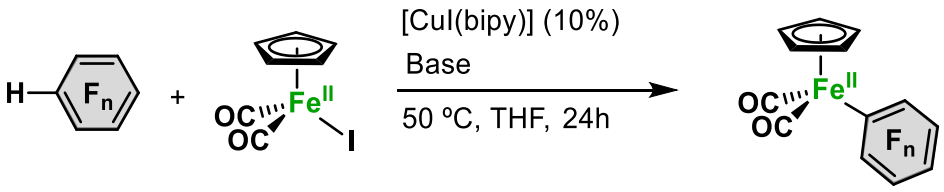

Entry	Arene	Base	Product	Yield (%)
1	$C_6F_3Cl_2H$	NaO^tBu	$[Fe(Cp)(C_6F_3Cl_2)(CO)_2]$	90
2	C_6F_5H	Cs_2CO_3	$[Fe(Cp)(C_6F_5)(CO)_2]$.	93
3	C_5HNF4	NaO^tBu	$[Fe(Cp)(C_5F_4N)(CO)_2]$	95
4	$C_7H_3F_4O$	NaO^tBu	$[Fe(Cp)(C_7H_3F_4O)(CO)_2]$.	86
5	$C_6H_3F_4N$	NaO^tBu	$[Fe(Cp)(C_6H_2F_4N)(CO)_2]$	n.d

Table 28. [CuI(bipy)] 10%, 1 eq. Base, 1 eq. of Arene, 1 eq. of $[FeCpI(CO)_2]$, 50 °C, 2 mL THF. 24h. [Cu] = 0.015 mol L^{-1}.

As we can see in the catalytic reaction conditions, although the transmetalation is relatively fast at room temperature, it is necessary to heat the reaction in order to give the C–H activation step.[174,177,186,187,188,189] The only substrate that did not generate the desired product was using tetrafluoroaniline (entry 5), which, as we have seen (Chapter I and III) in other systems, we are not able to activate, presumably due to the coordination of the N atom to the metal center. Note that when C_6F_5H is used as arene, Cs_2CO_3 is used as a base due to the nucleophilic attack of the $^tBuO^-$ rest to the fluorine atom in para position (see Chapter I for more details).

Furthermore, the products $[Fe(Cp)(C_5F_4N)(CO)_2]$ and $[Fe(Cp)(C_6F_3Cl_2)(CO)_2]$ could be characterized by X-ray diffraction, both shown in Figure 64.

[186] Aneeja, T.; Neetha, M.; Afsina, C. M. A.; Anilkumar, G. Progress and Prospects in Copper-Catalyzed C-H Functionalization. *RSC Adv*. **2020**, *10*, 34429–34458. DOI: 10.1039/d0ra06518h.
[187] Lesieur, M.; Lazreg, F.; Cazin, C. S. J. A Cooperative Pd-Cu System for Direct C-H Bond Arylation. *Chem. Commun.* **2014**, *50*, 8927–8929. DOI: 10.1039/c4cc03201b.
[188] Do, H. Q.; Khan, R. M. K.; Daugulis, O. A General Method for Copper-Catalyzed Arylation of Arene C-H Bonds. *J. Am. Chem. Soc.* **2008**, *130*, 15185–15192. DOI: 10.1021/ja805688p.
[189] Haines, B. E.; Kawakami, T.; Kuwata, K.; Murakami, K.; Itami, K.; Musaev, D. G. Cu-Catalyzed Aromatic C-H Imidation with N-Fluorobenzenesulfonimide: Mechanistic Details and Predictive Models. *Chem. Sci.* **2017**, *8*, 988–1001. DOI: 10.1039/c6sc04145k.

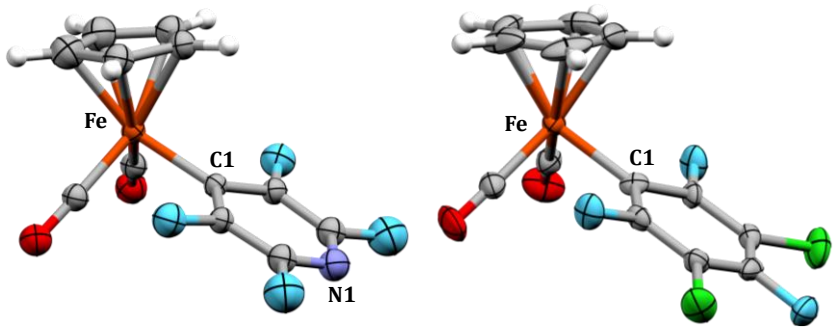

Figure 64. X-ray structure of [Fe(Cp)(C_5F_4N)($CO)_2$] and [Fe(Cp)($C_6F_3Cl_2$)($CO)_2$].

Upon verification of the catalytic system, the mechanism was studied. For this purpose, the [Cu(C_6F_5)(bipy)] (**3**) complex was reacted with the [Fe(Cp)I($CO)_2$] (**2**) complex in different solvents. Due to the low solubility of the [Cu(C_6F_5)(bipy)] (**3**) complex in some solvents (THF, CH_2Cl_2, $CHCl_3$ and toluene), DMF was used for the mechanistic studies. Interestingly, the reaction shows a peculiar kinetic profile, comparable to that mentioned above in the work of Hashmi et al. As we can see in Figure 65 the monitoring at ^{19}F NMR shows a considerably induction period (about 20 minutes).

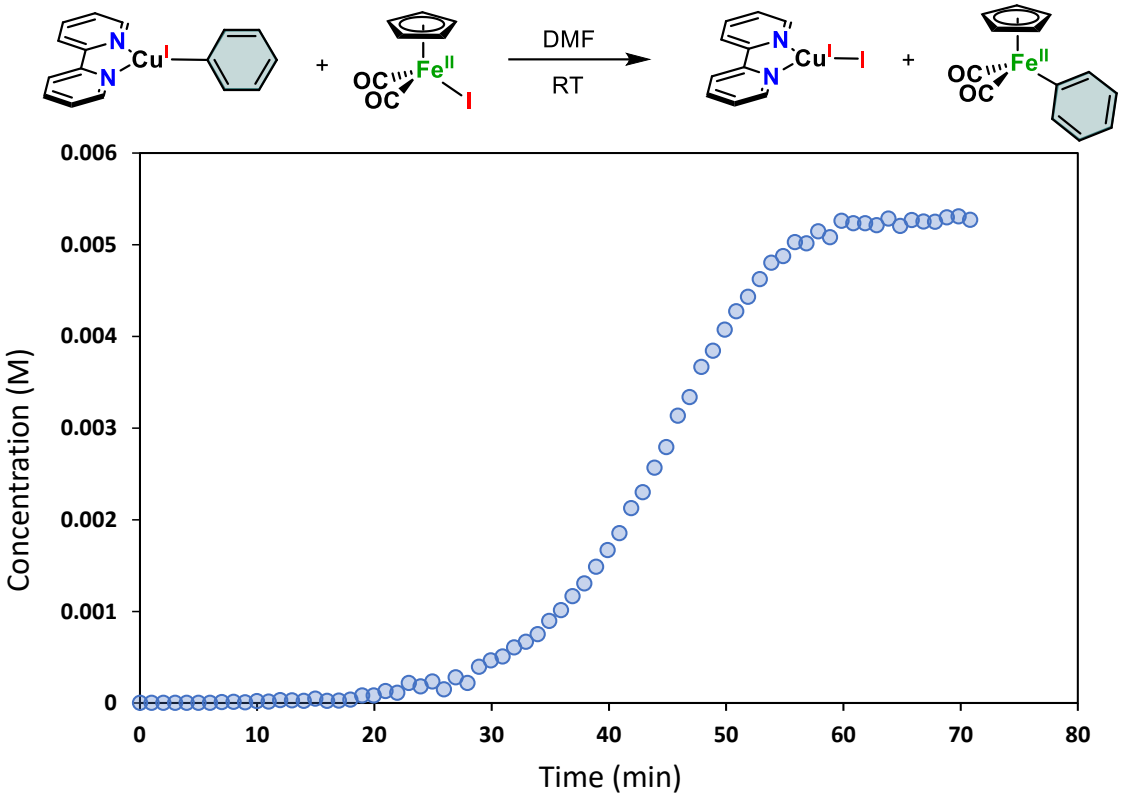

Figure 65. Concentration vs time plot of experimental data (dots) obtained by ^{19}F NMR monitoring of the formation of [Fe(Cp)(C_6F_5)($CO)_2$] in the reaction between [Cu(C_6F_5)(bipy)] (**3**) ($[3]_0$=6.5 x 10^{-3}

mol L^{-1}) and [Fe(Cp)I(CO)$_2$] (**2**) ([2]$_0$=6.5 x 10^{-3} mol L^{-1}) in dry DMF at 298 K. Blue aryl represents C_6F_5.

Different explanations for the induction period were initially put forward.

I) *Autocatalytic reaction*. This means that one of the products, either the [Fe(Cp)(C_6F_5)(CO)$_2$] complex or the [CuI(bipy)] complex, is able to catalyse the transmetalation between [Fe(Cp)I(CO)$_2$] (**2**) and [Cu(C_6F_5)(bipy)] (**3**). To test whether these products are able to catalyse the transmetalation reaction, 10% mol of these compounds are added as a reagent with respect to the initial reagents in two different experiments. The results of these experiments showed no variation in the reaction rate or in the induction period concluding that this is not an autocatalytic reaction.

II) *The reaction requires the temporary dissociation of one of the ligands*. This reaction requires the slow formation of a new species from the reactants by ligand substitution. Traditionally, this is very common in dissociative mechanisms.[190]This

[190] A) Hirner, J. J.; Shi, Y.; Blum, S. A. Organogold Reactivity with Palladium, Nickel, and Rhodium: Transmetalation, Cross-Coupling, and Dual Catalysis. *Acc. Chem. Res*. **2011**, *44*, 603–613 DOI: 10.1021/ar200055y. b) Amatore, C.; Jutand, A.; le Duc, G. Kinetic Data for the Transmetalation/Reductive Elimination in Palladium-Catalyzed Suzuki-Miyaura Reactions: Unexpected Triple Role of Hydroxide Ions Used as Base. *Chem. Eur. J.* **2011**, *17*, 2492–2503. DOI: 10.1002/chem.201001911. c) Carrow, B. P.; Hartwig, J. F. Distinguishing between Pathways for Transmetalation in Suzuki-Miyaura Reactions. *J. Am. Chem. Soc.* **2011**, *133*, 2116–2119. DOI: 10.1021/ja1108326. d) del Pozo, J.; Salas, G.; Álvarez, R.; Casares, J. A.; Espinet, P. The Negishi Catalysis: Full Study of the Complications in the Transmetalation Step and Consequences for the Coupling Products. *Organometallics* **2016**, *35,* 3604–3611. DOI: 10.1021/acs.organomet.6b00660. e) Hansmann, M. M.; Pernpointner, M.; Döpp, R.; Hashmi, A. S. K. A Theoretical DFT-Based and Experimental Study of the Transmetalation Step in Au/Pd-Mediated Cross-Coupling Reactions. *Chem. Eur. J.* **2013**, *19*, 15290–15303. DOI: 10.1002/CHEM.201301840. F) Meana, I.; Espinet, P.; Albéniz, A. C. Heterometallic Complexes by Transmetalation of Alkynyl Groups from Copper or Silver to Allyl Palladium Complexes: Demetalation Studies and Alkynyl Homocoupling. *Organometallics* **2014**, *33*, 1–7. DOI: 10.1021/om4005498. g) Toledo, A.; Meana, I.; Albéniz, A. C. Formal Gold-to-Gold Transmetalation of an Alkynyl Group Mediated by Palladium: A Bisalkynyl Gold Complex as a Ligand to Palladium. *Chem. Eur. J.* **2015**, *21*, 13216–13220. DOI: 10.1002/CHEM.201501813. h) García-Melchor, M.; Fuentes, B.; Lledós, A.; Casares, J. A.; Ujaque, G.; Espinet, P. Cationic Intermediates in the Pd-Catalyzed Negishi Coupling. Kinetic and Density Functional Theory Study of Alternative Transmetalation Pathways in the Me-Me Coupling of $ZnMe_2$ and Trans -[PdMeCl($PMePh_2$)$_2$]. *J. Am. Chem. Soc.* **2011**, *133*, 13519–13526. DOI: 10.1021/ja204256x. i) Espinet, P.; Echavarren, A. M. The Mechanisms of the Stille Reaction. *Angew. Chem. Int. Ed.* **2004**, *43*, 4704–4734. DOI: 10.1002/anie.200300638. j) Casares, J. A.; Espinet, P.; Fuentes, B.; Salas, G. Insights into the Mechanism of the Negishi Reaction: ZnRX versus ZnR_2 Reagents. *J. Am. Chem. Soc*. **2007**, *129*, 3508–3509 DOI: 10.1021/ja070235b. k) Oeschger, R. J.; Ringger, D. H.; Chen, P. Gas-Phase Investigations on the Transmetalation Step in Sonogashira Reactions. *Organometallics* **2015**, *34*, 3888–3892. DOI: 10.1021/acs.organomet.5b00491. l) Wang, X.; Song, Y.; Qu, J.; Luo, Y. Mechanistic Insights into the Copper-Cocatalyzed Sonogashira Cross-Coupling Reaction: Key Role of an Anion. *Organometallics* **2017**, *36*, 1042–1048. DOI: 10.1021/acs.organomet.7b00010. m) Hashmi, A. S. K.; Lothschütz, C.; Döpp, R.; Rudolph, M.; Ramamurthi, T. D.; Rominger, F. Gold and Palladium Combined for Cross-Coupling. *Angew. Chem. Int. Ed*. **2009**, *48*, 8243–8246. DOI: 10.1002/ANIE.200902942. n) Pérez-Temprano, M.

behaviour generated a free ligand situation in solution and can be quenched with the external addition of these ligands.[191,192] Therefore, the reaction was first tested in the presence of an equivalent of NBu_4I, an iodide source to study this possibility in our system, as we can see in Equation 14.

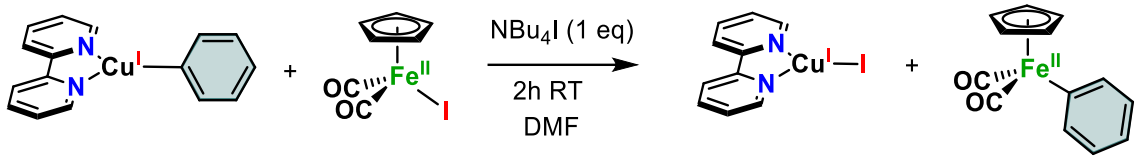

Equation 14. Transmetalation reaction between $[Fe(Cp)I(CO)_2]$ (**2**) and $[Cu(C_6F_5)(bipy)]$ (**3**) in presence of 1 equivalent of NBu_4I.

The reaction turns out not to undergo any variation with respect to the initial reaction. On the other hand, if the reaction was carried out under CO pressure, no product was observed after two hours, suggesting that it is this ligand that has to be dissociated to generate an active species instead the I^-, which is more common to be the dissociated ligand. Also, the cyclopentadiene ligand is able to change its coordination, generating vacancies. However, no evidence has been found in the literature that these complexes change their coordination mode in these systems.

There are different methods to favour reversibly and irreversibly dissociation of CO for these organometallic iron(II) complexes. The use of catalysts such as $[Fe(Cp)(CO)_2]_2]$,[193,194,195] or the use of organic reagents such as $ONMe_3$ are also good

H.; Casares, J. A.; de Lera, Á. R.; Álvarez, R.; Espinet, P. Strong Metallophilic Interactions in the Palladium Arylation by Gold Aryls. *Angew. Chem. Int. Ed.* **2012**, *124*, 5001–5004. DOI: 10.1002/ange.201108043.

[191] Villar, P.; Pérez-Temprano, M. H.; Casares, J. A.; Álvarez, R.; Espinet, P. Experimental and DFT Study of the $[AuAr(AsPh_3)]$-Catalyzed Cis/Trans Isomerization of $[PdAr_2(AsPh_3)_2]$ (Ar = C_6F_5or $C_6Cl_2F_3$): Alternative Mechanisms and Its Switch upon Pt for Pd Substitution. *Organometallics* **2020**, *39*, 2295–2303. DOI: 10.1021/acs.organomet.0c00245.

[192] Peñas-Defrutos, M. N.; Bartolomé, C.; García-Melchor, M.; Espinet, P. RhAr/AuAr′ Transmetalation: A Case of Group Exchange Pivoting on the Formation of M–M′ Bonds through Oxidative Insertion. *Angew. Chem. Int. Ed.* **2019**, *131*, 3539–3543. DOI: 10.1002/ange.201813419.

[193] Coville, N. J.; Darling, E. A.; Hearn, A. W.; Johnston, P. Metal Dimers as Catalysts. *J. Organomet. Chem.* **1987**, *328*, 375–385. DOI: 10.1016/0022-328X(87)80253-X.

[194] Coville, N. J.; Albers, M. O.; Ashworth, T. v.; Singleton, E. $[CpFe(CO)_2]_2$; a Versatile Catalyst for Ligand-Replacement Reactions on Transition-Metal Complexes. *Chem. Commun.* **1981**, *9*, 408–409. DOI: 10.1039/C39810000408.

[195] Gipson, S. L.; Liu, L.-K.; Soliz, R. U. The Reaction of $CpFe(CO)_2X$ (X = Cl, Br, I) with Phosphines Catalyzed by $[CpFe(CO)_2]_2$: Evidence for an Electron Transfer Chain Catalysis Mechanism. *J. Organomet. Chem.* **1996**, *526*, 393–395. DOI: 10.1016/S0022-328X(96)06586-2.

methods to carry out this displacement,[196] and the use of this methods have been studied in depth for years.[182] The reaction mechanisms are presented in Figure 66.

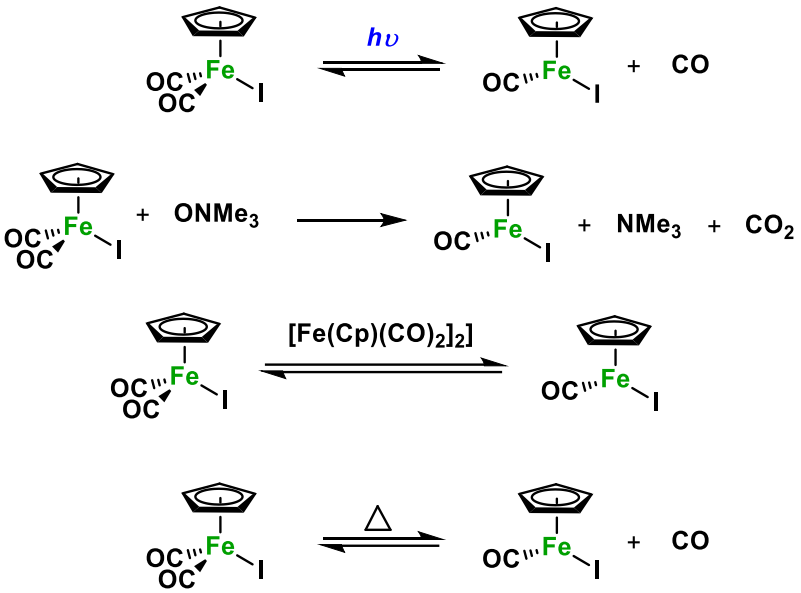

Figure 66. Different reactions for the displacement of the carbonyl ligand.

These ligand dissociation processes would allow the generation of a species with a vacancy that would facilitate the transmetalation process in the examples discussed above. To check if we can improve the stoichiometric or catalytic Fe/Cu systems using the mechanistic results obtained so far, we tested–the influence of different reagents, such as $ONMe_3$, which reacts irreversibly with a CO molecule, the iron(0) dimer $[Fe(Cp)(CO)_2]_2]$, which reversibly traps a CO molecule, and the use of blue light radiation, which facilitates the reversible dissociation of one of the two CO molecules.

As we can see in Figure 67 all methods reduce the induction period, but we do not observe an increase in the reaction rate in most cases. It should be noted that in the case of using the dimer, a small increase in the reaction rate is observed. First of all, the experiment with a catalytic amount of amine oxide (10 %), produce the transmetalation product in good yields. Note that is just necessary a minimum quantity of the active species [Fe(Cp)I(CO)] to generate the product in just 45

[196] Elzinga, J.; Hogeveen, H. Intermediate Complex in the Reduction of Trimethylamine Oxide by Pentacarbonyl Iron: Its Use as Catalyst in the Addition of Carbon Tetrachloride to Carbon–Carbon Double Bonds. *J. Chem. Soc. Chem. Commun.* **1977**, *20*, 705–706. DOI: 10.1039/C39770000

minutes. These results confirm that the transmetalation step goes throw this active specie.

Another experiments, using different amounts of $[Fe(Cp)(CO)_2]_2$ complex was tested. $[Fe(Cp)(CO)_2]_2$ is capable of capturing a CO molecule, generating this active specie and catalysing the transmetalation reaction. As we can see in Figure 67, the reaction rate using 5% (red dots) and 10% (yellow dots) is significantly faster than in the other cases. These complex not only generated the active species, but these kinetic profiles also suggest that the iron dimer could catalysed another process.

Finally, the other way to generate the complex [Fe(Cp)I(CO)] is using some irradiation source. As we commented in the introduction, Hashmi et al. catalysed the transmetalation reaction between organogold complexes and this iron (II) complexes using UV irradiation.[181] In our case, we use just 5 seconds of blue led, as we can see in Figure 67, to generate the active specie. When we try to improve this result with more exposition time to light, we obtained more than 20 % of the transmetalation product in the first spectra. Comparable kinetic monitoring is prevented by this rapid formation of the active specie, probably due to the high concentration of these complex.

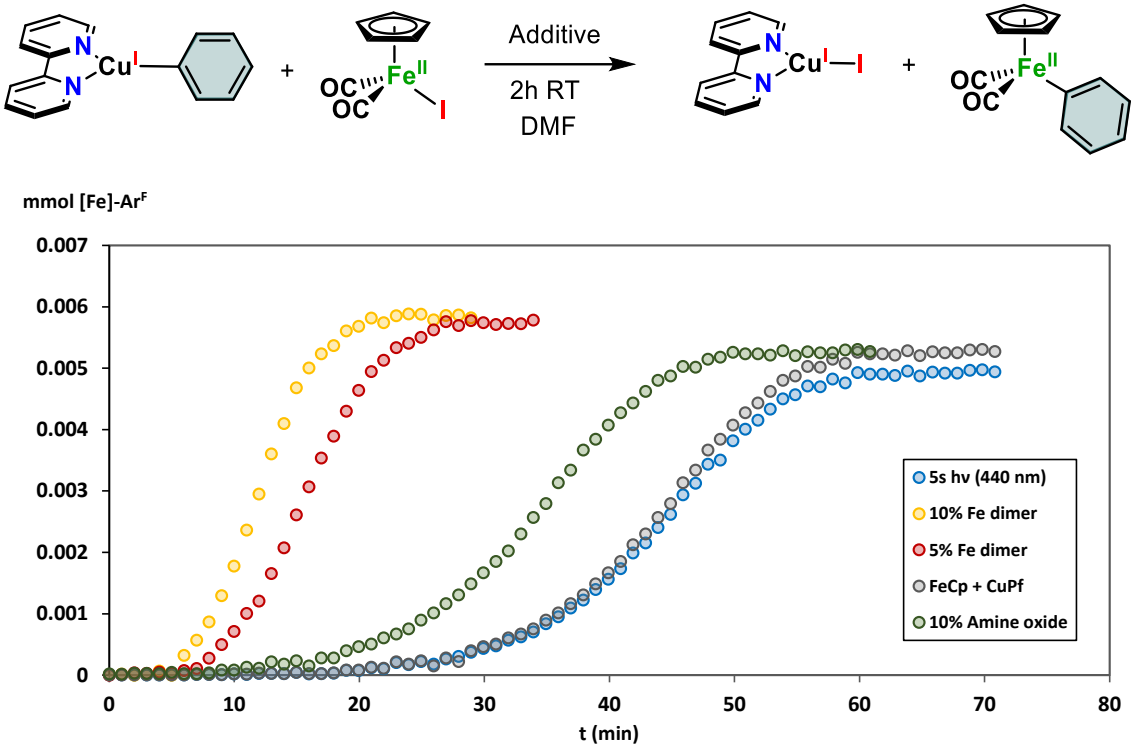

Figure 67. Concentration vs time plot of experimental data (dots) obtained by ^{19}FNMR monitoring of the formation of [Fe(Cp)(C_6F_5)(CO)$_2$] in the reaction between [Cu(C_6F_5)(bipy)] (**3**) ([3]$_0$=6.0 x 10^{-3} M) and [Fe(Cp)I(CO)$_2$] (**2**) ([2]$_0$=6.0 x 10^{-3} mol L^{-1}) and different additives in dry DMF at 298 K. ONMe$_3$ was used as amine oxide and [FeCp(CO)$_2$]$_2$] as iron dimer.

Although significant changes in induction time have been achieved, the kinetic profile remains the same. Therefore, in order to verify that our hypothesis is correct, qualitative study using kinetic simulations was made, to see if it has a good correlation with our system. The first proposed mechanism is shown in Scheme 24.

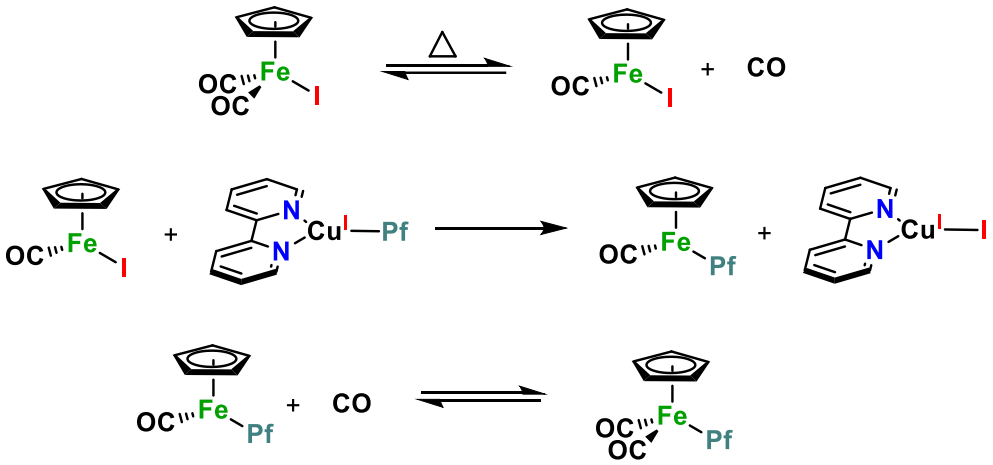

Scheme 24. Proposed kinetic model for the reaction represented in Figure 68.

As we can see, the mechanism initially proposed is formed by three elementary steps. The first is a CO dissociation process, which has been experimentally demonstrated using an excess of CO. The second is the transmetalation step, where the fluorinated aryl is transferred from the copper complex to the iron atom. And finally, the third step is the return of the CO ligand to the Fe^{II} complex to give the desired product.

As expected, the proposed mechanism does not fit well with the experimental results. As we can see in Figure 68, the kinetic simulation using this mechanism shows an induction period, but absolutely not similar to the kinetic profile experimentally obtained.

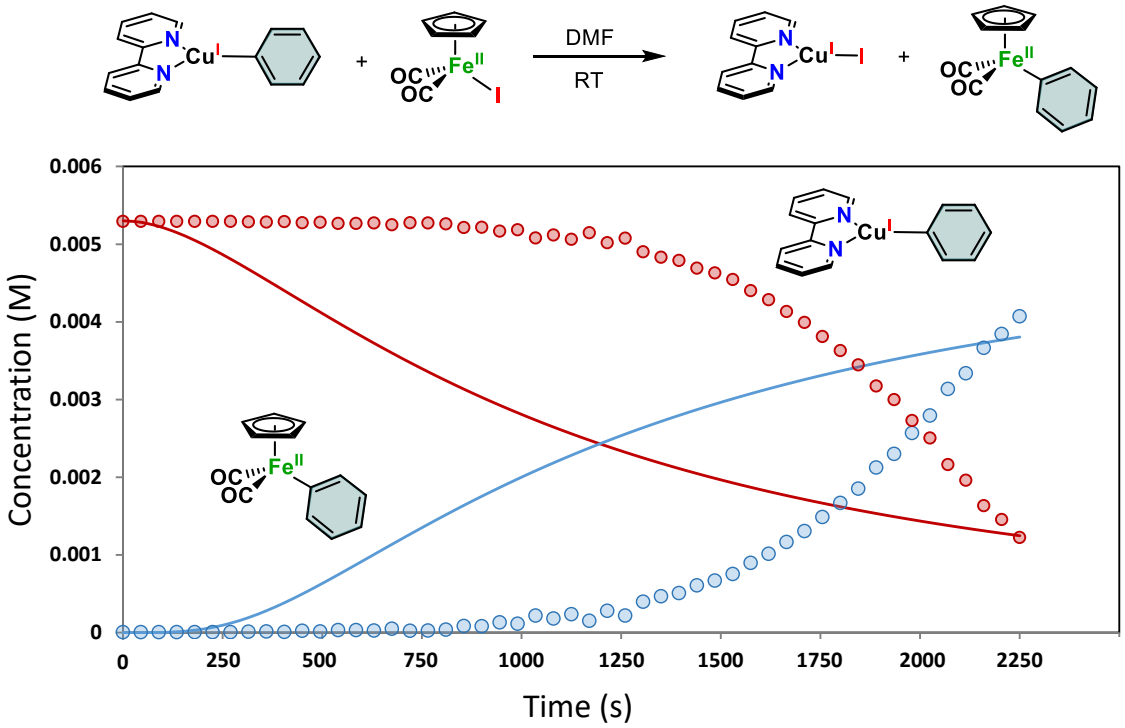

Figure 68. Concentration vs time plot of experimental data (dots) obtained by ^{19}F NMR monitoring of the formation of $[Fe(Cp)(C_6F_5)(CO)_2]$ (blue dots) in the reaction between $[Cu(C_6F_5)(bipy)]$ (**3**) ($[\mathbf{3}]_0$=5.5 x 10^{-3} mol L^{-1}) (red dots) and $[Fe(Cp)I(CO)_2]$ (**2**) ($[2]_0$=5.5 x 10^{-3} mol L^{-1}) in dry DMF at 298 K and the COPASI-fitted values (continuous lines) of the fluorinated-species observed.

This behaviour implies that more reactions must be involved in the mechanism. If we think about the proposed mechanism and the simulated kinetic profile, we realize that the explanation of the induction period lies in the formation of an active species, the interpretation of which is correct. The drawback is that for the induction

period to be longer, it is necessary that this intermediate reacts slowly to give the final product, *i.e.,* it is necessary that another Fe^{II} species of a carbonyl ligand reacts with this intermediate, giving the final product and generating another active species *via* transmetalation. This proposal is the most plausible considering that the reaction is slightly accelerated when the Fe^{0} dimer is used as a co-catalyst.

Again, this new mechanism is tested using the copasi software, adding the new reaction to the previous mechanistic proposal. In this way, there would be a mechanism where 4 elementary reactions would be involved. Both the kinetic simulation and the proposed mechanism can be seen in Figure 69.

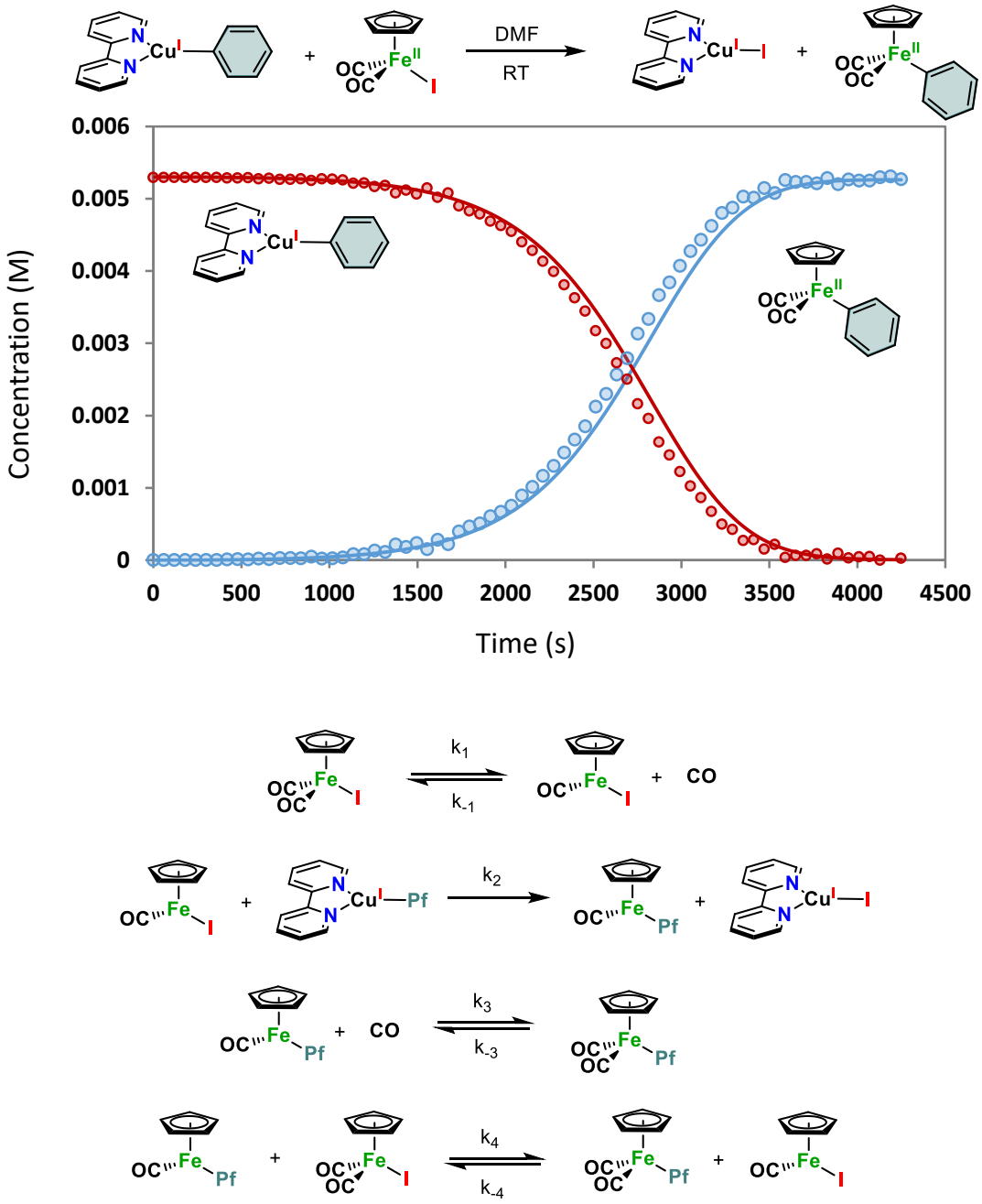

Figure 69. Concentration vs time plot of experimental data (dots) obtained by ^{19}F NMR monitoring of the formation of [Fe(Cp)(C_6F_5)$(CO)_2$] (blue dots) in the reaction between [Cu(C_6F_5)(bipy)] (**3**) ([**3**]$_0$=5.5 x 10^{-3} mol L^{-1}) (red dots) and [Fe(Cp)I$(CO)_2$] (**2**) ([**2**]$_0$=5.5 x 10^{-3} mol L^{-1}) in dry DMF at 298 K and the COPASI-fitted values (continuous lines) of the fluorinated-species observed. Kinetic model showed below.

As we can observe, the kinetic simulation fits perfectly with the experimental result, allowing to determine the real mechanism of this reaction. The table in Figure 70 shows the values obtained from the kinetic simulation of the velocity constants and their standard deviations.

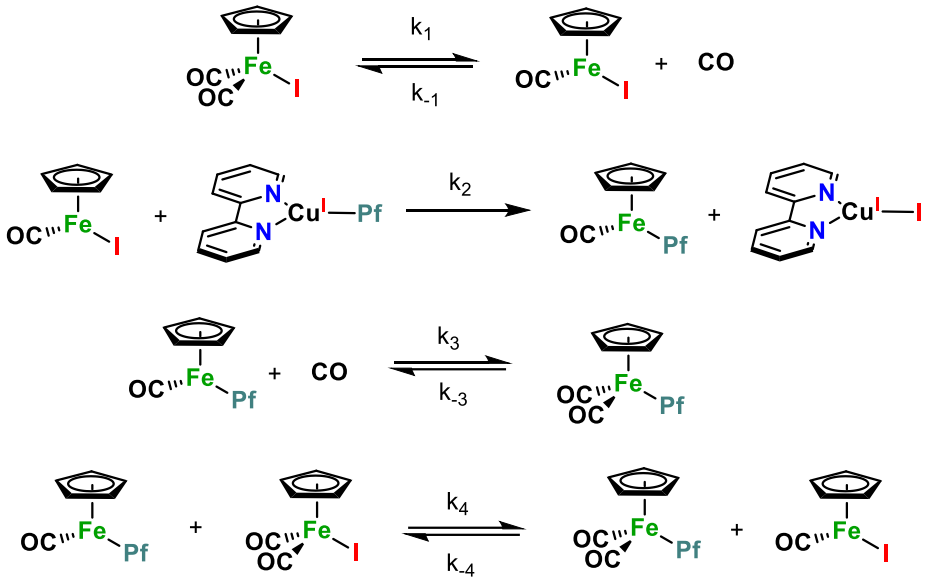

k	Value s^{-1} ; $M^{-1} \cdot s^{-1}$	Std. Desviation
k_1	1.00×10^{-8}	2.4×10^{-9}
k_{-1}	2.51×10^{-3}	3.0×10^{1}
k_2	5.77×10^{2}	8.1×10^{2}
k_3	1.49×10^{1}	1.9×10^{1}
k_{-3}	5.89×10^{-6}	1.4×10^{-6}
k_4	3.39×10^{2}	1.9×10^{2}
k_{-4}	2.36×10^{-6}	1.8×10^{-5}

Figure 70. Kinetic model proposed and value of the kinetic constants with their standard deviations.

To finalize the study, we proposed to carry out an exhaustive study by means of computational DFT calculations, trying to give the most realistic view possible of the reaction we were studying. This project is currently under development and the computational calculations are being done in collaboration with the Prof. Agustí Lledós Falcó.

For this, the main difficulty was to study the transmetalation between two metal complexes with metals of the first transition series by DFT calculations. The mechanism can be divided into two main steps. The first one is focus on the Cu cycle, where the C–H activation of the fluorinated arenes takes place. The mechanism of this stage has been studied in similar systems, as in the case of 1,10-phenanthroline, and for this reason it will not be studied at a theoretical level.[167] On the other hand,

the result of the catalysis shows that heating is necessary to give this activation of the C–H bond, contrary to the transmetalation studies, which occur at room temperature, which shows that the limiting step is the C–H activation. Since the C–H activation part has already been studied in depth by theoretical calculations, as we can see in the introduction of this chapter, we will focus only on the transmetalation step between [Cu(C_6F_5)(bipy)] (**3**) and [Fe(Cp)I($CO)_2$] (**2**).

The first step was to study the CO dissociation in the [Fe(Cp)I($CO)_2$] (**2**) complex, calculated by Bu et al. in 2011.[197] The structures of all the intermediates and transition states were optimized in dimethylformamide solvent (DMF, ε= 37.219) with the SMD continuum model using the B3LYP functional combined with the Grimme's D3 correction for dispersion. Basis Set includes the 6-31G(d,p) basis set for the main group elements, excluding iodine, and the scalar relativistic Stuttgart-Dresden SDD pseudopotential and its associated double-z basis set, complemented with a set of polarization functions, for the copper and iron (f polarization functions) and iodine (d polarization functions) atoms (more information in experimental section).

Figure 71 shows a representation of both the [Fe(Cp)I($CO)_2$] complex and the transition state associated with ligand dissociation. As we can observe, the Fe–CO bond distance increases from 1.786 Å to 2.586, which implies an elongation of 0.8 Å and has an energy value of $\Delta G^{\neq}$ = 24.7 kcal mol^{-1}.

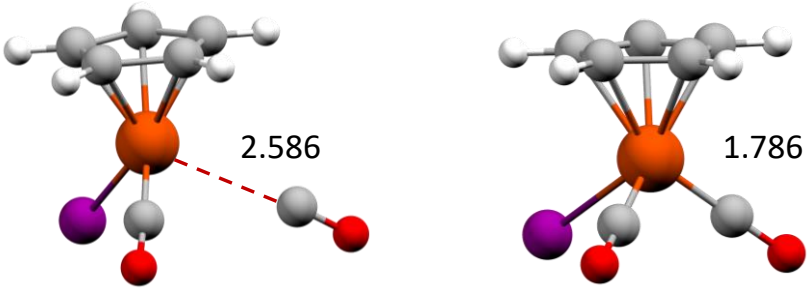

Figure 71. DFT calculations of: Right = Optimization geometry of **2** in DMF. Left = Transition state of the dissociation of the carbonyl group. Distances Cu–C are given in Å.

[197] Z. Zhang, Y. Bu. Arylation of styrene derivatives using aryliron complexes [CpFe($CO)_2$Ar] revealed by density functional theory calculations: Fe(II)-assisted group exchange through Fe–C bond cleavage and Fe–X bond formation. *J. Organomet. Chem.* **2011**, *24*, 3852–3860. DOI: 10.1016/j.jorganchem.2011.08.032.

Interestingly, some particularities can be commented on this process. First of all, this is not a "classical" dissociative substitution: the ligand that dissociates is not the leaving ligand (I^-). As the experimental results showed, the reaction does not undergo any modifications in the presence of I^- in solution, but it is radically blocked when the reaction is carried out in CO atmosphere. Furthermore, the evolution of the examined coordinate for the dissociation process to obtained the product [Fe(Cp)I(CO)] has not developed a enough stable structure yet. Furthermore, the stability and geometry of this $16e^-$ complexes were examined in detailed by Hoffman *et al*. where they conclude that the Jahn-Teller second-order theorem predicts that for a small HOMO-LUMO gap there exists a distortion of symmetry of the complexes [Fe(Cp)L(CO)] that opens up the HOMO-LUMO gap and stabilizes the system, obtaining by DFT calculations a pyramidal geometry.[198]

In addition, due to the ease of these complexes to modify the spin state,[185] a change in the spin of the [Fe(Cp)I(CO)] complex coming from the dissociation of the $[Fe(Cp)I(CO)_2]$ complex could take part on this process. For this, first of all, is the analysis of the molecular orbitals in the different stages. The analysis of the complex $[Fe(Cp)I(CO)_2]$ shows the molecular orbitals typically represented for purely octahedral complexes.[199] This complex must necessarily be singlet. On the other hand, as we can see in Figure 72, when the complex dissociates a CO ligand from the transition state depicted in Figure 71, an intermediate containing a vacancy appears. The analysis of molecular orbitals shows a splitting in the symmetry, allowing the appearance of different spin states, singlet, triplet and even quintuplet.

[198] a) Hofmann, P. Unsaturated Organometallics Intermediates: Electronic Structure and Structural Dynamics of $(\eta_5\text{-}C_5H_5)Mn(CO)_2$. *Angew. Chem. Int. Ed.* **1977**, *16*, 536–537. b) Ward, T. R.; Schafer, O.; Daul, C.; Hofmann, P. Geometry of Coordinatively Unsaturated Two-Legged Piano Stool Complexes with 16 Valence Electrons: A Theoretical Study. Organometallics **1997**, *16*, 3207–3215. DOI: 10.1021/om9700369.

[199] a) Kostic N.M.; R.F. Fenske. Molecular Orbital Study of Bonding, Conformations, and Reactivity of Transition-Metal Complexes Containing Unsaturated Organic Ligands. Electrophilic and Nucleophilic Additions to Acetylide, Vinylidene, Vinyl, and Carbene Ligands. *Organometallics* **1982**, *1*, 974-982. b) Schilling, B. E. R.; Hoffmann, R.; Faller, J. W. *J. Am. Chem. Soc.* **1979**, *101*, 592–598.

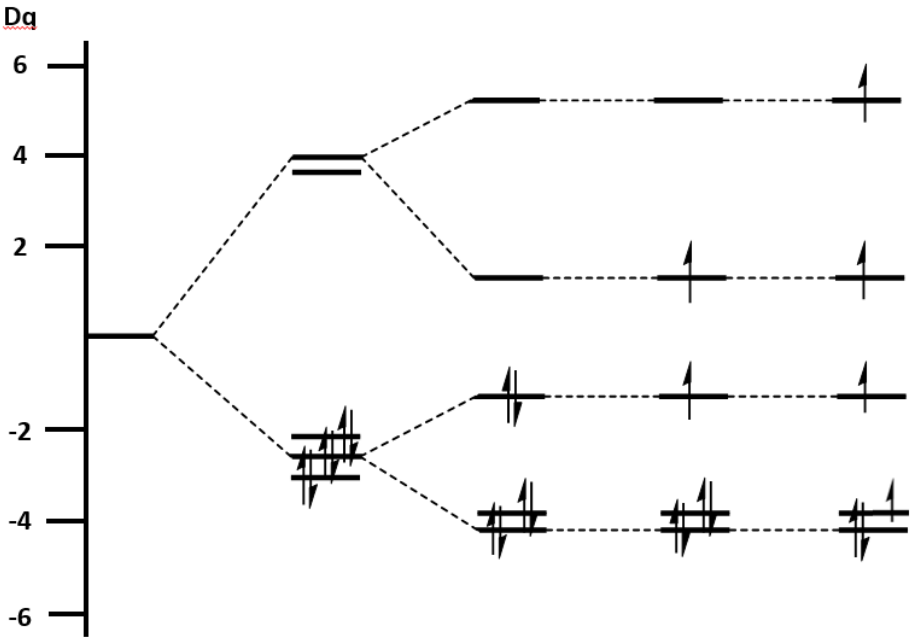

Figure 72. General representation of the molecular orbitals for complex **2** and their orbital splitting for singlet, triplet and quintuplet state.

At this point, the energy of these intermediates was calculated. As shown in Figure 73, the results are radically different. The values obtained for the energy in the states of [Fe(Cp)I(CO)] (**I2**) vary from 24.7 kcal mol^{-1} for the singlet state, to 12.7 kcal mol^{-1} for the triplet state, and finally 4.2 kcal mol^{-1} for the quintuplet state.

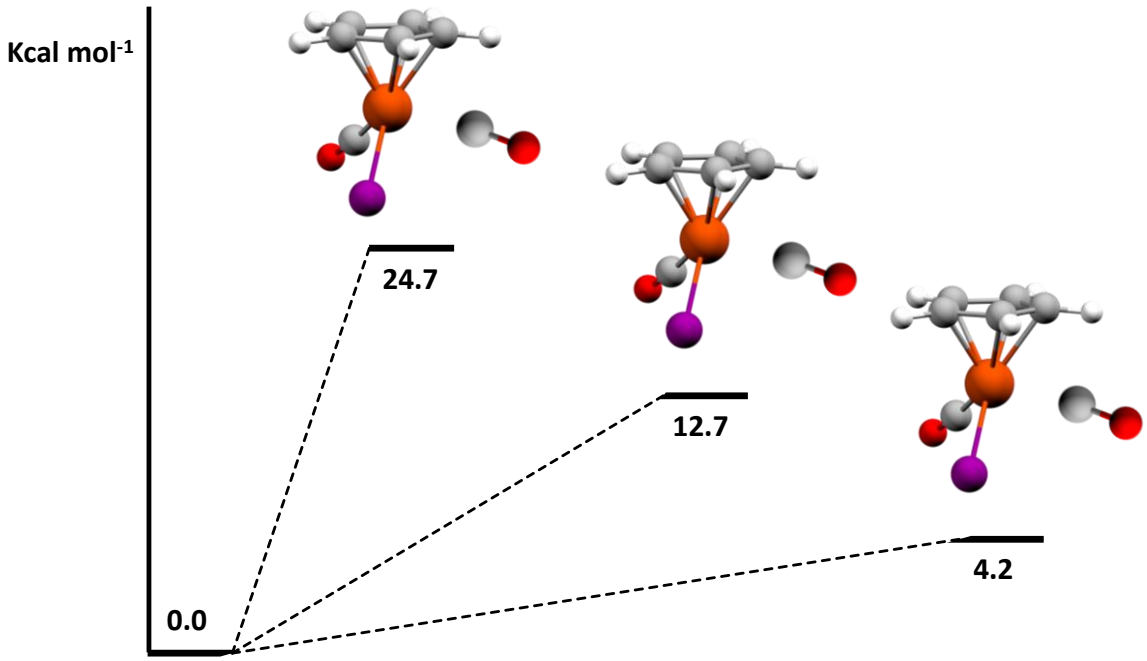

Figure 73. Energetic diagram of the different spin states of **I2.**

Because of these results, it is necessary to calculate all species to determine which parts of the energy profile go with a triplet or quintuplet state, and to find the crossovers between systems (MECP).

This reaction path would generate a first intermediate in a spin state other than singlet, through a MECP after the ligand dissociation step. These calculations are being carried out by Prof. Agustí Lledós, looking for the reaction path that makes the most chemical sense.

4.3 Summary and conclusions

In summary, the first catalytic system for the synthesis of Fe^{II} complexes of the $[Fe(Cp)(Ar^F)(CO)_2]$ type using copper as catalysts is presented. For this purpose, the C–H activation process of high fluorinated arenes in presence of base is employed. The transmetalation step is effective with bipyridine or carbene ligands, showing that the thermodynamics of the transmetalation is favorable. On the other hand, the election of the ligand is critical for the kinetic of this step.

The mechanistic study of the transmetalation reaction between the complexes [Cu(Pf)(bipy)] and $[Fe(Cp)I(CO)_2]$ shows in ^{19}F NMR a clear induction period, caused by the generation of the active species [Fe(Cp)I(CO)] by dissociation of one carbonyl group. This process is likely to lead to a concerted 4-membered transition state, where the aryl and halogen are exchanged between the Cu and Fe complexes.

It has been shown that different ways of facilitating such dissociation decrease the induction period time but do not increase the rate of transmetalation. Additionally, kinetic simulations demonstrate that an additional transmetalation between two Fe complexes to recover the carbonyl group and generate the desired product is mandatory.

On the other hand, the process has been studied by computational calculations, using DFT methods. The results show that a spin exchange could take part in the process, which allows a correct correlation between the experimental and computationally calculated energy.

4.4 Experimental section

General procedures and equipment have been described in the Experimental Section in Chapter I.

Synthesis of organoiron compounds

Stoichiometric reactions

Weighted amounts of complex [Cu(C_6F_5)(bipy)] (C_6F_5 = Pf) and [Fe(Cp)X$(CO)_2$] (1 equivalent) were added inside a screw cap NMR tube with the aid of a Schlenk NMR tube adaptor along with a flame sealed coaxial capillary containing acetone-d_6 to the lock deuterium signal. The tube was cooled to 195 K in an isopropanol and a volume of dry DMF or THF (0.5 mL) taken with a syringe was added. The tube was closed inside the adaptor and then, taken out of the cool bath, manually shaken until total dissolution of solids and transferred to the NMR probe, which had been preheated to the monitoring temperature. The kinetic profile is represented in Figure 65.

Weighted amounts of complex [Cu(C_6F_5)(bipy)] (C_6F_5 = Pf) and [Fe(Cp)I$(CO)_2$] were added inside a screw cap NMR tube with the aid of a Schlenk NMR tube adaptor along with a flame sealed coaxial capillary containing acetone-d_6 to the lock deuterium signal. Then, weighted amounts of $ONMe_3$ or [(η^5-C_5H_5)Fe$(CO)_2$]$_2$ (5 or 10%) was added. The tube was cooled to 195 K in an isopropanol and a volume of dry DMF or THF (0.5 mL) taken with a syringe was added. The tube was closed inside the adaptor and then, taken out of the cool bath, manually shaken until total dissolution of solids and transferred to the NMR probe, which had been preheated to the monitoring temperature. The kinetic profiles are represented in Figure 67.

Note that the use of blue light does not increase the reaction rate when the exposition to light is short.

General procedure for catalytic reactions

To a flame-dried screwed-capped Schlenk flask with a magnetic stirrer, CuI (4.8 mg, 2.5 x 10^{-2} mmol), 2,2'-bipyridine (6.8 mg, 3.7 x 10^{-2} mmol) the corresponding base (2.5 x 10^{-1} mmol) and [Fe(Cp)I$(CO)_2$] (2.5 x 10^{-1} mmol) were added. Then, the corresponding fluorinated arene (0.375 mmol), and dry THF (2 mL) were added to the flask. The Schlenk was stirred at 323 K for 24 hours. Then, 5 mL of non-dry THF was added. The solution was filtered through a path (2-3 cm) of silica gel to remove the salts. The results and the catalytic conditions are represented in Table 28.

[Fe(Cp)($C_6F_3Cl_2$)$(CO)_2$]

Following the general procedure for the synthesis of [Fe(Cp)($C_6F_3Cl_2$)$(CO)_2$] using $C_6F_3Cl_2H$ as arene. The aryl-iron(II) complex was obtained as a dark red microcrystalline solid after purification in silica gel (pentane as eluent). Crystals of [Fe(Cp)($C_6F_3Cl_2$)$(CO)_2$] valid for X-Ray diffraction analysis were obtained by slow diffusion of n-hexane in a solution of [Fe(Cp)($C_6F_3Cl_2$)$(CO)_2$] in CH_2Cl_2.

^{1}H NMR (499.72 MHz, Chloroform-*d*) δ 5.02 (m, 5H, Cp).

^{19}F NMR (470.17 MHz, Chloroform-*d*) δ -79.11 (s, 2F_o) -118.12 (s, 1F, F_p).

[Fe(Cp)(C_6F_5)$(CO)_2$]

Following the general procedure for the synthesis of [Fe(Cp)(C_6F_5)$(CO)_2$] using C_6F_5H as arene. The aryl-iron(II) complex was obtained as a dark orange microcrystalline solid after purification in silica gel (pentane as eluent). Characterization of [Fe(Cp)(C_6F_5)$(CO)_2$] is already reported.[200]

^{1}H NMR (499.72 MHz, Chloroform-*d*) δ 4.95 (m, 5H, Cp).

^{19}F NMR (470.17 MHz, Chloroform-*d*) δ -108.06 (m, 2F_o) -162.22 (t, 1F, F_p, J = 20 Hz), -165.15 (m, 2F, F_m).

[200] Chukwu, R.,Hunter, A. D.,Santarsiero, B. D.,Bott, S. G.,Atwood, J. L., Chassaignac, J. Organometallic complexes with electron bridges. Electrochemical, spectroscopic, and structural studies of mono- and bimetallic complexes of iron: x-ray crystal structures of $CpFe(CO)_2$-C_6F_5, 4-$CpFe(CO)_2$-C_5F_4N, and 1,4-$C_6F_4(CpFe(CO)_2)_2$. *Organometallics* **1992**, *11*, 589–597. DOI: 10.1021/om00038a015

[Fe(Cp)(C_5F_4N)$(CO)_2$]

Following the general procedure for the synthesis of [Fe(Cp)(C_5F_4N)$(CO)_2$] using C_6F_4NH as arene. The aryl-iron(II) complex was obtained as a dark orange microcrystalline solid after purification in silica gel (pentane as eluent). Characterization of [Fe(Cp)(C_5F_4N)$(CO)_2$] is already reported.[200] Crystals of [Fe(Cp)($C_6F_3Cl_2$)$(CO)_2$] valid for X-Ray diffraction analysis were obtained by slow diffusion of n-hexane in a solution of [Fe(Cp)(C_5F_4N)$(CO)_2$] in CH_2Cl_2.

^{1}H NMR (499.72 MHz, Chloroform-*d*) δ 4.97 (m, 5H, Cp).

^{19}F NMR (470.17 MHz, Chloroform-*d*) δ -98.36 (m, $2F_o$) -113.26 (m, 2F, F_m).

[Fe(Cp)($C_7H_3F_4O$)$(CO)_2$]

Following the general procedure for the synthesis of [Fe(Cp)($C_7H_3F_4O$)$(CO)_2$] using $C_7H_4F_4O$ as arene. The aryl-iron(II) complex was obtained as a dark red solid after purification in silica gel (pentane as eluent).

^{1}H NMR (499.72 MHz, Chloroform-*d*) δ 4.93 (s, 5H, Cp), 4.61 (s, 3H, OCH_3).

^{19}F NMR (470.17 MHz, Chloroform-*d*) δ -99.41 (m, $2F_o$) -114.12 (m, 2F, F_m).

Kinetic experiments

Weighted amounts of complex [Cu(C_6F_5)(bipy)] (C_6F_5 = Pf) (5.5 x 10^{-3} mmol) and [Fe(Cp)I($CO)_2$] (5.5 x 10^{-3} mmol, 1 equivalent) were added inside a screw cap NMR tube with the aid of a Schlenk NMR tube adaptor along with a flame sealed coaxial capillary containing acetone-d_6 to the lock deuterium signal. The tube was cooled to 195 K in an isopropanol and a volume of dry DMF (0.50 mL) taken with a syringe was added. The tube was closed inside the adaptor and then, taken out of the cool bath, manually shaken until total dissolution of solids, and transferred to the NMR probe, which had been preheated to 298 K. The kinetic monitoring was represented in Figure 65 and 67.

The kinetic rate constants were obtained by non-linear minimum square fitting of the experimental data points to kinetic models, with the aid of the software COPASI, as we can see in Scheme 24. For this experiment, the following kinetic model was used without any restriction.

Due to the bad results in the fitting between experimental data and the correlation with this simulation, no more investigation was carried out with this kinetic model. The additional information about the mechanism allowed us to add a new reaction in the kinetic model, showed in Figure 69 and 70.

Due to the good correlation between experimental data and the kinetic simulation, the next information about the kinetic constants and their corresponding standard deviation can be obtained.

For this correlation, the following kinetic model was used without any restriction or approximation, represented in Figure 69.

	'(Disociacion).k1'	'(Disociacion).k2'	'(Retrotransm).k1'	'(Retrotransm).k2'	'(Transmetalacion...	'(CO back).k1'	'(CO back).k2'
'(Disociacion).k1'	1	0.229467	0.478344	-0.0232123	-0.793295	0.271275	0.985063
'(Disociacion).k2'	0.229467	1	0.247677	-0.234072	-0.30395	0.136895	0.310142
'(Retrotransm).k1'	0.478344	0.247677	1	-0.0215698	-0.912007	0.810379	0.471896
'(Retrotransm).k2'	-0.0232123	-0.234072	-0.0215698	1	0.0288668	0.0101663	-0.0326395
'(Transmetalacion).k1'	-0.793295	-0.30395	-0.912007	0.0288668	1	-0.704722	-0.791254
'(CO back).k1'	0.271275	0.136895	0.810379	0.0101663	-0.704722	1	0.332489
'(CO back).k2'	0.985063	0.310142	0.471896	-0.0326395	-0.791254	0.332489	1

Figure 74. Correlation between kinetic constants of the proposed kinetic model of Figure 69.

Computational section

Theoretical calculations were performed at DFT level of theory using Gaussian16 software. The structures of all the intermediates and transition states were optimized in tetrahydrofuran solvent (DMF, ε= 37.219) with the SMD continuum model using the B3LYP functional combined with the Grimme's D3 correction for dispersion. Basis set BS1 was used for the optimizations. BS1 includes the 6-31G(d,p) basis set for the main group elements, excluding iodine, and the scalar relativistic Stuttgart-Dresden SDD pseudopotential and its associated double-ζ basis set, complemented with a set of polarization functions, for the copper (*f* polarization functions) and iodine (*d* polarization functions) atoms. Frequency calculations were carried out for all the optimized geometries in order to characterize the stationary points as either minima or transition states following the same criteria of the other chapters in this doctoral thesis.

Although the overall energy value of the energy profile is close to that seen experimentally, values lower than 26.3 kcal mol^{-1} could not be obtained for the intermediate after ligand dissociation in the singlet state. Therefore, we continued with the investigation in other spin states. Although the energy decreases with increasing spin state for this intermediate, the energy of the crossover points (MECP) must also be considered. This research is being carried out in collaboration with Prof. Agustí Lledos during the writing of this doctoral thesis

CHAPTER V: Study of the transmetalation step between Group 11 and *trans*-[PdCl(Rf)($AsPh_3$)$_2$]

5.1 Introduction

The transmetalation step

The C–C cross-coupling reactions are one of the most important bond formation methodologies nowadays.[201,202] In case of the organometallic catalysis, these reactions consist of two main reagents: an organic electrophile (R–X) and an organometallic nucleophile (R'–M). Traditionally, palladium organometallic complexes are one of the most powerful catalysts to carry out this transformation.[203,204] As a result of their relevance in organic synthesis, the 2010 Nobel Prize was awarded to the important contribution of Professor Richard F. Heck, Professor Eichi Negishi and Professor Akira Suzuki to the development and study of palladium catalysed C–C cross-coupling reactions.

Apart from this well-known cross-coupling reactions, some important transformations must be mentioned. The Sonogashira coupling,[205,206] that involves a C(sp)–C formation or the Stille reaction,[207,208] that use an organotin reagent as electrophile, are two of the most important cross-coupling reactions for the C–C bond formation in this category.

These reactions are generally proposed in a simplify mechanism that involves 3 elementary steps.

I) *Oxidative addition.* This reaction modifies the electronic of the metal center by the addition of the organic electrophile.

---

[201] Pérez Sestelo, J.; Sarandeses, L. A. Advances in Cross-Coupling Reactions. *Molecules* **2020**, *25*, 23–26. DOI: 10.3390/molecules25194500.

[202] Campeau, L. C.; Hazari, N. Cross-Coupling and Related Reactions: Connecting Past Success to the Development of New Reactions for the Future. *Organometallics* **2019**, *38*, 3–35. DOI: 10.1021/acs.organomet.8b00720.

[203] Biffis, A.; Centomo, P.; Del Zotto, A.; Zecca, M. Pd Metal Catalysts for Cross-Couplings and Related Reactions in the 21st Century: A Critical Review. *Chem. Rev.* **2018**, *118*, 2249–2295. DOI: 10.1021/acs.chemrev.7b00443.

[204] Jana, R.; Pathak, T. P.; Sigman, M. S. Advances in Transition Metal (Pd,Ni,Fe)-Catalyzed Cross-Coupling Reactions Using Alkyl-Organometallics as Reaction Partners. *Chem. Rev.* **2011**, *111*, 1417–1492. DOI: 10.1021/cr100327p.

[205] Wu, Y.; Huo, X.; Zhang, W. Synergistic Pd/Cu Catalysis in Organic Synthesis. *Eur. J. Chem.* **2020**, *26*, 4895–4916. DOI: 10.1002/chem.201904495.

[206] Chinchilla, R.; Nájera, C. N. Recent Advances in Sonogashira Reactions*: Chem. Soc. Rev.* **2011**, *12*, 5084–5121. DOI: 10.1039/c1cs15071e.

[207] Cordovilla, C.; Bartolomé, C.; Martínez-Ilarduya, J. M.; Espinet, P. The Stille Reaction, 38 Years Later. *ACS Catal.* **2015**, *5*, 3040–3053. DOI: 10.1021/acscatal.5b00448.

[208] Espinet, P.; Echavarren, A. M. The Mechanisms of the Stille Reaction. *Angew. Chem. Int. Ed.* **2004**, *43*, 4704–4734. DOI: 10.1002/anie.200300638.

II) *Transmetalation.* The organic moiety is transferred from an organometallic nucleophile to the metal center, replacing the halide/pseudo halide.

III) *Reductive elimination.* This step generates the new organic molecule and regenerate the palladium catalyst in low oxidation state.

Interestingly, from a mechanistic point of view, two of these steps (oxidative addition and reductive elimination) have been deeply studied.[209] However, delving into the mechanism, we see that there are some reactions that have not been taken into account in simplified versions of the catalytic cycles, as is the case of the transmetalation induced isomerization process.[210] The oxidative addition and transmetalation steps can result in the *cis* and *trans* arrangements of Pd^{II} complexes. In addition, the transmetalation step can maintain or exchange the geometry of the square-planar complex. Furthermore, reductive elimination process can only be carried out from the *cis* arrangement.[209] This implies that an isomerization process is necessary prior to reductive elimination if the transmetalation step places the complex in a *trans* arrangement. That is why the transmetalation takes an important role within the catalytic cycle, which can lead to improved catalytic reactions and thus obtain more quickly, and in better yield the desired products.

Mechanism of the transmetalation step in Pd^{II} complexes.

Traditionally, the transmetalation reaction on square-planar complexes of $16e^-$ has been proposed as a process that required a ligand substitution,[207,208,210] employing the following associative pathway,[211,212] represented in Scheme 25:

---

[209] Gioria, E.; del Pozo, J.; Martínez-Ilarduya, J. M.; Espinet, P. Promoting Difficult Carbon–Carbon Couplings: Which Ligand Does Best? *Angew. Chem. Int. Ed.* **2016**, *55*, 13276–13280. DOI: 10.1002/ANIE.201607089.

[210] Del Pozo, J.; Salas, G.; Álvarez, R.; Casares, J. A.; Espinet, P. The Negishi Catalysis: Full Study of the Complications in the Transmetalation Step and Consequences for the Coupling Products. *Organometallics* **2016**, *35*, 3604–3611. DOI: 10.1021/acs.organomet.6b00660.

[211] Osakada, K. *Fundamentals of Molecular Catalysis; Current Methods in Inorganic Chemistry*, **2003**, Elsevier: Amsterdam, Chapter 5, Transmetalation.

[212] A) Hirner, J. J.; Shi, Y.; Blum, S. A. Organogold Reactivity with Palladium, Nickel, and Rhodium: Transmetalation, Cross-Coupling, and Dual Catalysis. *Acc. Chem. Res.* **2011**, *44*, 603–613. DOI: 10.1021/ar200055y. b) Lennox, A. J. J.; Lloyd-Jones, G. C. Transmetalation in the Suzuki-Miyaura Coupling: The Fork in the Trail. *Angew. Chem. Int. Ed*, **2013**, *52*, 7362–7370. DOI: 10.1002/anie.201301737.c) Martínez de Salinas, S.; Mudarra, Á. L.; Benet-Buchholz, J.; Parella, T.; Maseras, F.; Pérez-Temprano, M. H. New Vistas in Transmetalation with Discrete "AgCF3" Species: Implications in Pd-Mediated Trifluoromethylation Reactions. *Eur. J. Chem.* **2018**, *24*, 11895–11898. DOI: 10.1002/chem.201802586. d) Pérez-Temprano, M. H.; Nova, A.;

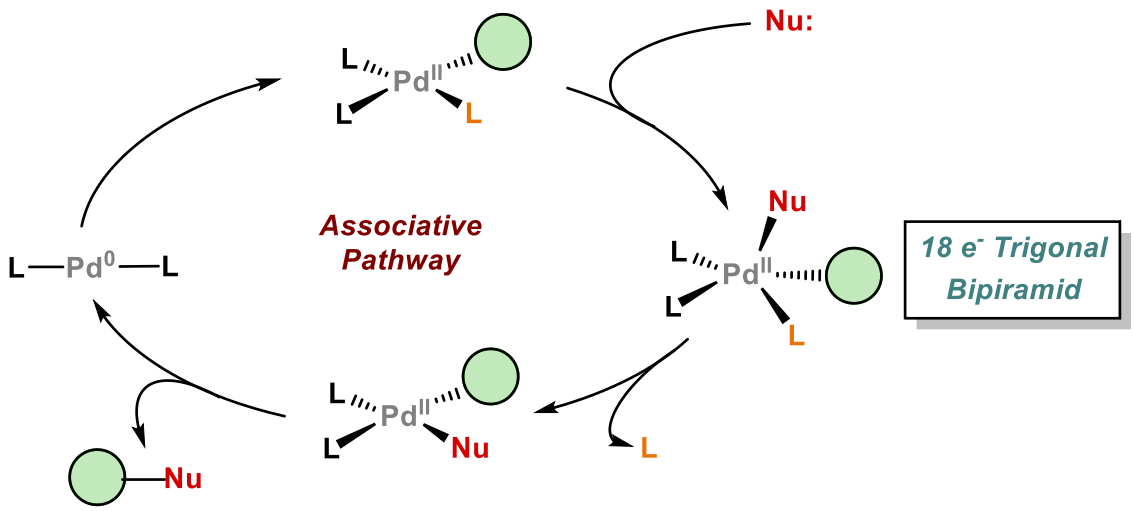

Scheme 25. Mechanism pathway of the ligand substitution in Pd^{II} complexes.

The associative pathway involves the formation of a pentacoordinate 18e⁻ complex, usually in the transition state (Scheme 25), and the position where the ligand will be substituted is determined by the ligand with the highest *trans effect*, which will determine the lowest activation free energy-(kinetic effect). In addition, different factors govern the transmetalation process. If we pay attention to thermodynamics, the breaking of bonds and the formation of new ones are the processes that sets the value of the free energy of the reaction, as we can see in Scheme 26.

Casares, J. A.; Espinet, P. Observation of a Hidden Intermediate in the Stille Reaction. Study of the Reversal of the Transmetalation Step. *J. Am. Chem. Soc.* **2008**, *130*, 10518–10520. DOI: 10.1021/ja802994v. e) Ricci, A.; Angelucci, F.; Bassetti, M.; Lo Sterzo, C. Mechanism of the Palladium-Catalyzed Metal-Carbon Bond Formation. A Dual Pathway for the Transmetalation Step. *J. Am. Chem. Soc.* **2002**, *124*, 1060–1071. DOI: 10.1021/ja011644p. f) Hansmann, M. M.; Pernpointner, M.; Döpp, R.; Hashmi, A. S. K. A Theoretical DFT-Based and Experimental Study of the Transmetalation Step in Au/Pd-Mediated Cross-Coupling Reactions. *Eur. J. Chem.* **2013**, *19*, 15290–15303. DOI: 10.1002/CHEM.201301840. G) Meana, I.; Espinet, P.; Albéniz, A. C. Heterometallic Complexes by Transmetalation of Alkynyl Groups from Copper or Silver to Allyl Palladium Complexes: Demetalation Studies and Alkynyl Homocoupling. *Organometallics* **2014**, *33*, 1–7. DOI: 10.1021/om4005498. H) García-Melchor, M.; Fuentes, B.; Lledós, A.; Casares, J. A.; Ujaque, G.; Espinet, P. Cationic Intermediates in the Pd-Catalyzed Negishi Coupling. Kinetic and Density Functional Theory Study of Alternative Transmetalation Pathways in the Me-Me Coupling of $ZnMe_2$ and trans-$[PdMeCl(PMePh_2)_2]$. *J. Am. Chem. Soc.* **2011**, *133*, 13519–13526. DOI: 10.1021/ja204256x. i) Mateo, C.; Ferná Ndez-Rivas, C.; Echavarren, A. M.; Cá, D. J. Isolation of the Transmetalation Step in the Hiyama Cross-Coupling Reaction of Organosilanes. *Organometallics* **1997**, 16, 1997–1999. DOI: 10.1021/om970085l. J) Amatore, C.; Grimaud, L.; Le Duc, G.; Jutand, A. Three Roles for the Fluoride Ion in Palladium-Catalyzed Hiyama Reactions: Transmetalation of $[ArPdFL_2]$ by $Ar'Si(OR)_3$. *Angew. Chem. Int. Ed.* **2014**, *53*, 6982–6985. DOI: 10.1002/ANIE.201400956. K) Casares, J. A.; Espinet, P.; Fuentes, B.; Salas, G. Insights into the Mechanism of the Negishi Reaction: ZnRX versus ZnR_2 Reagents. *J. Am. Chem. Soc.* **2007**, 129, 3508–3509. DOI: 10.1021/ja070235b.

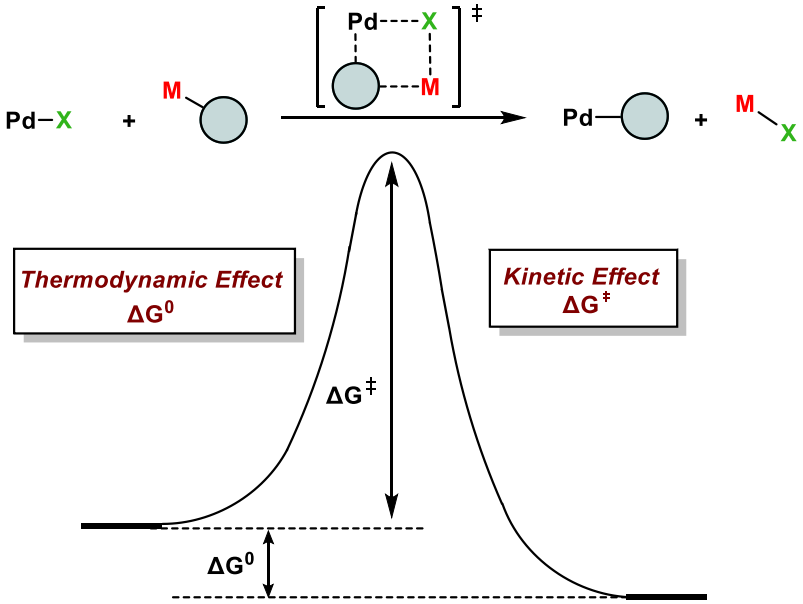

Scheme 26. Potential energy surface of the transmetalation step.

As a result, strong M–C bonds will difficult the transmetalation step whereas highly stable M–X compounds will play in favour of the process, as we saw in Chapter I.

Furthermore, if we focus on the kinetics of the reaction, we can find several factors capable of modifying the energy of the transition state involved in the transmetalation step, and thus the rate of the reaction. One of the most important factors is the steric effect of the M–R group that is transmetalated to the Pd complex. Depending on the volume of the molecule that must approach to the metal center, the rate of transmetalation will be different, as well as the electronic effects of the transition state produced by the ligands.

On the other hand, the M–Pd interactions that can be generated in this transition state are crucial for understanding the behaviour and nature of the transmetalation process.[210,213,214,215,216] There are strong evidences of the existence of metal-metal

[213] Oeschger, R. J.; Chen, P. Structure and Gas-Phase Thermochemistry of a Pd/Cu Complex: Studies on a Model for Transmetalation Transition States. *J. Am. Chem. Soc.* **2017**, *139*, 1069–1072. DOI: 10.1021/jacs.6b12152.
[214] Moret, M. E.; Chen, P. Interaction of Organoplatinum(II) Complexes with Monovalent Coinage Metal Triflates. *J. Am. Chem. Soc.* **2009**, *131*, 5675–5690. DOI: 10.1021/ja900449y.
[215] Oeschger, R. J.; Bissig, R.; Chen, P. Model Compounds for Intermediates and Transition States in Sonogashira and Negishi Coupling: d^8-d^{10} Bonds in Large Heterobimetallic Complexes Are Weaker than Computational Chemistry Predicts. *J. Am. Chem. Soc.* **2022**, *144*, 10330–10343. DOI: 10.1021/jacs.2c01641.
[216] Oeschger, R. J.; Ringger, D. H.; Chen, P. Gas-Phase Investigations on the Transmetalation Step in Sonogashira Reactions. *Organometallics* **2015**, *34*, 3888–3892. DOI: 10.1021/acs.organomet.5b00491.

interactions that might contribute to hold the two metals in close proximity when d^{10} organometallics are involved, by a labile d^8-d^{10} metallophilic bond, reported for several M–Pd systems, such us Zn–Pd (Negishi Coupling), Au–Pd, Ag–Pd or Cu–Pd (Sonogashira Coupling).[214,215,216] All of this studies demonstrated the importance of evaluate the M–Pd interactions, especially in the transition state, to understand the behaviour of the transmetalation step.

There are a lot of examples in which abnormally short distances between metals are observed, both in the ground state of several bimetallic complexes and in transition states of transmetalation steps.[217] These interactions range from very weak forces to moderate forces that are in the order of the strongest hydrogen bonds. These interactions have been studied in the last decade to have implications in the transmetalation step by the group of Chen. In fact, d^8-d^{10} interactions have been found in a variety of compounds between Pd and with Cu, Ag and Au.[205,218]
Due to the synergy between group 11 metals and Pd, it is not by chance that they have been used in most bimetallic systems. That is why we can find many works on Pd/Cu, Pd/Ag or Pd/Au bimetallic catalysis, but few mechanistic works focusing on the transmetalation step.

Among the studies that combine experimental data with theoretical calculations, where the transmetalation process is analysed, we find the work of Gooβen and co-workers, which we have already mentioned throughout this doctoral thesis in Chapters I and III. The results obtained in the decarboxylative C–C coupling using copper salts and a Pd complex was analysed by DFT calculations. The study shows how the decarboxylation step occurs in the Cu complex, with a $\Delta G_{solv} \approx 30$ kcal mol^{-1}. The [Cu(Ar)(Phen)] complex transmetalates the aryl moiety to the Pd^{II} complex, which will carry out the reductive elimination step, giving the desired biaryl.

Within the transmetalation step, it is important to highlight some aspects: no evidence of Cu–Pd interactions has been found during this step. The adduct formed

[217] Peñas-Defrutos, M. N.; Bartolomé, C.; García-Melchor, M.; Espinet, P. Rh I Ar/Au I Ar′ Transmetalation: A Case of Group Exchange Pivoting on the Formation of M–M′ Bonds through Oxidative Insertion. *Angew. Chem. Int. Ed.* **2019**, *131*, 3539–3543. DOI: 10.1002/ange.201813419.
[218] Wu, X.; Chen, D. G.; Liu, D.; Liu, S. H.; Shen, S. W.; Wu, C. I.; Xie, G.; Zhou, J.; Huang, Z. X.; Huang, C. Y.; Su, S. J.; Zhu, W.; Chou, P. T. Highly Emissive Dinuclear Platinum(III) Complexes. *J. Am. Chem. Soc.* **2020**, *142*, 7469–7479. DOI: 10.1021/jacs.9b13956.

prior to transmetalation process has a Cu–X–Pd bond, which is in contradiction with the data obtained by Chen and co-workers some years later.

So, what governs the process of transmetalation? Is it a kinetic problem, a thermodynamic problem or both? Are there really M–M' interactions in d^8-d^{10} configurations? Can we effectively predict these interactions to have a positive impact on the efficiency of a catalytic cycle?

The transmetalation step in Pd/Cu systems.

The C–C bonds formation using Pd/Cu catalytic systems is nowadays one of the most widely used due to its great versatility and efficiency.[201,219,220,221] Numerous research studies have demonstrated the great synergy between these two metals,[222,223,224] which over the years has allowed carried out complex synthetic reactions.[225,226]

Thus, the most studied reaction mechanism within the Pd/Cu synergy is the Sonogashira reaction.[206] From a mechanistic point of view, studies of transmetalation in Pd/Cu systems have focused on reactions in which the thermodynamic component is more favourable, *i.e.* in which the copper complex transmetalates an organic moiety (Cu–C bond) to a palladium complex with a halogen or pseudohalogen (Pd–X bond), forming a Pd–C bond and a Cu–X bond.

---

[219] Kazuhiko S.; Yoshiaki N. Cross Coupling Reactions by Cooperative Metal Catalysis. *J. Synth. Org. Chem., Jpn.* **2017**, *75*, 1133–1140. DOI: 10.5059/yukigoseikyokaishi.75.1133

[220] Semba, K.; Nakao, Y. Cross-Coupling Reactions by Cooperative Pd/Cu or Ni/Cu Catalysis Based on the Catalytic Generation of Organocopper Nucleophiles. *Tetrahedron* **2019**, *75*, 709–719. DOI: 10.1016/J.TET.2018.12.013.

[221] Oi, M.; Takita, R.; Kanazawa, J.; Muranaka, A.; Wang, C.; Uchiyama, M. Organocopper Cross-Coupling Reaction for C-C Bond Formation on Highly Sterically Hindered Structures. *Chem. Sci*., **2019**, *10*, 6107-6112. DOI: 10.1039/c9sc00891h.

[222] Rivada-Wheelaghan, O.; Comas-Vives, A.; Fayzullin, R. R.; Lledós, A.; Khusnutdinova, J. R. Dynamic PdII/CuI Multimetallic Assemblies as Molecular Models to Study Metal–Metal Cooperation in Sonogashira Coupling. *Eur. J. Chem.* **2020**, *26*, 12168–12179. DOI: 10.1002/CHEM.202002013.

[223] Ullah, Z.; Thomas, R. Markovnikov versus Anti-Markovnikov Addition and C–H Activation: Pd–Cu Synergistic Catalysis. *Appl. Organomet. Chem.* **2021**, *35*. DOI: 10.1002/AOC.6077.

[224] Bin-Kim, U.; Jung Jung, D.; Ji Jeon, H.; Rathwell, K.; Lee, S. Synergistic Dual Transition Metal Catalysis. *Chem. Rev*. **2020**, 120, 13382–13433. DOI: 10.1021/acs.chemrev.0c00245.

[225] Meana, I.; Espinet, P.; Albéniz, A. C. Heterometallic Complexes by Transmetalation of Alkynyl Groups from Copper or Silver to Allyl Palladium Complexes: Demetalation Studies and Alkynyl Homocoupling. *Organometallics* **2014**, *33*, 1–7 **2013**. DOI: 10.1021/om4005498.

[226] Zhou, C.; Dong, Y.; Yu, J.-T.; Sun, S.; Cheng, J.; Li, R.; Palladium/Copper-Catalyzed Multicomponent Reactions of Propargylic Amides, Halohydrocarbons and CO_2 toward Functionalized Oxazolidine-2,4-Diones. *Chem. Commun.* **2019**, *55*, 13685–13688. DOI: 10.1039/c9cc07027c.

However, there are also some studies where there are no halogens in the organometallic complexes, and the aryl scrambling is studied in Pd/Cu system.[227]

One of the first comprehensive mechanistic papers to be published was the mechanism of Cu/Pd catalysed decarboxylative cross-couplings, published by Gooβen in 2014, which shows a detailed overview of all steps, calculated by DFT and supported by previous experimental results.[228] The explicitly analysis of the transmetalation step, between the [Cu(Ar)(Phen)] and $[PdBr_2(Ar)(PMe_3)]^-$ complexes was commented (Figure 75). The first peculiarity found is that no energetically favourable interaction was found between the complexes, *e.g.*, when approaching the palladium and the π-system of the fluorophenyl ring, bringing palladium complex $[PdBr_2(Ar)(PMe_3)]^-$ into close proximity to the copper atom in [Cu(Ar)(Phen)] whereas bromine ligand results in the formation of a stable adduct (**I1**), as we can observe in Figure 75.

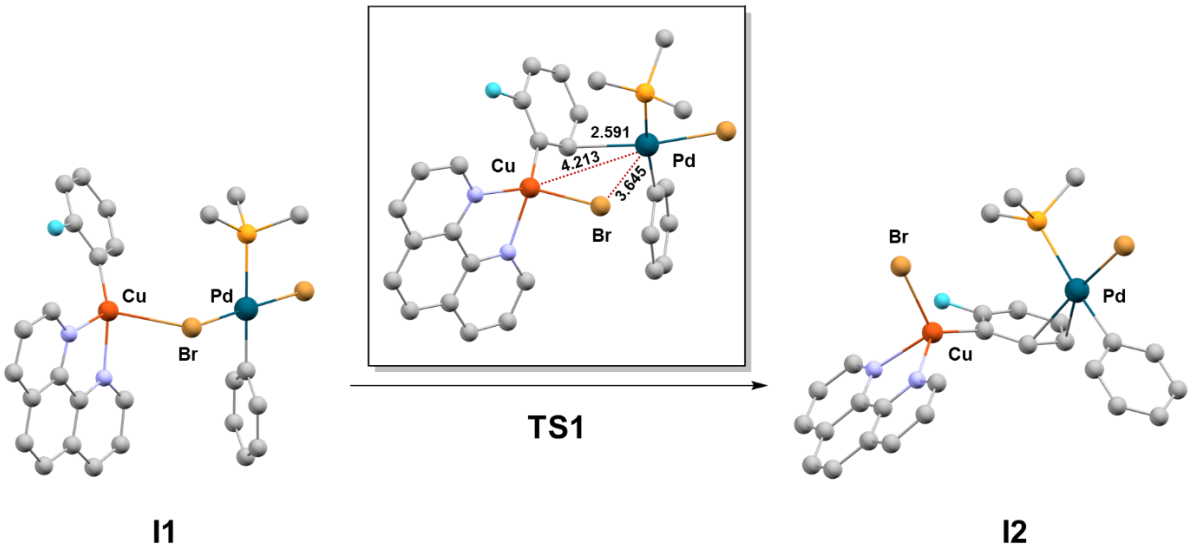

Figure 75. DFT calculations of the transmetalation step. Distances in Å.

The Cu–Br bond formation (2.82 Å) makes this step energetically favourable (ΔE_{tot} = −2.6 kcal mol^{-1}), which compensates the entropic hindrance and loss solvation energy associated with the formation of a bimolecular adduct. This adduct

[227] Pérez-Iglesias, M.; Lozano-Lavilla, O.; Casares, J. A.: An Extremely Efficient Catalyst for the Aryl Scrambling between Palladium Complexes. *Organometallics* **2019**, *38*, 739–742. DOI: 10.1021/acs.organomet.8b00885.
[228] Fromm, A.; van Wüllen, C.; Hackenberger, D.; Gooßen, L. J. Mechanism of Cu/Pd-Catalyzed Decarboxylative Cross-Couplings: A DFT Investigation. *J. Am. Chem. Soc.* **2014**, *136*, 10007–10023. DOI: 10.1021/JA503295X.

was the entry structure to a transmetalation reaction pathway in which the bromine halogen is transferred from the palladium complex $[PdBr_2(Ar)(PMe_3)]^-$ to [Cu(Ar)(Phen)] prior to transfer of the fluorophenyl group. The alternative transmetalation pathways was examined and no optimal results was obtained.

This adduct thus allows the transfer of Br halogen to the copper metal center, forming a pseudo tetrahedral complex via a moderate-energy transition state (19 kcal mol^{-1}). In addition, an interaction between the Pd atom and a carbon of the Ar group of the copper complex was observed. This transition state leads to a high energy intermediate where a clear π-interaction between the aryl and the Pd complex was considered. The evolution of this intermediate results in a transition state (**TS2**) of transfer from the Ar group to the Pd complex, which finally ends in another adduct between the palladium and the copper complexes, ending the transmetalation process, represented in Figure 76.

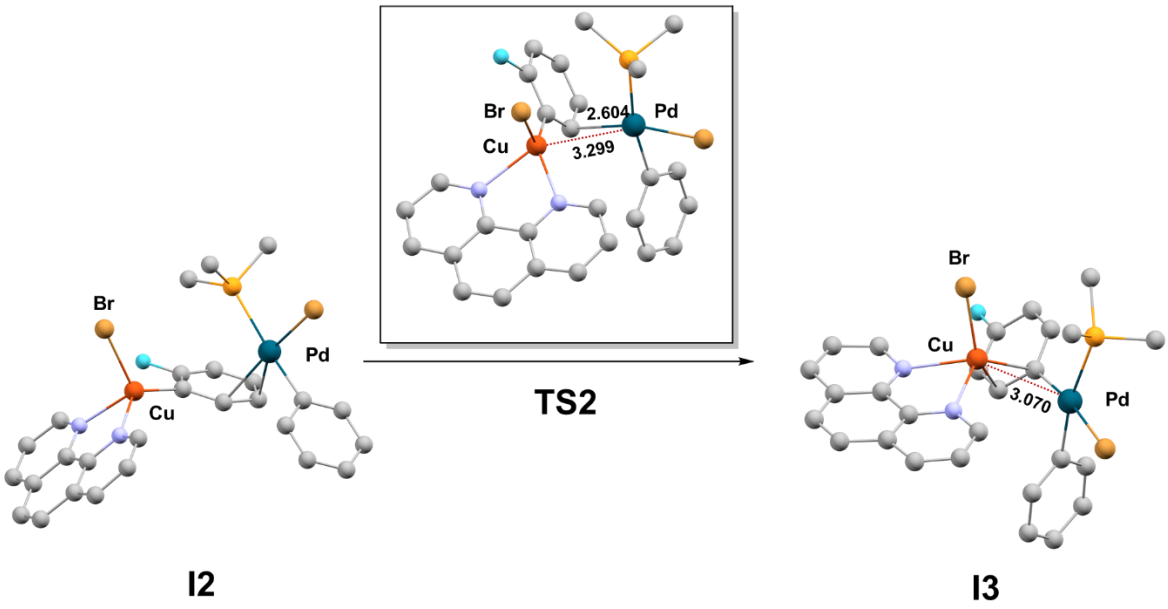

Figure 76. DFT calculations of the evolution of the transmetalation step. Distances in Å.

Some important conclusions can be drawn from this study:

1) As previously stated, it has not been possible to demonstrate the existence of metal-metal interactions in the transmetalation process, but authors suggest that attractive interaction between two metals play a role in the transmetalation step.

2) It is an irreversible process due to the high energy stabilization of the products with respect to the reactants (thermodynamic component).

3) It is a multistep reaction. The authors have not been possible to find an alternative reaction pathway in which the halogen and the organic moiety were transferred in the same transition state. The transfer of the Ar group and the halogen are the highest energy barrier processes (kinetic component). Moreover, this transmetalation process can be carried out in one or in several steps, the organic moiety and the halogen do not necessarily have to be simultaneously transferred. This behaviour can modify the reaction rate of the reaction.

Peter Chen and co-workers published in 2015, a gas-phase investigations on the transmetalation step in Sonogashira reactions, as we can see in Figure 77. In this study they prepared a bimetallic intermediate that hat is considered as a hypothetical intermediate in such reactions.

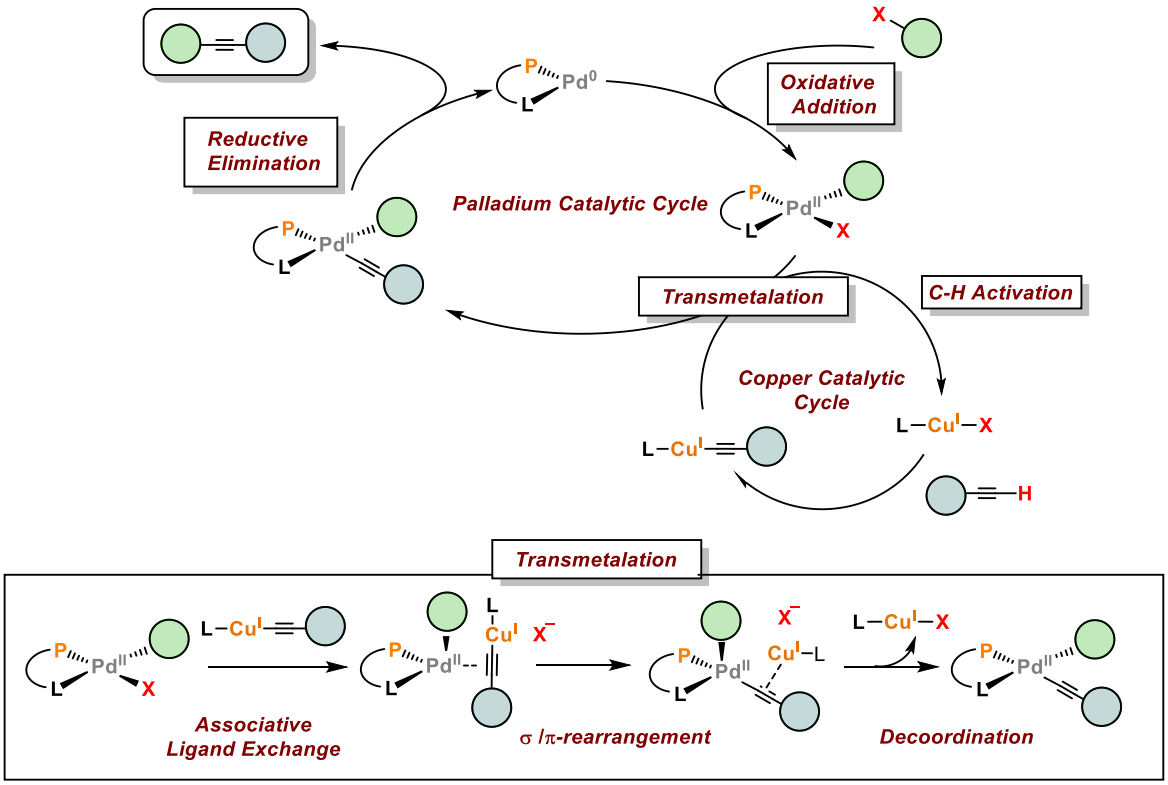

Figure 77. Classical Sonogashira catalytic-cycle and a mechanistic proposal of the transmetalation step.

This complex has been prepared with Cu, Ag and Au, and the optimized intermediates showed strong heterobimetallic bonding interactions, which appear to be responsible for the overall low rearrangement barriers. DFT studies of the transmetalation step in the Sonogashira reaction suggested that the reaction starts from a Cu acetylide with Pd coordinated to the π bond and goes through a transition state with a close Pd^{II}–Cu^{I} contact and a trigonal ipso carbon to a Pd acetylide with Cu coordinated to the triple bond. This result is absolutely different from that obtained by Gooβen et al. where the mechanistic approach shows that there is no interaction between the two metals and shows clear contradictions between the two processes.

This feature might be applicable to other bimetallic transition-metal-catalysed reactions involving a transmetalation step and potentially gives access to more efficient catalysts.

Two years later, in 2017, they reported the first the first crystal structure of a bimetallic complex with a Pd^{II}–Cu^{I} d^8–d^{10} bond.[213,215,216] The measured crystal structure (Figure 78) shows a short Pd^{II}–Cu^{I} distance of only 2.55 Å, which is significantly shorter than the sum of the covalent radii (2.71 Å).[229]

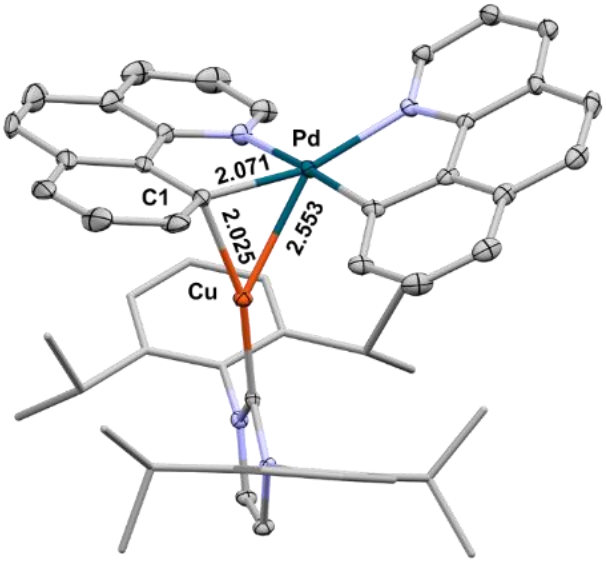

Figure 78. X-ray diffraction of the Pd-Cu bimetallic complex. Distances in Å. Cif obtained from Ref 213.

[229]Cordero, B.; Gómez, V.; Platero-Prats, A. E.; Revés, M.; Echeverría, J.; Cremades, E.; Barragán, F.; Alvarez, S. Covalent Radii Revisited. *Dalton Trans.* **2008**, *21*, 2832–2838. DOI: 10.1039/b801115j.

They proposed that the concept of transmetalation steps being facilitated by metal–metal interactions might be applicable to other bimetallic reactions, and a detailed knowledge about these interactions can potentially lead to the development of more efficient catalytic reactions and more specific mechanistic studies.

In 2019, Uchiyama and co-workers published an organocopper cross-coupling reaction for C–C bond formation on highly sterically hindered structures.[230] This work combines experimental results with an exhaustive computational analysis for the formation of large organic molecules, where the copper complex transfers a bulky organic group. With respect to previous Gooβen's work, there are some differences. The computational work (studied by *Natural Bond Orbital* analysis) concludes that the unique ability of copper to facilitate efficient transmetalation via a compact transition state arising from an efficient metal–metal interaction is the key to the success of this reaction. In addition, in this reaction the transmetalation step occurs in only one step. The halogen and the organic moiety is transferred in the same transition state, represented in Figure 79 with the NBO analysis.

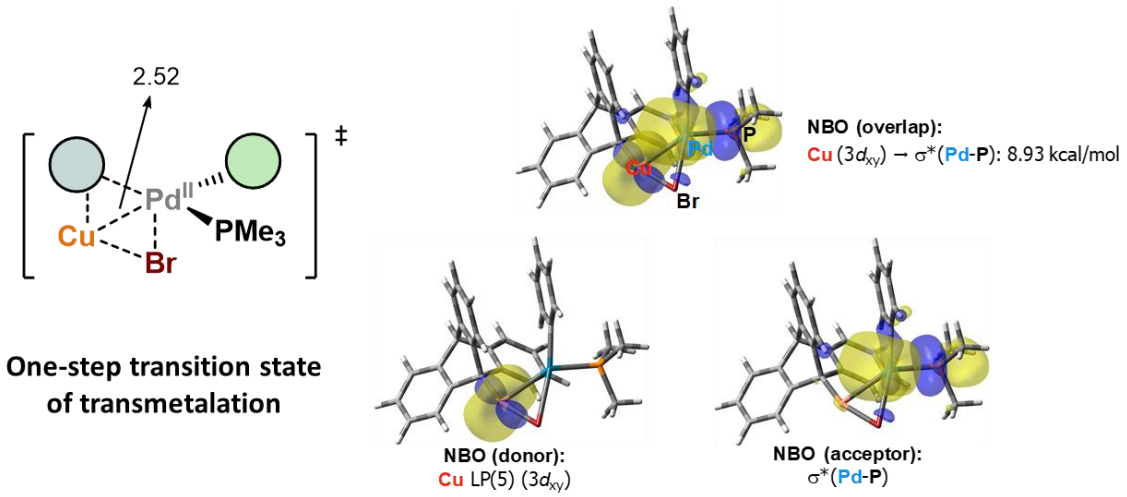

Figure 79. Transmetalation Transition State (distances in Å) NBO analysis from the TS. Figure of the NBO analysis obtained from ref. 230.

[230] Oi, M.; Takita, R.; Kanazawa, J.; Muranaka, A.; Wang, C.; Uchiyama, M. Organocopper Cross-Coupling Reaction for C-C Bond Formation on Highly Sterically Hindered Structures *Chem. Sci.* **2019**, *10*, 6107–6112. DOI: 10.1039/c9sc00891h.

Based on these studies, we can conclude that metal-metal interactions are apparently necessary for transmetalation processes in Pd/Cu processes.

Furthermore, when this interaction is proposed, is frequently assigned to be the key of the transmetalation process.

On the contrary, results obtained by DFT where metal-metal interactions are evaluated suggest that the computed metal-metal interaction overestimates the bond strength, which correspondingly distorts the computed potential energy surface for transmetalation.[215] This work by Chen and co-workers presents different complexes with M−Pd bonds or interactions (M = Au, Ag, Cu) that they propose as possible transmetalation intermediates or transition states in Sonogashira and Negishi reactions. In some cases, in this type of reactions, the transmetalation step is proposed as the rate limiting stage of the catalytic process, often obtaining the values by DFT calculations. In this research, the authors isolate different compounds with these characteristics, and study by experimental techniques and DFT calculations the bond strength or M−M' interaction and observe that the experimental values differ quite a lot from those obtained by DFT calculations. For this reason, they conclude that the computational calculations overestimate the strength of these interactions, which generates distortions in the energetic surface of the transmetalation process, which can influence in a wrong interpretation of the activation barriers.

The transmetalation step in Pd/Ag systems.

In general, it is logical to think that organometallic silver complexes are slower than copper complexes in the transmetalation step to Pd^{II} complexes due to different factors, such as the reactivity of Ag^{I} complexes, as they descend in the same group, the reactivity is reduced. On the other hand, as we have commented above, M−M' interactions can play a determinant role in the transmetalation step, so orbital interactions, especially in the transition state, can be determinant to understand the reaction rate in transmetalation. The orbital overlap will be worse in the case of Ag than in the case of Cu, generating worse interactions and destabilizing the transition state. Nevertheless, silver salts are one of the most widely used additives in

transition metal catalysis, especially in palladium catalysed cross-coupling reactions.[231]

Silver species can play different roles in Pd catalysed transformations, their performance as transmetalating agents being critical for a successful reaction in Pd/Ag bimetallic systems. Despite the promising advances in this area of knowledge is fundamental understand how the corresponding organic moiety is transferred from Ag^{I} to Pd^{II}. Just a limited number of examples of stoichiometric reactions between well-defined AgR (R = aryl or fluorinated aryl, CF_3) species and Pd^{II} organometallic complexes have been reported, and the number of well-known catalytic processes is even smaller.[232,233]

Traditionally, Ag^{I}–R (aryl or fluorinated aryl) has been employed as an aryl source to form aryl or fluorinated-aryl palladium complexes. These reactions proceed smoothly presumably due to the stabilization of the transition state and the insolubility of the formed silver salts. This methodology can be used in the context of C–H activations, as well as in Pd/Cu systems. This particularity makes Ag/Pd systems very attractive for different synthesis protocols. Particularly noteworthy is the work of Sanford and co-workers.[234] In this research, they study a bimetallic Pd/Ag system to generate the homocoupling of aryls, including the aforementioned C_6F_5-C_6F_5. NMR spectroscopy and H/D exchange studies of the stoichiometric reactions revealed a role for [Ag(OPiv)] in the C–H cleavage reaction, generating Ag–C_6F_5 as an intermediate (Figure 80). This proposal is supported by DFT calculations, which show energetically feasible pathways for concerted metalation–deprotonation of pentafluorobenzene at two molecules of [Ag(OPiv)].

---

[231] Mudarra, Á. L.; Salinas, M. de. Biomolecular Chemistry Beyond the Traditional Roles of Ag in Catalysis: The Transmetalating Ability of Organosilver(I) Species In Pd-catalysed reactions. *Org. Biomol. Chem*. **2019**, *17,* 1655–1667. DOI: 10.1039/c8ob02611d.

[232] Pye, D. R.; Mankad, N. P. Bimetallic Catalysis for C–C and C–X Coupling Reactions. *Chem. Sci.* **2017**, *8*, 1671–2466. DOI: 10.1039/c6sc05556g.

[233] Pérez-Temprano, M. H.; Casares, J. A.; Espinet, P. Bimetallic Catalysis Using Transition and Group 11 Metals: An Emerging Tool for C-C Coupling and Other Reactions. *Eur. J. Chem.* **2012**, *18*, 1864–1884. DOI: 10.1002/CHEM.201102888.

[234] Lotz, M. D.; Camasso, N. M.; Canty, A. J.; Sanford, M. S. Role of Silver Salts in Palladium-Catalyzed Arene and Heteroarene C-H Functionalization Reactions. *Organometallics* **2017**, *36*, 165–171. DOI: 10.1021/acs.organomet.6b00437.

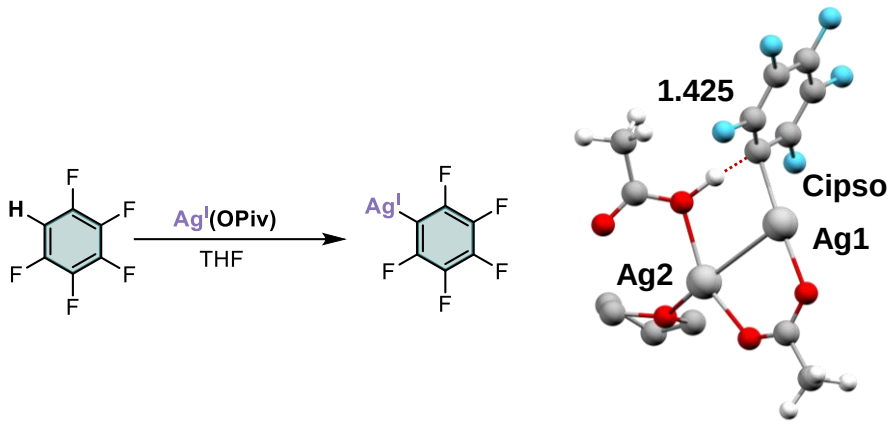

Figure 80. Potential transition structures for concerted metalation–deprotonation (CMD) of and pentafluorobenzene at binuclear silver centers proposed by Sandford and coworkers.

These studies suggest that initial metalation of C–H substrates at silver(I) carboxylates should be considered as a plausible pathway in C–H functionalization reactions involving mixtures of silver carboxylates and palladium(II) complexes.

In the same way that the Ar–Ar coupling reaction had been carried out using a Pd/Cu system through the activation of carboxylic acids,[235] commented in the last section (*The transmetalation step in Pd/Cu systems) of this chapter*, this methodology was transferred to silver salts. This co-catalyst also proved to be very effective in this type of reaction, which was perfected over the following years, extending to a large number of substrates. In 2007, Goossen and co-workers, published the first example of Pd/Ag catalysed decarboxylative coupling of aromatic carboxylates with aryl halides using over stoichiometric silver salts, as we can see in Figure 81.[236] .

[235] Gooßen, L. J.; Deng, G.; Levy, L. M. Synthesis of Biaryls via Catalytic Decarboxylative Coupling. *Science* **2006**, *313*, 662–664. DOI: 10.1126/science.1128684.

[236] Goossen, L. J.; Rodríguez, N.; Melzer, B.; Linder, C.; Deng, G.; Levy, L. M. Biaryl Synthesis via Pd-Catalyzed Decarboxylative Coupling of Aromatic Carboxylates with Aryl Halides. *J. Am. Chem. Soc*. **2007**, *129*, 4824–4833. DOI: 10.1021/ja068993.

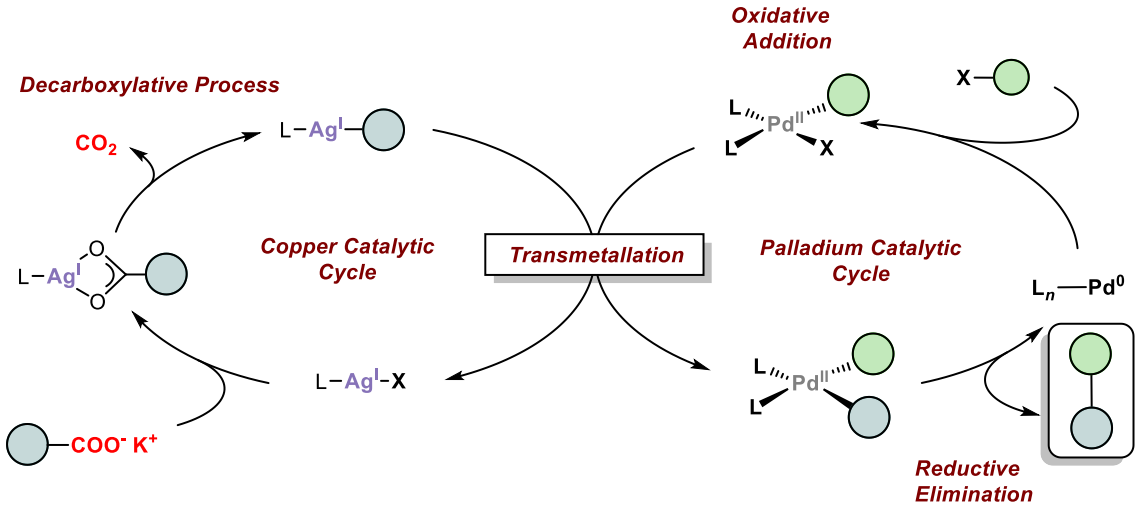

Figure 81. Bimetallic catalytic cycle proposed by Gooßen. Circles represent generic aryl moieties.

In the same year, Wagner et al. published the synthesis of biaryls using the same methodology.[237] For that, $PdCl_2/AsPh_3$ catalytic system in the presence of Ag_2CO_3 in DMSO was found to be particularly efficient to perform this transformation. This reaction was carried out at 150 °C to obtain the desired product in moderated yields. Furthermore, the reaction can be extended to the synthesis of several biaryls, including sterically hindered biaryls and with different substituents, represented in Scheme 27.

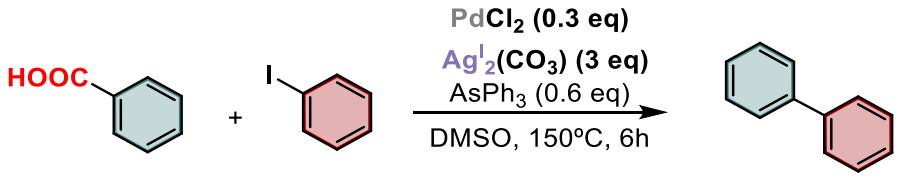

Scheme 27 Synthesis of biaryls via decarboxylative Pd-catalysed cross-coupling reaction using silver salts.

Finally, in 2010, Gooβen and co-workers improved this system using microwave reaction, which drastically reduced the reaction time.[238] On the contrary, it was not possible in any case to reduce the reaction temperatures from 120 °C (in the best case), leaving as the main drawback of this methodology the drastic reaction conditions. Compared to Pd/Cu systems, silver catalyst has proven to be

[237] Becht, J.-M.; Catala, C.; le Drian, C.; Wagner, A. Synthesis of Biaryls ViDecarboxylative Pd-Catalyzed Cross-Coupling Reaction. *Org. Lett.* **2007**, *9*, 1781–1783. DOI: 10.1021/ol070495y.

[238] Gooßen, L. J.; Lange, P. P.; Rodríguez, N.; Linder, C. Low-Temperature Ag/Pd-Catalyzed Decarboxylative Cross-Coupling of Aryl Triflates with Aromatic Carboxylate Salts. *Eur. J. Chem.* **2010**, *16*, 3906–3909. DOI: 10.1002/CHEM.200903319.

significantly more inert than copper catalysts, giving lower yields and longer reaction times.

It was in 2016, when J. Hartwig's group carried out the allyl arylation reaction in cooperation with a Pd/Ag bimetallic system (Scheme 28).[239] They have discovered a methodology for the highly selective formation of C(aryl)–C(sp^3) bonds by the Pd-catalysed and Ag-functionalized allylation of aryl C–H bonds with allylic pivalates to generate linear (E)-allyl-arenes in good yields.

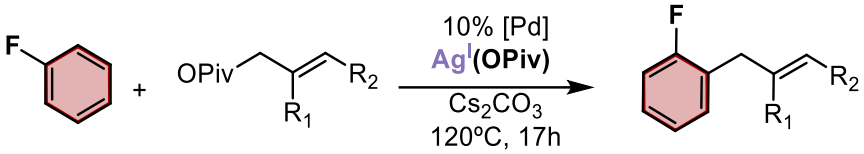

Scheme 28. The allyl arylation reaction in cooperation with a Pd/Ag bimetallic system.

The mechanistic investigation suggests that the C–H bond cleavage proceeds through a concerted metalation–deprotonation (CMD) pathway at the most acidic C–H bond via Ag(I) catalysed C–H activation. The authors synthesized the proposed intermediates and characterized them by X-ray crystallography. They observed the allylation product under stoichiometric conditions and demonstrated the synergy of both metal complexes in the transmetalation step. The main drawback of this work is that it does not provide more data, neither experimental or computational, for an in-depth study of the transmetalation step, showing, as in the case of copper, the possible substrate exchange pathways and evaluating the existence of transitions states or non-observable intermediates with a Pd–Ag interactions.

Furthermore, the nature of the silver species and the speciation of these complexes is an important concept to consider if we are to understand the transmetalation step between these two metals. In 2018, the Pérez-Temprano group explored the reactivity of novel, well-defined and isolable "$AgCF_3$" complexes as trifluoromethyl source for cross-coupling reactions.[240] This study showed for the

[239] Lee, S. Y.; Hartwig, J. F. Palladium-Catalyzed, Site-Selective Direct Allylation of Aryl C–H Bonds by Silver-Mediated C–H Activation: A Synthetic and Mechanistic Investigation. *J. Am. Chem. Soc.* **2016**, *138*, 15278–15284. DOI: 10.1021/jacs.6b10220.

[240] Martínez de Salinas, S.; Mudarra, Á. L.; Benet-Buchholz, J.; Parella, T.; Maseras, F.; Pérez-Temprano, M. H. New Vistas in Transmetalation with Discrete "$AgCF_3$" Species: Implications in Pd-Mediated Trifluoromethylation Reactions. *Eur. J. Chem.* **2018**, *24*, 11895–11898. DOI: 10.1002/chem.201802586.

first time how silver nucleophiles outperformed the traditional trifluoromethyl sources like the Togni's reagent. However, the main drawback of the reaction outcome is the highly dependent on the nature and speciation in solution of the silver trifluoromethyl complex. For example, it is well know the nature of some complexes in solution, that experiment an equilibrium between the neutral form ([AgR(L)]) and the anionic/cationic species ($[Ag(L_2)]^+$ and $[AgR_2]^-$) or the $(Cs)[Ag(CF_3)_2]$, which present an unexpected geometry represented in Figure 82.[240]

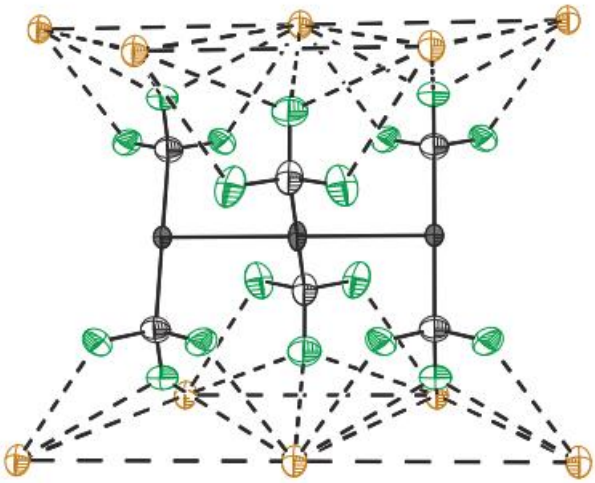

Figure 82. X-ray structure of the complex $Cs[Ag(CF_3)_2]$. Cif obtained from the reference.[240]

Furthermore, it demonstrates the great importance of the understanding of the speciation of this type of complexes in solution when studying the transmetalation step. Indeed, the extraordinary transmetalating capability of this type of complex gave access to $[Pd(R)(CF_3)(Xantphos)]$ from [Pd(Ph)I(Xantphos)] in one-pot, overcoming the challenges associated to the transmetalation step for the CF_3.

The transmetalation step in Pd/Au systems.

Bimetallic Pd/Au catalysed C–C coupling is currently a very attractive research topic.[241,242,243] It requires R-group transmetalation from Au to Pd, but despite the

[241] Hirner, J. J.; Shi, Y.; Blum, S. A. Organogold Reactivity with Palladium, Nickel, and Rhodium: Transmetalation, Cross-Coupling, and Dual Catalysis. *Acc. Chem. Res.* **2011**, *44*, 603–613. DOI: 10.1021/ar200055y.
[242] Alshammari, A.; Kalevaru, V. N.; Martin, A. Catalysts Bimetallic Catalysts Containing Gold and Palladium for Environmentally Important Reactions. *Catalysts* **2016**, *6*, 97–121. DOI: 10.3390/catal6070097.
[243] Hashmi, A. S. K.; Lothschütz, C.; Döpp, R.; Rudolph, M.; Ramamurthi, T. D.; Rominger, F. Gold and Palladium Combined for Cross-Coupling. *Angew. Chem. Int. Ed.* **2009**, *48*, 8243–8246. DOI: 10.1002/ANIE.200902942.

extraordinary attention recently paid to these Pd/Au systems in synthesis, not too much mechanistic studies have been reported.[244,245,246,247,248] The first evidence of such Pd/Au transmetalation in a catalytic reaction was recognized, as a reversible process, in the gold-catalysed *trans*-to-*cis* isomerization of $[PdRf_2(tht)_2]$ complexes, for which isomerization at the Pd center was proposed to occur through aryl exchange in a bimetallic Au/Pd intermediate supported by an Au–Pd bond.[249] In addition, several contributions in this field have been proposed by this research group over the years.

In 2012, our research group published a study of the transmetalation of Au^I complexes of the type $[AuCl(AsPh_3)]$ to palladium complexes $[Pd(Ar)_2(AsPh_3)_2]$, represented in Scheme 29.[245] Interestingly, it is observed that the transmetalation product formation is thermodynamically unfavourable, and that the reaction occurs in the opposite direction (retro-transmetalation), even at low temperatures. This is due to the thermodynamics of the reaction. For this reason, the retro-transmetalation reaction is very effective.

---

[244] Verlee, A.; Heugebaert, T.; van der Meer, T.; Kerchev, P.; van Hecke, K.; Breusegem, F. van; Stevens, C. Gold and Palladium Mediated Bimetallic Catalysis: Mechanistic Investigation through the Isolation of the Organogold(I) Intermediates. *ACS Catal*. **2019**, *9*, 7862–7869. DOI: 10.1021/acscatal.9b02275.

[245] Pérez-Temprano, M. H.; Casares, J. A.; de Lera, Á. R.; Álvarez, R.; Espinet, P. Strong Metallophilic Interactions in the Palladium Arylation by Gold Aryls. *Angew. Chem. Int. Ed.* **2012**, *12*, 5001–5004. DOI: 10.1002/ange.201108043.

[246] Villar, P.; Pérez-Temprano, M. H.; Casares, J. A.; Álvarez, R.; Espinet, P. Experimental and DFT Study of the $[AuAr(AsPh_3)]$-Catalyzed Cis/Trans Isomerization of $[PdAr_2(AsPh_3)_2]$ (Ar = C_6F_5 or $C_6Cl_2F_3$): Alternative Mechanisms and Its Switch upon Pt for Pd Substitution. *Organometallics* **2020**, *39*, 2295–2303. DOI: 10.1021/acs.organomet.0c00245.

[247] Toledo, A.; Meana, I.; Albéniz, A. C. Formal Gold-to-Gold Transmetalation of an Alkynyl Group Mediated by Palladium: A Bisalkynyl Gold Complex as a Ligand to Palladium. *Eur. J. Chem* **2015**, *21*, 13216–13220. DOI: 10.1002/CHEM.201501813.

[248] Khaledifard, Y.; Nasiri, B.; Javidy, S. A.; Sereshk, A. V.; Yates, B. F.; Ariafard, A. Phosphine-Scavenging Role of Gold(I) Complexes from $Pd(PtBu_3)_2$ in the Bimetallic Catalysis of Carbostannylation of Alkynes. *Organometallics* **2017**, *36*, 2014–2019. DOI: 10.1021/acs.organomet.7b00237.

[249] Casado, A. L.; Espinet, P. A Novel Reversible Aryl Exchange Involving Two Organometallics: Mechanism of the Gold(I)- Catalyzed Isomerization of Trans-$[PdR_2L_2]$ Complexes (R = Aryl, L = SC_4H_8). *Organometallics* **1998**, *17*, 3677–3683.

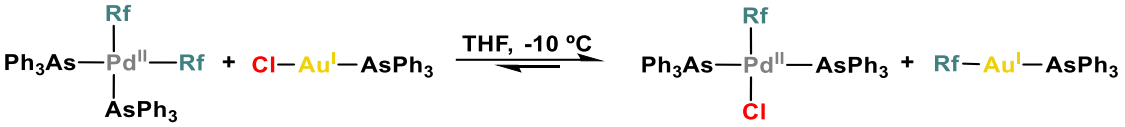

Scheme 29. Retro-transmetalation in Au/Pd system.

Kinetic experiments followed by ^{19}F NMR spectroscopy afforded critical information. Interestingly, addition of $AsPh_3$ (free ligand) slowed down the reaction, and the observed reaction order with respect to the concentration of arsine, determined from initial rates was -0.52. Note that fitting the observed reaction order with respect to the concentration of arsine required the existence of two transition states, the second one having higher free energy than the first one. This implies that a ligand dissociation is required in one of the steps. This is either replaced by the Pd complex or by a ligand dissociation. Moreover, DFT calculations provide details of the mechanistic profile and other interesting features of the system. First of all, they show that the transition state with the highest energy in the transmetalation multistep process is TS2, which has a structure in which Au and Pd are exchanging Cl for R. This agrees with the results obtained in the kinetic experiments. The overall energy obtained by DFT calculation for the transmetalation between gold and palladium was 26.1 kcal mol^{-1}. This value is considerably higher than those seen previously for Pd/Cu transmetalation, which were around 20 kcal mol^{-1}.

Some interesting conclusions about the mechanism of Au/Pd transmetalation can be drawn from this study. The Au/Pd systems shows that aryl transmetalation from [Au(Ar)($AsPh_3$)] to [PdCl(Ar)($AsPh_3$)$_2$]] complexes is thermodynamically disfavoured and will require a subsequent irreversible reductive elimination from [Pd(Ar)$_2$L$_2$] to form Ar–Ar, modifying the overall thermodynamics of the reaction. In this case, as we saw in Chapter I, the challenging reductive elimination of two high-fluorinated aryls cannot take place with the triphenylarsine as a ligand. Moreover, the transition state exchanging the Ar and Cl group shows a strong interaction between the two metals, in agreement to examples of transmetalation in Pd/Cu systems. Furthermore, the transmetalation reactions was proposed with a multi-step mechanism, with an activation barrier considerably higher than the energy barriers for the Pd/Cu and Pd/Ag systems. These results show a clear trend between

the three metals, where the rate of transmetalation appears to decrease as we move down through Group 11.

One year later, in 2013, Hashmi and co-workers conducted a comprehensive study on the transmetalation step at theoretical and experimental level in Pd/Au-mediated cross-coupling reactions.[250] Detailed mechanistic and energetic studies of the transmetalation step were commented and compared for different substrates and ligands on the catalytic Pd center. Several transmetalation pathways were studied in detail, which the lower energetic barrier has some important aspects. First of all, is a non-concerted process, where the transmetalation step takes place in several steps. As in the previous cases (and in the cases with Ag and Cu), a substitution of one of the palladium ligands is mandatory. On the other hand, Au–Pd interactions prove to be vital in order to obtain adequate energetic values (around 24 kcal mol^{-1}). In addition, it is also shown that the thermodynamics of the reaction is unfavourable, being an endergonic process, which means that it requires a subsequent step (reductive elimination) that acts as a driving force to pull the thermodynamics of the whole process.

Another important behaviour in such bimetallic systems is the ability of Cu/Ag/Au to catalyse slow isomerization in Pd^{II} complexes. In 2020, our research group published a large study on the of the [Au(Ar)($AsPh_3$)]-catalysed cis/trans isomerization of [$Pd(Ar)_2(AsPh_3)_2$].[246] As in the previous study, ligand dissociation turns out to be a critical step for the interaction between the two metals. The aryl exchanges between *cis*- or *trans*-[$Pd(Ar)_2L_2$] and [Au(Ar')L] complexes can occur with or without *cis/trans* isomerization at Pd, depending on the pathway, as we can see in Figure 83.

[250] Hansmann, M. M.; Pernpointner, M.; Döpp, R.; Hashmi, A. S. K. A Theoretical DFT-Based and Experimental Study of the Transmetalation Step in Au/Pd-Mediated Cross-Coupling Reactions. *Eur. J. Chem.* **2013**, *19*, 15290–15303. DOI: 10.1002/CHEM.201301840.

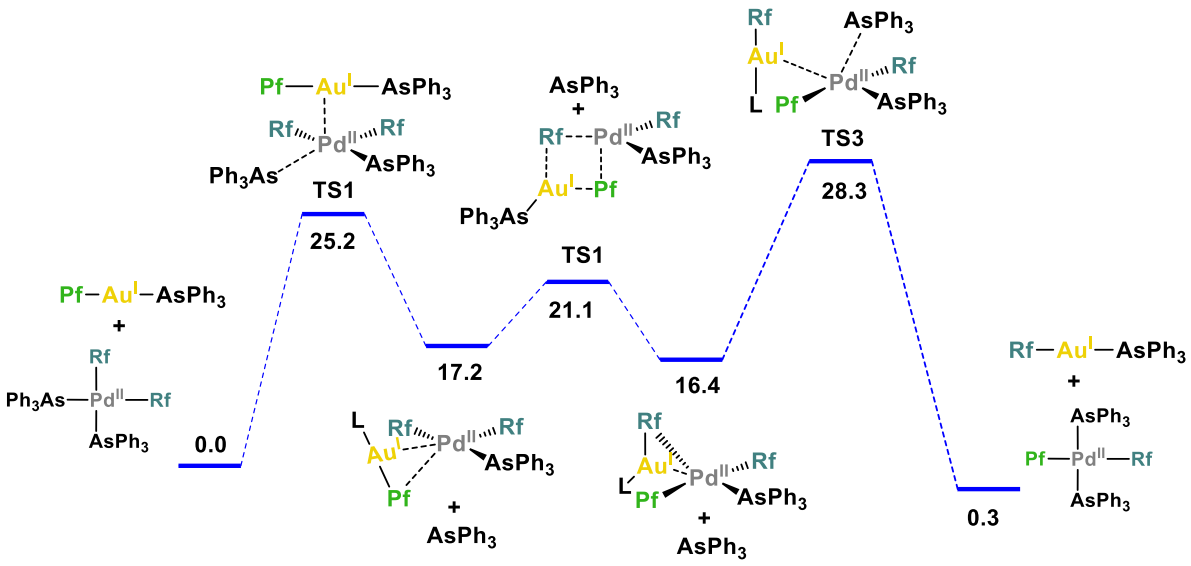

Figure 83. Reaction energy profile of the aryl exchange and isomerization in Au/Pd system. [246]

The reaction is always initiated by substitution of one $AsPh_3$ in Pd for the Au–C_{ipso} bond of the entering [Au(Ar)($AsPh_3$)] molecule, generating strong interactions between both metals, detected by DFT calculations in several transitions states and intermediates, and in QTAIM calculations. [246]

In summary, there were few differences in the Cu/Ag/Au and Pd bimetallic systems, especially in the most important step, the transmetalation was found. Depending on the metal, kinetic differences (different energy barriers, possibly caused by the existence or not of metal-metal interactions and the nature of it) generate activation energies barriers around 20 kcal mol^{-1} for copper, up to 25-26 kcal mol^{-1} in the best cases for gold. On the other hand, the thermodynamic component has a great influence on the effectiveness of the reactions in the cases of Cu and Ag, and critical in the case of Au/Pd bimetallic reactions, which may even need a subsequent reductive elimination step in order to have a favourable product formation.

All of this suggests answering various questions to shed some light on this step, which is important for improving various catalytic processes. What is the reason for the different reactivity of these three metals? Are there always metal-metal interactions for the same reaction, and how does this affect to the kinetics of the reaction? Are the energy profiles similar or different?

5.2 Results and discussion

To try to explain some of the particularities mentioned above, we have carried out the transmetalation kinetic studies using as a model the system formed by the complexes *trans*-[PdCl(Rf)($AsPh_3$)$_2$] and [M(Pf)(NHC)] (Pf = C_6F_5; Rf = $C_6Cl_2F_3$; M = Cu, Ag, Au), represented in Scheme 30. The use of palladium and group 11 metals complexes bearing different high fluorinated aryl groups is aimed at distinguishing the possible aryl exchanges with and without isomerization and studying both phenomena independently. These high fluorinated aryls (Pf and Rf) are very similar thermodynamically, and their presence allows to monitor exchanges by ^{19}F NMR in a way quite similar to isotopic labelling. Because ligand substitution is expected, $AsPh_3$ is chosen as the ligand in Pd. Although phosphines are more common ligands in Pd catalysis, they were discarded because of the extreme slowness of the reaction in this case because they are stronger ligands than $AsPh_3$. In addition, for the group 11 metals, carbene-type ligands have been chosen to ensure that the geometry of the complexes is the same in all cases (linear geometry) and that the ligand in solution does not change from one metal to another. Additionally, from the results obtained during the optimization of conditions in Chapter I, when bulky carbene-type ligands are used, no ligand exchange is observed between the complexes with group 11 metals and the Pd complex. This is probably due to the thermodynamics of the exchange, since the binding energy between carbenes and metal is favourable compared to that of carbene and Pd.[249]

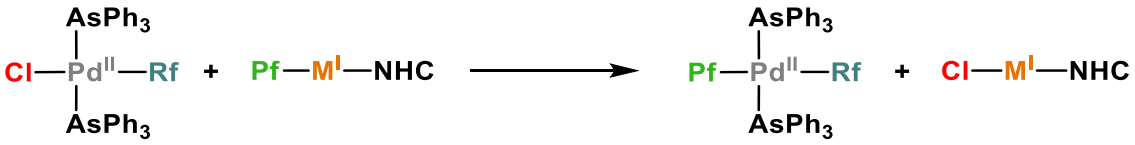

Scheme 30. General reaction to study the transmetalation process.

Our first idea was to study the transmetalation between linear Cu^I/Ag^I/Au^I complexes with Pf as fluorinated aryl, to the *trans*-[PdCl(Rf)($AsPh_3$)$_2$] (**1**) complex and try to identify the differences in reactivity between these metals. The choice of the *trans*-[PdCl(Rf)($AsPh_3$)$_2$] (**1**) complex is not trivial, due to the thermodynamics of the isomerization, which is favourable to the trans isomer. The use of *cis*-[PdCl(Rf)($AsPh_3$)$_2$] (**3**) was not possible due to the not accessible to isolate it. For

this study, different kinetic experiments are proposed, which are carried out systematically for the three metals of group 11, in order to analyse the similarities and differences between them. For this purpose, each metal is dealt with in a separate section, and the results will be studied individually initially, and jointly at the end of the study.

The transmetalation step in Cu/Pd systems.

Stoichiometric Reaction

The stoichiometric reaction between the *trans*-[PdCl(Rf)($AsPh_3$)$_2$] (**1**) complex and the [Cu(Pf)(DPI)] (**2-Cu**) complex (DPI = diphenylimidazole) is shown in Figure 84. This reaction was carried out in dry CH_2Cl_2 due to the good solubility of the reagents and was measured at 15 °C. As expected from previous work, the reaction mixture is complex due to the large number of organometallic complexes in solution. Thanks to these investigations,[246,245] the formation of the complexes *cis/trans*-[Pd(Pf)(Rf)($AsPh_3$)$_2$](**4** and **5**), *cis/trans*-[Pd(Pf)$_2$($AsPh_3$)$_2$](**6** and **7**) and *cis/trans*-[Pd(Rf)$_2$($AsPh_3$)$_2$] (**8** and **9**) corresponding to the transmetalation reaction, and successive retro-transmetalations, have been observed.

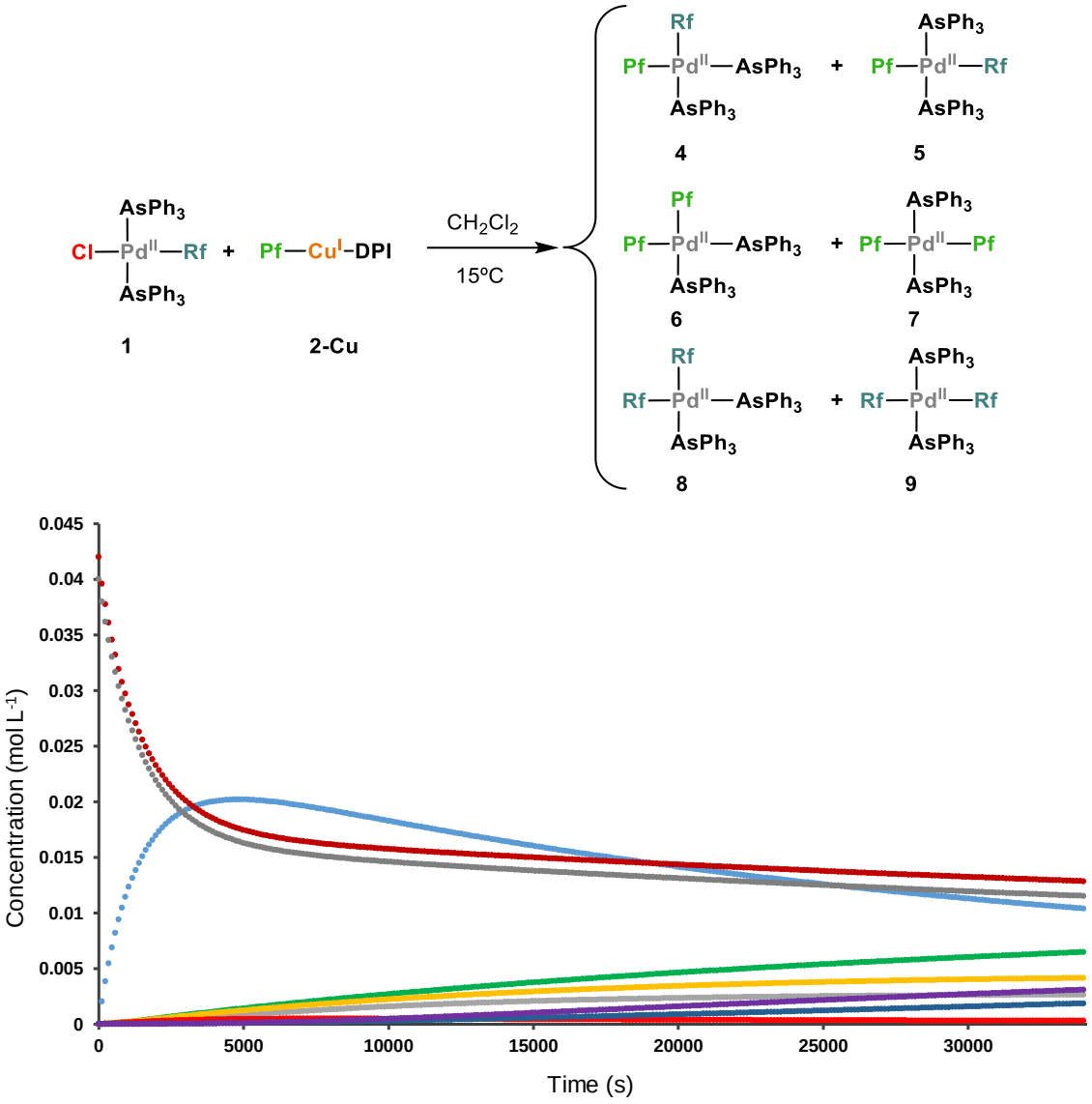

Figure 84. Concentration vs time plot of experimental data obtained by ^{19}FNMR monitoring of the stoichiometric reaction between trans-[PdCl(Rf)(AsPh$_3$)$_2$] (**1**) [0.040 mol L^{-1}] complex and the [Cu(Pf)(DPI)] (**2-Cu**) [0.042 mol L^{-1}] complex in dry CH_2Cl_2 at 15°C. Color code: Red **2-Cu,** Grey **1**, Blue *cis*-[Pd(Pf)(Rf)(AsPh$_3$)$_2$] (**4**), Green *trans*-[Pd(Pf)(Rf)(AsPh$_3$)$_2$] (**5**), Yellow *cis*-[Pd(Pf)$_2$(AsPh$_3$)$_2$] (**6**), Light Grey *cis*-[Pd(Rf)$_2$(AsPh$_3$)$_2$] (**7**), Purple *trans*-[Pd(Pf)$_2$(AsPh$_3$)$_2$] (**8**), Dark blue *trans*-[Pd(Rf)$_2$(AsPh$_3$)$_2$] (**9**), Light Red C_6F_5H.

If we pay attention to the first part of the kinetic monitoring represented in Figure 84, we identify that the compounds whose concentration decreases are the starting reagents, both the *trans*-[PdCl(Rf)(AsPh$_3$)$_2$] (**1**) and the [Cu(Pf)(DPI)] (**2-Cu**) complexes. The blue line is the *cis*-[Pd(Rf)(Pf)(AsPh$_3$)$_2$] (**3**) with mixed fluorinated aryls formed by a transmetalation reaction between **1** and **2-Cu**. Surprisingly, the arrangement of this complex is the *cis* one (kinetic product), much less stable than

its *trans* isomer (thermodynamic product). This means that transmetalation proceeds without geometry retention, generating the less thermodynamically favourable isomer. This complex has been unequivocally identified by X-ray diffraction, as shown in Figure 85.

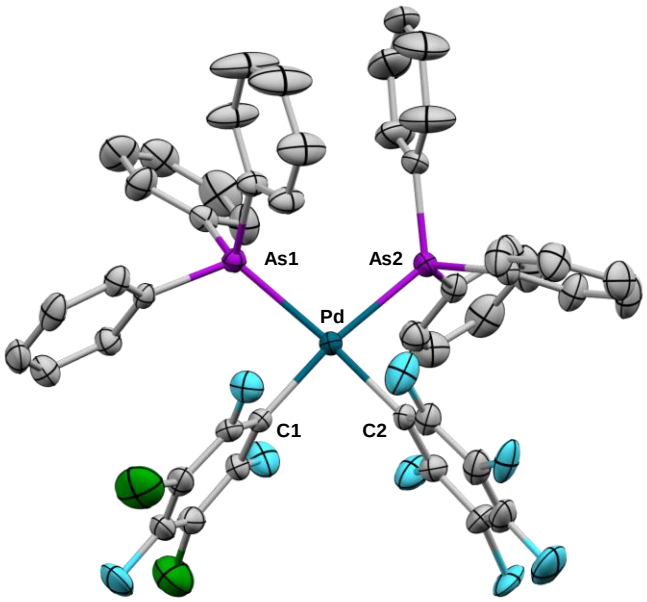

Figure 85. X-Ray diffraction of the intermediate *cis*-[Pd(Rf)(Pf)($AsPh_3$)$_2$] (**4**). Hydrogen atoms are omitted for clarity.

This structure shows normal and expected bond distances for this complex. The distance Pd–C_{ipso}(Rf) = 2.033 Å, while the distance Pd–C_{ipso}(Pf) = 2.058 Å. On the other hand, the trans influence of both aryls, which can be determined by the distance between the Pd and the trans ligand to each of the aryls, also turns out to be practically identical (Pd–As1 = 2.428 Å, Pd–As2 = 2.450 Å), which shows that the Rf and Pf aryls are electronically similar. [246]

Next, if we look at the lower concentration lines, we can identify many compounds, as we can see in Figure 86. Among them is, for example, the *trans*-[Pd(Rf)(Pf)($AsPh_3$)$_2$] (**4**) complex. [246]

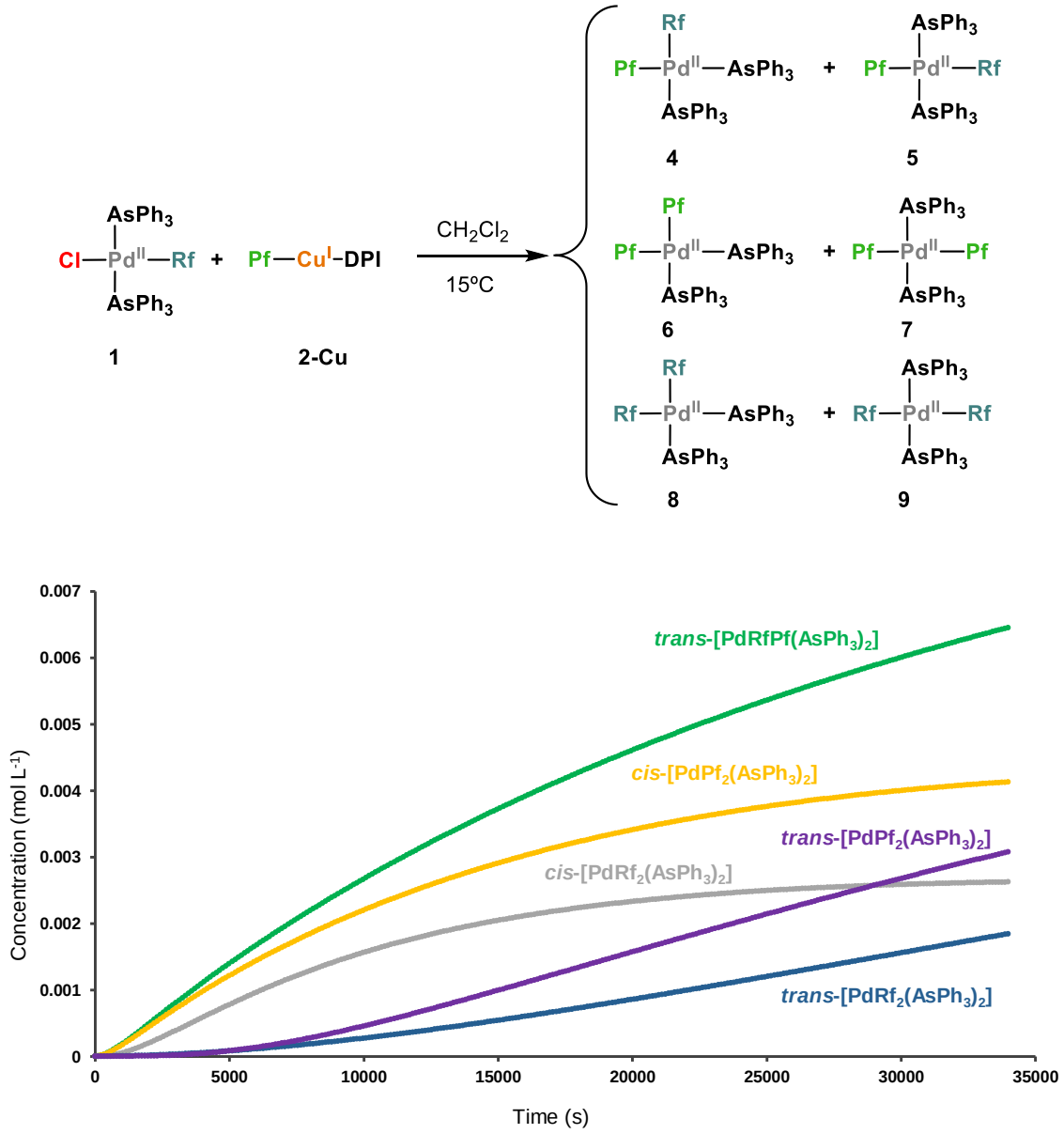

Figure 86. Concentration vs time plot of experimental data obtained by ^{19}FNMR monitoring of the stoichiometric reaction between *trans*-[PdCl(Rf)(AsPh$_3$)$_2$] (**1**) complex and the [Cu(Pf)(DPI)] (**2-Cu**) complex in dry CH_2Cl_2 at 15 °C. Zoom of minority compounds of Figure 84.

The appearance of complex **4** is interesting because as discussed in the introduction, the isomerization of *cis*-[Pd(Rf)$_2$(AsPh$_3$)$_2$] to *trans*-[Pd(Rf)$_2$(AsPh$_3$)$_2$] was studied by ^{19}F NMR in $CDCl_3$ at 323 K. In the absence of any catalyst the spontaneous isomerization in $CDCl_3$ is very slow (24 hours at 323 K, the conversion is only 8%).[246] This means that **2-Cu** complex is not only able to transmetalate efficiently the aryl moiety to complex **1**, also catalyzes the isomerization of the *cis* to *trans* complexes effectively. On the other hand, it is observed that the formation of the *cis*-[Pd(Pf)$_2$(AsPh$_3$)$_2$] complex is faster than the formation of the *cis*-

$[Pd(Rf)_2(AsPh_3)_2]$ complex, due to the slight excess of the **2-Cu** complex in the reaction. More importantly, from a mechanistic perspective, the cis-geometry complex always forms first. This implies that transmetalation and retro-transmetalation steps must necessarily occur at the position where a triphenylarsine ligand was previously present, leaving the organic moiety in that position, changing the initial geometry from trans to cis. Furthermore, it is well known the aryl exchange between Cu/Pd or Pd/Pd complexes. This transmetalations and retro-transmetalations explains the presence of *cis*-Pd^{II} species in the reaction mixture, and their trans isomers are formed faster than expected by copper catalysed cis/trans isomerization.[227]

Kinetic Analysis

The kinetic results obtained by ^{19}F NMR, and the additional experimental data allow us to make a mechanistic proposal and try to fit it by Copasi kinetic simulator, as we can see in Figure 87, and the results are given in Figure 88.

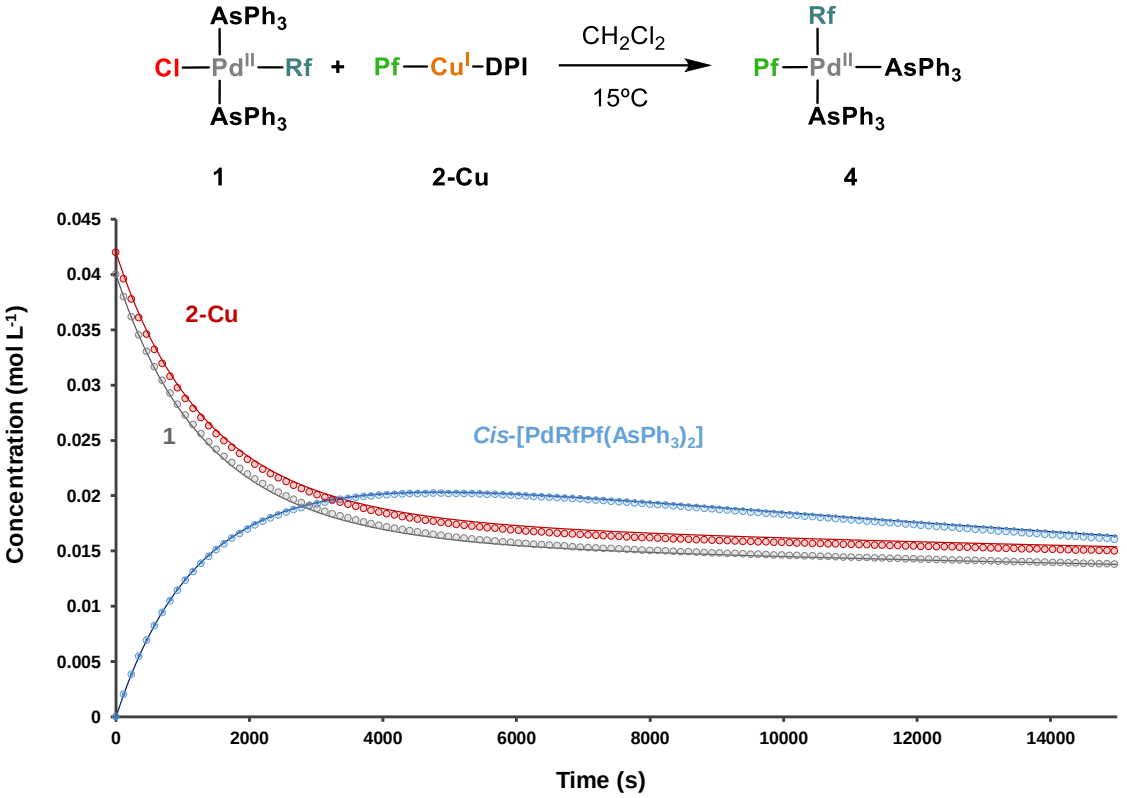

Figure 87. Concentration vs time plot of experimental data (dots) obtained by ^{19}FNMR monitoring and -fitted values (continuous lines) of the fluorinated-species in the transmetalation step between **1** and [**2-Cu**].

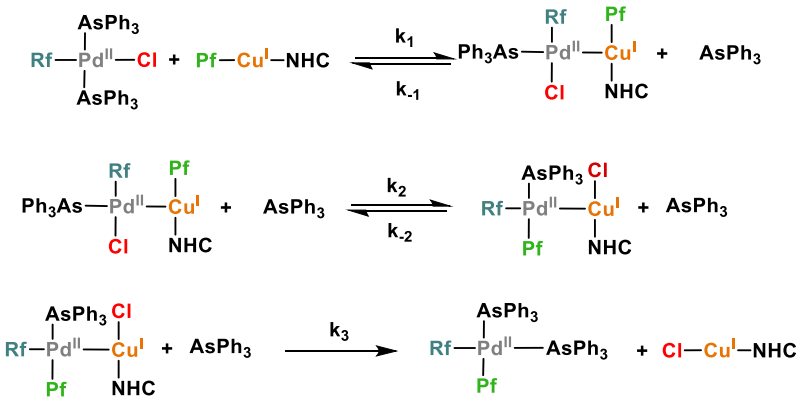

	Value ($s^{-1}Lmol^{-1}$)	**Stand. Desv.**
k_1	3.97×10^{-2}	2.3×10^{-4}
k_{-1}	39.7	2.5×10^{-2}
k_2	3.50×10^{-2}	1.1×10^{-4}
k_{-2}	3.92×10^{-7}	1.8×10^{-8}
k_3*	Fast	-

Figure 88. Complete kinetic model, summarizing the plausible reaction pathways, to explain the transmetalation step between **1** and **2-Cu** and fitted rate constants with their respective Standard deviations. * For this kinetic analysis, k_3 was fixed with an arbitrary value due to the other kinetic constants do not experiment any variation because they are not correlated.

In this kinetic model, three elementary reactions are used for the transmetalation step. The first equation represents the substitution of arsine by the copper complex. This reaction is posited as an equilibrium which would be shifted towards the reactants. This would imply that, in the reaction profile, the assumed bimetallic intermediate would be higher in energy than the reactants. On the other hand, a transmetalation step, where the fluorinated aryl of the copper complex would be exchanged for the halogen of the Pd complex. In this case, it is important to note that the equilibrium is very much shifted towards the products, being a thermodynamically favourable process. Finally, the formation of the *cis*-[Pd(Rf)(Pf)($AsPh_3$)$_2$] + [CuCl(DPI)] complex is fitted as a fast reaction. The value of the k_3 constant is locked at 1000 $s^{-1}Lmol^{-1}$, as this is understood to be a fast reaction, but the change in this value above a certain value does not change the fitted values. As we have seen, the kinetic fitting with three elementary reactions is able to reproduce the experimental results with good values, allowing a good fit. For this

reason, an attempt is made to fit the complete system, adding the isomerization reactions, as reproduced in previous works, as we can see in Figure 89 and Scheme 31. [246]

It is important to emphasize that this is a simplification of the system, and that not all reactions that can coexist have been considered. The kinetic model is designed to interpret the mechanistic approach of the transmetalation step, and the exchange and isomerization processes have not been studied in depth.

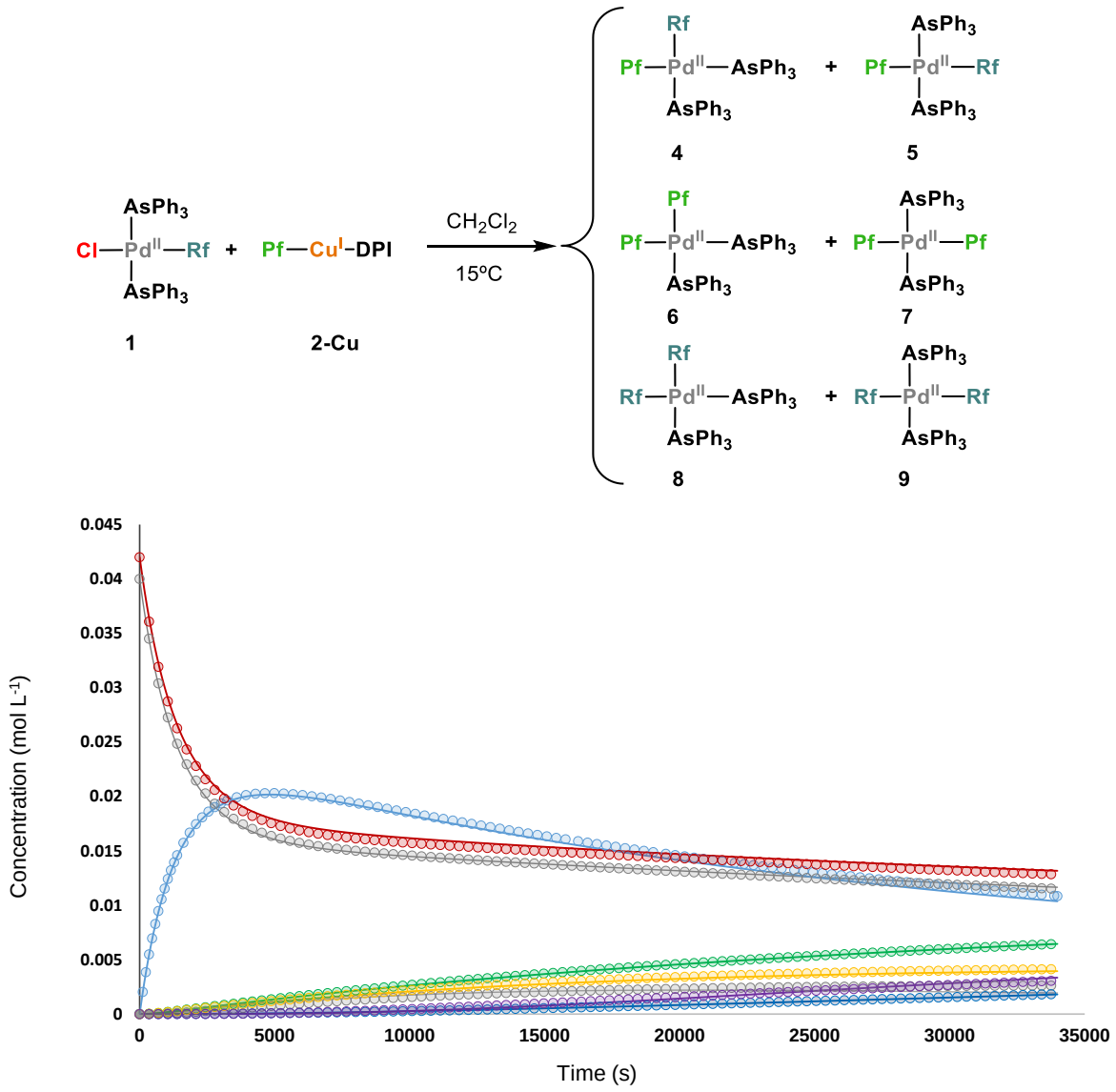

Figure 89. Concentration vs time plot of experimental data (dots) obtained by ^{19}F NMR monitoring and COPASI-fitted values (continuous lines) of the fluorinated-species in the transmetalation step and aryl exchange/retro-transmetalations between **1** and [**2-Cu**]. Color code: Red **2-Cu,** Grey **1**, Blue *cis*-[Pd(Pf)(Rf)($AsPh_3$)$_2$] (**4**), Green *trans*-[Pd(Pf)(Rf)($AsPh_3$)$_2$] (**5**), Yellow *cis*-[Pd(Pf)$_2$($AsPh_3$)$_2$] (**6**),

Light Grey *cis*-[Pd(Rf)$_2$(AsPh$_3$)$_2$] (**7**), Purple *trans*-[Pd(Pf)$_2$(AsPh$_3$)$_2$] (**8**), Dark blue *trans*-[Pd(Rf)$_2$(AsPh$_3$)$_2$] (**9**).

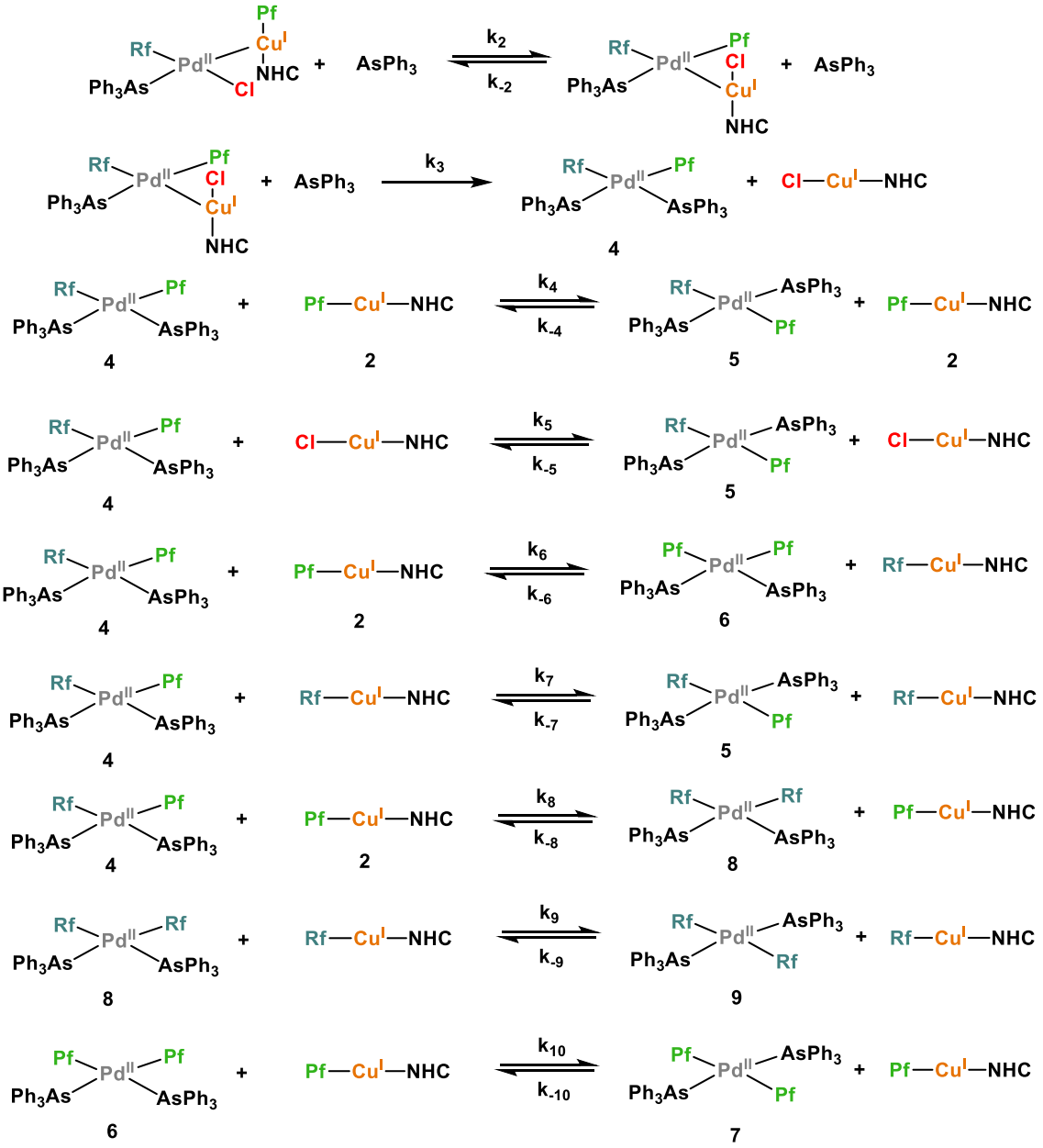

Scheme 31. Kinetic model used for the non-linear fitting shown in Figure 90.

In addition, five kinetic experiments with different amounts of arsine have been adjusted simultaneously, observing the decrease of the reaction rate. In this model an attempt is made to represent the ligand substitution. As expected, the kinetic fit was very satisfactory, and allows us to affirm that the ligand displacement is a real and explainable step in this reaction, and that it is not the rate limiting step of the process, as has been previously demonstrated.

Since there are a large number of reactions that can be carried out in this system, independently of transmetalation, a simpler kinetic model can be obtained that fits the experimental results, as we can show in Table 29:

Reaction	Parameter	Value ($s^{-1}Lmol^{-1}$)	Std. Deviation
t-[Pd(Rf)Cl($AsPh_3$)$_2$ + [Cu(Pf)(DPI)] = c-[Pd(Rf)(Pf)($AsPh_3$)$_2$] + [CuCl(DPI)]	k_1	1.11E-02	1.1E-05
	k_{-1}	5.53E-03	7.3E-06
c-[Pd(Rf)(Pf)($AsPh_3$)$_2$]+ [Cu(Pf)(DPI)] -> t-[Pd(Rf)(Pf)($AsPh_3$)$_2$]+ [Cu(Pf)(DPI)]	k_2	7.86E-04	2.5E-07
c-[Pd(Rf)(Pf)($AsPh_3$)$_2$]+ [Cu(Pf)(DPI)] -> c-[Pd(Pf)$_2$($AsPh_3$)$_2$] + [Cu(Rf)(DPI)]	k_3	7.26E-04	1.4E-07
c-[Pd(Pf)$_2$($AsPh_3$)$_2$] + [Cu(Pf)(DPI)]-> t-[Pd(Pf)$_2$($AsPh_3$)$_2$] + [Cu(Pf)(DPI)]	k_4	1.34E-03	5.2E-07
t-[Pd(Rf)(Pf)($AsPh_3$)$_2$] + [Cu(Rf)(DPI)] = c-[Pd(Rf)$_2$($AsPh_3$)$_2$]+ [CuCl(DPI)]	k_{-4}	3.35E-02	2.0E-05
	k_5	1.00E-08	1.7E-06
c-[Pd(Rf)$_2$($AsPh_3$)$_2$]+ [Cu(Rf)(DPI)] -> t-[Pd(Rf)$_2$($AsPh_3$)$_2$] + [Cu(Rf)(DPI)]	k_6	1.36E-01	6.2E-05

Table 29. Complete kinetic model, summarizing the plausible reaction pathways, to explain the transmetalation step between **1** and **2-Cu** and Fitted rate constants with their respective Standard deviations.

These results not only show faster transmetalation rates than traditional bimetallic reactions, such as the Negishi,[210,251] Stille[207,208] or Suzuki reactions,[252] but they are also an alternative to these transmetalating agents, due to the ability of Cu to functionalized molecules that it is then able to transmetalate. In this way, a very attractive alternative to traditional bimetallic catalysis, which requires stoichiometric agents at best as transmetalating reagents, is obtained. On the other hand, it is established as a safer alternative, since many of these traditional transmetalating agents have major drawbacks, both for health and for the environment security.

[251] Casares, J. A.; Espinet, P.; Fuentes, B.; Salas, G. Insights into the Mechanism of the Negishi Reaction: ZnRX versus ZnR_2 Reagents. *J. Am. Chem. Soc*. **2007**, *129*, 3508–3509. DOI: 10.1021/ja070235b.

[252] Amatore, C.; Jutand, A.; Le Duc, G. Kinetic Data for the Transmetalation/Reductive Elimination in Palladium-Catalyzed Suzuki-Miyaura Reactions: Unexpected Triple Role of Hydroxide Ions Used as Base. *Eur. J. Chem* **2011**, *17*, 2492–2503. DOI: 10.1002/chem.201001911.

Once the stoichiometric reaction has been studied and all the species involved in the reaction have been identified, it is decided to study in depth the mechanism of the first step, which is the transmetalation between complexes *trans*-[PdCl(Rf)($AsPh_3$)$_3$] **(1)** and [Cu(Pf)(DPI)] **(2-Cu).**

a) *Kinetic order with respect to the copper complex.*

To determine the order with respect to the **2-Cu** complex, different reactions are measured keeping the quantities of **1** constant, to obtain a relation on how the transmetalation rate varies with respect to the quantity of **2-Cu**.

The transmetalation reaction is first-order in [**2-Cu**] as shown in Figure 90 and Table 30. The plot of ln(*r0*) *vs.* ln([**2-Cu**]) is a straight line with slope 0.98. Therefore, the transmetalation rate is proportional to the concentration of [**2-Cu**].

Table 30. Initial rates for the transmetalation between **1** and **2-Cu:**

[Cu] mol L^{-1}	**r_0 mol L^{-1} s^{-1}**	**ln[Cu]**	**ln(r_0)**
4.01E-03	6.19E-06	5.52	1.20E+01
8.02E-03	4.09E-06	4.83	1.24E+01
1.20E-02	2.50E-06	4.42	1.29E+01
1.60E-02	1.83E-06	4.14	1.32E+01
3.01E-02	9.80E-07	3.51	1.38E+01

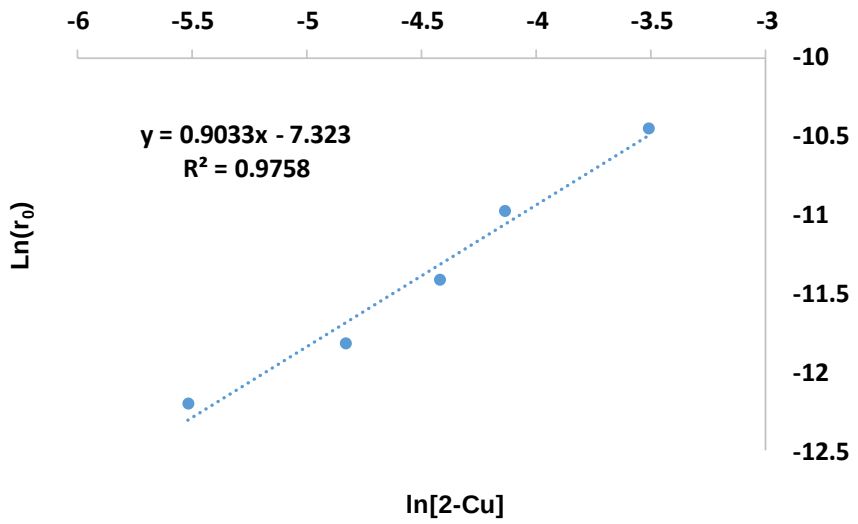

Figure 90. Effect of [**2-Cu**] on the transmetalation of *trans*-[Pd($C_6Cl_2F_3$)Cl($AsPh_3$)$_2$] (**1**) in CH_2Cl_2 at 15°C. r_0 is the initial transmetalation rate. [**2-Cu**]$_0$ (mol L^{-1}) = 4.01 x 10^{-3}, 8.02 x 10^{-3},1.20 x 10^{-2},1.60 x 10^{-2},3.01 x 10^{-2}. [**1**]$_0$ (mol L^{-1}) = 4.00 x 10^{-3}.

b) *Retardation by addition of $AsPh_3$.*

The presence of added $AsPh_3$ retards the transmetalation reaction between **1** and **2-Cu**. The corresponding data is collected in Table 31 and represented in Figure 91. The kinetic law shows minus first order with respect to the concentration of $AsPh_3$ (the plot of ln(*r*0) *vs* ln[$AsPh_3$]$_{added}$ is a straight line with slope -0.93). As commented above, the minus first order with respect to the concentration of $AsPh_3$ implies that the energy profile consists of several stages. One of them involves the dissociation or exchange of the $AsPh_3$ group for the **2-Cu** complex, and that this stage is not the rate limiting step of the reaction.

Table 31. Initial rates for the transmetalation between **1** and **2-Cu:**

[$AsPh_3$] mol L^{-1}	r_0 mol L^{-1} s^{-1}	ln[$AsPh_3$]	ln(r_0)
3.99 E-03	5.00E-06	5.52E+00	-1.22E+01
8.02E-03	7.40E-06	4.83E+00	-1.18E+01
1.21E-02	1.10E-05	4.42E+00	-1.14E+01
1.61E-02	1.71E-05	4.14E+00	-1.10E+01
3.00E-02	2.90E-05	3.51E+00	-1.04E+01

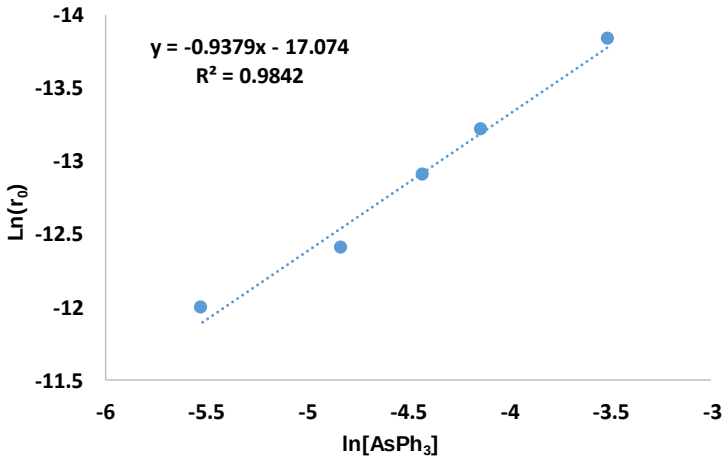

Figure 91. Effect of free $AsPh_3$ on the transmetalation of [Cu(Pf)(DPI)] [**2-Cu**] and trans-[$Pd(C_6Cl_2F_3)Cl(AsPh_3)_2$] (**1**) in CH_2Cl_2 at 15°C. r_0 is the initial transmetalation rate. [**2-Cu**]$_0$ (mol L^{-1}) = 4.00 x 10^{-3} [**1**]$_0$(mol L^{-1}) = 4.00 x 10^{-3}. [$AsPh_3$]$_0$ (mol L^{-1}) = 3.99 x 10^{-3}, 8.02 x 10^{-3}, 1.21 x 10^{-3}, 1.61 x 10^{-2}, 3.00 x 10^{-2}.

c) *Deduction of theoretical kinetic equations.*

Experimental results show a decrease in reaction rate in the presence of free $AsPh_3$. This leads us to raise the hypothesis shown in the Scheme 32. Since our measurements have been made at the early stages of the reactions, we have considered that the reactions are irreversible during the duration of the study.

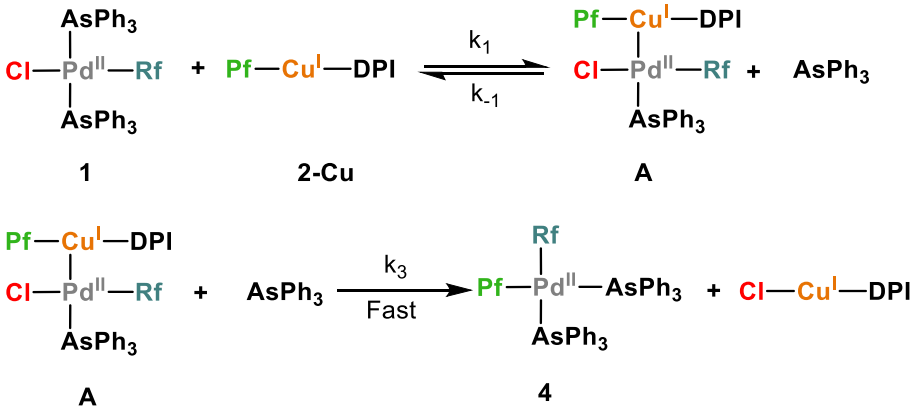

Scheme 32. Mechanistic proposal for the kinetic approximations.

Kinetic Equations applying the steady state approximation: Applying the steady-state approximation to the reaction scheme, the rate law is:

$$\frac{d[A]}{dt} = 0 = k_1[1]_0[2]_0 - k_{-1}[A][AsPh_3] - k_2[A] = 0$$

$$A = \frac{k_1[1]_0[2]_0}{k_2 + k_{-1}[AsPh_3]}$$

$$Rate(r) = \frac{k_1 k_2[1]_0[2]_0}{k_2 + k_{-1}[AsPh_3]} = \frac{a[1]_0[2]_0}{b + [AsPh_3]}$$

$$(r) = \frac{a[1]_0[2]_0}{b + [AsPh_3]}$$

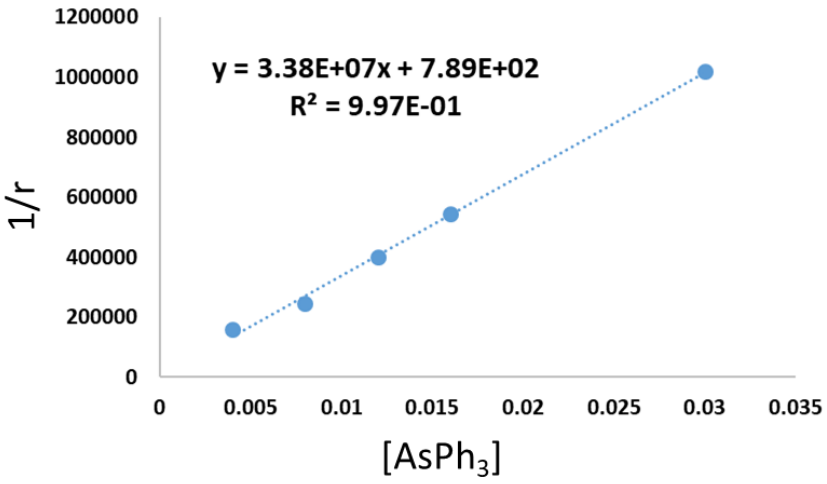

Figure 92. Retardation effect due to the addition of $AsPh_3$ on the transmetalation in CH_2Cl_2 at 283.0 K. $[trans\text{-}[Pd(Rf)(Cl)(AsPh_3)_2]]_0$ = 0.04 mol L^{-1}; $[\mathbf{2\text{-}Cu}]_0$ = 0.0416 mol L^{-1}. r is the initial transmetalation rate.

Thus, the transmetalation process is first-order with respect to [Pd] and [Cu], and minus first order with respect to the concentration of $AsPh_3$. In agreement with this, the numerical analysis of the previous data leads to the rate law:

$$(r) = \frac{a[1]_0[2]_0}{b + [AsPh_3]}$$

$$\mathbf{a = 2.96\ 10^{-8}\ s^{-1}}$$

$$\mathbf{b = 2.33\ 10^{-5}\ mol\ L^{-1}}$$

This rate expression agrees with two different kinetic models: a pre-equilibrium involving $AsPh_3$ releasing, followed by a step that it is rate controlling (prior-equilibrium approximation); or a fast equilibrium to form a reactive intermediate that does not accumulate at an appreciable level compared with reagents and products, (steady-state approximation) followed by the rate-controlling step. Using these results in the previous equations, we can obtain an approximation for the rate constants:

$$\frac{d[A]}{dt} = 0 = k_1[1]_0[2]_0 - k_{-1}[A][AsPh_3] - k_2[A] = 0$$

$$A = \frac{k_1[1]_0[2]_0}{k_2 + k_{-1}[AsPh_3]}$$

$$Rate(r) = \frac{k_1k_2[1]_0[2]_0}{k_2 + k_{-1}[AsPh_3]} = \frac{a[1]_0[2]_0}{b + [AsPh_3]}$$

$$(r) = \frac{a[1]_0[2]_0}{b + [AsPh_3]}$$

These results are consistent with a reaction profile with two steps, where $k_2 < k_{-1}$ at a value of $k_2/k_{-1} \approx 10^{-3}$, and the energy profile (Figure 93) with the approximate values would be:

$$\Delta G‡ = -RTln(Keq) + \Delta G‡(k2) = 20 - 22\ kcal\ x\ mol^{-1}$$

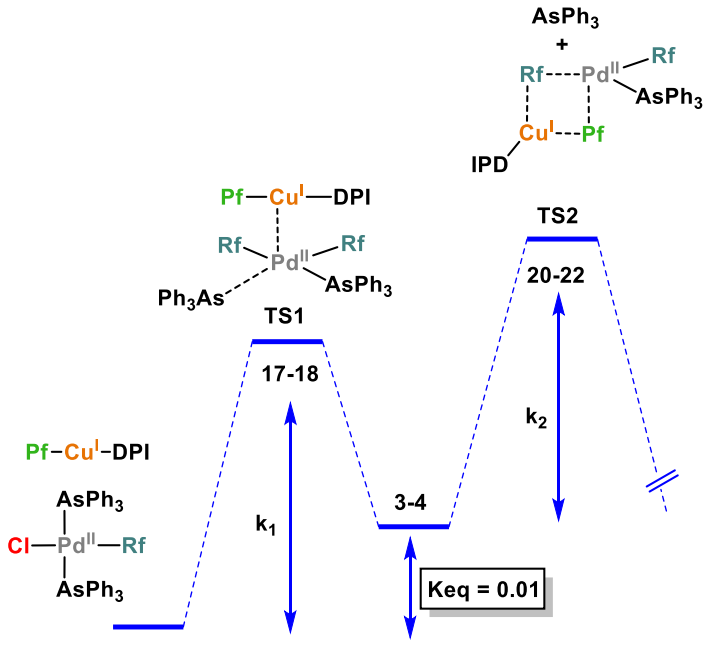

Figure 93. Proposed energy profile for the transmetalation stage. Values obtained from experimental data.

The observed initial rates fit well, which is a typical rate law for a two-step mechanism where the first step is the substitution of one $AsPh_3$ by the incoming reagent (**2**), and the second (and rds one) leads to the final products. The activation energy of this reaction is 20-22 kcal/mol. This is in agreement with the previous studies.[245,246]

Other experiments

*Equilibria between trans-[PdCl(Rf)(AsPh$_3$)$_2$] (**1**)* and *[PdRf(μ-Cl)(AsPh$_3$)]$_2$*

It is common for this type of palladium(II) organometallic complexes to undergo rapid equilibration at room temperature to form the dimeric species.

For that, a low-temperature study could show the two species in solution, so we could measure the equilibrium constant and calculate how much dimer would be present in our reaction. For this experiment, complex **1** is dissolved in CH_2Cl_2 and ^{19}F NMR is measured at 100 °C. The result shows that there is no variation in the ^{19}F NMR signals (Figure 94), and no new species appear in solution, so the equilibrium is strongly shifted towards the monomeric species, and it is assumed that it does not act in our reaction.

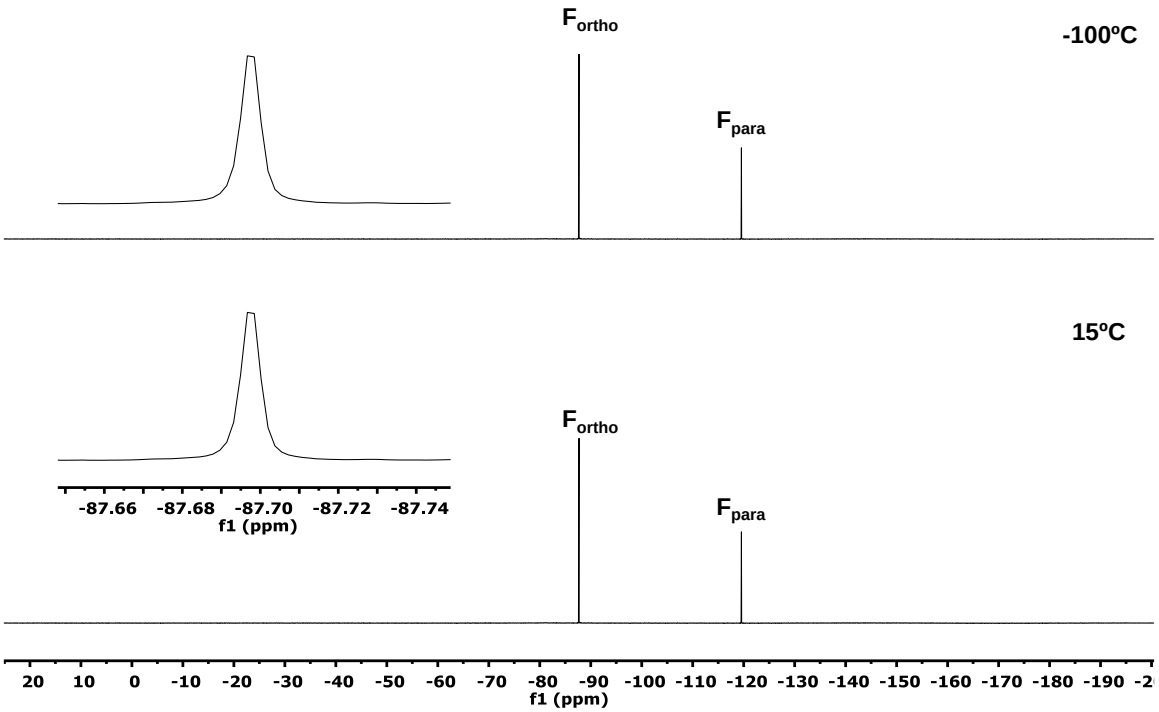

Figure 94. ^{19}F NMR of complex 1 at 15 °C (bottom) and -100 °C (up) in CH_2Cl_2. $[\mathbf{1}]_0$ = 0.041 mol L^{-1}.

Transmetalation between trans-[PdCl(Rf)(AsPh$_3$)$_2$] and [Cu(Pf)(DPI)] in presence of NH$_4$Cl.

Due to the possibility of the presence of chloride anions in the reaction, which may come from the chlorinated solvents, the following experiment is carried out to check whether these anions may be having any influence. The transmetalation reactions was carried out in CH_2Cl_2 or $CHCl_3$, which may contain traces of chloride anions. This experiment aimed to test whether the reaction rate depends or not on the presence of chloride. Therefore, the reaction was carried out adding a certain amount of these anions.

The transmetalation experiment was carried out between the complex *trans*-[PdCl(Rf)(AsPh$_3$)$_2$] (0.040 mol L^{-1}), [Cu(Pf)(DPI)] (0.041 mol L^{-1}) and 5% of NH_4Cl at 285 K in dry CH_2Cl_2. We observed in ^{19}F NMR that the transmetalation does not undergo any variation in the reaction rate with respect to the reaction without NH_4Cl at 2 hours. In summary, the reaction pathway was not been affected by de presence of chloride anions.

Summary and conclusions of the transmetalation step in Cu/Pd systems.

The reaction between the *trans*-[PdCl(Rf)($AsPh_3$)$_2$] complex and the [Cu(Pf)(DPI)] complex shows an expected complexity mixture of products. The transmetalation reaction generates the complex with configuration exchange *cis*-[Pd(Pf)(Rf)($AsPh_3$)$_2$]. Different isomerization/aryl exchange reactions are generated within the reaction. Kinetic and data analysis results as well as kinetic simulations allow us to confirm different steps within the overall reaction.

1) The transmetalation occurs with an isomerization reaction. This process is important when designing catalytic reactions because the reductive elimination step can only be carried out from *cis* arrangement.

2) The first step of the reaction is the displacement of the $AsPh_3$ ligand from the Pd complex by the Cu complex. This process occurs in a single step. Its existence is confirmed by kinetic experiments with different amounts of free ligand and kinetic fits supporting these results.

3) It is shown that Cu complexes are able to catalyse *cis/trans* isomerization in Pd complexes due to transmetalation and aryl exchange processes.

4) The transmetalation rate between the Cu and Pd complexes of the system studied, demonstrates that Pd/Cu catalytic systems are a real alternative to traditional bimetallic systems, not only increasing the transmetalation rate, but also being a more economical alternative, as it can be used catalytically, and safer.

The transmetalation step in Ag/Pd systems.

Stoichiometric Reaction

The stoichiometric reaction between the *trans*-[PdCl(Rf)($AsPh_3$)$_2$] (**1**) complex and the [Ag(Pf)(DPI)] (**2-Ag**) complex (DPI = diphenylimidazole) (Scheme 33) shows the same behaviour as in the case of copper, but with some differences.

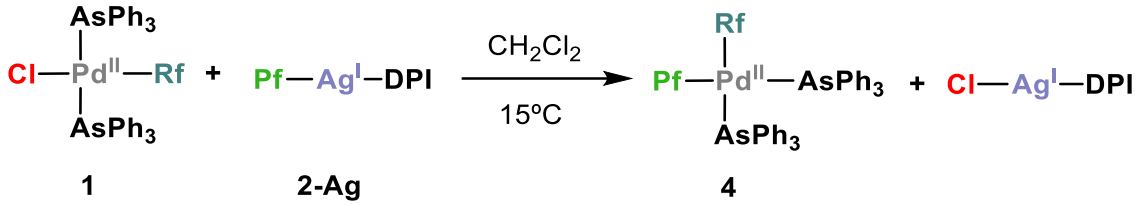

Scheme 33. Reaction model for the transmetalation between **2-Ag** and **1**.

As we observe in Figure 95, the main product characterized as *cis*-[Pd(Rf)(Pf)($AsPh_3$)$_2$] again has the same characteristics as in the transmetalation step in Cu/Pd systems. This complex, as we have already seen, evolves to its more stable trans isomer. Thanks to previous investigations,[246,245] and with the experiments carried out in this systems, the formation of the complexes cis/trans-[Pd(Pf)(Rf)($AsPh_3$)$_2$](**4** and **5**), cis/trans-[Pd(Pf)$_2$($AsPh_3$)$_2$](**6** and **7**) and cis/trans-[Pd(Rf)$_2$($AsPh_3$)$_2$] (**8** and **9**) corresponding to the transmetalation reaction, and successive retro-transmetalations, have been observed.

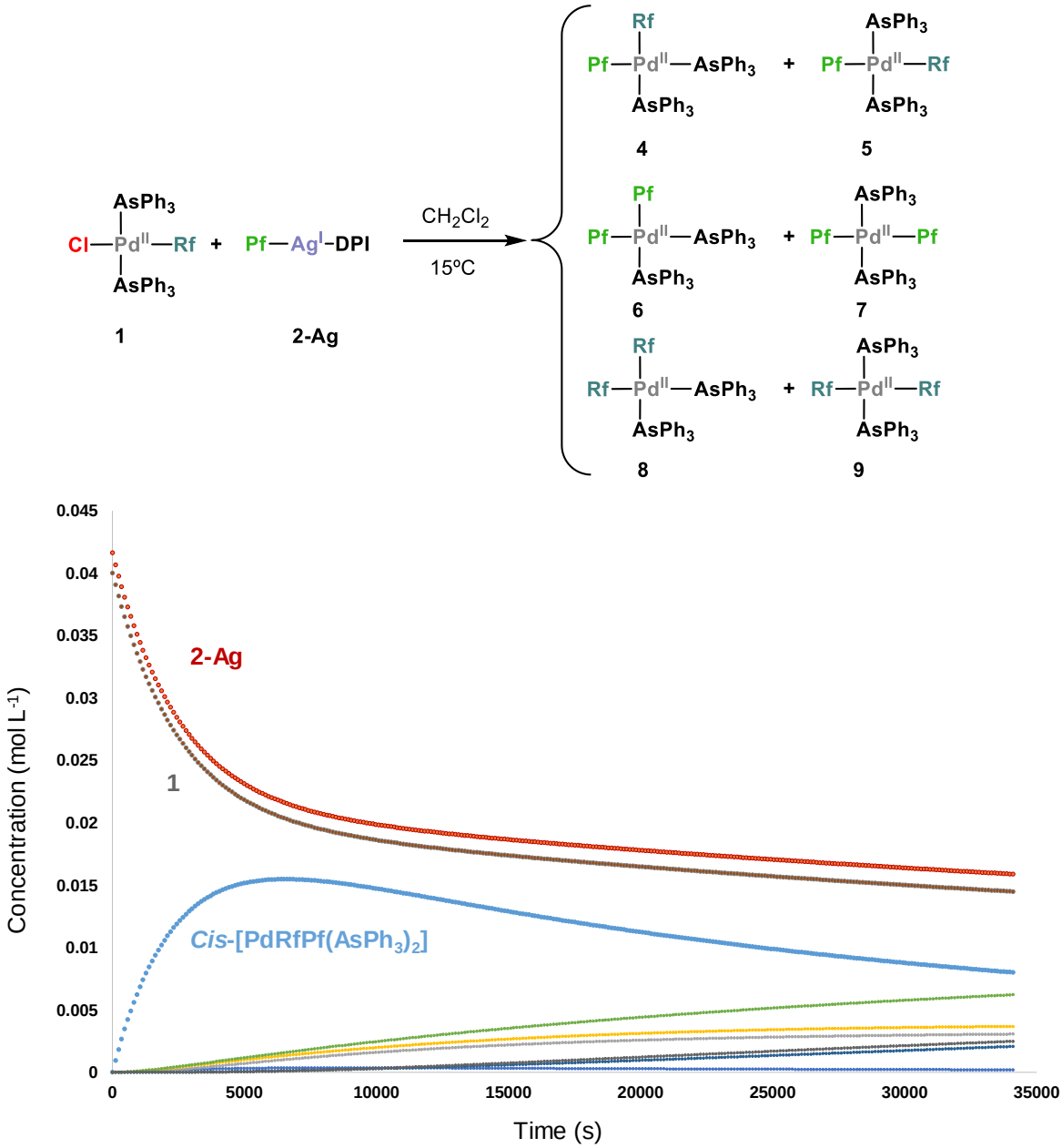

Figure 95. Concentration vs time plot of experimental data obtained by ^{19}FNMR monitoring of the stoichiometric reaction between *trans*-[PdCl(Rf)($AsPh_3$)$_2$] (**1**) [**1**]$_0$ = 0.040 mol L^{-1} complex and the [AgPf(DPI)] (**2-Ag**) [**2-Ag**]$_0$ = 0.0420 mol L^{-1} complex in dry CH_2Cl_2 at 15 °C. Grey **1**, Blue *cis*-[Pd(Pf)(Rf)($AsPh_3$)$_2$] (**4**), Green *trans*-[Pd(Pf)(Rf)($AsPh_3$)$_2$] (**5**), Yellow *cis*-[Pd(Pf)$_2$($AsPh_3$)$_2$] (**6**), Light Grey *cis*-[Pd(Rf)$_2$($AsPh_3$)$_2$] (**7**), Purple *trans*-[Pd(Pf)$_2$($AsPh_3$)$_2$] (**8**), Dark blue *trans*-[Pd(Rf)$_2$($AsPh_3$)$_2$] (**9**).

Interestingly, the concentration of this intermediate in solution is lower in the case of using Ag as a transmetalating agent than in the case of Cu. A possible explanation is that the reaction that makes **2-Ag** disappear (isomerization process) is faster. As we have commented in the previous case, these isomerization processes in Pd square-planar complexes are slow at room temperature, so at the reaction

temperature (15 ˚C) it is impossible for it to be a spontaneous isomerization, *i.e.*, it must be catalysed by the Ag complex. Moreover, the decrease of the concentration by half of the reactants requires approximately 5000 s in the case of silver, compared to approximately 2000 s in the case of copper. This allows us to conclude at first sight that the transmetalation reaction is slower in the case of silver than in the case of copper, but that the isomerization reaction of the *cis*-[Pd(Rf)(Pf)($AsPh_3$)$_2$] complex is faster in the case of silver than in the case of copper.

The secondary reactions of aryl exchange and isomerization follow the same pattern as in the previous case, which is in agreement with the similar reactivity of both metals.

For a more exhaustive comparison, a kinetic fit is made using the same model as in the case of transmetalation with aryl-copper derivatives, which will allows a discussion of the reactivity of both metals.

Kinetic Analysis

Using the same kinetic profile as in the case of copper, a non-linear kinetic fitting is made for the case of silver with the experimental data obtained so far, as shown in Figure 96. As we can see, the model used for the fitting fits with the experimental data, as in the previous case.

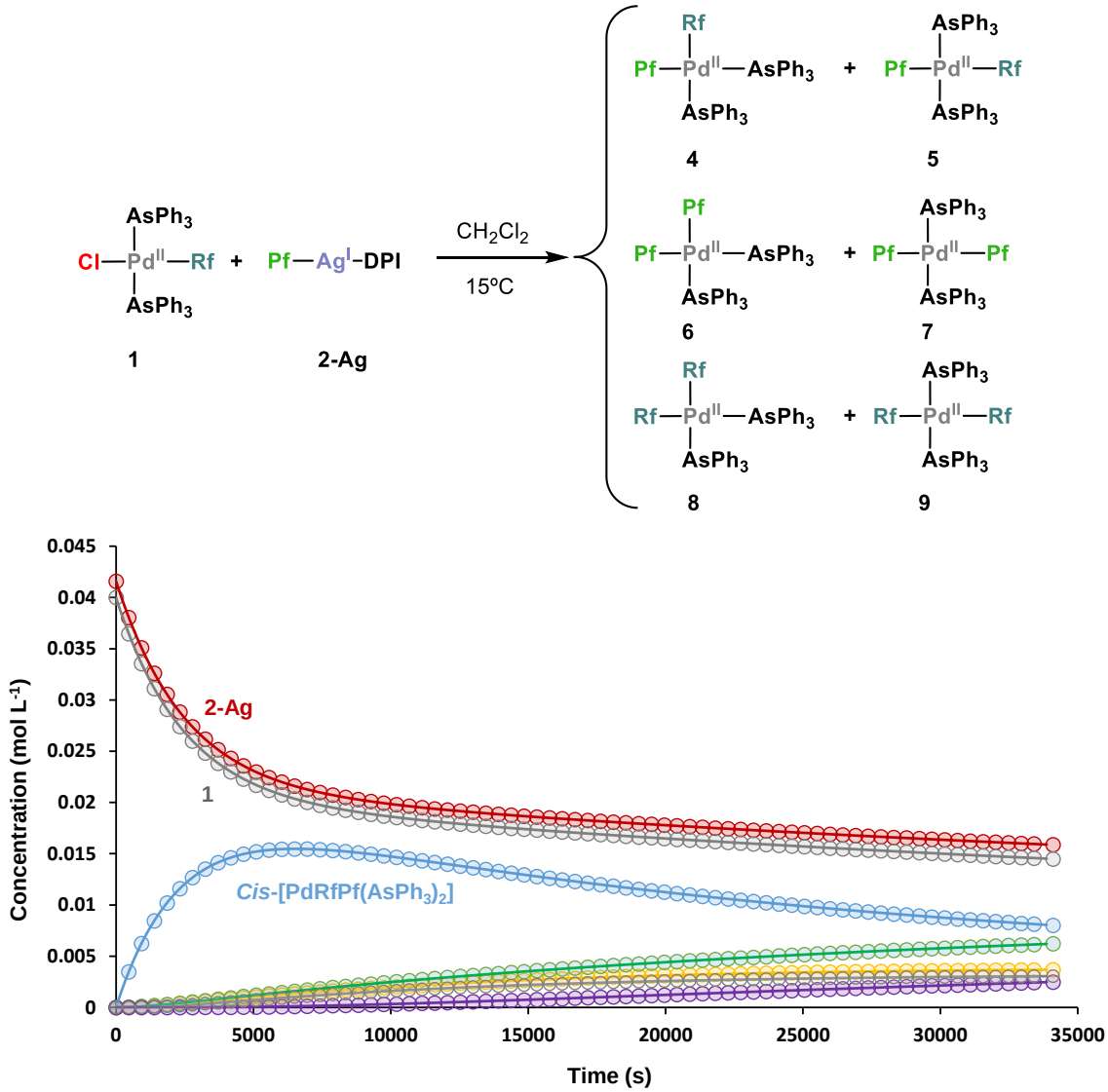

Figure 96. Concentration vs time plot of experimental data (dots) obtained by ^{19}FNMR monitoring and COPASI-fitted values (continuous lines) of the fluorinated-species in the transmetalation step and aryl exchange/retro-transmetalations between **1** and [**2-Ag**]. Color code: Red **2-Ag,** Grey **1**, Blue *cis*-[Pd(Pf)(Rf)(AsPh$_3$)$_2$] (**4**), Green *trans*-[Pd(Pf)(Rf)(AsPh$_3$)$_2$] (**5**), Yellow *cis*-[Pd(Pf)$_2$(AsPh$_3$)$_2$] (**6**), Light Grey *cis*-[Pd(Rf)$_2$(AsPh$_3$)$_2$] (**8**), Purple *trans*-[Pd(Pf)$_2$(AsPh$_3$)$_2$] (**7**).

Two types of kinetic models have been used to study the transmetalation step and the subsequent isomerization and retro-transmetalations. The first one, as in the case of Cu, tries to add as many reactions as possible that can take place. As we

can see, the simulated values are in good agreement with the experimental ones. The complete model is shown in the Scheme 34:

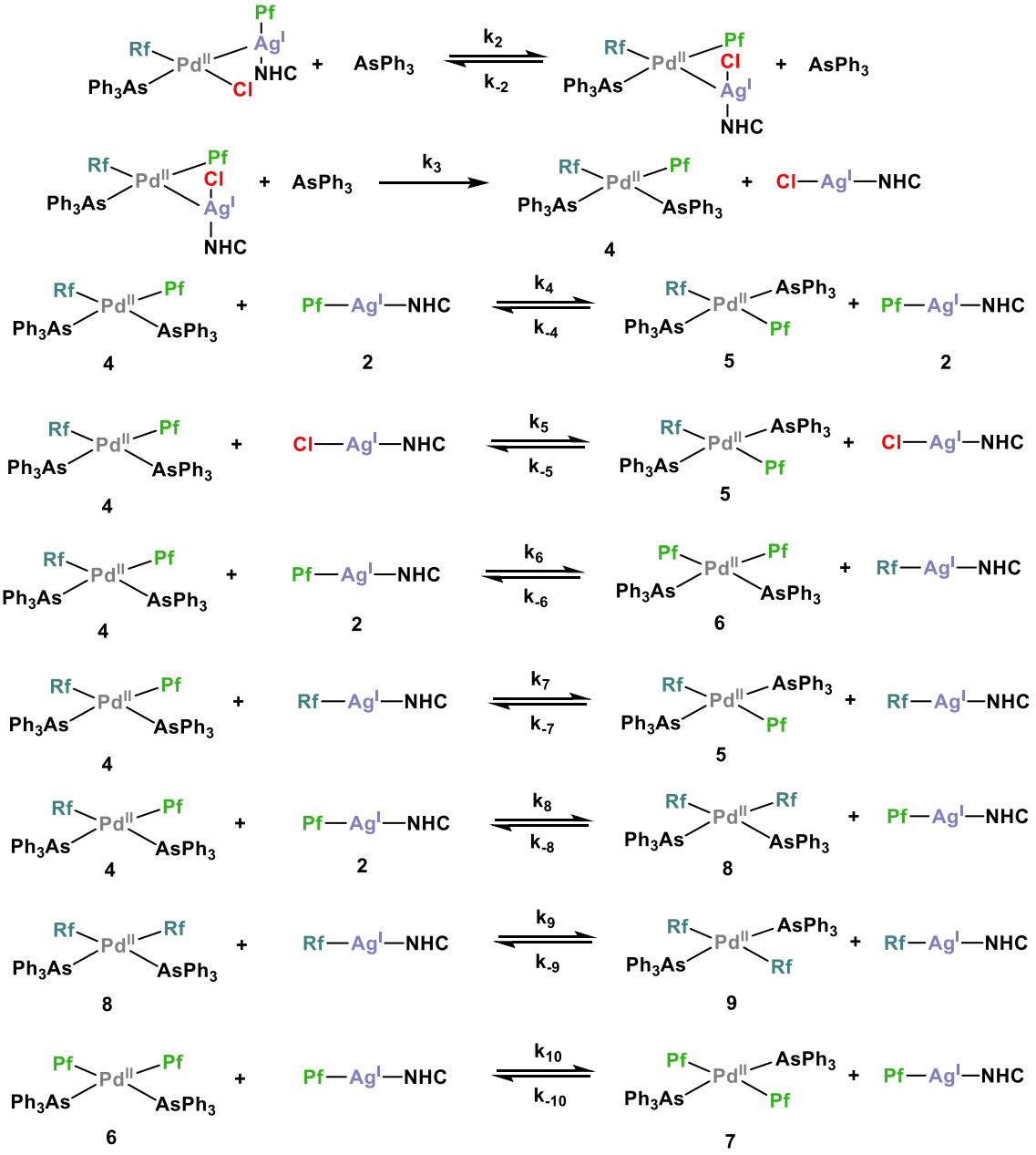

Scheme 34. Kinetic model used for the non-linear fitting shown in Figure 96. NHC represents diphenylimidazole.

On the other hand, for a more precise discussion of the comparison between the two metals, the simplified system has been used, which again also adjusts the experimental values. The results obtained for this adjustment are shown in the Table 32:

Reaction	Parameter	Value ($s^{-1}Lmol^{-1}$)	Std. Deviation
t-[Pd(Rf)Cl($AsPh_3$)$_2$ + [Ag(Pf)(DPI)] = c-[Pd(Rf)(Pf)($AsPh_3$)$_2$] + [AgCl(DPI)]	k_1	5.00E-03	3.9E-08
	k_{-1}	5.51E-03	5.9E-08
c-[Pd(Rf)(Pf)($AsPh_3$)$_2$]+ [Ag(Pf)(DPI)] -> t-[Pd(Rf)(Pf)($AsPh_3$)$_2$]+ [Ag(Pf)(DPI)]	k_2	8.03E-04	2.3E-09
c-[Pd(Rf)(Pf)($AsPh_3$)$_2$]+ [Ag(Pf)(DPI)] -> c-[Pd(Pf)$_2$($AsPh_3$)$_2$] + [Ag (Rf)(DPI)]	k_3	7.43E-04	1.3E-09
c-[Pd(Pf)$_2$($AsPh_3$)$_2$] + [Ag(Pf)(DPI)]-> t-[Pd(Pf)$_2$($AsPh_3$)$_2$] + [Ag(Pf)(DPI)]	k_4	1.36E-03	4.4E-09
t-[Pd(Rf)(Pf)($AsPh_3$)$_2$] + [Ag(Rf)(DPI)] = c-[Pd(Rf)$_2$($AsPh_3$)$_2$]+ [AgCl(DPI)]	k_{-4}	3.32E-02	1.6E-07
	k_5	1.00E-06	1.4E-08
c-[Pd(Rf)$_2$($AsPh_3$)$_2$]+ [Ag(Rf)(DPI)] -> t-[Pd(Rf)$_2$($AsPh_3$)$_2$] + [Ag(Rf)(DPI)]	k_6	1.30E-01	5.1E-07

Table 32. Complete kinetic model, summarizing the plausible reaction pathways, to explain the transmetalation step between **1** and **2-Cu** and fitted rate constants with their respective standard deviations.

As we can see by comparing the two settings, the difference between the direct constants of the transmetalation step is practically of an order of magnitude, which would imply a difference of practically 1 kcal mol^{-1} in the energy of the process. On the other hand, the transmetalation equilibrium is much more displaced in the case of Cu (k_1 = 1.11 x 10^{-2} $s^{-1}Lmol^{-1}$ and k_{-1} = 5.53 x 10^{-3} $s^{-1}Lmol^{-1}$) than in the case of silver. On the other hand, the constants for the rest of the processes are very similar, thus confirming that silver also effectively catalysed isomerization in these Pd(II) complexes. As already mentioned, this is of vital importance when perfecting catalytic systems, either Cu/Pd or Ag/Pd.

a) <u>Kinetic order with respect to the silver complex.</u>

The transmetalation reaction is first-order in **2-Ag** as shown in Figure 97. The plot of ln(*r0*) *vs.* ln([**2-Ag**]) is a straight line with slope 0.98. Therefore, the transmetalation rate is proportional to the concentration of **2-Ag**.

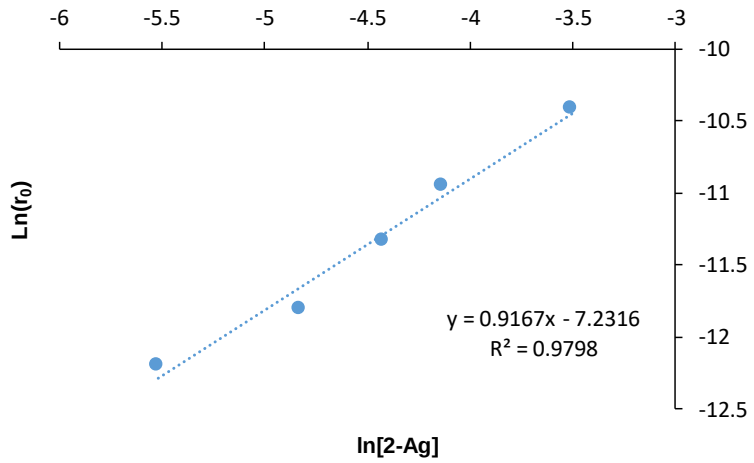

Figure 97. Effect of [**2-Ag**] on the transmetalation of trans-[Pd($C_6Cl_2F_3$)Cl($AsPh_3$)$_2$] (**1**) in CH_2Cl_2 at 15 °C. r_0 is the initial transmetalation rate.

b) Retardation by addition of $AsPh_3$.

The presence of added $AsPh_3$ retards the transmetalation reaction between **1** and **2-Ag**. The kinetic law suggests minus first order with respect to the concentration of $AsPh_3$ (the plot of ln(*r*0) *vs.* ln[$AsPh_3$] added is a straight line with slope -0.91). Thus, it can be concluded that the self-dissociation of $AsPh_3$ in the starting complexes is not taking place or, at least, it has not kinetic consequences in the mechanism of the reaction. As commented in the last case, the minus first order with respect to the concentration of $AsPh_3$ implies that the energy profile consists of several stages. One of them involves the dissociation or exchange of the $AsPh_3$ group for the **2-Ag** complex, and that this stage is not the rate limiting step of the reaction.

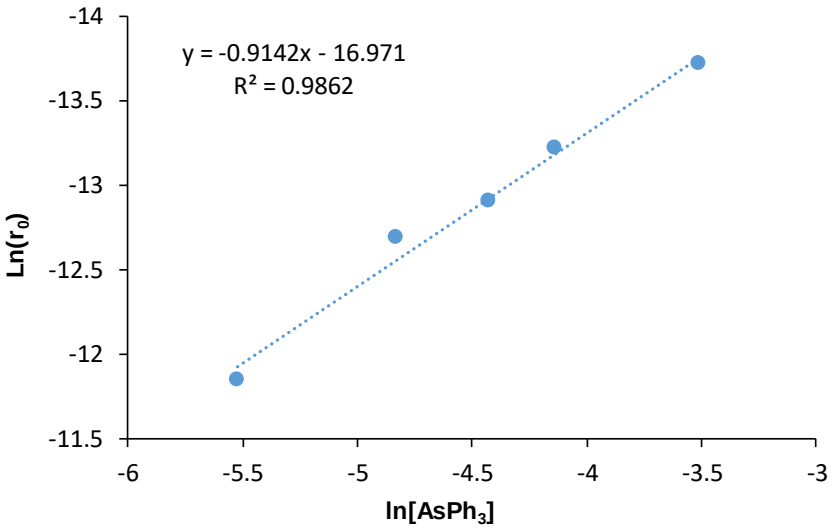

Figure 98. Effect of free $AsPh_3$ on the transmetalation of [**2-Ag**] and *trans*-[PdCl(Rf)($AsPh_3$)$_2$] (**1**) in CH_2Cl_2 at 15 °C. r_0 is the initial transmetalation rate.

Summary and Conclusions of the transmetalation Step in Ag/Pd systems.

The transmetalation reaction generates the complex with configuration *cis*-[Pd(Rf)(Pf)($AsPh_3$)$_2$], Different isomerization/aryl exchange reactions are generated within the reaction. Kinetic and data analysis results as well as kinetic simulations allow us to confirm different stages within the overall reaction.

1) The transmetalation occurs with an isomerization reaction. This process is important when designing catalytic reactions because the reductive elimination step can only be carried out from *cis* arrangement.

2) The first step of the reaction is the displacement of the $AsPh_3$ ligand from the Pd complex by the Ag complex. This process occurs in a single step. Its existence is confirmed by kinetic experiments with different amounts of free ligand and kinetic fits supporting these results.

3) It is shown that Ag complexes are able to catalyses *cis/trans* isomerization in Pd complexes due to transmetalation and aryl exchange processes.

Evaluation and conclusions of transmetalation step using a Cu/Pd and Ag/Pd systems.

The transmetalation step between the **2-Cu** and **2-Ag** complex to the *trans*-[PdCl(Rf)($AsPh_3$)$_2$] organometallic complex has similarities and differences. In both cases the reaction produces the same *cis*-[Pd(Rf)(Pf)($AsPh_3$)$_2$] complex with geometry exchange. The formation of this complex reflects that the thermodynamics of the reaction between complexes **2** and **1** is favourable. Moreover, the stereocontrol of the reaction is governed by the position of the exiting ligand, in this case $AsPh_3$. The incoming **2-Cu** or **2-Ag** complex replaces the ligand, and through a 4-centre transition state generates the isomer with configuration exchange.

Interestingly, although the thermodynamics of the process are favourable, the reaction is an equilibrium shifted slightly toward the products, leading to the fact that the disappearance of the reactant **2-Cu** or **2-Ag** is not observed until long times. Moreover, analysing the kinetic profiles, we observe that the thermodynamics of the transmetalation is more favourable for Cu than for Ag, due to the accumulation of the intermediate *cis*-[Pd(Rf)(Pf)($AsPh_3$)$_2$]. These results agree with the kinetic data obtained from copasi software. The values for the transmetalation process, considered a reversible stage, are for the Cu case ($k_1 = 1.11x10^{-2}\ s^{-1}$ and $k_{-1} = 5.53x10^{-3}\ s^{-1}$) and for the Ag case ($k_1 = 5.00x10^{-3}\ s^{-1}$ and $k_{-1} = 5.51x10^{-3}\ s^{-1}$), which shows that the equilibrium in the copper case is much more shifted than in the silver case.

On the other hand, the kinetics effect of the reaction also shows a clear predominance in the case of **2-Cu**, which rate constant for the direct step of transmetalation is higher than in the case of **2-Ag**. This is in agreement with the value of the kinetic constants. The transmetalation step between **1** and **2-Cu** ($k_2 = 1.11x10^{-2} \pm 1.15x10^{-5}\ s^{-1}$) has an energetic barrier about 20 kcal mol^{-1}. On the other hand, the transmetalation step between **1** and **2-Ag** ($k_2 = 5.00x10^{-3} \pm 3.9x10^{-8}\ s^{-1}$) has an energetic barrier about 21 kcal mol^{-1}. Although the kinetic differences are not very large between the two metals, there are significant differences in other areas. Ag(I) organometallic complexes are considerably more expensive, and equally sensitive to moisture and oxygen as their Cu(I) counterparts. In addition, they are usually photosensitive complexes, and often undergo redox processes, which can

impair the outcome of our reaction. On the other hand, as mentioned in the introduction, the speciation of Ag(I) complexes can be very complex, especially in some systems. Therefore, copper catalytic systems are considered to be a much more attractive alternative to the silver counterparts.

Additionally, both complexes are able to efficiently catalyse the cis/trans isomerization of the Pd^{II} complexes involved in the process, generating all possible species in solution.[246]

The transmetalation step in Au/Pd systems.

The stoichiometric reaction between the *trans*-[PdCl(Rf)($AsPh_3$)$_2$] (**1**) complex and the [Au(Pf)(DPI)] (**2-Au**) complex (DPI = diphenylimidazole) shows a completely different behavior from the two previous ones. First of all, the reaction cannot be carried out at 15 °C in CH_2Cl_2 as in the previous cases, but it is necessary to heat up to 50 °C and change the solvent to $CHCl_3$. On the other hand, as we see in Figure 99, the kinetic profile is very different. The appearance of the *cis*-[Pd(Rf)(Pf)($AsPh_3$)$_2$] complex is not seen at any time. However, the complex that appears is the *trans*-[PdCl(Pf)($AsPh_3$)$_2$], *i.e.*, the aryl exchange complex.

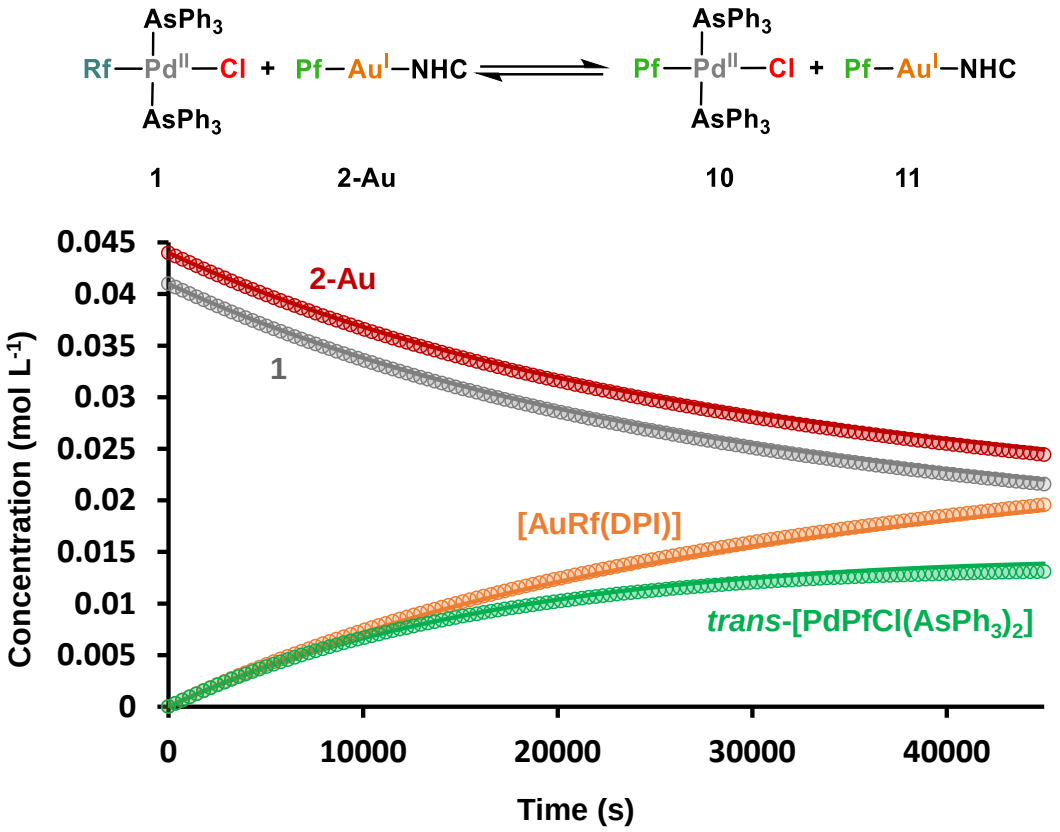

Figure 99. Concentration vs time plot of experimental data obtained by ^{19}FNMR monitoring of the stoichiometric reaction between *trans*-[PdCl(Rf)($AsPh_3$)$_2$] (**1**) [**1**]$_0$ = 0.041 mol L^{-1} complex and the [Au(Pf)(DPI)] (**2-Au**) [**2-Au**]$_0$ = 0.045 mol L^{-1} complex in dry CH_3Cl at 323 K. Color code : Light Grey (**1**), Red (**2-Au**), Orange (**11**) and Green (**10**).

As we can observe, the disappearance of the reagents is slow at 323 K. This reaction produces the aryl exchange complexes, leading to the formation of the [Au(Rf)(DPI)] complex (orange dots), and *trans*-[Pd(Pf)Cl($AsPh_3$)] (green dots).

At first sight, these results fit with the thermodynamics expected for this system, which have already been previously studied.[245,246] As mentioned in the introduction, the gold complex prefers to exchange the aryl rather than give the classical transmethylation step, due to the thermodynamics of the system marked by the formation of the Pd−C and Au−X bonds. Interestingly, as a result of the aryl exchange reaction the complex formed is *trans*-[PdCl(Pf)($AsPh_3$)]. This result is not uncommon due to the notorious difference in the stability of the cis/trans isomers.[246] This implies that the mechanism can go through a 4-member transition state between the two aryls, with or without Pd−Au interactions, as in the previous cases, but the cis product is not detected. This process could be catalysed by gold complex or not, because the spontaneous isomerization process should be fast al 323 K.

In the same way as in the previous cases, different stoichiometric experiments are carried out to try to determine some of the step of the mechanism.

Furthermore, the **2-Au** complex is able to catalyses the isomerization of Pd complexes with cis-configuration (kinetic products) to trans-configuration (thermodynamic products) as previously commented. [246]

a) *Kinetic order on the gold complex.*

The transmetalation reaction is first-order in **[2-Au]**. The plot of ln(*r0*) *vs.* ln([**2-Au**]) is a straight line with slope 0.93. Therefore, the transmetalation rate is proportional to the concentration of [**2-Au**].

b) *Retardation by addition of $AsPh_3$.*

The presence of added $AsPh_3$ retards the aryl exchange reaction between **1** and **2-Au** using the same methodology as in the copper and silver cases. The kinetic law show-minus first order with respect to the concentration of $AsPh_3$ (the plot of ln(*r*0) *vs.* ln[$AsPh_3$] added is a straight line with slope -0.90) represented in Figure 100. Thus, it can be concluded that the self-dissociation of $AsPh_3$ in the starting complexes is not taking place or, at least, it has not kinetic consequences in the mechanism of the reaction. As commented in the last cases, the minus first order with respect to the concentration of $AsPh_3$ implies that the energy profile consists of

several steps. One of them involves the dissociation or exchange of the $AsPh_3$ group for the **2-Au** complex, and that this stage is not the rate limiting step of the reaction, in agreement with the other metals.

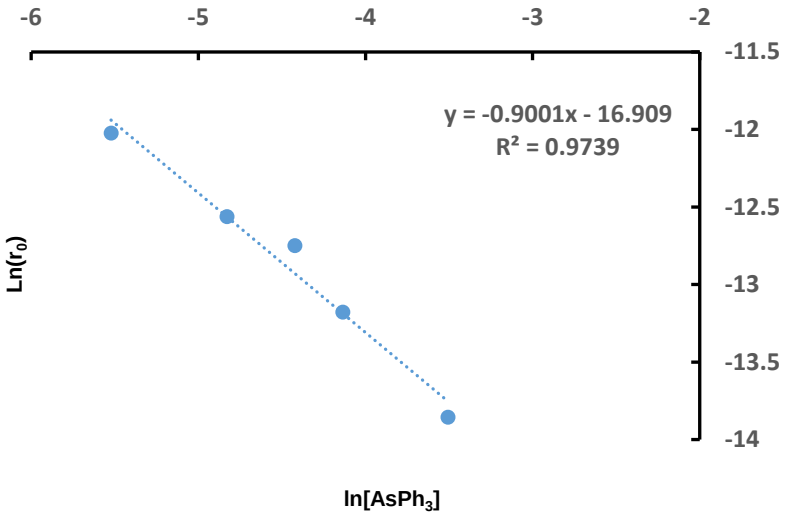

Figure 100. Effect of free $AsPh_3$ on the aryl exchange of [**2-Au**] and trans-[$Pd(C_6Cl_2F_3)Cl(AsPh_3)_2$] (**1**) in CH_2Cl_2 at 50 °C. r_0 is the initial transmetalation rate.

Kinetic Analysis.

The kinetic results obtained by ^{19}F nuclear magnetic resonance, and the additional experimental data allow us to make a mechanistic proposal and try to fit it by Copasi kinetic simulator, as we can see in Figure 101.

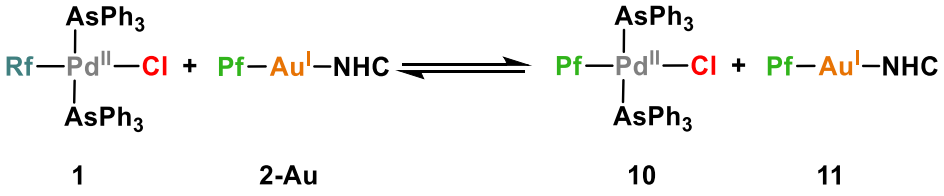

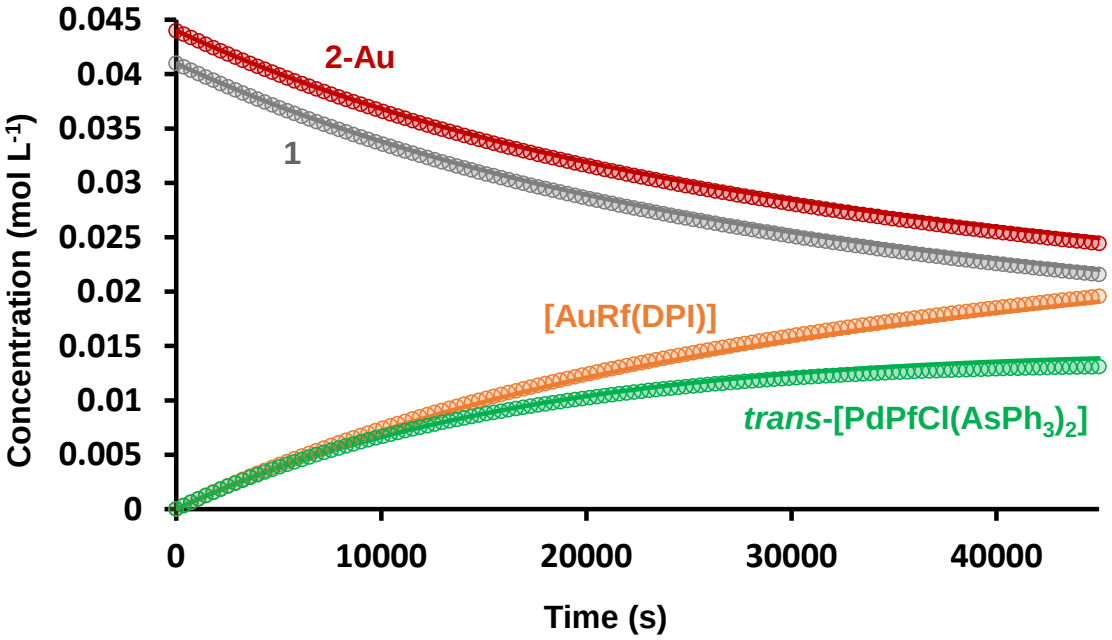

Figure 101. Concentration vs time plot of experimental data obtained by ^{19}FNMR and COPASI-fitted values (continuous lines) monitoring of the stoichiometric reaction between *trans*-[PdCl(Rf)(AsPh$_3$)$_2$] (**1**) [**1**]$_0$ = 0.041 mol L^{-1} complex and the [AuPf(DPI)] (**2-Au**) [**2-Au**]$_0$ = 0.045 mol L^{-1} complex in dry CH$_3$Cl at 323 K.

As we can see in Figure 101, the experimental results and the kinetic model using the copasi software fits well, which allows us to assume that the associated mechanistic proposal is correct, or at least close to reality. For this fitting, the following reactions have been used. It is important to emphasize that this is a simplification of the system, and that not all reactions that can coexist have been considered (Scheme 35).

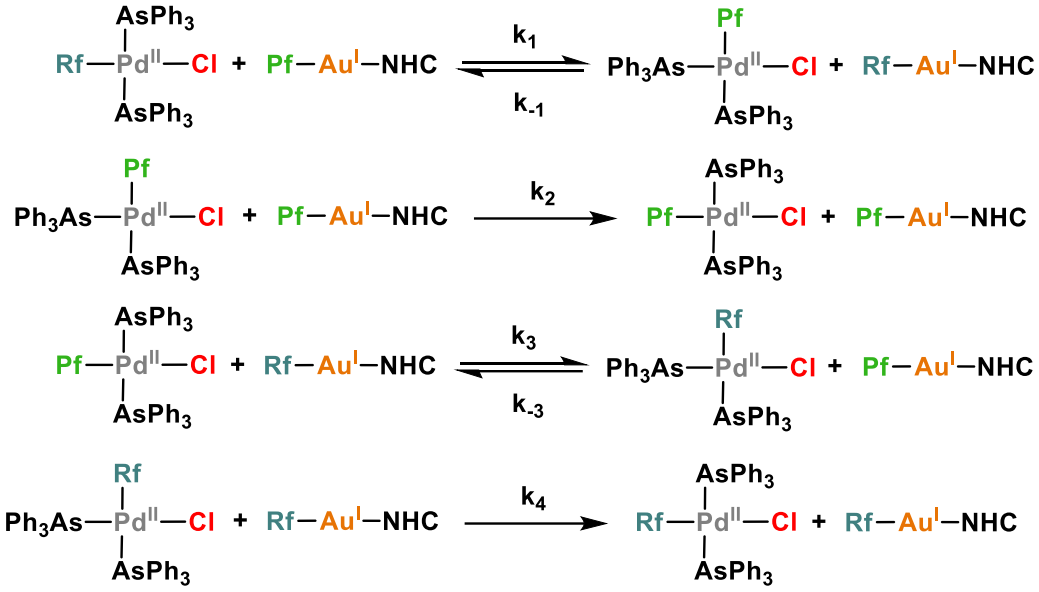

Scheme 35. Kinetic model using for the non-linear fitting shown in Figure 101.

The kinetic fit was satisfactory, as we can observe in the following table, and allows us to affirm that the ligand displacement is a real and explainable step in this reaction, and that it is not the rate limiting step of the process, as has been previously demonstrated. The complete kinetic model is summarized in Table 33:

Reaction	Parameter	Value($s^{-1}Lmol^{-1}$)	Std. Deviation
t-[Pd(Rf)Cl($AsPh_3$)$_2$+ [Au(Pf)(DPI)] = c-[Pd(Pf)Cl($AsPh_3$)$_2$ + [Au(Rf)(DPI)]	k_1	4.11E-04	1.3E-08
	k_{-1}	4.89E-04	1.1E-07
c-[Pd(Pf)Cl($AsPh_3$)$_2$ + [Au(Rf)(DPI)] -> t-[Pd(Rf)Cl($AsPh_3$)$_2$ + [Au(Pf)(DPI)]	k_2	1.01E+00	8.3E-04
t-[Pd(Rf)Cl($AsPh_3$)$_2$+ [Au(Rf)(DPI)] = c-[Pd(Rf)Cl($AsPh_3$)$_2$ + [Au(Pf)(DPI)]	k_3	4.83E-04	1.8E-09
	k_{-3}	2.01E-04	9.1E-06
c-[Pd(Rf)Cl($AsPh_3$)$_2$ + [Au(Rf)(DPI)] -> t-[Pd(Rf)Cl($AsPh_3$)$_2$+ [Au(Rf)(DPI)]	k_4	6.21E-04	4.2E-08

Table 33. Complete kinetic model, summarizing the plausible reaction pathways, to explain the reaction between **1** and **2-Au** and Fitted rate constants with their respective Standard deviations.

As a result, a value of $k_1 = 4.11x10^{-4} \pm 1.3x10^{-8}$ s^{-1} L mol^{-1} ($\Delta G^{\ddagger}_{323} \approx 24$ kcal mol^{-1}) is obtained, exceeding by more than 4 kcal mol^{-1} the values obtained for Cu and Ag in the simplified kinetic model.

On the other hand, using the information obtained from the simplified kinetic model, a more complete model can be examined, as we can see in Scheme 36, including the ligand substitution between the organometallic complex **2-Au** and the palladium complex **1**.

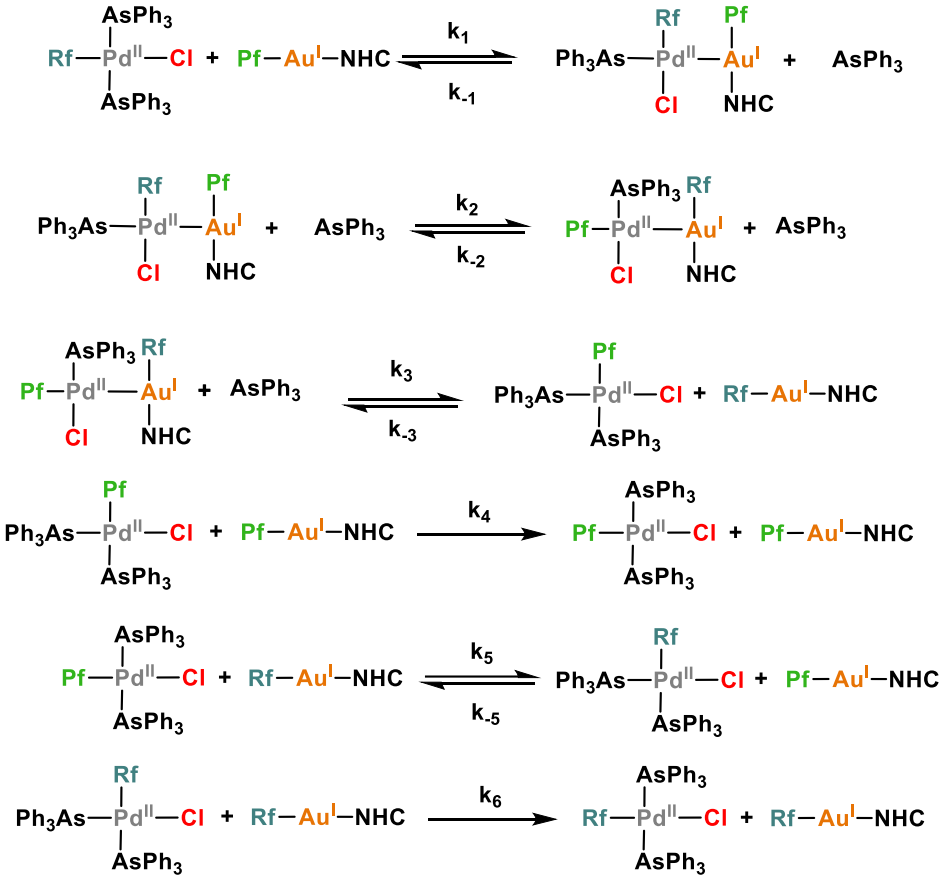

Scheme 36. Kinetic model using for the non-linear fitting shown in Figure 102.

As we can see in the Figure 102, and in the following table (Table 34), these results are consistent with the mechanistic proposal.

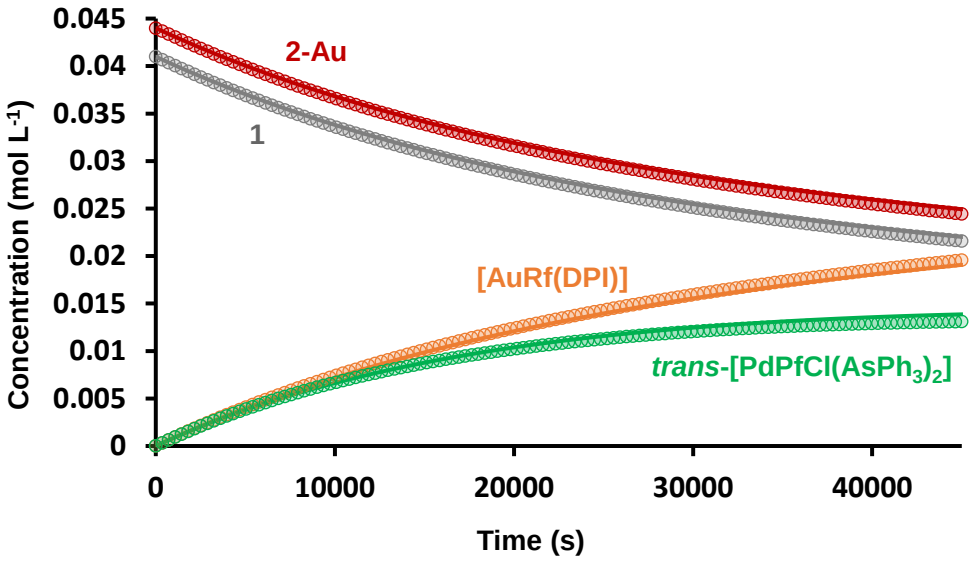

Figure 102. Concentration vs time plot of experimental data obtained by ^{19}FNMR and COPASI-fitted values (continuous lines) monitoring of the stoichiometric reaction between *trans*-[PdCl(Rf)(AsPh$_3$)$_2$] (**1**) [**1**]$_0$ = 0.041 mol L^{-1} complex and the [AuPf(DPI)] (**2-Au**) [**2-Au**]$_0$ = 0.045 mol L^{-1} complex in dry CH$_3$Cl at 323 K.

Reaction	Parameter	Value ($s^{-1}Lmol^{-1}$)	Std. Deviation
t-[Pd(Rf)Cl(AsPh$_3$)$_2$]+ [Au(Pf)(DPI)] = c-[Pd(Rf)(Cl)(AsPh$_3$)Au(Pf)] + AsPh$_3$	k_1	4.14E-04	2E-06
	k_{-1}	5.09E-04	4E-05
= c-[Pd(Rf)(Cl)(AsPh$_3$)Au(Pf= c-[Pd(Pf)(Cl)(AsPh$_3$)Au(Rf)]	k_2	1.69E-03	1E-04
	k_{-2}	6.33E-04	6E-05
c-[Pd(Pf)(Cl)(AsPh$_3$)Au(Rf)]+ AsPh$_3$ = c-[Pd(Pf)Cl(AsPh$_3$)$_2$] + [Au(Rf)(DPI)]	k_3	1.01E+02	5E+00
	k_{-3}	2.59E-06	1E-07
c-[Pd(Pf)Cl(AsPh$_3$)$_2$] + [Au(Pf)(DPI)] -> t-[Pd(Pf)Cl(AsPh$_3$)$_2$+ [Au(Pf)(DPI)]	k_4	9.97E+01	4E+02
t-[Pd(Pf)Cl(AsPh$_3$)$_2$]+ [Au(Rf)(DPI)] = t-[Pd(Rf)Cl(AsPh$_3$)$_2$]+ [Au(Pf)(DPI)]	k_5	4.86E-04	1E-07
	k_{-5}	1.46E-05	1E-06
c-[Pd(Rf)Cl(AsPh$_3$)$_2$] + [Au(Pf)(DPI)] -> t-t-[Pd(Pf)Cl(AsPh$_3$)$_2$] + [Au(Rf)(DPI)]	k_6	5.86E-04	1E-05

Table 34. Kinetic model for the aryl exchange between *trans*-[PdCl(Rf)(AsPh$_3$)$_2$] (**1**) and [Au(Pf)(DPI)] (**2-Au**).

With the results obtained, we can see that the mechanism initially proposed is confirmed. First, an equilibrium would occur where the **2-Au** organometallic complex would displace a triphenylarsine ligand. This equilibrium is not very displaced and would be one of the slow steps of the reaction, its direct kinetic barrier

being 4.14 x 10^{-4} ± 3 x 10^{-6} s^{-1}, to give a complex with cis arrangement. This complex would undergo aryl exchange, which is likely to be determined by a 4-membered transition state, with a direct kinetic barrier of 1.69 x 10^{-3}± 1 x 10^{-4} s^{-1}.

The complex with cis-fluorinated aryl exchange would rapidly isomerization process, catalysed or not by a gold complex, to give the much more stable trans isomer, which is the one detected by ^{19}F NMR. Although it has already been mentioned above that gold complexes are able to catalyses cis-trans isomerization in Pd(II) complexes, in this case, the reaction may or may not be catalysed, as the spontaneous isomerization of cis-trans in the *cis*-[Pd Cl(Pf)($AsPh_3$)$_2$] complex will be relatively fast at 323 K.[253]

These kinetic results are comparable to the data obtained by our group in previously investigations of gold-catalysed aryl exchange or isomerization process in Pd(II) complexes.[245,246]

c) *DFT calculations.*

All computational results in this chapter have been carried out by Prof. Rosana Álvarez of the University of Vigo. Preliminary computational calculations allow us to understand some elementary steps in this reaction. First of all, as we can observed in Figure 103, an adduct is formed between the two complexes, with the two metals in apical position, whose energy would be 17.3 kcal mol^{-1}. This apical position, was computed in some research previously, generating good results in the overall energy of the process. [245,246,254]

This intermediate ***I1***, evolves through a low-energy process to another intermediate ***I2***, where the gold complex is placed almost perpendicular to the Pd coordination plane, as we can see in Figure 103.

[253] Casado, A. L.; Espinet, P. On the Configuration Resulting from Oxidative Addition of RX to Pd(PPh_3)$_4$ and the Mechanism of the Cis-to-Trans Isomerization of [PdRX(PPh_3)$_2$] Complexes (R) Aryl, X)Halide) . *Organometallics* **1998**, *17*, 954–959. DOI: 10.1021/om9709502.

[254] Aryl, R.; Sc, L. H.; Casado, A. L.; Espinet, P.: Mechanism of the Gold (I) -Catalyzed. *Organometallics* **1998**, *7333*, 3677–3683.

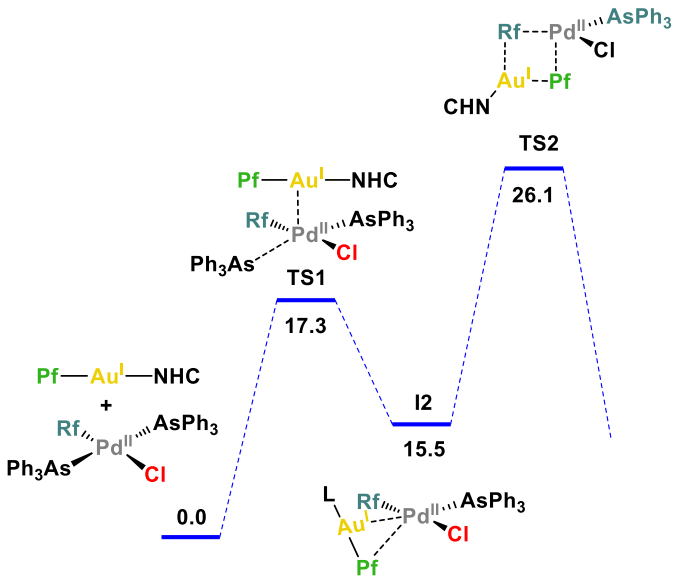

Figure 103. Preliminary computational calculations for the energetic profile of the aryl exchange system.

Finally, this intermediate ***I2*** will evolve through a four member bridged aryls transition state to the complex with the exchanged aryls. As we see in Figure 104, this transition state clearly shows short distances between the ipso carbons of Rf and Pf with the two metal centres (Au-C_{ipso}(Rf)=2.400, Au-C_{ipso}(Pf)=2.344, Pd-C_{ipso}(Rf)=2.094, Pd-C_{ipso}(Pf)=2.146). Interestingly, the distance between the two metal atoms is surprisingly short (Au–Pd = 2.94 A) which shows a clear interaction between the metals, represented in Figure 104.

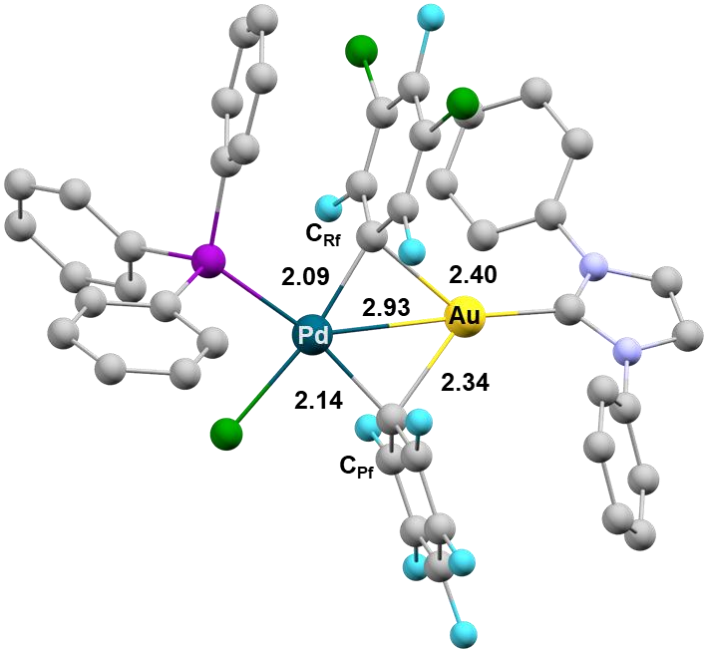

Figure 104. Transition state for the aryl exchange between **1** and **2-Au**. Distances in Å. The coordinates of the structure have been provided by Prof. Rosana Álvarez.

This transition state is found at 26.1 kcal mol^{-1}, which fits quite well with the energies obtained from the copasi software and the experimental data. Moreover, it shows a clear dependence on $AsPh_3$, considering the transition from ***I1*** to ***I2*** by ligand substitution. This would imply a negative order of $AsPh_3$. Additionally, the fact that it is more than 4 kcal mol^{-1} below ***TS1*** implies that the ligand order would be minus one, which fits perfectly with the experimental results.

Moreover, these calculations also fit perfectly with others obtained in previous work. For example, for the study of [Au(Pf)($AsPh_3$)]-catalysed cis/trans

isomerization of $[Pd(Rf)_2(AsPh_3)_2]$, the aryl exchange transition state shows quite similarities with the one obtained for this case, as we can see in Figure 105.

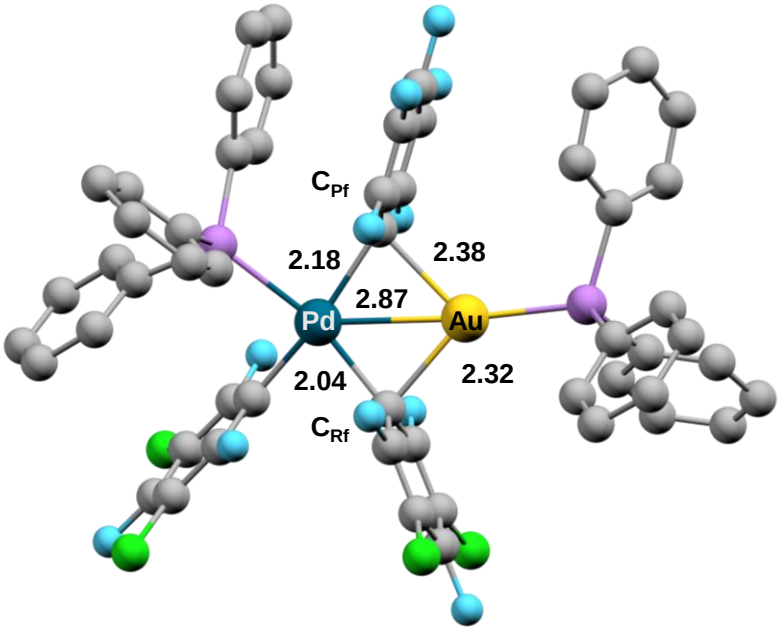

Figure 105 Transition state for the aryl exchange between $[Pd(Rf)_2(AsPh_3)_2]$ and $[Au(Pf)(AsPh_3)]$. Distances in Å.[246]

The four atoms involved in the concerted rearrangement are close to coplanar, as in our case. The Au–Pd distance is in the order of a covalent bond, and the bridging distances to Pd (2.14 and 2.18 Å), practically the same as in Figure 104 are rather shorter than to gold (2.32 and 2.38 Å), which agrees with the distances obtained for our system. Although in our case, the ligand coordinating to the gold atom is a carbene-type ligand, with a much higher sigma-donor character than in the case of $AsPh_3$, which has traditionally been considered a labile ligand, the distances of both transition states are very similar, which could reflect that the ligand coordinated to the transmetalating agent is not very determinant. Interestingly, the Au–Pd distances are also quite similar, which would indicate that both in the previous intermediate I1 and in the transmetalation transition state, there would be distances that would indicate an M–M' interaction. However, as discussed in the introduction to Chen and co-workers' investigation,[215] it is important to treat such interactions with caution, and not to attribute exaggerated stabilization to them for both intermediate and transition states.

Summary and conclusions of the aryl exchange step in Au/Pd systems.

The reaction between the *trans*-[PdCl(Rf)($AsPh_3$)$_2$] complex and the [Au(Pf)(DPI)] complex shows a different reactivity but expected. The transmetalation reaction does not generate the complex with configuration *cis*-[Pd(Rf)(Pf)($AsPh_3$)$_2$], instead of that, the aryl exchange process takes place Different isomerization reactions are generated within the reaction. Kinetic and data analysis results as well as kinetic simulations and DFT calculations allow us to confirm different steps within the overall reaction.

1) The aryl exchange reaction occurs without isomerization. This process is important when designing catalytic reactions because the reductive elimination step is important to modulate the overall thermodynamics of the process and to obtain a C–C coupling.

2) The first step of the reaction is the displacement of the $AsPh_3$ ligand from the Pd complex by the Au complex. This process occurs in a single step. Its existence is confirmed by kinetic experiments with different amounts of free ligand kinetic fits and DFT calculations supporting these results.

4) It is shown that Au complexes are able to catalyse *cis/trans* isomerization in Pd complexes due to aryl exchange processes.

Summary and conclusions of transmetalation step in M/Pd (M = Cu, Ag, Au) systems.

The reaction between the *trans*-[PdCl(Rf)($AsPh_3$)$_2$] complex and the [M(Pf)(DPI)] complex show differences in reaction rates and selectivity. To analyze the observed differences, we will briefly discuss them using thermodynamic and kinetic differences.

a) Thermodynamic component

The most notable difference is that the Cu and Ag systems show a clear tendency to form the M–Cl vs. M–C bond, which leads to an effective transmetalation reaction, generating the *cis*-[Pd(Rf)(Pf)($AsPh_3$)$_2$] complex. This transmetalation occurs with exchange of the configuration, possibly due to then involved bridge transition state. Although the transmetalation step in palladium-copper or silver systems is known to work, it is worth commenting on the thermodynamics of this process. In a simplistic manner, M–C and Pd–X bonds are broken and Pd–C and M–X bonds are formed.

Concerning the copper species, experimental data of various Cu–X bond dissociation energies (BDE) are available.[255] Considering X–Cu dissociation energies series, the Cu–C bond dissociation energy (BDE) is 53 kcal·mol^{-1}, whereas the formed Cu–Cl energy is 91 kcal·mol^{-1}.[255] The affinity of halogens for copper centers are indeed well known, and it acts as the thermodynamic driving force of the transmetalation. This behaviour is similar in the case of silver bonds.

In the case of Pd–halogen bonds of actual complexes, calculated and experimental energies are available. The energy balance between the Pd–X and the Pd–C bonds is endergonic, (from about 14 kcal·mol^{-1} for Pd–I, up to 30 kcal·mol^{-1} if a Pd–Cl bond is broken).[256] Nevertheless, much smaller differences are handled if compared with the copper ones, which would have a greater contribution to the overall ΔG (the

[255] Luo, Y. R. Comprehensive Handbook of Chemical Bond Energies. *Comprehensive Handbook of Chemical Bond Energies* **2007**, 1–1656. DOI: 10.1201/9781420007282.
[256] Casares, J. A.; Coco, S.; Espinet, P.; Lin, Y. S. Observation of a Slow Dissociative Process in Palladium(II) Complexes. *Organometallics* **1995**, *14*, 3058–3067. DOI: 10.1021/om00006a055.

energy balance between the Cu–X and the Cu–C bonds is 41 kcal·mol^{-1} for X=Cl).[257] On the other hand, the thermodynamics of transmetalation in the case of the Au complex is unfavourable for the formation of the Au–Cl bond, with a BDE for the Au–Cl bond of 62 kcal·mol^{-1}, and 90 kcal·mol^{-1} for the Au–C(C_6F_5). [258]

This large difference in the bonding energies between the reactants and products of the transmetalation process is the reason why there are such significant differences between the Cu and Ag transmetalation compared to the aryl exchange produced by Au and could explain the behaviour differences between metals.

Furthermore, due to the electronic similarities between the Rf and Pf, it leads to the aryl exchange complex. This thermodynamic difference leads to obtain different products, leaving Cu and Ag complexes more attractive for the design of new bimetallic catalysis.

b) Kinetic component

Regardless of the products obtained, which are governed by the thermodynamics of the system, differences in the reaction rate are also observed. The activation barrier values obtained by kinetic calculations, kinetic simulations or DFT calculations show a clear trend within the group. The **2-Cu** complex is the fastest to give the reaction (approximately 20 kcal mol^{-1}), followed by **2-Ag** (approximately 21 kcal mol^{-1}) and finally the **2-Au** organometallic complex with an activation barrier of approximately 26 kcal mol^{-1}. With the data that we have and based on the mechanistic proposals discussed in the introduction, we can assume that the transition state that marks the reaction rate will be the same in all cases. Due to the kinetic results obtained, where an order -1 is observed for the triphenylarsine ligand, suggesting that a substitution or dissociation step of this ligand is needed, and furthermore that the dissociation or association of $AsPh_3$ cannot be the rate limiting step, only the transmetalation transition state (or aryl

[257] Golubeva, E. N.; Zubanova, E. M.; Zhidomirov, G. M. The Nature of Cu-C Bond and Copper Oxidation State in Chloroorganocuprates [$CuClnCH_3]_2$-n. *J Phys Org Chem* **2013**, *26*, 724–729. DOI: 10.1002/poc.3093.

[258] Pérezpérez-Iglesias, M.; Espinet, P.; Casares, J. A. Comparing Protonolysis and Transmetalation Reactions: Microcalorimetric Studies of C–Au I Bonds in [AuRL] Complexes. *Inorg. Chem* **2018**, *57*, 46. DOI: 10.1021/acs.inorgchem.8b01758.

exchange in the case of Au) con be considered as the most energetically in the reaction profile.

Assuming that in all cases the transition state associated to the transmetalation step would be like the represented in Figure 105, we can assume that the M–Pd interactions will be stronger as we go down in the group, so the interaction Au–Pd > Ag–Pd > Cu–Pd. This interaction, which generates orbital overlap, can play a fundamental role stabilizing the intermediate **I1** in all cases, but in greater proportion the greater this interaction is. This would leave a greater energetic separation between **I2** and **TS2**, leaving Au as the most sluggish metal for this type of reaction. For the transition state between Cu/Pd and Ag/Pd, the energy difference between the two will be quite small, as the direct rate constants only vary by one order of magnitude (about 1 kcal mol^{-1}). This difference can be explained by orbital interactions. As the Cu atom is smaller than the Ag atom, it is easier to generate a more effective counterionic orbital overlap, which stabilizes, albeit subtly, the transition state lowering its activation energy.

5.3 Experimental section

General experimental section

General procedures and equipment have been described in the Experimental Section in Chapter I. *trans*-[PdCl(Rf)($AsPh_3$)$_2$], *cis*-[Pd(Pf)(Rf)($AsPh_3$)$_2$] *trans*-[Pd(Pf)(Rf)($AsPh_3$)$_2$] *trans*-[Pd(Rf)$_2$($AsPh_3$)$_2$] *cis*-[Pd(Rf)$_2$($AsPh_3$)$_2$], *trans*-[Pd(Pf)$_2$($AsPh_3$)$_2$] *cis*-[Pd(Pf)$_2$($AsPh_3$)$_2$] was synthesized as previously reported.[245,246]

2-Cu and **2-Ag** were synthesized following the Chapter 2 procedure. **2-Au** was synthesized as previously reported.[259]

[259] Johnson, A.; Gimeno, M. C. An Efficient and Sustainable Synthesis of NHC Gold Complexes. *Chem. Commun.* **2016**, *52*, 9664–9667. DOI: 10.1039/c6cc05190a.

Stoichiometric reactions

General Procedure for Kinetic Study of the Transmetalation Step between [M(C_6F_5)(DPI)] (M = Cu, Ag, Au) and trans-[Pd($C_6Cl_2F_3$)Cl($AsPh_3$)$_2$].

Weighted amounts of complex [M(C_6F_5)(DPI)] (M = Cu, Ag, Au) (0.021 mmol) and *trans*-[Pd($C_6Cl_2F_3$)Cl($AsPh_3$)$_2$]. (0.020 mmol, 1 equivalent) were added inside a screw cap NMR tube with the aid of a Schlenk NMR tube adaptor along with a flame sealed coaxial capillary containing acetone-d_6 to the lock deuterium signal. The tube was cooled to 195 K in an isopropanol and a volume (0.50 mL) of dry CH_2Cl_2 (for Cu and Ag) or $CHCl_3$ (for Au) taken with a syringe was added. The tube was closed inside the adaptor and then, taken out of the cool bath, manually shaken until total dissolution of complexes, and transferred to the NMR probe, which had been preheated to the monitoring temperature. After letting the sample thermally equilibrate for ~30 s, single-scan ^{19}F NMR spectra were collected. Shimming and 90° pulse calibration were performed according to the ^{19}F signals of a dummy sample.
The signal of the heteroaryl palladium complexes not isolated are the following:[246]
trans-[Pd($C_6Cl_2F_3$)(C_6F_5)($AsPh_3$)$_2$]: NMR ^{19}F (282.31 MHz, CH_2Cl_2/acetone-cap, 298 K) δ -88.91 (s, o–$C_6Cl_2F_3$), -113.22 (m, o–C_6F_5), -119.97 (s, p– $C_6Cl_2F_3$), -161.68 (t, p–C_6F_5), - 163.96 (m, m– C_6F_5).
trans-[Pd($C_6Cl_2F_3$)(C_6F_5)($AsPh_3$)$_2$]: NMR ^{19}F (282.31 MHz, CH_2Cl_2/acetone-cap, 298 K) δ -89.81 (m, o– $C_6Cl_2F_3$), -115.36 (m, o– C_6F_5), -121.06 (s, p– $C_6Cl_2F_3$), -162.46 (t, o– C_6F_5), -163.87 (m, m– C_6F_5).

*Equilibria between trans-[PdCl(Rf)(AsPh$_3$)$_2$] (**1**)* and *[PdRf(μ-Cl)(AsPh$_3$)]$_2$*

A low-temperature study could show the two species in solution, so we could measure the equilibrium constant and calculate how much dimer would be present in our reaction. Weighted amounts of complex *trans*-[PdCl($C_6Cl_2F_3$)($AsPh_3$)$_2$]. (0.020 mmol, 1 equivalent) were added inside a screw cap NMR tube with the aid of a Schlenk NMR tube adaptor along with a flame sealed coaxial capillary containing acetone-d_6 to the lock deuterium signal. The tube was cooled to 195 K in an isopropanol and a volume (0.50 mL) of dry CH_2Cl_2 taken with a syringe was added. The tube was closed inside the adaptor and then, taken out of the cool bath, manually shaken until total dissolution of complexes, and transferred to the NMR probe, which had been precooled to the monitoring temperature (-100°C). After letting the sample thermally equilibrate for ~30 s, single-scan ^{19}F NMR spectra were collected. Shimming and 90° pulse calibration were performed according to the ^{19}F signals of a dummy sample.

The result shows that there is no variation in the ^{19}F NMR signals, and no new species appear in solution, so the equilibrium is strongly shifted towards the monomeric species, and it is assumed that it does not act in our reaction.

Kinetic order with respect to the copper complex.

Weighted amounts of complex *trans*-[Pd($C_6Cl_2F_3$)Cl($AsPh_3$)$_2$]. (0.020 mmol, 1 equivalent) and different amounts of **2-Cu** were added inside a screw cap NMR tube with the aid of a Schlenk NMR tube adaptor along with a flame sealed coaxial capillary containing acetone-d_6 to the lock deuterium signal. The tube was cooled to 195 K in an isopropanol and a volume (0.50 mL) of dry CH_2Cl_2 taken with a syringe was added. The tube was closed inside the adaptor and then, taken out of the cool bath, manually shaken until total dissolution of complexes, and transferred to the NMR probe, which had been precooled to the monitoring temperature. After letting the sample thermally equilibrate for ~30 s, single-scan ^{19}F NMR spectra were collected. Shimming and 90° pulse calibration were performed according to the ^{19}F signals of a dummy sample.

To determine the order with respect to the **2-Cu** complex, different reactions are measured keeping the quantities of **1** constant, to obtain a relation on how the transmetalation rate varies with respect to the quantity of **2-Cu**.

The transmetalation reaction is first-order in [**2-Cu**] as shown in Figure 90. The plot of ln(*r0*) *vs.* ln([**2-Cu**]) is a straight line with slope 0.98. Therefore, the transmetalation rate is proportional to the concentration of [**2-Cu**].

Retardation by addition of $AsPh_3$.

Weighted amounts of complex *trans*-[Pd($C_6Cl_2F_3$)Cl($AsPh_3$)$_2$]. (0.020 mmol, 1 equivalent) of **2-Cu** were added inside a screw cap NMR tube with the aid of a Schlenk NMR tube adaptor along with a flame sealed coaxial capillary containing acetone-d_6 to the lock deuterium signal. Additionally, different amounts of free triphenylarsine were added to the mixture in different experiments, as we can see in Figure 91. The tube was cooled to 195 K in an isopropanol and a volume (0.50 mL) of dry CH_2Cl_2 taken with a syringe was added. The tube was closed inside the adaptor and then, taken out of the cool bath, manually shaken until total dissolution of complexes, and transferred to the NMR probe, which had been precooled to the monitoring temperature. After letting the sample thermally equilibrate for ~30 s, single-scan ^{19}F NMR spectra were collected. Shimming and 90° pulse calibration were performed according to the ^{19}F signals of a dummy sample.

The presence of added $AsPh_3$ retards the transmetalation reaction between **1** and **2-Cu**. The kinetic law shows minus first order with respect to the concentration of $AsPh_3$ (the plot of ln($r0$) *vs* ln[$AsPh_3$]$_{added}$ is a straight line with slope -0.93). As commented above, the minus first order with respect to the concentration of $AsPh_3$ implies that the energy profile consists of several stages. One of them involves the dissociation or exchange of the $AsPh_3$ group for the **2-Cu** complex, and that this stage is not the rate limiting step of the reaction. Data collected in Figure 91.

Kinetic order with respect to the silver complex.

Weighted amounts of complex *trans*-[Pd($C_6Cl_2F_3$)Cl($AsPh_3$)$_2$]. (0.020 mmol, 1 equivalent) and different amounts of **2-Ag** were added inside a screw cap NMR tube with the aid of a Schlenk NMR tube adaptor along with a flame sealed coaxial capillary containing acetone-d_6 to the lock deuterium signal. The tube was cooled to 195 K in an isopropanol and a volume (0.50 mL) of dry CH_2Cl_2 taken with a syringe was added. The tube was closed inside the adaptor and then, taken out of the cool bath, manually shaken until total dissolution of complexes, and transferred to the NMR probe, which had been precooled to the monitoring temperature. After letting the sample thermally equilibrate for ~30 s, single-scan ^{19}F NMR spectra were collected. Shimming and 90° pulse calibration were performed according to the ^{19}F signals of a dummy sample.

To de termine the order with respect to the **2-Ag** complex, different reactions are measured keeping the quantities of **1** constant, to obtain a relation on how the transmetalation rate varies with respect to the quantity of **2-Cu**.
The transmetalation reaction is first-order in [**2-Cu**] as shown in Figure 97. The plot of ln(*r0*) *vs.* ln([**2-Ag**]) is a straight line with slope 0.98. Therefore, the transmetalation rate is proportional to the concentration of [**2-Ag**].

Retardation by addition of $AsPh_3$.

Weighted amounts of complex *trans*-[Pd($C_6Cl_2F_3$)Cl($AsPh_3$)$_2$]. (0.020 mmol, 1 equivalent) of **2-Ag** were added inside a screw cap NMR tube with the aid of a Schlenk NMR tube adaptor along with a flame sealed coaxial capillary containing acetone-d_6 to the lock deuterium signal. Additionally, different amounts of free triphenylarsine were added to the mixture in different experiments, as we can see in Figure 98. The tube was cooled to 195 K in an isopropanol and a volume (0.50 mL) of dry CH_2Cl_2 taken with a syringe was added. The tube was closed inside the adaptor and then, taken out of the cool bath, manually shaken until total dissolution of complexes, and transferred to the NMR probe, which had been precooled to the monitoring temperature. After letting the sample thermally equilibrate for ~30 s, single-scan ^{19}F NMR spectra were collected. Shimming and 90° pulse calibration were performed according to the ^{19}F signals of a dummy sample.

The presence of added $AsPh_3$ retards the transmetalation reaction between **1** and **2-Ag**. The kinetic law shows minus first order with respect to the concentration of $AsPh_3$ (the plot of ln($r0$) *vs* ln[$AsPh_3$]$_{added}$ is a straight line with slope -0.91). As commented above, the minus first order with respect to the concentration of $AsPh_3$ implies that the energy profile consists of several stages. One of them involves the dissociation or exchange of the $AsPh_3$ group for the **2-Ag** complex, and that this stage is not the rate limiting step of the reaction. Data collected in Figure 98.

Kinetic order with respect to the gold complex.

Weighted amounts of complex *trans*-[Pd($C_6Cl_2F_3$)Cl($AsPh_3$)$_2$]. (0.020 mmol, 1 equivalent) and different amounts of **2-Au** were added inside a screw cap NMR tube with the aid of a Schlenk NMR tube adaptor along with a flame sealed coaxial capillary containing acetone-d_6 to the lock deuterium signal. The tube was cooled to 195 K in an isopropanol and a volume (0.50 mL) of dry $CHCl_3$ taken with a syringe was added. The tube was closed inside the adaptor and then, taken out of the cool bath, manually shaken until total dissolution of complexes, and transferred to the NMR probe, which had been preheating to the monitoring temperature. After letting the sample thermally equilibrate for ~30 s, single-scan ^{19}F NMR spectra were collected. Shimming and 90° pulse calibration were performed according to the ^{19}F signals of a dummy sample.

To determine the order with respect to the **2-Au** complex, different reactions are measured keeping the quantities of **1** constant, to obtain a relation on how the transmetalation rate varies with respect to the quantity of **2-Au**.
The transmetalation reaction is first-order in [**2-Au**]. The plot of ln(*r0*) *vs.* ln([**2-Au**]) is a straight line with slope 0.93. Therefore, the transmetalation rate is proportional to the concentration of [**2-Au**].

Retardation by addition of $AsPh_3$.

Weighted amounts of complex *trans*-[Pd($C_6Cl_2F_3$)Cl($AsPh_3$)$_2$]. (0.020 mmol, 1 equivalent) of **2-Au** were added inside a screw cap NMR tube with the aid of a Schlenk NMR tube adaptor along with a flame sealed coaxial capillary containing acetone-d_6 to the lock deuterium signal. Additionally, different amounts of free triphenylarsine were added to the mixture in different experiments, as we can see in Figure 100. The tube was cooled to 195 K in an isopropanol and a volume (0.50 mL) of dry CH_2Cl_2 taken with a syringe was added. The tube was closed inside the adaptor and then, taken out of the cool bath, manually shaken until total dissolution of complexes, and transferred to the NMR probe, which had been precooled to the monitoring temperature. After letting the sample thermally equilibrate for ~30 s, single-scan ^{19}F NMR spectra were collected. Shimming and 90° pulse calibration were performed according to the ^{19}F signals of a dummy sample.

The presence of added $AsPh_3$ retards the transmetalation reaction between **1** and **2-Au**. The kinetic law shows minus first order with respect to the concentration of $AsPh_3$ (the plot of ln($r0$) *vs* ln[$AsPh_3$]$_{added}$ is a straight line with slope -0.90). As commented above, the minus first order with respect to the concentration of $AsPh_3$ implies that the energy profile consists of several stages. One of them involves the dissociation or exchange of the $AsPh_3$ group for the **2-Au** complex, and that this stage is not the rate limiting step of the reaction. Data collected in Figure 100.

X-ray crystallographic data

A crystal was attached to a glass fiber and transferred either to an Agilent Supernova diffractometer with an Atlas CCD area detector (Valladolid University facilities). The crystal was kept at constant temperature during data collection. Data collection was performed with Mo-Kα radiation (0.71073 Å). Data integration, scaling and empirical absorption correction were carried out using the CrysAlisPro program package. Using Olex2, the structure was solved with the olex2.solve structure solution program and refined with ShelX program. The non-hydrogen atoms were refined anisotropically and hydrogen atoms were placed at idealized positions and refined using the riding model. Refinement proceeded smoothly to give the residuals shown in CCDC contains the supporting crystallographic data for this paper. These data can be obtained free of charge at www.ccdc.cam.ac.uk/conts/retrieving.html [or from the Cambridge Crystallographic Data Centre, 12, Union Road, Cambridge CB2 1EZ, UK; fax: (internat.) +44-1223/336-033;

Identification code	cis-[Pd(Rf)(Pf)($AsPh_3$)$_2$]
CCDC deposition N°	2131401
Empirical formula	$C_{48}H_{30}As_2Cl_4F_6Pd$
Formula weight	1085.86
Temperature/K	294
Crystal system	triclinic
Space group	P-1
a/Å	9.6475(8)
b/Å	11.5994(9)
c/Å	21.6027(12)
α/°	97.498(5)
β/°	90.397(5)
γ/°	112.377(8)
Volume/Å3	2212.1(3)
Z	2
ρcalcg/cm3	1.630
μ/mm-1	2.092
F(000)	1072.0
Crystal size/mm3	0.587 × 0.351 × 0.325
Radiation	MoKα (λ = 0.71073)
2Θ range for data collection/°	7.014 to 59.19
Index ranges	-13 ≤ h ≤ 11, -14 ≤ k ≤ 12, -21 ≤ l ≤ 29
Reflections collected	15442
Independent reflections	10101 [Rint = 0.0287, Rsigma = 0.0666]
Data/restraints/parameters	10101/0/550
Goodness-of-fit on F2	1.070
Final R indexes [I>=2σ (I)]	R1 = 0.0561, wR2 = 0.1261
Final R indexes [all data]	R1 = 0.0832, wR2 = 0.1446
Largest diff. peak/hole / e Å-3	1.06/-1.28

Conclusiones generales

Capítulo 1: En resumen, hemos desarrollado un nuevo sistema eficiente para preparar biarilos altamente fluorados en rendimientos excelentes, utilizando un sistema catalítico bimetálico Pd/Cu, empleando reactivos Ar^F–H disponibles comercialmente y sin necesidad de preparación previa de nucleófilos para el ciclo catalítico de cobre, y bromuros o cloruros de arilo fluorados para el ciclo catalítico de paladio.

La elección de ligandos para Pd y Cu es crucial para el buen resultado de la reacción, ya que todos los pasos en el mecanismo pueden ser limitantes para la velocidad de reacción general. La elección del ligando carbeno IPr para el complejo de cobre y la fosfina XPhos tipo Buchwald para el paladio ha demostrado ser perfectamente sinérgica en este sistema catalítico. Estos ligandos facilitan el acoplamiento rápido y selectivo incluso para arilos altamente fluorados, reduciendo la hidrólisis no deseada y los productos de homoacoplamiento, producidos por ciclos catalíticos externos y permite una aplicación general y en condiciones suaves. Además, la elección de los ligandos también permite evitar el intercambio de ligandos. La investigación mecanicista muestra un comportamiento cooperativo clave entre ambos metales, demostrando que las diferentes etapas limitantes dependen de la naturaleza de los reactivos. Eso hace factible el proceso y genera una interesante sinergia entre metales, que puede permitir mejorar la nueva catálisis bimetálica de Pd/Cu.

Capítulo 2: Como conclusión del capítulo II, podemos destacar que la reactividad y estereoquímica de la adición oxidante en complejos de Cu(I) del tipo [Cu(L)(C_6F_5)] (L=Carbeno) puede ser modificada por el halógeno o pseudohalógeno que se emplea, y no es necesario cambiar la vía mecanística. Además, la activación del enlace $C_6F_3Cl_2$–I por el complejo de 14e– [Cu(C_6F_5)(DPI)] ocurre a través de la interacción de dos complejos de cobre con un mismo yoduro de arilo. Este modo de activación no requiere la formación de un dímero de cobre, sino que se basa en la formación previa de una interacción de yoduro de arilo con un complejo de cobre en una concentración cinéticamente relevante, que se ha detectado experimentalmente. Este grupo reacciona con un segundo complejo de cobre, sobre

el que se produce la adición oxidante. La estabilización es eficiente en los estados de transición para la ruptura y formación del enlace C–I, que es donde el átomo de yodo tiene un mayor carácter aniónico. La estabilización del estado de transición puede atribuirse a una polarización de la densidad electrónica del yodo por el segundo cobre, confirmado por análisis de NBO. El funcionamiento de estos mecanismos tiene un efecto dramático en la estereoselectividad de la reacción: dado que conduce a la disposición *trans*-[CuI(C_6F_5)($C_6F_3Cl_2$)(DPI)] en lugar de a la disposición *cis*, no se observan productos de acoplamiento cruzado en estas condiciones de reacción, sino que se produce la metátesis del halógeno.

Capítulo 3: En conclusión, presentamos una metodología novedosa y moderna para la formación de biarilo fluorado y altamente fluorado a partir de los benzoatos abundantes y estables. Enfocados en la metodología, realizamos la síntesis de biarilos simétricos y asimétricos altamente fluorados en condiciones suaves utilizando un sistema catalítico de cobre. También se elimina el uso de sales estequiométricas, largos tiempos de reacción o metales no abundantes.

Por otro lado, esta metodología fotoquímica es el primer ejemplo de reacción de acoplamiento cruzado C–C utilizando una fotodescarboxilación vía LMCT utilizando cobre como catalizador. Esta innovadora reacción abre la puerta a varios procesos de acoplamiento utilizando ácidos carboxílicos/carboxilatos como fuente de reactivos para la formación de los enlaces más importantes para generar moléculas complejas.

Algunas características del mecanismo son particularmente relevantes: i) la activación fotoquímica podría operar en dos pasos consecutivos del ciclo catalítico, y ii) la escisión fotoquímica Ar–COO conduce principalmente al enlace Cu–Ar. Estas aportaciones, junto con las descritas anteriormente, nos permiten estar un poco más cerca de una comprensión completa del mecanismo de este tipo de reacciones.

Capítulo 4: Se presenta el primer sistema catalítico para la síntesis de complejos Fe^{II} del tipo [Fe(Cp)(ArF)$(CO)_2$] utilizando cobre como catalizador. Para ello, se emplea el proceso de activación C–H de arenos altamente fluorados en presencia de base. La etapa de transmetalación es efectiva con ligandos bipiridina o carbeno,

mostrando que la termodinámica de la transmetalación es favorable. Por otro lado, la elección del ligando es crítica para la cinética de este paso.

El estudio mecanistico de la reacción de transmetalación entre los complejos [Cu(C_6F_5)(bipy)] y [Fe(Cp)I($CO)_2$] muestra en RMN de ^{19}F un claro período de inducción, causado por la generación de la especie activa [Fe(Cp)I(CO)] por disociación de un grupo carbonilo. Es probable que este proceso conduzca a un estado de transición concertado de 4 miembros, donde el arilo y el halógeno se intercambian entre los complejos Cu y Fe.

Se ha demostrado que diferentes formas de facilitar dicha disociación disminuyen el tiempo del período de inducción, pero no aumentan la velocidad de transmetalación. Además, las simulaciones cinéticas demuestran que es obligatoria una transmetalación adicional entre dos complejos de Fe para recuperar el grupo carbonilo y generar el producto deseado.

Por otro lado, el proceso ha sido estudiado mediante cálculos computacionales, utilizando métodos DFT. Los resultados muestran que un intercambio de espín podría participar en el proceso, lo que permitiría una correlación correcta entre la energía experimental y calculada computacionalmente.

Capítulo 5: La reacción entre el complejo *trans*-[PdCl(Rf)($AsPh_3)_2$] y los complejos [M(Pf)(DPI)] (M = Cu, Ag, Au) muestra diferencias en las velocidades de reacción y selectividad. Para analizar las diferencias observadas, se discuten brevemente utilizando diferencias termodinámicas y cinéticas.

Componente termodinámico

La diferencia más notable es que los sistemas con Cu y Ag muestran una clara tendencia a formar el enlace M–Cl vs. M–C, lo que conduce a una reacción de transmetalación efectiva, generando el complejo *cis*-[Pd(Rf)(Pf)($AsPh_3)_2$]. Esta transmetalación ocurre con intercambio de la configuración, posiblemente debido al estado de transición involucrado. Aunque se sabe que el paso de transmetalación en los sistemas de paladio-cobre o plata funciona, vale la pena comentar sobre la termodinámica de este proceso. De una manera simplista, los enlaces M–C y Pd–X

se rompen y se forman los enlaces Pd–C y M–X. En cuanto a las especies de cobre, se dispone de datos experimentales de diversas energías de disociación del enlace Cu-X . Considerando las series de energías de disociación X–Cu, la energía de disociación del enlace Cu–C es de 53 kcal·mol$^{-1,}$ mientras que la energía del enlace Cu–Cl formado es de 91 kcal·mol^{-1}. La afinidad de los halógenos por los centros de cobre es bien conocida, y actúa como la fuerza motriz de la termodinámica de la etapa de transmetalación. Este comportamiento es similar en el caso de los complejos de plata.

En el caso de enlaces Pd–halógenos de complejos reales, se dispone de energías calculadas y experimentales. El balance de energía entre los enlaces Pd–X y Pd–C es endergónico, (desde aproximadamente 14 kcal·mol^{-1} para Pd–I, hasta 30 kcal·mol^{-1} si se rompe un enlace Pd–Cl). Sin embargo, se manejan diferencias mucho menores si se comparan con las de cobre, que tendrían una mayor contribución al ΔG global (el balance de energía entre los enlaces Cu–X y Cu–C es de 41 kcal·mol^{-1} para X = Cl). Por otro lado, la termodinámica de la transmetalación en el caso del complejo Au es desfavorable para la formación del enlace Au–Cl, con una energía para el enlace Au–Cl de 62 kcal·mol^{-1}, y 90 kcal·mol^{-1} para el Au–C(C_6F_5), lo que repercute en que la reacción de transmetalación no se produzca, y se observe únicamente el intercambio de los grupos arilo.

Esta gran diferencia en las energías de enlace entre los reactivos y los productos del proceso de transmetalación es la razón por la cual existen diferencias tan significativas entre la transmetalación Cu y Ag en comparación con el intercambio arilo producido por Au y podría explicar las diferencias de comportamiento entre los metales.

Componente cinético

Independientemente de los productos obtenidos, que se rigen por la termodinámica del sistema, también se observan diferencias en la velocidad de reacción. Los valores de barrera de activación obtenidos mediante cálculos cinéticos, simulaciones cinéticas o cálculos DFT muestran una clara tendencia dentro del grupo. El complejo **2-Cu** es el más rápido para dar la reacción (aproximadamente 20 kcal mol^{-1}), seguido de **2-Ag** (aproximadamente 21 kcal mol^{-}

^{1}) y finalmente el complejo organometálico **2-Au** con una barrera de activación de aproximadamente 26 kcal mol^{-1}. Con los datos que tenemos y en base a las propuestas mecanicistas comentadas en la introducción, podemos suponer que el estado de transición que marca la velocidad de reacción será el mismo en todos los casos. Debido a los resultados cinéticos obtenidos, donde se observa un orden -1 para el ligando trifenilarsina, lo que sugiere que es necesaria una etapa de sustitución o disociación de este ligando, y además que la disociación o asociación de $AsPh_3$ no puede ser el paso limitante de la velocidad, solo el estado de transición de transmetalación (o intercambio arilo en el caso de Au) se considera como el más energético en el perfil de reacción.

Suponiendo que en todos los casos el estado de transición asociado al paso de transmetalación sería como el representado en la Figura 105, podemos suponer que las interacciones M–Pd serán más fuertes a medida que descendemos en el grupo, por lo que la interacción Au–Pd > Ag–Pd > Cu–Pd. Esta interacción, que genera solapamiento orbital, puede jugar un papel fundamental estabilizando el intermedio I1 en todos los casos, pero en mayor proporción cuanto mayor sea esta interacción. Esto dejaría una mayor separación energética entre **I2** y **TS2**, dejando al Au como el metal más lento para este tipo de reacción. Para el estado de transición entre Cu/Pd y Ag/Pd, la diferencia de energía entre los dos será bastante pequeña, ya que las constantes de velocidad directa solo varían en un orden de magnitud (aproximadamente 1 kcal mol^{-1}). Esta diferencia puede explicarse por interacciones orbitales. Como el átomo de Cu es más pequeño que el átomo de Ag, es más fácil generar una superposición orbital más efectiva, que estabiliza, aunque sutilmente, el estado de transición reduciendo su energía de activación.

List of abbreviations and acronyms

acac: Acetylacetonate

Ad: Adamantyl

Alk: Alkyl

Ar: Aryl

Bn: Benzyl

Bpin: Pinacolboryl

bpy: 2,2′-Bipyridine

Bz: Benzoyl

CAAC: Cyclic (alkyl)(amino)carbene

Cat: Catalytic

COD: 1,5-Cyclooctadiene

Cy: Cyclohexyl

DFT: Density functional theory

DMA: N,N-Dimethylacetamide

DMF: N,N-Dimethylformamide

DMSO: Dimethyl sulfoxide

dppbz: 1,2-Bis(diphenylphosphino)benzene

dppe: 1,2-Bis(diphenylphosphino)ethane

Equiv: equivalent

Het: Heterocyclic

HMPA: Hexamethylphosphoramide

HRMS: High resolution mass spectrometry

iBu: Isobutyl

iPr: Isopropyl

L: Ligand

M: Metal

Mes: Mesityl

MECP: Minimum Energy Crossing Point

NBO = Natural Bond Orbitals

nBu: Butyl

NHC: N-Heterocyclic carbene

n-hex: Hexyl

NMR: Nuclear magnetic resonance

NR: No reaction

Nu^-: Nucleophile

Tf: Trifluoromethanesulfonyl

Ts: p-Toluenesulfonyl

phen: 1,10-Phenanthroline

py: Pyridine

pyBOX: Pyridine bisoxazoline

RT: Room temperature

SET: Single electron transfer

T: Temperature

TBAB: Tetrabutylammonium bromide

TBAC: Tetrabutylammonium chloride

TBAF: Tetrabutylammonium fluoride

^{t}Bu: Tert-Butyl

TEMPO: 2,2,6,6-Tetramethylpiperidine 1-oxyl

TFA: Trifluoroacetic acid

THF: Tetrahydrofuran

TMEDA: Tetramethylethylenediamine

TMS: Trimethylsilyl

Tol: Tolyl

Xantphos: 4,5-Bis(diphenylphosphino)-9,9-dimethylxanthene